

Understanding Powder Blending Mechanics for Applications in Pharmaceutical Continuous Direct Compression

By

Owen Jones-Salkey

A thesis submitted to
the University of Birmingham
for the degree of
DOCTOR OF ENGINEERING

Formulation Engineering CDT
School of Chemical Engineering
College of Engineering and Physical Sciences
University of Birmingham
December 2024

UNIVERSITY OF
BIRMINGHAM

University of Birmingham Research Archive

e-theses repository

This unpublished thesis/dissertation is copyright of the author and/or third parties. The intellectual property rights of the author or third parties in respect of this work are as defined by The Copyright Designs and Patents Act 1988 or as modified by any successor legislation.

Any use made of information contained in this thesis/dissertation must be in accordance with that legislation and must be properly acknowledged. Further distribution or reproduction in any format is prohibited without the permission of the copyright holder.

© Copyright by OWEN JONES-SALKEY

On behalf of University of Birmingham, AstraZeneca & EPSRC - 2024

All Rights Reserved

ABSTRACT

This thesis presents a holistic example of accelerating pharmaceutical process development by integrating experimental platforms, user-centric process design, and data-driven modelling. At the heart of this approach lies the modular process optimisation suite, the MACH-1, a Good Laboratory Standard (GLS) equipment suite operating in parallel with a fully fledged Good Manufacturing Practice (GMP) development facility. This dual setup not only expands the experimental capacity but also allows project-specific work packages to seamlessly integrate into AstraZeneca's established workflows for oral product development. Beyond its on-site utility, the GLS suite has supported off-site mechanistic studies, highlighting its flexibility for delivering diverse R&D needs.

Accordingly, Positron Emission Particle Tracking (PEPT), a unique noninvasive measurement technique, was leveraged to characterise steady-state powder behaviours in continuous blending. Through the tracking of discrete particle spatial-temporal data, the study revealed how adjusting incline linear blender parameters, such as rotational speed and blade configuration, can enhance content uniformity and even induce a 'folding region', where powder is transported away from and returned to a bed of bulk mass residing at the base of the inclined blender, in a convection-like cycle. These insights also provide the means for calibrating and validating future Discrete Element Method (DEM) simulations.

Building on these experimental insights, the relationship between product formulation and process conditions was modelled using three distinct AI/ML approaches: Random Forest Regression, Symbolic Regression, and Artificial Neural Network (ANN). When predicting fill levels in inclined linear blenders, the ANN outperformed other methods, achieving an r^2 of 0.97 and generalising effectively to multicomponent commercial formulations. By

reducing experimental trials by up to 60–70%, these models substantially cut material use and development time.

An additional innovation is the digital layer integrated into the MACH-1 workflow: a democratised ANN for real-time assessment of blending quality. This user-friendly platform, accessible via a hyperlink on the intranet, empowers scientists and engineers to refine process parameters independently, minimising the reliance on specialised expertise. Consequently, the interface increases both operational agility and the broader adoption of advanced analytics.

This holistic approach ultimately yielded the following benefits per experimental campaign:

- **Reduced experimentation:** Up to a 60–70% reduction in the number of experiments, significantly conserving high-cost APIs.
- **Cost efficiency:** Decreasing the need for expensive materials translates into a projected savings of £112k.
- **Environmental sustainability:** Cutting down on experimental runs reduces carbon emissions by almost 6 tonnes of CO_2.
- **Accelerated timelines:** Replacing multi-day *in-vitro* trials with minutes long *in silico* studies, facilitated by real-time, democratised access to advanced modelling tools.

In summary, this thesis illustrates the core objective of an industrially based Engineering Doctoral programme– conducting research that not only advances the broader scientific field, but also directly serves the needs of AstraZeneca. Through the fusion of modular process design and digital transformation, it advances process understanding, sustainability, innovation, and cost efficacy. In so doing, it demonstrates that, despite decades of brilliant work, there is a growing market for opportunities to make drug product development more environmentally and economically responsible.

DEDICATION

Dedicated to my:

Mother (Lisa), Nanny & Grandad (Olivia & George), Father (Anthony).

& my late grandparents (Mavis & Byron).

ACKNOWLEDGMENTS

I am truly grateful for the support and encouragement throughout my journey. This work is largely due to the unwavering love and guidance of my family, the patience and companionship of my friends and colleagues, and the insightful mentorship that has shaped my growth.

I first extend special thanks to Dr. Andy Ingram, Professor Kit Windows-Yule, and Dr. Richard Greenwood. Your collective expertise, generosity with your time, and constructive challenges have provided me with a solid foundation on which to build my career. I could not have asked for a more supportive network of advisors; you cultivated an environment where no question was too trivial, and your guidance has been instrumental in nurturing the skills I will carry forward into industry.

To Niamh, Tara and Martin (Hawes), thank you for welcoming me into your family. Your kindness and support greatly enriched my life and my work. I will always cherish the lessons and, most importantly, the memories that we shared together. Thank you.

Lastly, I am incredibly grateful to my father, whose perspective (often shared over a pint) helped me through difficult times. I equally cherish the warmth and support of Nanny (Olivia) and Grandad (George). Above all, the strength, kindness and resolve of my mother, who inspires me to strive for more while ensuring I am a grounded person with a duty to care for others.

Engineering Doctoral (EngD) thesis: *Understanding Powder Blending Mechanics for Applications in Pharmaceutical Continuous Direct Compression*

Contents

Page

1 Introduction: Oral Solid Dosage Forms & Continuous Direct Compression 1

1.1 Overview of Oral Solid Dosage Forms 1

1.2 Thesis Motivation 3

1.3 Project Focus: Continuous Powder Blending 6

1.3.1 Understanding Powder Blending on Tablet Performance 7

1.4 Thesis Aims 9

2 Literature Review 10

2.1 Preface 10

2.2 Published Review Article: Reviewing the Impact of Powder Cohesion on Continuous Direct Compression (CDC) Performance. 11

2.2.1 Powder Feeding 11

2.2.2 Feeding Summary 31

2.2.3 Blending 33

3 Business Impact: AstraZeneca, Oral Product Development 56

3.1 Introduction: Continuous Blending Equipment 56

3.2 Business Criticality: The Role of MACH-1 57

3.2.1 What is the MACH-1? 57

3.2.2 The Role of MACH-1 59

3.2.3 Required Modifications for the Prototype Blender 62
3.3 MACH-1 Integration 64
3.4 The Impact of the MACH-1 66
3.4.1 MACH-1 Enabled Experimentation, Modelling & Simulation 67
3.4.2 Model Democratization 72
3.5 Closing Remarks 74

4 Application of Positron Emission Particle Tracking (PEPT) for the Evaluation of Powder Behaviour in an Incline Linear Blender for Continuous Direct Compression (CDC) 76

4.1 Preface 76
4.2 Abstract 77
4.3 Introduction 78
4.4 Equipment, Materials and Methods 81
4.4.1 Equipment 81
4.4.2 Materials 83
4.4.3 Experimental Set-Up 84
4.4.4 Experimental Design 85
4.4.5 Experimental Method 86
4.4.6 Analysis 88
4.5 Results & Discussion 95
4.5.1 Traversal Classification 96
4.5.2 Lagrangian Micromixing 98
4.5.3 Auto-Correlation 102
4.5.4 Axial Spatial Residence Time Distribution 105
4.6 Conclusion 108

5 Using AI/ML to Predict Blending Performance and Process Sensitivity for Continuous Direct Compression (CDC) 111

5.1 Preface . . . 111

5.1.1 Preface: Model Democratisation & Re-training/parameterisation . . . 112

5.2 Introduction . . . 113

5.3 Equipment . . . 114

5.3.1 Prototype GEA, CDB-1, Linear Blender . . . 114

5.3.2 GEA, Compact Powder Feeder . . . 117

5.3.3 Mettler Toledo, Catch Scale . . . 117

5.4 Materials & Characterisation . . . 118

5.4.1 Material List . . . 118

5.4.2 Material Characterisation & Methods . . . 120

5.5 Methods . . . 123

5.5.1 Feeder Calibration . . . 123

5.5.2 Residence Mass (RM) Measurements . . . 124

5.5.3 Calculations . . . 127

5.5.4 Predictive Modelling . . . 128

5.5.5 Symbolic Regression – M^2E^3D . . . 141

5.6 Results . . . 145

5.6.1 General Data Trends . . . 145

5.6.2 Model: Random Forest Regression . . . 148

5.6.3 Model: PyTorch ANN Feature analysis & Contour Mapping . . . 150

5.6.4 Model: M^2E^3D's Symbolic Regression . . . 152

5.7 Discussion . . . 154

5.7.1 Blind Formulation Validation and Model Comparison. . . . 154

5.7.2 Predicting Mixing Performance . . . 156

5.7.3 Application: Identifying the Strain Window . . . 163

5.8 Conclusion 165

6 Conclusion **168**

6.1 Thesis Conclusion 168

6.1.1 Industrial Conclusion 168

6.1.2 Technical Conclusion 169

6.2 Future Work 172

6.2.1 Scaling Over & Technology Transfers 172

6.2.2 Advanced Drug Formulation 173

6.2.3 Improving Upstream Processing — Powder Feeding 174

A Attached Publication for Chapter 2 **177**

B Attached Publication for Chapter 4 **226**

C Attached Publication for Chapter 5 **238**

References **256**

List of Figures

2.1 **Left**: Graphs highlighting the difference in characteristics (Flow Function (FFC), Cohesion, and angle of internal friction) of the two excipients: Hypromellose and Dicalcium Phosphate Anhydrous with and without colloidal silica. **Right**: Scanning Electron Microscope (SEM) of the two excipients mixed with 1% w/w colloidal silica. Adapted from: Leung et al. [42]. 15

2.2 **Top Left**: Mass per screw pitch as a function of cohesive stiffness (K_{adh}). **Bottom Left**: Mass per Watt as a function of cohesive stiffness (K_{adh}). **Top Right**: Visualisation of the powder arching/bridging within the hopper volume. The images show both the back and front of the hopper from two different simulations using the same K_{adh}. **Bottom Right**: Irregular filling of the conveying volume due to cohesive stiffness (K_{adh}). The images compare $K_{adh} = 0.3$ and $K_{adh} = 0.5$. Gathered with permission from Lopez et al. [48]. 17

2.3 (**A**) Comparing the differences in the dynamic cohesive index (σ) with the addition of different types and weight percentages of Mesoporous Silicates (MPS). (**B**) Dynamic influence of MPS on the cohesive index, demonstrated through plotting the cohesive index over different rotating speeds. (**C**) Comparison of Charge Density (nC/g) in two excipients and resultant performance with the addition of 2% weight silicates. Where: +S244 is Syloid® 244FP, +SAL1 is Syloid® AL–1FP, and +SXDP is Syloid® XDP3050. Adapted from Lumay et al. [50]. 21

2.4 **Top**: Two graphs detailing the feed factor throughout the volumetric empty, with absolute values (**left**) and normalised values (**right**), the key indicates the material used. Where: FF316 is Lactose Fast Flo® 316, SD711 is Sodium Croscarmellose Ac-Di-Sol® SLS is Sodium Lauryl Sulphate, PH102 is MCC Avicel® PH-102, APAP is Acetaminophen, and MgSt is Magnesium Sterate. **Bottom**: Three graphs compare feeder performance to bulk characteristics. Adapted from Van Snick et al. [32]. 23

2.5 Correlation heat map (Escotet-Espinosa [54]) showing the magnitude of the linear correlation (R) between bulk powder characteristics and the regressed feed-factor parameters. Acronyms: R = Pearson correlation coefficient; UYS = unconfined yield stress; AIF = angle of internal friction; cBD = conditioned bulk density; TBD = tapped bulk density; FFC = flow function coefficient; WFA = wall friction angle; BFE = basic flowability energy; d_{10}, d_{50}, d_{90} = particle-size percentiles; MCS = main consolidation stress; FRI = flow rate index; SE = Specific Energy; Compressibility@15 kPa = compressibility at 15 kPa normal stress; Permeability, cm^3 @15 kPa = permeability at 15 kPa normal stress per square centimetre. 25

2.6 (**A**–**C**) Shows the feeder performance for just semi-fine APAP & 0.25% silica over 3 refill levels, each with 10 manual refills. (**A**) Maximum deviation from setpoint (kg/h), (**B**) Time of deviation (s), and (**C**) Total deviation (kg). (**D**–**F**) Similarly, shows the comparison between zinc oxide powder and semi-fine APAP & 0.25% silica blend. (**D**) Maximum deviation from setpoint (kg/h), (**E**) Time of deviation (s), and (**F**) Total deviation (kg). The deviation is defined as the sum of the surplus powder delivered during refill. Adapted from Engisch & Muzzio [30]. 27

2.7 Cohesive mixtures described by homogeneity vs influence factor (Equation (2.2)). Adapted from Fan et al. [84]. 35

2.8 Example linear blender used in Portillo et al. [93]. Profile view of the blender (**A**) view of the agitator shaft and blade angle orientation (**B**). 37

2.9 Acetaminophen residence time distribution plots from Portillo et al. [93], demonstrating the effect of blender volume inclination and RPM on RTD; (**a**) 78 RPM, (**b**) 16 RPM. 39

2.10 Blade configurations refer to a series of different blade orientations along the agitator's axis. **Top left**: side-by-side comparison of transport blade and radial mixing blade (RMB). **Top right**: example of a blade combination that would take a position along the agitator's axis, denoted by a number in the configurations D8 and P16 below. D8 and P16 depict blade configurations; all positions that are not labelled as RMBs are transport blades, and each collar position sees the blade combination rotate 60° clockwise to the direction of the impeller. Adapted from Van Snick et al. [32]. 40

2.11 Tablet uniformity corresponding to the blade configurations seen in Figure 2.10 (D8 and P16); Upper graphs: content uniformity as a function of impeller speed and mass rate (green triangle = 24 kg/h, blue square = 30 kg/h, red triangle = 36 kg/h). Lower graphs: relative density distribution based on the target API dosage at the centre point of the experimental design (250 rpm and 30 kg/h). Gathered with permission from Van Snick et al. [32]. 41

2.12 Periodic section of a continuous blender including two blades (**a**) Isometric View, (**b**) Side profile view with dimensions. Gathered with permission from Gao et al. [97]. 42

2.13 Contour plots of normalized mean axial velocity: (**a**) control, (**b**) lower density, (**c**) larger particle size, and (**d**) cohesive particles. Gathered with permission from Gao et al. [97]. 44

2.14 (**A**) Impeller and scraper continuous mixer with arrows detailing rotation direction, (**B**) APAP RTD spike response. Adapted from Tomita et al. [99]. . 45

2.15 Tablet assay RSD plotted against Strain (see Equation (2.3)), an exponential decay model is fitted to the data. Gathered with permission from Palmer et al. [76]. 47

2.16 Peclet Number (Pe) and Strain relationship plotted on a log–log graph, grouped by throughput. Gathered with permission from Palmer et al. [76]. 47

2.17 Contour plots mapping the impeller speed, number of mixing blades, and fill level at a throughput of 26.25 kg/h (**a**) Micronized APAP, (**b**) powder APAP, (**c**) special granular APAP. Gathered with permission from Palmer et al. [76]. 48

2.18 SEM images showing the surface coatings of **Top**: excipient (lactose) and **bottom**: API (Ascorbic Acid). **Left**: Non-coated and **Right**: 1% w/w Aerosil® R972 colloidal silica coating. Gathered with permission from Huang et al. [23]. 52

3.1 Simplified Computer-Aided Design (CAD) drawing of the MACH-1 equipment arranged within the powder booth, equipment and arrangement are to scale. The set scale can be seen by the 1-meter scale bar (of the 10 consecutive 10cm squares) outside the powder booth. 58

3.2 Colour labelled Simplified CAD Drawing of the MACH-1 equipment. Colours correspond to the following equipment: blue, Gericke LIW powder feeder; gold, GEA LIW powder feeder; green, fabricated stainless steel frames/trolleys; red, GEA CDB-1 prototype blender; purple, Mettler Toledo catch scale. . . . 60

4.1 Picture of the Experimental Set-up; supporting frame holding the blender and feeder in the ADAC detector's FoV 85

4.2 Schematic of the Experimental Set-up; showing the blender, and the dimensions, within the ADAC detector's FoV. The Region of Interest (RoI) is indicated by the red box. 86

4.3 Blade dimensions and angle arrangement for the 8H and 16H configurations. The red dashed-line box indicates the FoV of the detector. 87

4.4 Graphical supplementation of the axial classification calculation. The units of the 3D scatter plots are in millimetres. Overlayed examples are not to scale. 92

4.5 Graphical Representation of the Lagrangian micromixing metric discussed in section.4.4.6 94

4.6 Graphical Representation of Table. 4.1 discussed in section.4.5.1 97

4.7 Example tracers plotted in 3D (with units mm), where each trace is labelled by its corresponding classification, RPM and blade configuration. While the colour bar indicates the time in seconds. 99

4.8 Lagrangian micro mixing along the axis between: Point 1, 220mm and Point 2, 420mm. The Mixing Blade Zone (MBZ) starts at 310mm and 390mm for the 16H and 8H configurations respectively. 101

4.9 Auto-Correlation ($C_r(x)$) of the [y, z] radial plane as a function of [x] the axis length. Detailing predictability of the radial position along the barrel. $AC = 0$ shows no predictability between the radial and axial plane, suggesting a high level of radial dispersion. N is the number of traces in the AC calculation, and therefore an indicator of confidence. 103

4.10 Spatial Residence Time plots, normalised by the area under the graph, for the various speeds and their given blade configuration. The region of interest for the calculation spans between 220mm to 420mm. A black dashed line denotes the Mixing Blade Zone and corresponds to where the mixing zone starts along the axial length (mm), the zones start at 310mm and 390mm for the 16H and 8H respectively. To remove any erroneous tracers, a filter was applied to the calculation excluding points which had; traces shorter than 200mm, min velocity of 0.01m/s, max velocity of 3m/s, and points with relative error $>95^{th}$ percentile. 107

5.1 Demonstration of using the Web-Based Artificial Neural Network Application. 112

5.2 The above figure graphically describes the Experimental Set-Up, Blade Arrangement, and Impeller configuration used for the experiments 116

5.3 Three example feed factor profiles, showcasing the profiles for the three different grades of the same material, Avicel (MCC). Error bars indicate the range of values from the duplicate/triplicate calibration runs (indicated by $n =$ in the graph's title). The red dashed lines indicate the feed factor at which the top-up occurred. The following windows were used for the three powders: FF1 to FF4 (0.8L top-up) for Avicel 101, FF2 to FF6 (0.8L top-up) for Avicel 102, and FF4 to FF6 (0.4L top-up) for Avicel 105 125

5.4 Example of a '450 RPM Empty', where the offset (remaining mass in the blender) would then be added to the asymptote collected from the curve fitting to gain the final residence mass at steady state. 127

5.5 Random Forest Regression (RFR) Model Parameter Tuning. Results were ordered from worst (left) to best (right) r^2 value, with the secondary axis plotting the assessment of the residual's normal distribution using the Shapiro-Wilk Test (SWT)– higher SWT scores indicate a normal distribution. The x-axis shows the combination of the following 5 hyperparameters (in respective order): number of estimators, maximum depth, minimum number of samples to split, minimum number of samples for a leaf and maximum features. . . . 129

5.6 Random Forest Regression (RFR) Model Performance. The top left graph shows a parity plot of the measured vs predicted fill level. Top right, training data (only) k-fold cross-validation. Bottom left, RFR's residual histogram. Finally, the bottom right shows the Feature Importance (FI) of each of the parameters on the RFR's predictive capability, higher indicates more importance. The error bars show the standard deviation of the FI across the $n = 20$ generated estimators. 130

5.7 ANN training and performance: Left, parity plot of the measured vs. predicted fill level percentage. Centre, training and validation losses (in MSE (Mean Squared Error)) of the model vs. the number of epochs. Right, histogram of the residuals (measured - predicted). The relative root mean squared error was 12%. 135

5.8 ANN SHAP analysis, showing the mean of the modulus SHAP Values. Effectively, the average impact of each of the variables on the output magnitude. This is then ranked-ordered from the most influential feature to the least. The scale quantifies the relative importance of the variables. 140

5.9 M^2E^3D representation of an example analytical model (bottom right), built as a tree with its nodes (circles) representing input parameters (purple), constants which need fitting (green), binary operators (blue) and unary operators (orange). 142

5.10 M^2E^3D Parity Plot, Measured vs Predicted. With an r-squared of 0.83, a Mean Absolute Error of 0.04 and a Relative Mean Squared Error of 0.05 . . 144

5.11 Correlation Heatmap (-1 to +1) between Process Parameters, Material Properties and Response Variable (Fill Level). The colour bar indicates the positive correlation (+1, Red) and negative correlation (-1, Blue) 146

5.12 Scatter graphs showing the fill level response of the materials used for the experiment with respect to the three processing parameters: RPM, Mixing Blades, and Feedrate (kg/hr) 147

5.13 Decision Tree (35 of 50) from the Random Forest Regression Model, with darker colours indicating high Fill Level. Samples refer to the number of data points, and value is the mean Fill Level for those samples– in percentage (%)– for that node. 149

5.14 Fill Level Contour Plot Prediction using the ANN as a function of RPM and WFA. The (shared) colour bar indicates the fill level in percentage for the 3 plots. The held values for the contour plot are as follows: RPM (150-450), MB (8, 12, 16), Feed Rate (22 kg/hr), BFE (188 mJ), WFA (5-50), d10 (61μm), d50 (122μm), d90 (206μm), 1/FFC (0.189) 151

5.15 Parity Plot between the experimental and predicted fill levels. The parity plot shows the three different models predicting the fill level. Each experiment was repeated 3 times, the mean is shown and the bars indicate the range of values (on the x-axis). Each model demonstrates the operating space between the RPM and mixing blades. The three models are ranked by the MAE (Mean Absolute Error) prediction of the experiment. Subsequently, an example of the design space showing the two most important processing parameters is plotted for each of the models. The model's contour plots are indicated by the graph's title. Furthermore, all contour graphs share the same colour bar and number of gradient steps (12) between the min and max. 155

5.16 Surface plots showing the strain by the three processing parameters for the drug surrogate formulation. The continuous parameters (those that can change during operation) share the same plot as the strain. The colour bar indicates the ANN predicted fill level, the three graphs share the same colour scale– allowing comparison. 157

5.17 Graphical Representation of the Strain Window (ω_W). Points 2, 3, and 4, indicate guided experiments to find the Strain Point (ω_P)– or the expansion of the current Strain Window (ω_W). 164

List of Tables

2.1 Material properties of the APAP grades used in Palmer et al. [76]. 46

4.1 Tracer classification based on the definitions provided in section 4.4.6, followed with the number of trajectories collected. 96

5.1 Characterisation results for the ten materials and the surrogate formulation. 120

5.2 ANOVA Table for the generated M^2E^3D equation (See Eq. 5.6) based on the split terms (See Eq. 5.7 and Eq. 5.8), showing the sum squared variance (sum_sq), degrees of freedom (df), F-Statistic (F) and P-Statistic (PR(>F)) 153

Acronyms

AC AutoCorrelation. 104

AI Artificial Intelligence. 111

ANN Artificial Neural Network. 112

APAP Acetaminophen. 37

API Active Pharmaceutical Ingredient. 5

ATEX ATmospheres Explosibles. 64

BAU Business as Usual. 9

BBD Box-Behnken Design. 67

BFE Basic Flowability Energy. 121

CAD Computer Aided Design. 57

CCD Central Composite Design. 67

CDC Continuous Direct Compression. 3

CPP Critical Process Parameters. 3

CQA Critical Quality Attributes. 3

$CSTR$ Continuous Stirred Tank Reactor. 56

DEM Discrete Element Method. 11

$DSEAR$ Dangerous Substances and Explosive Atmospheres Regulations. 64

FFC Good Manufacturing Practice. 121

FI Feature Importance. 131

FoV Field of View. 84

Fr Froude Number. 46

GLS Good Laboratory Standards. 57

GMP Good Manufacturing Practice. 57

GUI Graphical User Interface. 111

HSE Health and Safety Executive. 64

$HVAC$ Heating Ventilation And Cooling. 51

ICH International Council for Harmonisation of Technical Requirements for Pharmaceuticals for Human Use. 78

LIW Loss-in-Weight. 59

MAS Magnesium Aluminosilicates. 52

MB Mixing Blades. 85

MBZ Mixing Blade Zone. 100

ML Machine Learning. 111

MPS Mesoporous Silica. v, 21

MRT Mean Residence Time. 125

MSE Mean Squared Error. 134

OEB Operational Exposure Band. 65

OSD Oral Solid Dosages. 1

PAT Process Analytical Technology. 3

PCA Principle Component Analysis. 29

$PEPT$ Positron Emission Particle Tracking. 9

PID Proportional Integral Derivative. 63

PLS Partial Least Squares. 131

PSD Particle Size Distribution. 121

Pe Peclet Number. 46

QbD Quality by Design. 3

RH Relative Humidity. 51

RM Residence Mass. 125

RMB Radial Mixing Blade. 42

$RMSE$ Root Mean Squared Error. 133

RPM Rotations Per Minute. 125

RSD Relative Standard Deviation. 37

RTD Residence Time Distribution. 38

SEM Scanning Electron Microscopy. 51

$SHAP$ SHapley Additive exPlanations. 139

SLS Sodium Lauryl Sulphate. 24

$SMEs$ Subject Matter Experts. 72

SOP Standard Operating Procedure. 65

SWT Shapiro-Wilk Test. 131

WFA Wall Friction Angle. 121

ff Feed Factor (grams/revolution). 24

$mAPAP$ Micronised APAP. 48

$pAPAP$ Powdered APAP. 48

$sgAPAP$ Special Granular APAP. 48

Chapter One

Introduction: Oral Solid Dosage Forms & Continuous Direct Compression

1.1 Overview of Oral Solid Dosage Forms

Oral solid dosage forms (OSD) are a method of therapeutic drug delivery that includes tablets, capsules, and similar preparations and are the cornerstone of pharmaceutical therapy. Their development over the centuries has been a journey of innovation and refinement, evolving from rudimentary herbal pills to sophisticated, controlled-release formulations [1, 2]. In the early 20th century, the advent of compressed tablets revolutionised drug delivery, offering more precise dosing and stability compared to their predecessors [3].

Moreover, despite their simplicity, OSDs offer several advantages over alternative dosage forms in modern medicine, including greater patient compliance due to their ease of administration and convenience [4]. They require simple storage conditions that help preserve therapeutic efficacy without the need for refrigeration or specialist equipment [5]. In addition, OSDs utilise the gastrointestinal tract for drug absorption, a natural and resilient system that does not require breaching physical biological barriers, reducing the risk of infections

and complications associated with invasive methods such as intravenous therapy [4]. These benefits contribute to the preference for OSDs over intravenous therapies in many clinical situations.

Consequently, the second half of the 20th century saw remarkable advancements in OSDs. The introduction of coated tablets, multilayer tablets, and extended-release formulations marked significant steps in improving patient compliance and therapeutic efficacy [1]. These innovations were driven by a deeper understanding of secondary manufacture, pharmacokinetics, and drug-release mechanisms, as well as advances in materials science and characterisation [6].

In recent years, innovation has shifted towards developing two primary paradigms for patients. The first is personalised medicines, which seek to improve therapeutic effects by meeting the unique needs of patients. Developments in this area include products such as orally disintegrating tablets for patients with swallowing difficulties (effectively varying the mechanical properties of OSD according to the patient's needs) [7] and paediatric formulations with adjustable therapeutic doses (allowing one to provide variability in the potency of the therapeutic effect based on the physiological development of the individual) [8]. This is realised through the advancement of novel technology, such as 3D printing, which is poised to revolutionise OSD further by enabling the production of patient-centric dosage forms [9].

The second is to improve production and manufacturing processes. This emphasis is driven by the need to improve cost efficiency and environmental sustainability in a global market that is growing for medications. An ageing population and an increasing prevalence of chronic diseases require large-scale production of OSDs, which are commonly used for long-term therapies [5]. Consequently, pharmaceutical companies are compelled to optimise manufacturing processes to reduce costs while minimising environmental impact, all within stringent regulatory frameworks [10]. Advances in manufacturing technologies not only lead

to more efficient production, but also contribute to sustainability goals by reducing waste and energy consumption [11]. These improvements are essential to ensure the availability of affordable medications and maintain competitiveness in the global market.

1.2 Thesis Motivation

The primary goal of this thesis is to understand the powder blending stage in a relatively novel method of continuous secondary manufacturing, Continuous Direct Compression (CDC) [12].

The narrow focus on this particular unit operation seeks first to address critical challenges such as cost efficiency and environmental sustainability in manufacturing processes, and second to contribute to the broader efforts of the scientific and engineering community.

To begin with, it is crucial to review the current landscape to improve manufacturing results, which is closely related to enhancing manufacturing efficiency. The start of modern methods dates back to the Quality by Design (QbD) concept introduced by Joseph M. Juran in 1992 [13]. QbD is a systematic, science-based, and risk-based approach to development and manufacturing, focused on understanding processes and designing them to consistently meet predefined quality criteria. This concept has been adopted by a broad spectrum of industrial and academic stakeholders [14, 15, 16, 17] that span understanding, regulatory support, and application. Central to this conversation is the idea of Critical Quality Attributes (CQA), which essentially measure a product's performance. Understanding these CQAs requires measuring the relevant variables that lead to them, known as Critical Process Parameters (CPP). The need to measure these parameters has driven the adoption and advancement of Process Analytical Technology (PAT), which helps to develop either mechanistic relationships or data-driven solutions linking CPPs to CQAs.

As these new methods have evolved, the pharmaceutical industry has seen the potential to use innovative tools to explore new manufacturing approaches. A key opportunity lies in continuous manufacturing, enabling thorough monitoring and measurement of CQAs throughout production. This method is crucial due to strict safety regulations that require a deep understanding of the process to produce complex formulation products accurately and reliably. This importance is amplified in the production of potent therapeutics, where slight inaccuracies in dosage or physical properties can cause serious problems.

Other manufacturing sectors have long established the principles of continuous and centralised manufacturing, offering several advantages [18, 19]:

- Improved processing efficiency per unit, both in cost and waste reduction
- Reduced supply chain length and responsiveness
- Enhanced consistency in product quality
- Higher production throughput, improving scheduling
- Lower manual intervention and reduced human error risk

The emergence of new (manufacturing and analytical) technologies, together with the QbD principles, has allowed the move towards continuous manufacturing of OSDs, with the aim of making products more affordable and sustainable for patients [19].

However, despite these benefits, the adoption of such manufacturing techniques presents challenges, including significant capital investment in equipment, process method development, and issues with processing flexibility, especially when changing between potential drug product candidates presenting varying material properties. Overcoming these challenges is at the heart of this thesis, as outlined in the research objectives. With the manufacturing

industry moving towards more flexible, digital and sustainable methods, the insights from this thesis can be applied to a variety of production processes [20].

Continuous Direct Compression (CDC) represents the most straightforward modality within the continuous manufacturing landscape for OSDs. Unlike more complex continuous manufacturing systems, such as Continuous Wet Granulation, CDC simplifies the production process by using three main stages [21]. The sequential stages in the CDC process are described below:

1. **Feeding**: This stage involves the precise and consistent delivery of the constituent powder components to achieve a complete formulation at a rate that matches the desired production throughput. The precision of this step is critical to ensure the quality and efficacy of the final product.

2. **Blending**: Here, the constituent powders are thoroughly mixed to ensure uniformity in the final blend. This uniformity is vital for the consistency and quality of the active pharmaceutical ingredient (API) within the overall formulation of the OSD, which impacts the therapeutic and mechanical effectiveness of the medication.

3. **Tabletting**: This final stage involves accurately dosing the tablet press with the well-mixed formulation and compacting it under controlled conditions to form the OSD. The precision in the dosing and compaction parameters is crucial for achieving the desired properties of the tablet.

Moreover, all CM OSD modalities can incorporate intermediate unit operations between process stages to further enhance output quality and mitigate additional CQA risks– this may be done for particularly difficult-to-handle substances. A notable example includes the integration of a cone mill [1] between the feeding and mixing stages. The use of a cone mill

[1] A cone mill (sometimes referred to as a comill) is designed for the continuous processing of powdered

has been shown to improve process performance, in terms of mixing accuracy or consistency [22, 24].

Lastly, a further advantage of employing CM modalities, such as CDC, lies in its scalability from development to production. The equipment (and spatial footprint) is often the same or at least very similar in terms of scale, facilitating rapid transitions from small-scale clinical trials to large-scale commercial production (high throughput)[19]. That is, any pre-production fundamental work or development work leading to furthering process understanding of these processing stages is directly representative of commercial production environments.

1.3 Project Focus: Continuous Powder Blending

Of the three CDC stages, the focus of this thesis resides with the **blending** stage, which at times expands to detail aspects of powder handling (upstream and downstream) in an effort not only to describe how the mixing stage fits into the CDC process, but its processing similarities and end-to-end influence on the quality of the resultant OSD. This is particularly pertinent for the literature review (Chapter 2), which includes sections detailing the literature for the stages of feeding (Chapter 2.2.1) and blending (Chapter 2.2.3). The inclusion of the feeding section is intentional, in order to emphasise the challenges associated with powder handling and conveying, because the blending process requires these actions in addition to mixing.

material, facilitating the breakdown of agglomerated or aggregated clumps of powder into finer particles. This is achieved by feeding the material through a funnel onto an impeller/spreader positioned above a mesh. The rotational motion of the impeller forces the material through the mesh, using high-shear forces, which works well against cohesive powder species and incidentally mixes the various powder species in the formulation. Several studies cite their usage [22, 23, 24].

The motivations for elucidating the blending stage reside in the development optimisation, cost effectiveness, and the available literature landscape at the beginning of the thesis project. Much work has been done on powder compaction as many batch-based systems use translatable or similar equipment at the compression stage [25]. However, research on both powder feeding and continuous blending is relatively limited. It is crucial to grasp the context in which the data is acquired within these fields. In the case of powder feeding, different powder types might be processed through the feeder under different conditions to establish a connection or comprehension between Critical Process Parameters (CPPs), which in turn allows the assessment of their effects on Critical Quality Attributes (CQAs). Upon completion of a feeding trial, the powder is retrieved after feeding and retains a (quasi-) representative form of the initial sample, with only a slight loss of fine particles. The potential reuse until it has lost its representative or characteristic bulk behaviour. The same cannot be said for blending, as blending requires the evaluation of the mixing performance of at least one species with another; thus, unless one can separate the powder species from another, it means the powder may be required to be discarded if it cannot be used for alternative development activities, incurring cost and waste. Thus, for development batches, where the cost of API is particularly expensive, this is highly unfavourable. Thus, adopting a right-first-time strategy through the QbD methodology in experiments is essential. This involves enhancing process understanding to identify optimal experiments that yield valuable data, thereby minimising cost and waste while accelerating and simplifying process development.

1.3.1 Understanding Powder Blending on Tablet Performance

It is **vital** that the constituent species within the formulation are homogeneously mixed. Improper mixing leads to poor content uniformity, resulting in a variation in powder behaviour, therefore, leading to variability in manufacturability; giving rise to variability in both me-

chanical and therapeutic effects. Then it is of the utmost importance that the mixing stage within the CDC process performs well.

Mixing performance can be broken down into two main metrics, consistency of mix (scale) and quality of mix (intensity), and under ideal conditions, both are delivered. To attain a high-quality mixture, it would require intimate mixing of the constituents of the formulation, such that as the scrutiny of scale decreases (on assessing the content uniformity) the ratio(s) of the desired constituents remains the same. However, consistency of the mix requires more bulk motion that involves the diffusive capacity of powder species across the entire powder volume. Improved definitions of mixture performance can be seen in Chapter 2.2.3. In the context of the introduction, these mixing metrics can be considered, in an over-simplified manner, as representing the precision and dependability of achieving a thoroughly mixed formulation.

Naturally, questions arise: under nonideal conditions, what constitutes sufficient mixing for a given formulation and its intrinsic properties? Or, what is the relationship between formulation properties and processing parameters that influence mixing? Ultimately, addressing such questions enables the development of experimental plans alongside a deeper understanding of the continuous blending process. Despite these knowledge gaps, it remains relatively clear that a true understanding of the intrinsic mixing mechanisms is required to achieve the idealised goal: for any given powder formulation, how much mixing is needed and what process parameters are required, within the constraints of the available equipment, to induce effective mixing behaviour?

This becomes challenging for particular continuous blending geometries, as the micro- and macromixing metrics may be coupled, meaning that varying the processing parameters to optimise for one of the two results in a reduction of the other. Therefore, balancing this trade-off, within the bounds of the desired parameter space (e.g. throughput), is paramount

to delivering a consistent-high-quality mixture. This is particularly difficult for APIs because of its often cohesive nature and low bulk density- handling the powder can present challenges, thus leading to variability.

1.4 Thesis Aims

This thesis primarily seeks to enhance the knowledge and optimisation of continuous direct compression by thoroughly examining the powder blending phase. It combines experimental characterisation, process-integrated approaches, and predictive modelling to improve development efficiency, sustainability, and robustness. These challenges form the foundation for the thesis's objectives, outlined as follows:

1. Gain an understanding of the underpinning mixing mechanics in the continuous blender via. the use of Positron Emission Particle Tracking (PEPT), which is described in Chapter 4.

2. Develop and establish the experimental means and methodology to investigate the CDC integration, including the way of working and integration into Business-as-Usual (BaU) [2] for AstraZeneca.

3. Develop a modelling tool to predict mixing performance based on the bulk characteristics of the drug formulation and processing parameters, leading to cross-project application (generalised application). Finally, implement this tool into Business-as-Usual (BaU) at AstraZeneca for use in the early stages to reduce the risks associated with formulation and processing and to aid in product advancement.

[2]BAU, in this instance, is best described as ensuring sufficient embedding and standardisation of working activities which complement and build upon the already established ways of working.

Chapter Two

Literature Review

2.1 Preface

Understanding how different powder species interact in blending environments is essential to achieving optimal mixing specifications. Cohesive powders, in particular, are among the most challenging to blend due to their strong interparticle forces– often gained through small particle size and high aspect ratio particles. Given that most APIs are low in density and high in cohesion, consistent feeding and blending by-in-large encompasses the current best practice for CDC.

The following extracts from the upcoming review paper provide a comprehensive overview of research on how cohesive species (APIs) are blended and fed through a triage of methods, covering a range of aspects from Discrete Element Method (DEM) simulations to experimental approaches. To aid in understanding the complexities of powder handling and manipulation, the section dedicated to powder feeding has been included, emphasising the importance of consistent feeding to avoid disturbances that could affect downstream blending processes, in addition to the challenges of powder handling and processing. The performance of the blender is crucial because it must smooth out these disturbances to

achieve high-quality mixing, which is essential to maintain specified content uniformity.

The following text comprises the 'Powder Feeding' and 'Blending' sections from the review article (Jones-Salkey et al. [25]) published in ***MDPI****'s Pharmaceutics Journal (Impact Factor = 5.4, available at https://doi.org/10.3390/pharmaceutics15061587). These sections were authored by O. Jones-Salkey. In the original review, the 'Abstract', 'Introduction', 'Summary Table', and 'Conclusions' were jointly written by O. Jones-Salkey and Z. Chu, and are therefore included in the Appendix (Section 1).*

2.2 Published Review Article: Reviewing the Impact of Powder Cohesion on Continuous Direct Compression (CDC) Performance.

2.2.1 Powder Feeding

Feeding Introduction

Powder feeding for CDC processes must be accurate and consistent for CDC performance success. Feeding modes are commonly defined by the delivery and maintenance of material, in a given time frame. As such, there are two main categories for feeders: volumetric and gravimetric, which supply material according to volume per unit time, and mass per unit time, respectively [26, 27, 28, 29, 30]. Volumetric feeding is often used to understand the characteristics of powder behaviour within the hopper, whereas gravimetric feeding seeks to smooth out any volumetric perturbation through feedback control, arguably resulting in gravimetric being the superior of the two modes for mass delivery [26, 31, 27, 28, 29, 30]. Powder feeding is the first unit of operation in the CDC process; therefore, disturbance

or variation from the set point can propagate downstream, fundamentally impacting tablet quality [32, 28].

One of the tasks of the blending stage in ensuring that constituents are well-mixed is to smooth out the perturbations from the feeder. The lower the intensity and frequency of these perturbations, the lower the chance that content uniformity or manufacturability issues will arise downstream [27, 33, 34]. Moreover, note that not all disturbances have a detrimental impact. It depends both on the magnitude and duration of such disturbances—Gyürkés et al. [35] aptly discuss this concept with the use of funnel plots.

Powder cohesion affects feeding performance by introducing variation through complex bulk behaviour, resulting in variation of flow behaviour [27, 28]. This contributes to both the restriction of power into the converting screws, and the resistance to flow within the swept volume of the screws. In addition, these materials are prone to electrostatic charging, causing attraction-repellent behaviour, which can lead to deposits of material that reside and adhere to surfaces after feed [36, 37]. This buildup can migrate into the bulk feeder, dosing it with a spike of material, which therefore results in a compositional imbalance [36, 37]. The following section aims to discuss the work of several publications, exploring the complexity surrounding powder feeding.

The variation in complex behaviour originates at the particle scale. Collections of particles, homogeneous or heterogeneous, form the bulk and their individual properties, together with their population distributions, determine the macroscopic response (e.g. flowability, the readiness of a bulk powder to flow in a desired manner [38]). A non-exhaustive set of relevant attributes includes particle size, shape, and surface roughness (and their distributions), as well as surface energy/chemistry, hygroscopicity, and electrostatic propensity. Smaller particles and broader size distributions increase the specific surface area, promoting particle–particle contact and strengthening the adhesive and capillary forces. Likewise, angular

or high-aspect ratio shapes promote mechanical interlocking; hydrophobic or high-surface-energy chemistries modify van der Waals and liquid-bridge contributions; and ambient relative humidity shifts the balance between tribocharging and capillary cohesion [39, 40, 36, 37]. These intrinsic attributes are expressed through laboratory bulk measurements (discussed in the following) and are often correlated to identify practical predictors of manufacturability.

Powders with good manufacturability are considered to exhibit stable conditions over a broad operating range because they require fewer adjustments (during accommodation) and are less sensitive to process perturbations. The process of defining manufacturability is therefore to identify empirical correlations between a formulation, or a set of formulations, and one or more of the aforementioned bulk powder measurements. These measurements characterise behaviours such as flowability, which can serve as practical proxies for how a powder performs during unit operations.

Feeding Discussion

The difficulty associated with powder feeding directly derives from the handling of larger volumes of powder (in the hopper) and the conversion of this into smaller, consistent streams (at the outlet). Essentially, this refers to the driving of powder down a pathway of lowering power-to-powder contact, to instead increase powder-to-wall contact. When there is resistance to this gradient of increasing powder-to-wall interactions, it suggests that there is a lack of flowability, which commonly manifests itself in the form of cohesivity. Though cohesion is ultimately a microscopic process (i.e., it occurs at the scale of particle-particle contacts), at present its effects are currently predominantly characterised by macroscopic (bulk) measurements [41].

The Flow Function Coefficient (FFC) is a measurement used to quantify the amount of stress required to cause a powder to yield, and is one of several manners in which a powder's

'flowability' may be characterised [39, 40]. Gathered from a ring shear tester, for example, the measurement applies a normal consolidation force to a powder bed and measures the tangential force required to cause failure (incipient flow). A yield locus of shear stress versus normal stress is plotted and, applying Mohr–Coulomb failure theory, the major principal yield stresses of the consolidated and unconfined material are obtained. FFC is the ratio of these values. The theory and methodology is discussed in various degrees of detail in the following papers: [42, 43, 39, 40]. Leung et al. [42] performed a comprehensive analysis on 1130 ring shear measurements and effectively assumed that particle friction coefficients are negligible in FFC measurements, suggesting that cohesion is the primary characteristic that influences measurement. In addition, the authors state that mitigating the effects of cohesion is much more influential than mitigating the frictional aspect(s) of the powder when it comes to improving powder flow, and also suggest that altering interparticle forces is the best approach to take when combating cohesive powders.

Leung et al. [42] demonstrated the effect of introducing 1% w/w of colloidal silicon dioxide into two excipients on FFC, cohesion and angle of internal friction. The first excipient—hypromellose—showed a significant drop in cohesion and an increase in FFC (Figure 2.1). Meanwhile, the second excipient—dicalcium phosphate anhydrous—showed the inverse behaviour, but to a much lower degree. No significant changes in the angle of internal friction were observed for both materials. Additional work on the use of colloidal silicon dioxide nanoparticles for formulation adjustment is shown in [44, 45]. The mechanism at work involves the surface coating of SiO_2 nanoparticles, which introduce additional distance, therefore lowering the strength of the van der Waals attraction between the two surfaces of the more cohesive species [42, 44, 45, 46]. Furthermore, Leung et al. state that particles with uneven shapes and rough surfaces may receive little beneficial effect from the SiO_2 surface coating, and therefore minimal improvement in flowability. The SiO_2 will fail to act as a barrier to the contact of the carrier species, as it is shown that the use of SiO_2

as an additive can be detrimental to FFC.

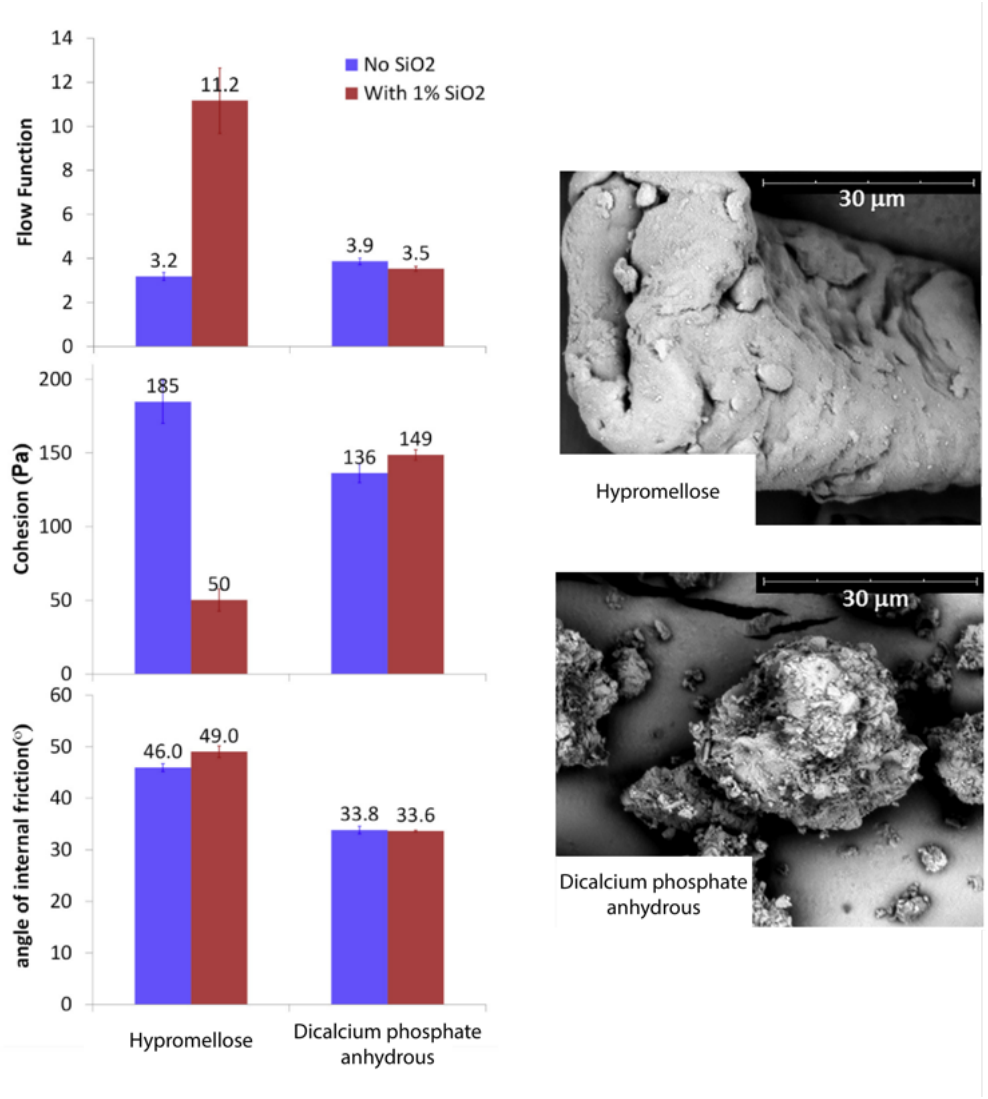


Figure 2.1: **Left**: Graphs highlighting the difference in characteristics (Flow Function (FFC), Cohesion, and angle of internal friction) of the two excipients: Hypromellose and Dicalcium Phosphate Anhydrous with and without colloidal silica. **Right**: Scanning Electron Microscope (SEM) of the two excipients mixed with 1% w/w colloidal silica. Adapted from: Leung et al. [42].

Tran et al. [47], investigated these underpinning mechanisms that govern flow modification through the use of colloidal silica–their findings agree with those of Leung et al. [42].

Tran et al. studied the differences in silica loading for two different excipients using flow characterisation, static image analysis, and particle size distribution. It was found that materials with a higher surface area (described as rugged) were able to accommodate higher silica loads, and that the optimal amount of silica loading depends both on the surface area and the size of the carrier particle but, most notably, their results discussed the possibility of taking a 'quality by design approach by determining silicate (glidant) loading by carefully assessing the physical properties of the carrier powder.

Lopez et al. [48] published a DEM study on the effect of increasing cohesion on feeding performance. The researchers began by calibrating the powder used in the system, first identifying and assigning the physical properties and particle shape of paracetamol, before performing a sensitivity analysis across different adhesive stiffness values (K_{adh}) and conveying impeller rotation rates. Where, K_{adh} is the DEM adhesion parameter that controls the normal cohesive force component between particles; higher K_{adh} increases the effective cohesion. In essence, K_{adh} acts as a proxy for various physical properties, such as surface roughness, chemistry, and hydroscopicity. Thus, the value K_{adh} must approximate these adhesive characteristics of the powder particles, despite the lack of explicit mechanisms in the DEM solver's contact model to account for the physical phenomena causing adhesion. Additionally, this approximation decreases computational complexity and costs, since the mechanisms are not explicitly solved for.

When the conveying impeller was kept at a constant rotation rate (10 rad/s), the particles saw an increase in translational velocity in the conveying barrel with increasing K_{adh} (ranging from 0 to 0.5). This effect was less, but it was present at the interface between the conveying barrel and the hopper. On the other hand, keeping K_{adh} at a constant 0.2, across increasing conveying speeds (10, 20, and 50 rad/s) saw an increase in the overall translational velocity of the particles. Perhaps unsurprisingly, for the range of parameters explored, increasing conveying speed was observed to have a greater influence on particle velocity in

the hopper than altering cohesion.

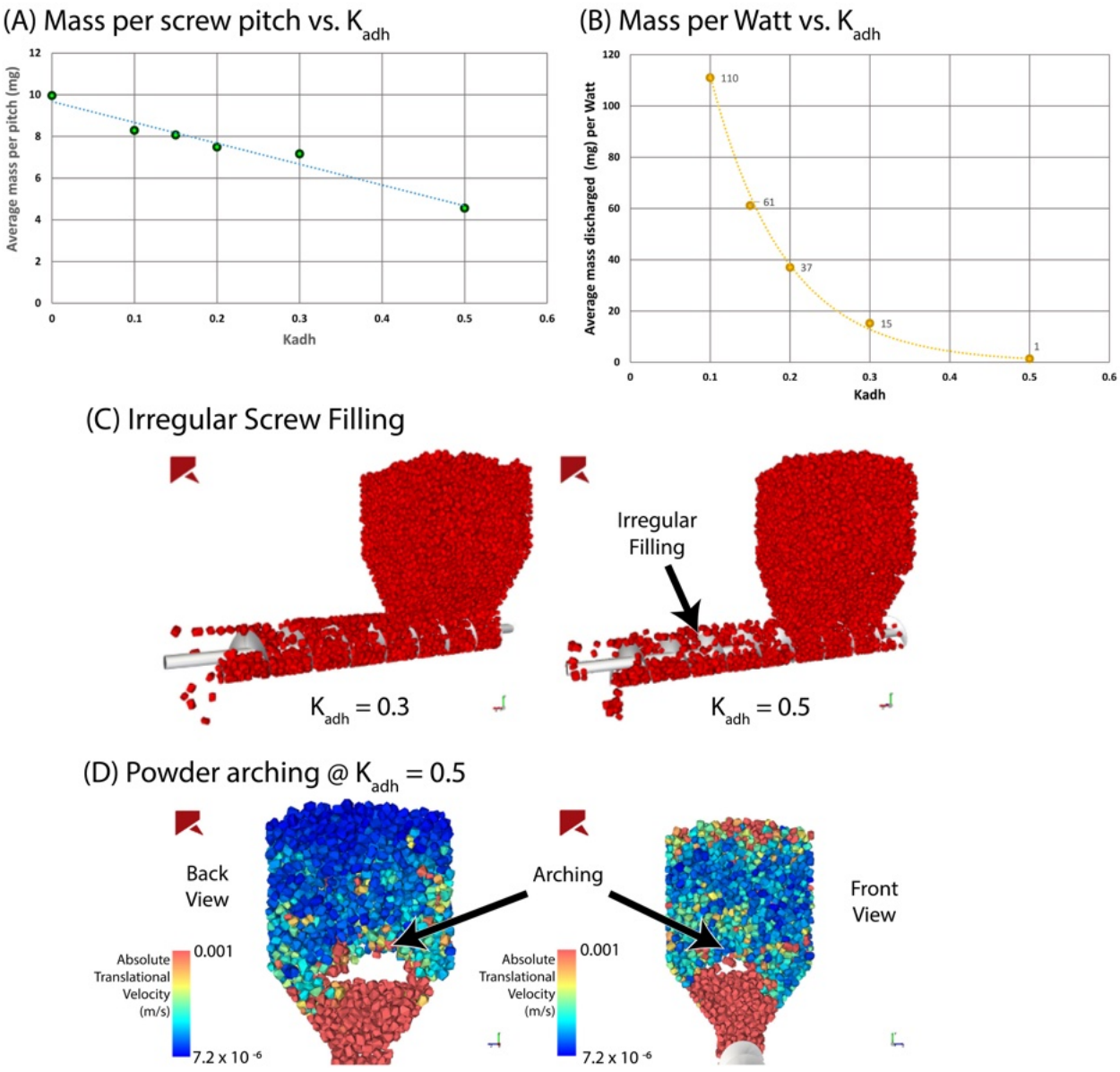


Figure 2.2: **Top Left**: Mass per screw pitch as a function of cohesive stiffness (K_{adh}). **Bottom Left**: Mass per Watt as a function of cohesive stiffness (K_{adh}). **Top Right**: Visualisation of the powder arching/bridging within the hopper volume. The images show both the back and front of the hopper from two different simulations using the same K_{adh}. **Bottom Right**: Irregular filling of the conveying volume due to cohesive stiffness (K_{adh}). The images compare $K_{adh} = 0.3$ and $K_{adh} = 0.5$. Gathered with permission from Lopez et al. [48].

The DEM simulation of Lopez et al. [48] also provides valuable information on the expected power draw; Since the CDC system is continuous, it would mean that the process would be running for days, if not weeks, at a time, making this an important consideration. The authors demonstrated the average mass discharged per Watt as a function of the K_{adh} (between 0.1 to 0.5 K_{adh}), which showed an exponential decay with increasing K_{adh} Figure 2.2. Consequently, K_{adh} values higher than 0.5 showed arching: a phenomenon that occurs when the cohesive forces between particles are stronger than the forces due to gravity. Arching (also referred to as bridging) is a semi-stable instance of particles forming particle–particle structures suspended in a hopper or opening, which are resistant to the displacement of powder beneath them [28]. For additional information on the influence of particle properties on arching, see the following papers: [49, 28, 39]. Lopez et al. described this behaviour with absolute translational velocity where they revealed instances that lead to inconsistent feeding of the conveying screw, which in turn leads to flow irregularities Figure 2.2. The authors link this artefact of transient macro behaviour to the micro by stating that inconsistencies in flow result in improper filling of the screw pitch, giving rise to an inconsistent mass flow rate. This is best demonstrated by the plot of mass per screw pitch vs. K_{adh} shown in Figure 2.2). Finally, the researchers indicated what future work would be of value, notably suggesting the mapping of the transient cohesive behaviour by altering the particle properties, feeder's geometry and rotational speed.

To build on the above suggestions, it would be interesting to see the implementation of a DEM study on a more commercially representative feeder, which possesses both a hopper agitator and twin screw conveying elements. Allow exploration of concepts such as agitator design and rotation speed to increase barrel/screw filling consistency or the breakage/mitigation of arching. What is more, the research conducted by Leung et al. [42], which discussed the minimal effect of friction on powder flow consistency, could use simulation tools such as DEM to more directly support their claims.

Escotet-Espinoza et al. [46] present a publication showcasing the use of silica to improve feeder performance. The researchers began by pre-blending the three different APIs explored with 1% silica, before characterising the bulk behaviour of the pre-and post-silicated API. The APIs (and their silicated counterparts) were then fed through the feeder, while a catch scale continuously measured the mass that exited the feeder. The response was then measured over time, with attention being paid to the consistency and accuracy of the feeding process.

Like Leung et al. [42], Escotet-Espinoza et al. [46] also found that the introduction of silica improved flowability by reducing interparticle cohesion. Feeding improved with the addition of silica, with each of the API case studies showing improved screw speed consistency, a reduction of mass flow RSD (relative standard deviation), a reduction in powder adhesion to the hopper surfaces, and a reduction of remaining mass. This suggests that the addition of silica is hugely advantageous for feeding. The improvement can potentially be attributed to an increase in flowability, allowing the powder to better fill the swept volume of the screws, which leads to an increase in mass per revolution with the addition of silica.

Furthermore, Leung et al. [42] highlight that such improvements arise because flow aids (glidants, such as colloidal silicon) reduce interparticle cohesive forces by acting as spacers between particle–particle contacts, rather than by decreasing interparticle friction. This underscores the dependence of surface area contact and surface chemistry of the primary API particles in driving cohesive behaviour, with particle size and shape distributions directly influencing the available surface area.

This observation is supported by the work of Lopez et al. [48] which shows that, with a reduction of K_{adh}, there follows an increase in mass per screw pitch. Furthermore, with FFC (as previously discussed) being a strong indicator of powder cohesion, it would suggest that it would be useful to understand this screw-filling behaviour. This conveniently

leads to another suggestion for furthering the work of Lopez et al. [48], whereby similar DEM studies could be carried out to understand the effect of additives on the feeding and conveying of powders. Escotet-Espinoza et al. [46] also describe the material used generating the electrostatic charge, which allowed the API to adhere to the agitator. However, in the silicated API case study, there was very low powder adhesion, suggesting that the addition of silica also acted to suppress the effects of electrostatic adhesion.

A study by Lumay et al. [50] explicitly investigated the influence and mechanisms of mesoporous silica (MPS) on electrostatic charge, again finding that the addition of silica species improves powder flow. The experiments differed from those discussed previously in several ways. Firstly, the study differed in the materials and methods used: the authors tested three different grades of silica, varying in particle size and pore size, in three common excipients (microcrystalline cellulose, lactose, and maize starch) using a rotating drum. Secondly, the authors applied different experimental analyses: In this case, the dynamic effect of silication was evaluated by measuring the *cohesive index* [51] of the materials (with and without MPS) across a range of rotation speeds. Finally, using a standardised charge density measurement technique [52], the charge density of the material blends is shown in the presence of different types and amounts of MPS.

It was found that MPS with the smallest particle size provided the greatest improvement in flowability. Furthermore, the addition of just 0.5% w/w made a considerable impact on the cohesive index—see Figure 2.3A. The authors attribute this improvement to the particle size of the MPS, explaining that there would be an increase in the effective surface area, which would suggest greater coverage, and thus intervention between, cohesive species.

An additional striking finding of the study was that the addition of silica was also found to change the shear-dependent rheological properties of certain tested materials, with typically rheotropic materials becoming thixotropic when mixed with a small volume

of silica. Specifically, the study evaluated the cohesive index of the powder by testing the excipients against their 2% w/w silica counterparts over a range of rotation rates (see Figure 2.3B). Both materials, maize and lactose, were shown to be more cohesive (thickening) with increasing rotating speed (ranging from 2 to 10 rpm) and in the presence of silica less cohesive (thin) with increasing rotating speed. The silicated maize showed a greater decrease in cohesion than the silicated lactose with increasing rotation speed.

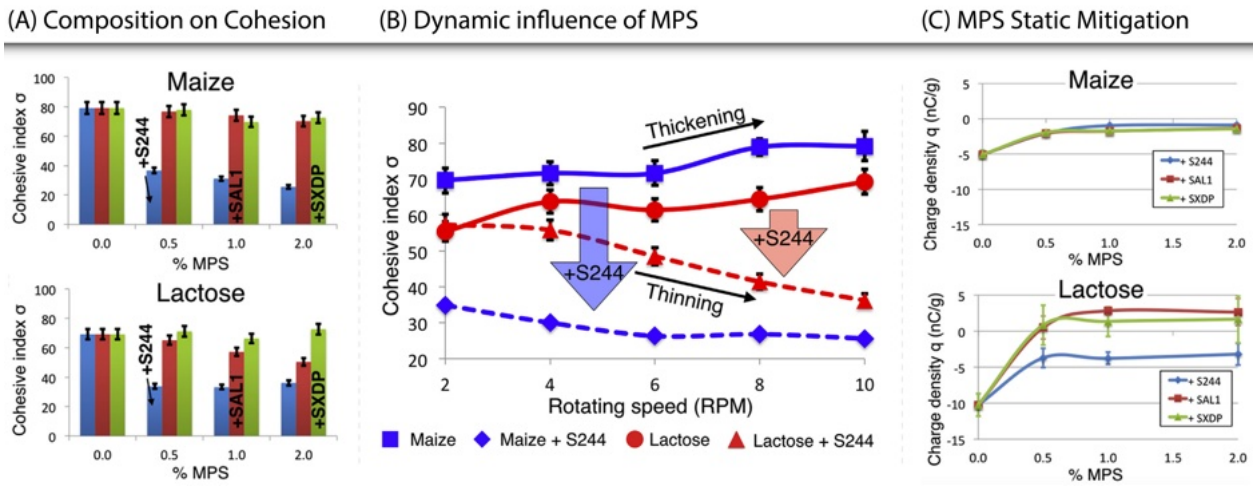


Figure 2.3: (**A**) Comparing the differences in the dynamic cohesive index (σ) with the addition of different types and weight percentages of Mesoporous Silicates (MPS). (**B**) Dynamic influence of MPS on the cohesive index, demonstrated through plotting the cohesive index over different rotating speeds. (**C**) Comparison of Charge Density (nC/g) in two excipients and resultant performance with the addition of 2% weight silicates. Where: +S244 is Syloid® 244FP, +SAL1 is Syloid® AL–1FP, and +SXDP is Syloid® XDP3050. Adapted from Lumay et al. [50].

Finally, the inclusion of MPS was shown to decrease the static charge density of the powder—see Figure 2.3C. Across all materials and MPS grades, the addition of 1% (of MPS) saw similar results to the addition of 2 —- suggesting that 1% was sufficient for charge mitigation, with any greater amount being surplus. MPS incorporated into the maize saw

a decrease in charge after just 0.5% w/w, with the grade of MPS used making a minimal difference. In contrast, MPS in lactose still produced a decrease in the magnitude of charge density, though different grades responded differently. This suggests that there may be some complexity associated with the use of MPS with lactose. It is potentially important to note that Lumay et al. [50] stated that the lactose varied in positive or negative charge on the day, which depended on the relative humidity of the air. Given that the magnitude is roughly the same but the charge differs, if the S244 (Syloid®FP244) was positive, it would suggest that the grade of MPS used would have little effect on the charge density and vice versa for SXDP (Syloid®XDP3050). Research by Ramires-Dorronsoro et al. [53] supports this: when completing a similar study—with a different measurement technique—they also observed spray-dried lactose exhibiting a positive charge density. Ultimately, this suggests that the use of silica in poorly flowing hygroscopic powders greatly improves the flowability, and decreases the sensitivity to triboelectric charging.

The previously discussed papers showcase the underpinning behaviour of cohesive powders during feeding, and the discussion of silication demonstrates the advantage of understanding the mechanism underlying a powder's cohesive properties. Despite this, when considering CDC in its entirety, the predictive capability is a large part of reducing experimentation and understanding the process. Therefore, it is desirable to be able to predict the feeding performance from a few key characteristics of the powder [54, 31, 32], one of which is cohesion.

Van Snick et al. [32] and Garcia-Munoz et al. [34] provided some of the first in-depth analysis of the end-to-end CDC process, thus by definition including aspects of feeding. The authors discuss the correlation of bulk density, tapped bulk density, and FFC with feeding consistency (Figure 2.4). The experiments involved the comparison of different materials that were running volumetrically (with a constant screw speed) from full to empty, while measuring the response of the feed factor over time. The maximum (ff_{max}) and minimum

(ff_{min}) feed factors (g/revolution) were then taken and used for further calculation. Feed factors change throughout the hopper fill as the powder above the hopper bears down upon the powder below, due to gravity. When the hopper is at low fill, there is not only a reduction of gravitational bulk powder compaction but a potentially inconsistent feed into the conveying volume.

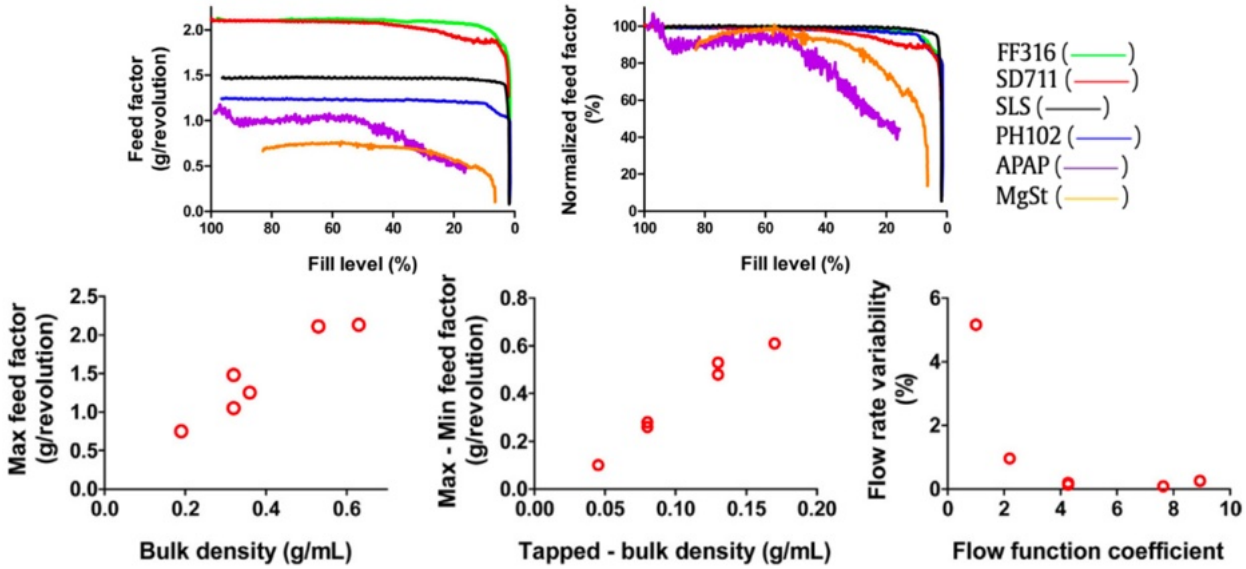


Figure 2.4: **Top**: Two graphs detailing the feed factor throughout the volumetric empty, with absolute values (**left**) and normalised values (**right**), the key indicates the material used. Where: FF316 is Lactose Fast Flo® 316, SD711 is Sodium Croscarmellose Ac-Di-Sol® SLS is Sodium Lauryl Sulphate, PH102 is MCC Avicel® PH-102, APAP is Acetaminophen, and MgSt is Magnesium Sterate. **Bottom**: Three graphs compare feeder performance to bulk characteristics. Adapted from Van Snick et al. [32].

As a result, the bulk density increased linearly with the maximum feed factor, the tapped bulk density increased linearly with the delta feed factor (where the delta feed factor is: $ff_{\Delta} = ff_{max} - ff_{min}$), and finally flow rate variability exponentially decayed with increasing FFC. Since both bulk density and FFC are common descriptors for powder cohesion, it can be used as a proxy to describe behaviour. The study highlighted FFC values greater

than 3 would give sub-1% flow rate variability, and that powders with low bulk density and low tapped bulk density are prone to large ff_{Δ}—— suggesting instability when processing. Escotet-Espinosa [27, 55] also investigated the influence of powder properties on the feed factor and the modelling of such behaviour using the following (simplified) equation.

$$ff_w = ff_{max} * (ff_{max} - ff_{min}) exp[-\beta * w] \tag{2.1}$$

where ff_w is the feed factor as a function of $'w'$ the weight, while ff_{max}, ff_{min} and β are the maximum feed factor, minimum feed factor, and a fitting constant based on feeder geometry, respectively.

The ff_{max} and ff_{min} were then plotted on a correlation heat map (Figure 2.5), relating the responses to a plethora of recorded bulk characteristics. Interestingly, the highest correlation was seen for cBD, conditioned bulk density (g / ml). cBD is similar to the bulk density tapped, obtained from the initial standardised conditioning step of a powder rheometer. It involves a blade passing through a volume of powder with a set torque before measuring the weight of the known volume. Observing the units, it is a given that there is a correlation between the two density measurements, but the interest is with 'compressibility at 15 kPa which also scored high for ff_{min}, which would be a method to achieve a higher bulk density. This suggests that a powder capable of being compressed, and has a high conditioned bulk density, will deliver a high ff_{min}. Similar studies by Shier et al. [56] and Bekaert et al. [31] look similar to predict feeder performance using bulk characteristic properties.

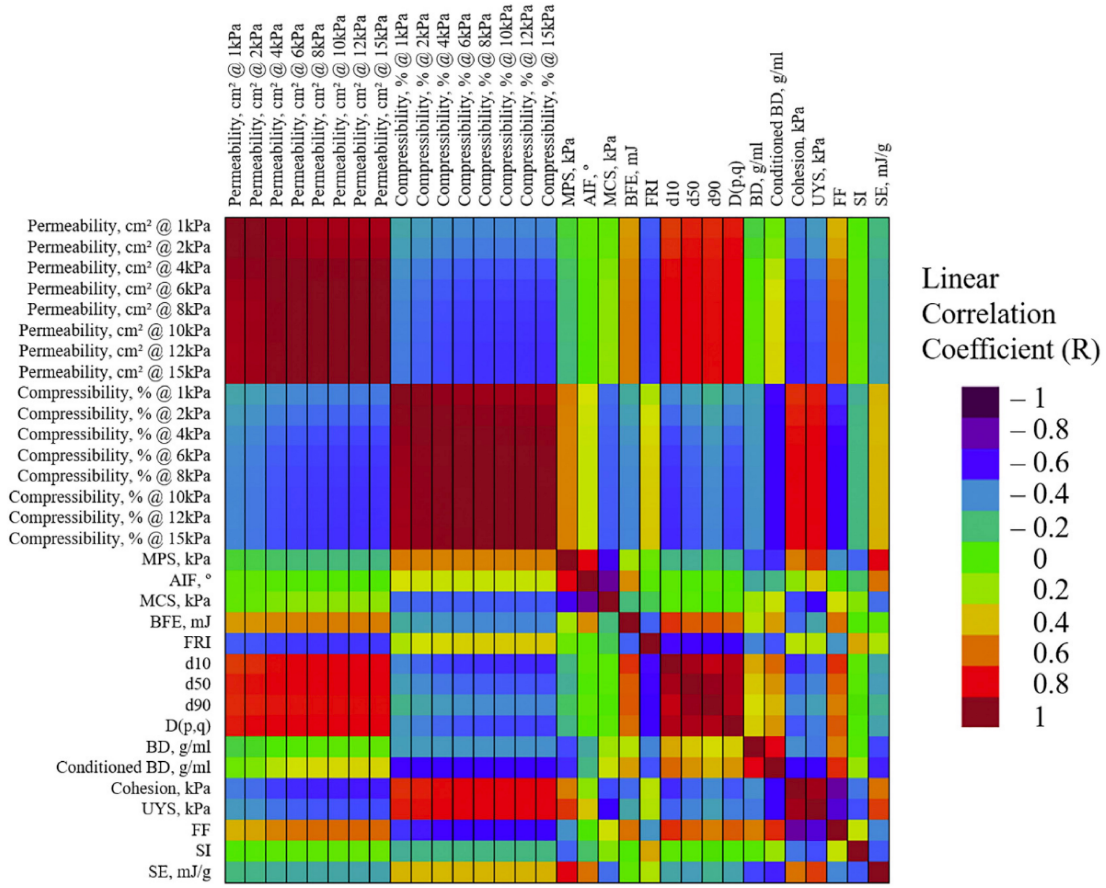


Figure 2.5: Correlation heat map (Escotet-Espinosa [54]) showing the magnitude of the linear correlation (R) between bulk powder characteristics and the regressed feed-factor parameters. Acronyms: R = Pearson correlation coefficient; UYS = unconfined yield stress; AIF = angle of internal friction; cBD = conditioned bulk density; TBD = tapped bulk density; FFC = flow function coefficient; WFA = wall friction angle; BFE = basic flowability energy; d_{10}, d_{50}, d_{90} = particle-size percentiles; MCS = main consolidation stress; FRI = flow rate index; SE = Specific Energy; Compressibility@15 kPa = compressibility at 15 kPa normal stress; Permeability, cm^3 @15 kPa = permeability at 15 kPa normal stress per square centimetre.

Engisch & Muzzio [30] performed a study on varying hopper refill conditions on powders with varying cohesiveness and measured the resultant effect on feeding accuracy and consistency. Typical loss-in-weight (LIW) feeder operation is gravimetric, until topping up (or refilling), where the system operates volumetrically to ensure a consistent feed is maintained whilst an influx of mass is registered on the feeder's load cell. This method results in a trade-off between the number of times the system has to enter the 'less accurate' volumetric mode and ensuring the hopper is sufficiently full, such that the feed factor is stable. For an example of the effect of decreasing fill on feed factor, see Figure 2.4. The conclusion from Engisch & Muzzio is that refilling the feeders with less material, and therefore more frequently, results in better overall performance. This should be taken into account when paying attention to the duration of time that the system enters volumetric mode and reducing the overall disturbance from the setpoint over the whole duration of running the feeder. Regardless of the frequency and volume of fill, Engisch & Muzzio state refilling should be gentle, as this causes the least disruption to feeding. Furthermore, it is shown that the refilling sensitivity is much lower at higher refill levels, Figure 2.6. Refilling at higher fill levels reduces the maximum set-point deviation, time of deviation, and the total amount of mass during deviation.

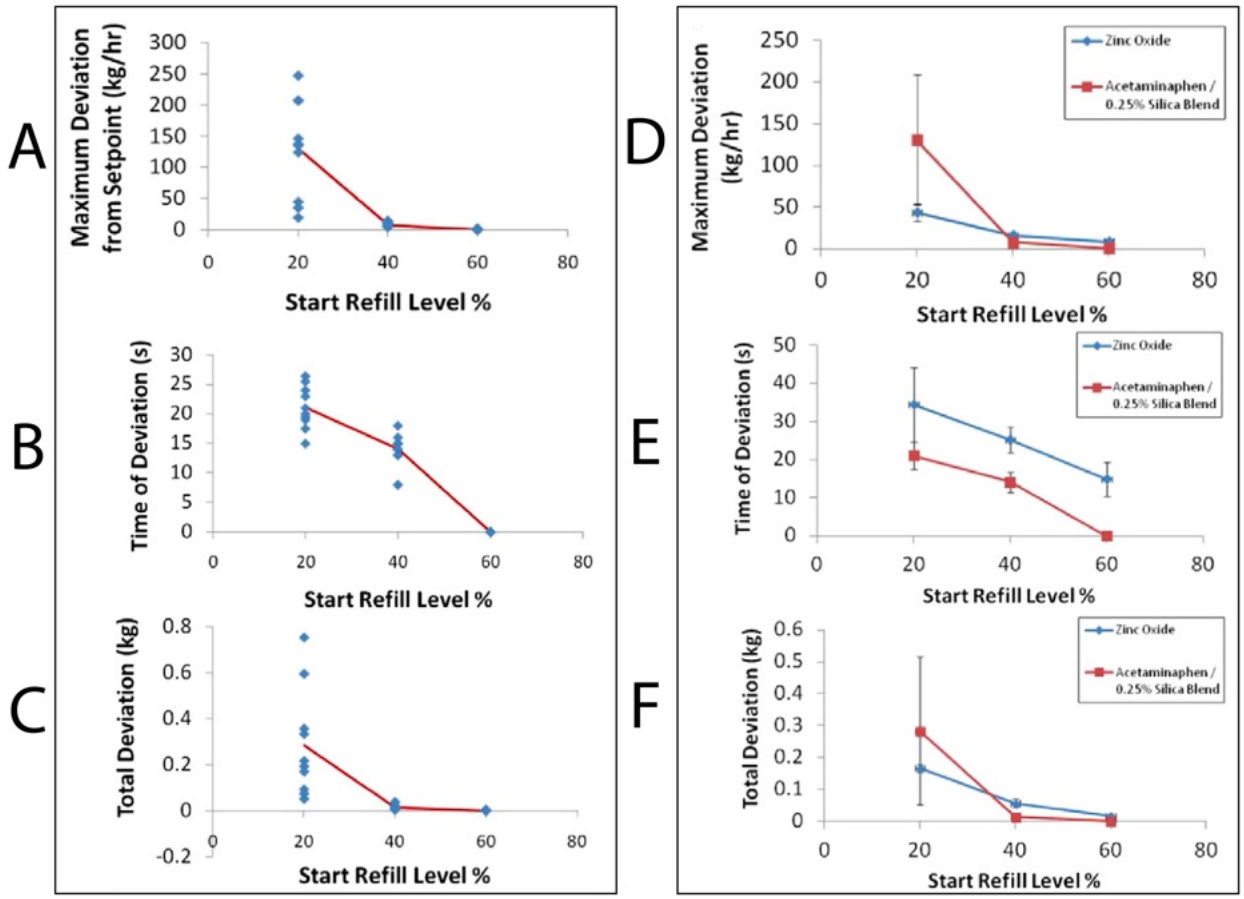


Figure 2.6: (**A**–**C**) Shows the feeder performance for just semi-fine APAP & 0.25% silica over 3 refill levels, each with 10 manual refills. (**A**) Maximum deviation from setpoint (kg/h), (**B**) Time of deviation (s), and (**C**) Total deviation (kg). (**D**–**F**) Similarly, shows the comparison between zinc oxide powder and semi-fine APAP & 0.25% silica blend. (**D**) Maximum deviation from setpoint (kg/h), (**E**) Time of deviation (s), and (**F**) Total deviation (kg). The deviation is defined as the sum of the surplus powder delivered during refill. Adapted from Engisch & Muzzio [30].

A similar methodology could also be applied to combat cohesive powders through compaction during refilling, by attempting to keep the hopper volume as constant as possible, during their most stable ff_w. To build a theoretical case study, using the APAP that is fed volumetrically in Van Snick et al. [32] (Figure 2.4) and the supporting evidence of

refill stability from Engisch & Muzzio [30], see Figure 2.6. A top-up of 25–30% of the volume of the hopper could be used and activated at the fill level of 50—- 60%, refilling to 75—- 80%. This would occur during the most stable feed factor window, whilst the hopper is already half full. During the window in which the powder is dumped into the system, there is a transient influx of powder into the existing powder bed. This impulse of vertical pressure on the powder would increase the powder compression within the bed, increasing the bulk density of the powder local to the conveying screws. Corroboration is seen by adding Escotet-Espinosa's [27] correlation measures, as there is an improvement in the conditioned bulk density, which increases ff_{min} reducing the ff_{Δ}, essentially reducing the feeder inconsistency related to lower fill levels. However, this theoretical case study is generalised without considering phenomena such as disturbances due to air flows during discharging mass, and an increased volume of powder that may be prone to triboelectric charging due to the agitator. DEM studies, such as Lopez et al. [48], open the stage to explore some of the fundamental behaviours seen in these systems, in particular when looking to evaluate the micro and macro behaviour attributed to conveying inconsistency.

Finally, Yadav et al. conducted a comprehensive study with a loss in weight feeder [57] that used a range of screw speeds, gear ratios, and screw types, across a range of materials. The result was a PCA model that identified the influence of these processing parameters and how they interacted with the bulk characteristics of the materials. The principal components consisted of one comprising the powder's bulk characteristics, a second representing the feeder's processing parameters, and a third representing an interaction component. Most notably, the interaction component related screw free volume (cm^3) to density, particle size (d_{10}, d_{50}, d_{90}), wall friction angle, and Feed Factor. The authors note that a different screw type will have a different screw-free volume, which means that the comparison between a smaller or larger volume to dispense per revolution must be taken into consideration when evaluating the feed factor. Similar findings are seen with Engisch et al. [29], where their

suggestion is the use of both self-cleaning concave screws and the removal of any outlet screens for very cohesive materials.

Gamble et al. [58] further support this notion by demonstrating that bulk descriptors alone, such as bulk density or FFC, do not always provide sufficient resolution to explain observed processing behaviour. Their study highlights that powders with comparable particle size distributions may still behave differently due to underlying differences in particle shape, fines content, or the distribution of elongation and width. Using image analysis in combination with Principle Component Analysis (PCA), the authors produced morphological distribution maps that allowed the comparison of powders with similar particle sizes but differing shape characteristics. This approach is analogous to the use of PCA in feeder studies such as those by Yadav et al. [57], although extended here by embedding a morphological fingerprint in the analysis of powder behaviour. The implication is that combining morphology-driven data with bulk characterisation offers a more comprehensive framework for predicting feeder performance and downstream stability, particularly in cases where conventional metrics alone cannot sufficiently capture the complexity of powder behaviour.

Pereira Diaz et al. [59] show that routine physical properties alone can be leveraged to predict flow behaviour with high fidelity. Using a library of 112 pharmaceutical powders that span wide ranges of particle size / shape distributions, bulk densities, and measured FFCs, the authors trained supervised models that classify flow behaviour with accuracies exceeding 80% under cross–validation. Feature importance (discussed in more detail in Chapter 5.5.4) consistently elevated size metrics (D_{10}, D_{50}) and an aspect ratio descriptor, reinforcing that distributional and geometric information embedded in standard characterisation carries an actionable signal for flow prediction - without recourse to custom tests or extensive process trials.

Based on this, Owasit et al. [60] extend the data–driven approach to *blends*, train

supervised models on constituent–level descriptors (particle size/morphology, bulk densities, surface energy) along with dry coating parameters, and report strong predictive performance in multiple flow categories. Their feature importance analyses consistently prioritise coating parameters and size/morphology, highlighting nonlinear and higher-order interactions that simple linear correlations miss. In parallel, Chapter 5 applies similar AI/ML techniques to CDC using targeted bulk / process descriptors (e.g., wall friction angle, feed rate, blender RPM, region size) to predict process performance and process sensitivity [61]. Together, these studies point to a clear and practical conclusion for elucidating the link between product and process for CDC: Novel machine learning methods, trained in carefully curated physical descriptors, can deliver predictive and interpretable tools for feeding and blending, reducing experimental burden, sharpening risk triage, and improving control robustness beyond what bulk metrics alone can provide.

Supervised regression techniques are a vital subset of machine learning. They convert numeric inputs like bulk powder measurements or process parameters into measurable outputs. This process allows for predicting responses at the process level from characterization data. As the model learns from experimental datasets, it effectively captures complex nonlinear relationships that traditional empirical methods struggle to describe [62].

Three classes of supervised regression models are of particular relevance to this thesis and are explored in detail in Chapter 5:

- **Random Forest Regression (RFR):** An ensemble method based on decision trees, useful for capturing nonlinear interactions and providing interpretable measures of variable importance [63].
- **Artificial Neural Networks (ANNs):** An adaptable nonlinear function approximator capable of capturing intricate dependencies and demonstrating strong generalisation when trained on diverse datasets [64].

- **Symbolic Regression:** An approach that searches for analytical expressions that best fit the data, offering interpretability alongside predictive capability [65, 66].

2.2.2 Feeding Summary

Cohesion has been shown, across multiple studies, to worsen the flowability of powders, in turn reducing the consistency with which powder flows into the conveying volume [48, 42, 32]. The transient inconsistency of material flowing into this volume persists and has been shown to result, in turn, in an inconsistency in the mass powder flow of the material delivered, and therefore a deviation from the desired set point [29, 48, 30, 67]. Thus, it is very important to ensure that the powder, despite its cohesive nature, is consistently motivated to enter and be transported through the conveying section of the feeder.

This review outlines just a few examples that have been used so far to reduce the negative influence of cohesion on feeding: reducing interparticle contact between cohesive species [50, 42]; reducing the effect of triboelectric charging [50]; refilling the hopper at moderate fill levels [30, 67]; and adjusting screw speed and screw type [57, 29].

When applying the knowledge gained from Lumay et al. [50] to the work of Escotet-Espinoza et al. [46] and Lopez et al. [48] it would perhaps be sensible to suggest that smaller silica nanoparticles would be ideal to improve flowability at this stage of the CDC process. Silica nanoparticles have also been shown to change the blend from shear-thickening to shear-thinning, implying that, when the powder contacts the hopper's agitator or the conveying screws, one might expect a further transient, localised increase in flowability.

Despite silicates holding the much of spotlight for discussion, surrounding improving powder flowability, it should be noted that several alternative materials could be selected. However, every material in question, for flow modification, would need to be considered for

its end-to-end impact on the process. Silicates, for instance, have been shown to negatively impact compatibility [68, 69] but also improve flowability and therefore improve feeder processing consistency [48, 42, 32], while magnesium stearate (a powder lubricant) has also been shown to increase flowability, but due to its hydrophobicity—coating the surface of API would hinder the dissolution of API within the formulation [70]. This would result in the material being greatly undesirable for any scenario that may involve the intimate blending, or over-mixing, of magnesium stearate with API. However, pre-blending API with other materials such as tricalcium phosphates or microcrystalline cellulose [71, 23] propose the ability to improve flow behaviour at a minimised trade-off, and as such, more research should be carried out on both the use (to improve feeding performance) and the end-to-end implications of selecting such materials.

Moreover, this review of the literature has also highlighted the benefit of future DEM studies which could be undertaken to better understand the fundamental powder movement that governs powder feeding, in particular using commercially-relevant geometries. Notable areas of study could include modelling the effect of silication; altering, and potentially optimising, agitator and screw design; further investigation of the influence of refill regimes in the hopper. The development of dynamic DEM simulations could also be used to develop and test various control strategies, both existing and novel. Intuitively, it could be possible to develop a control proposition for shear thickening powders involving a sudden reduction in RPM followed by a slow build-up of screw speed back to setpoint.

2.2.3 Blending

Blending Introduction

Despite diverse designs available commercially and in the academic literature, continuous blenders can, in general, be reduced to four main components: an inlet, an outlet, a mixing volume, and a mechanism for promoting blending while in the volume of the blender. Typically, this last component will be some form of rotating agitator, the geometry of which may differ from mixer to mixer, or even formulation to formulation. Recognising the different types and geometries of mixers that exist within this space is fundamental when evaluating the role of powder mixing in CDC performance, as the features that differentiate one mixer from another can have significant impacts on the behaviour of the powders being blended, and thus may require different measures to handle the blending of cohesive powders.

Achieving good mixing is integral to the performance of any given pharmaceutical tablet; the therapeutic efficacy and mechanical properties of the tablet will suffer without the effective distribution of its constituent materials, ultimately compromising the safety of the product [72, 73, 74, 32, 75, 76]. Thus, mixing inherently defines the final quality of the formulation (although the final product cannot be delivered without the consistency and precision of the upstream and downstream processes [32, 34]).

Practically defining whether a formulation is well mixed is a complex endeavour with issues such as frequency of sampling [77, 72, 78], location of sampling [77, 72, 78], and scrutiny (size) of the sample [77, 72, 78]. However, describing the mechanisms of mixing may be ever-so-slightly easier, and is of more direct relevance to the present work.

The two commonly defined types of mixing—macro- and micro-mixing—are both essential when looking to create ideal mixtures [72, 76, 73, 79, 80]. Macromixing is responsible for large, global movements, of material—or bulk transport—allowing the material to flow

and circulate around the vessel [72, 76, 81, 82, 83, 80]. Micro-mixing, on the other hand, involves the movement and displacement of material at the particle scale, i.e., the local interactions between particle species [80, 72]. Accordingly, micromixing achieves the detail of the mixing action due to the mixing occurring at the smallest possible scale: the particle–particle level [80, 72], whereas macro-mixing serves to smooth out the upstream mass flow rate perturbations due to the flow and bulk motion of the powder [80, 72].

Fan et al. [84], succinctly discuss the evaluation of mixing in terms of cohesive mixtures. Figure 2.7 and Equation (2.2) encapsulate the majority of this discussion. It is shown that by increasing the surface force —- which is also a function of particle size, and therefore surface area—it is possible to reduce the influence factor defined in Equation (2.2). A low influence factor means surface forces dominate, and the particle species adhere to the surface of another particle species, creating a perfectly ordered blend. Small, less dense particles would be the ones that adhere to the more dense carrier particles, because of gravitational forces. Then, if the surface forces are minimal, gravity dominates, and thus the mixture would involve non-cohesive species, following more typical solids mixing criteria.

$$Influence\ Factor = \frac{Gravitational\ Force}{Surface\ Force} \tag{2.2}$$

Conversely, de-mixing occurs through several mechanisms, such as: segregation, the separation of a formulation into constituent particles of similar properties, for example, size and density [72, 77, 85]; agglomeration, the formation of particle–particle dense macro-particles, due to interparticle attractive forces [86, 87]; and electrostatic repulsion, or attraction, due to inter-particle charge imbalances, which predominantly result from contact-induced electron transfer, as particles move relative to each other and the equipment surfaces [88, 89]. The part cohesion plays differs significantly in each of these mechanisms, and can either subdue or exacerbate de-mixing [85]. For instance, electrostatic charges could be worked

into powder, through the triboelectric effect, creating attractive or repulsive forces between different species [78, 89]. These interactions underpin much of the following discussion of how cohesion affects the mixing process and the competition between mixing and de-mixing.

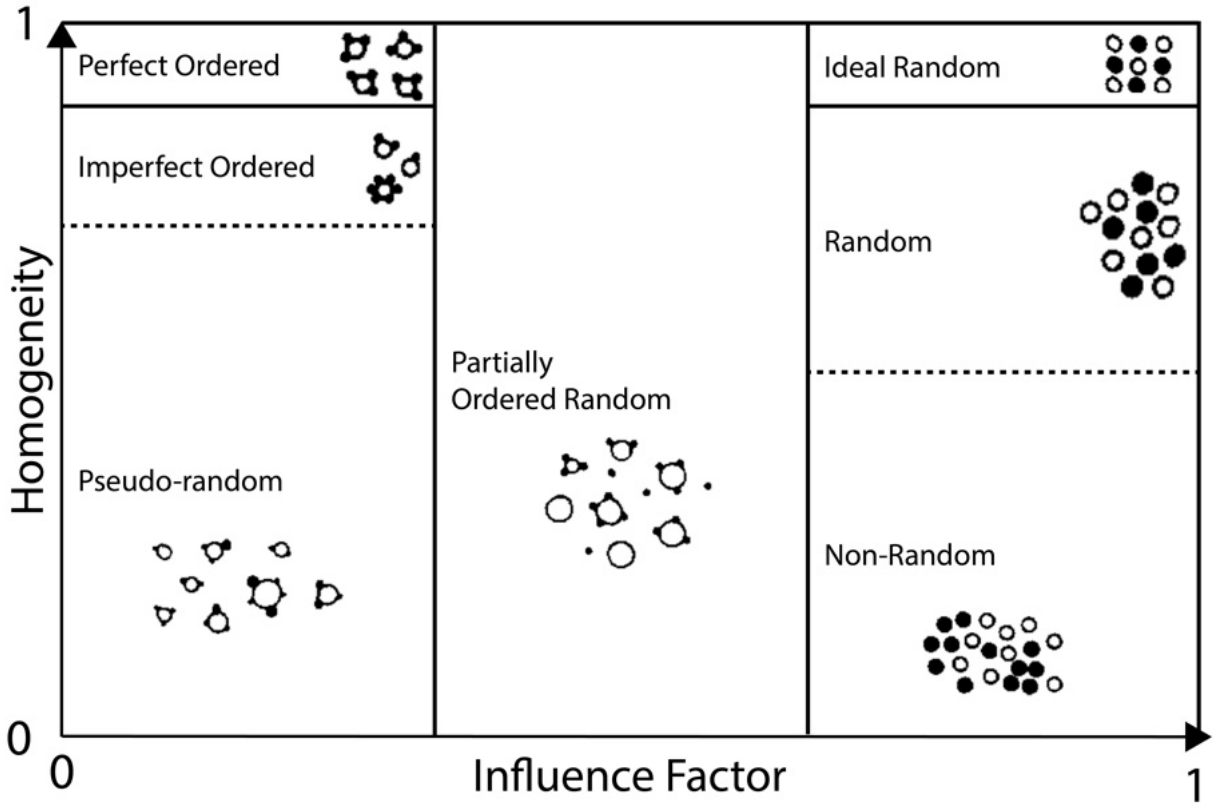


Figure 2.7: Cohesive mixtures described by homogeneity vs influence factor (Equation (2.2)). Adapted from Fan et al. [84].

Blending Discussion

Processing parameters such as the RPM of the agitator, the feed rate (throughput), and agitator design, are the primary methods of manipulating the powder through a given blending volume [32, 90, 76]. For example, trends have been identified to improve the quality of the mixing through the use of processing parameters: macro mixing as a function of the mean residence time; micro mixing as a function of RPM (agitation); residence time is a function

of throughput [32, 76, 24, 91, 83]. These examples show the importance of the process parameters in mixing performance. However, the intricacies of powder behaviour in response to these systems are rarely discussed in the wider literature.

As discussed in the preceding section, cohesion can be overcome through the use of formulation additives and/or changes to the process [92, 50, 42, 79]. Additives, such as glidants (for example, SiO_2), are typically used to make bulk powder properties easier to deal with, by increasing flowability [92, 50, 42]. However, additives change the overall composition of the formulation, which can have detrimental effects on downstream processing-namely tabletting [69, 68]. In contrast, process changes (processing parameters) can potentially overcome issues related to cohesion without altering the composition of the formulation [32, 90, 76]. Using these favourable processing parameters is thus the more practical of the two solutions for CDC processes, but the development and transfer of knowledge between different systems appears to be a substantial hurdle. This is largely due to this approach requiring a much deeper understanding of the specific unit operation being used in the study. Therefore, the knowledge gained is often less transferable; each particular set of process parameters may be unique to system geometry, orientation, or method of operation. With this in mind, it is useful to note the use of dimensionless numbers/groups within the discussed research, as it allows greater understanding and application of relative powder behaviour between publications.

Portillo et al. [93] performed trials on an axial continuous blender (see Figure 2.8)), the axis of which was adjustable between $\pm 30°$ to the horizontal. The researchers found that at ($+30°$) incline there was an increase in mean residence time which led to a decrease in the relative standard deviation (RSD) of acetaminophen (APAP) concentration in two lactose grades. This demonstrates the effect of longer mean residence time on macro-mixing and a reduction in APAP RSD. The lactose grades differed in terms of average particle size and size range: Lactose 100 (70–250 μm, average 130 μm) and Lactose 125 (55 μm), whereas

APAP (36 μm) remained the same in both tests, and made up 3% w/w of the mass flow rate. They also discussed that, despite typical behaviour, the smaller (and more cohesive) grade of lactose did not affect mixing performance at high or low rotation speeds. It was observed that, while the cohesive material readily formed agglomerates, these were relatively weak and agitation from the impeller was sufficient in breaking the clusters and dispersing the powder.

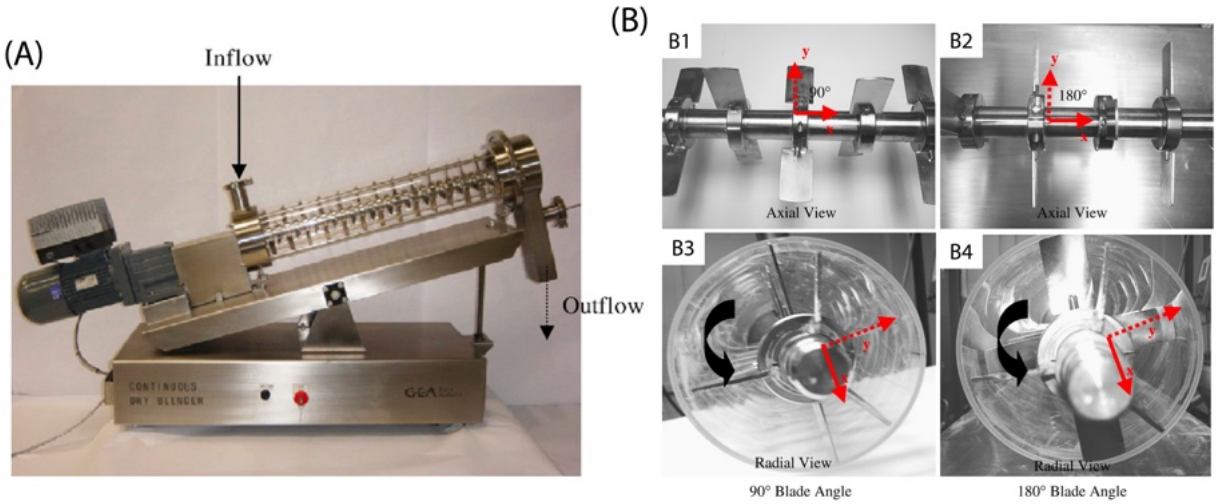


Figure 2.8: Example linear blender used in Portillo et al. [93]. Profile view of the blender (**A**) view of the agitator shaft and blade angle orientation (**B**).

Later work by the same group [79] discussed the influence of cohesivity on powder behaviour in a different continuous mixer (albeit similar to the blender shown in Figure 2.8), inclined at $+17^{o}$. The study used two different grades of lactose, Fast Flo and Edible, which displayed flow indices (measured using a Gravitational Displacement Rheometer) of 24.9 and 34.8, respectively, suggesting that both are highly flowable powders. In addition, the bulk density tapped density of the Fast Flo Lactose were 0.626 (g/mL) and 0.704 (g/mL), respectively, while the Edible Lactose measured 0.629 (g/mL) and 0.981 (g/mL), respectively. Portillo et al. [79] found that cohesivity negatively impacted axial mixing, becoming a statistically significant factor at higher levels of agitation; thus demonstrating the effect of cohesion

in resisting the separation or relative movement of particles. In addition, the authors observed that particles with high cohesion experience longer residence times, with similar path lengths, suggesting that the particles move at slower velocity through the blender. This postulates that methods that increase the shear rate, and therefore the relative particle velocity, can combat the effects of cohesion by increasing dispersion [94], and consequently improve micro-mixing. This could also be described as an increase in the dynamic granular temperature as a function of the increased shear rate [95, 96]. This finding may, at face value, seem to contradict the findings discussed in the previously mentioned study by Lopez et al. [48], in which the translational velocity of the powder going through the conveying portion of the system was observed to be higher with increasing cohesivity. However, despite the *net* velocity being higher, the *relative* velocity (which drives micro-mixing) may nonetheless be lower.

It should be noted that any residence time distribution (RTD) data will be a function of both the volume % of the tracer and the interaction of the tracer within the bulk that it aims to measure. For more detail on RTD behaviour in continuous blenders see Escotet-Espinoza et al. [81, 54], where the authors provide a comprehensive two-part study, analysing the behaviour of tracers with different properties.

Vanarase et al. [24] investigated the blending performance of a horizontal linear blender, both with and without the addition of a co-mill. The authors stated that under optimal macro-mixing conditions, micro-mixing was identified as the limiting factor, leading to poor mixing performance. The inverse was also found for optimum micro-mixing conditions. This highlights the independence of these two types of mixing, and the consequent requirement, to balance a blending system's capability to deliver both sufficient micro and macro mixing.

Interestingly, research by Portillo. et al. [93] contains contradictory findings, when

compared to Vanarase et al.'s study [24]. They found that using an incline blender increases the overall residence time when compared to a horizontal system—see Figure 2.9. Thus, for the same residence time as was demonstrated by Vanarase et al. and therefore similar macro behaviour, Portillo et al. showed that the agitator speed could be increased, which in turn provides greater shear, achieving improved micro-mixing conditions with cohesive powders.

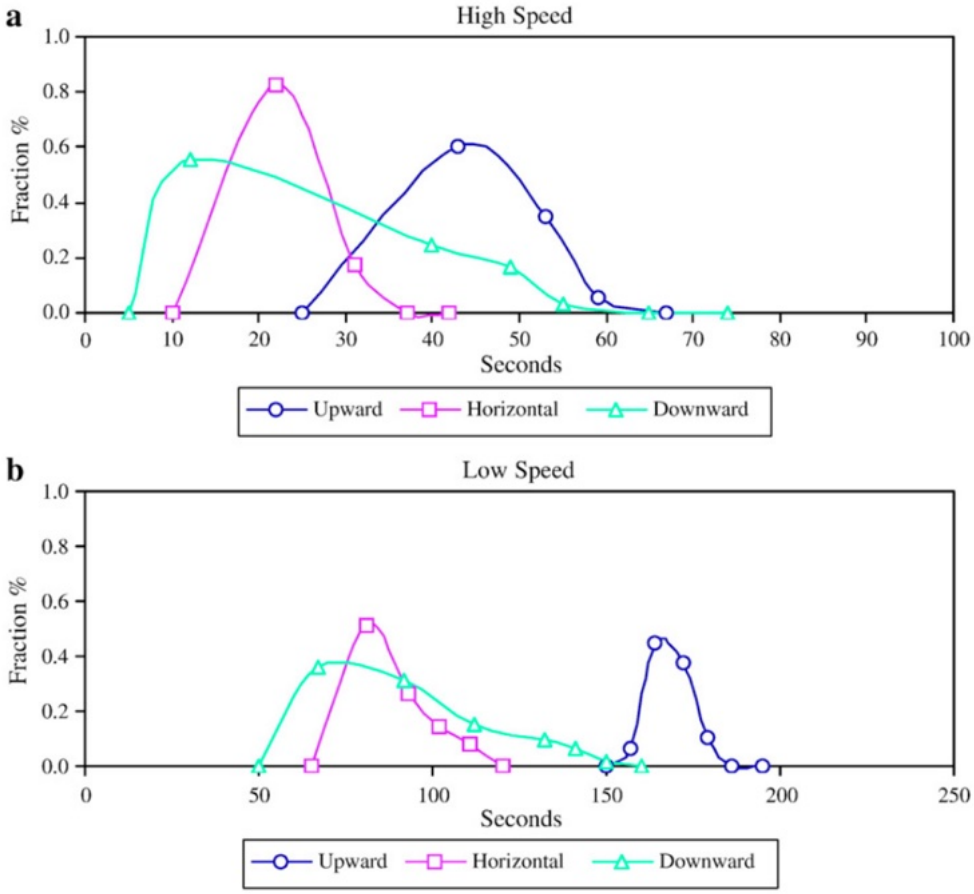


Figure 2.9: Acetaminophen residence time distribution plots from Portillo et al. [93], demonstrating the effect of blender volume inclination and RPM on RTD; (**a**) 78 RPM, (**b**) 16 RPM.

Van Snick et al. [32] investigated the performance of different mixing blade configurations (Figure 2.10, graphically demonstrates the orientation of blades along the agitator's axis) and found that despite the 'P16' blade configuration not delivering the highest dis-

persion, it offered the best consistency (see Figure 2.11). The 'P16' blade config' utilised a series of two sets of transport blades (45°), followed by a set of radial mixing blades (90°). Whereas the other example—'D8'—delivered the highest powder dispersion, with the downside of higher variability.

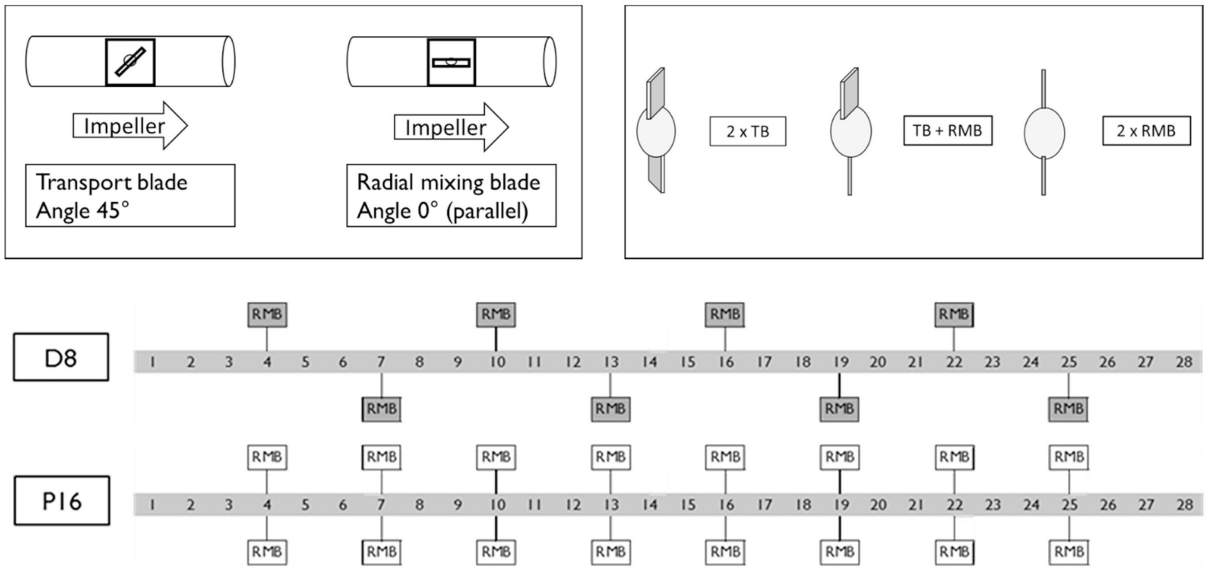


Figure 2.10: Blade configurations refer to a series of different blade orientations along the agitator's axis. **Top left**: side-by-side comparison of transport blade and radial mixing blade (RMB). **Top right**: example of a blade combination that would take a position along the agitator's axis, denoted by a number in the configurations D8 and P16 below. D8 and P16 depict blade configurations; all positions that are not labelled as RMBs are transport blades, and each collar position sees the blade combination rotate 60° clockwise to the direction of the impeller. Adapted from Van Snick et al. [32].

This is supported by Vanarase et al.'s [24] findings, with both surmising that a balance is required between micro and macro mixing. Based on 'P16's performance, in Van Snick et al. [32], it seems as if the 'D8' configuration provides a surplus of dispersion- lending to poor macro conditions. The authors also attribute the good performance of 'P16' to the increased mass hold-up within the blender's volume, as the mixing blades are shown to

increase fill level, and therefore total mass hold-up [32]. Ultimately, the study suggests that varying position, number, and angle of the blades could aid in controlling API within the blending phase, and that different blade configurations may be selected according to the formulations' properties, such that the desired throughput is attained, whilst output variation is minimised.

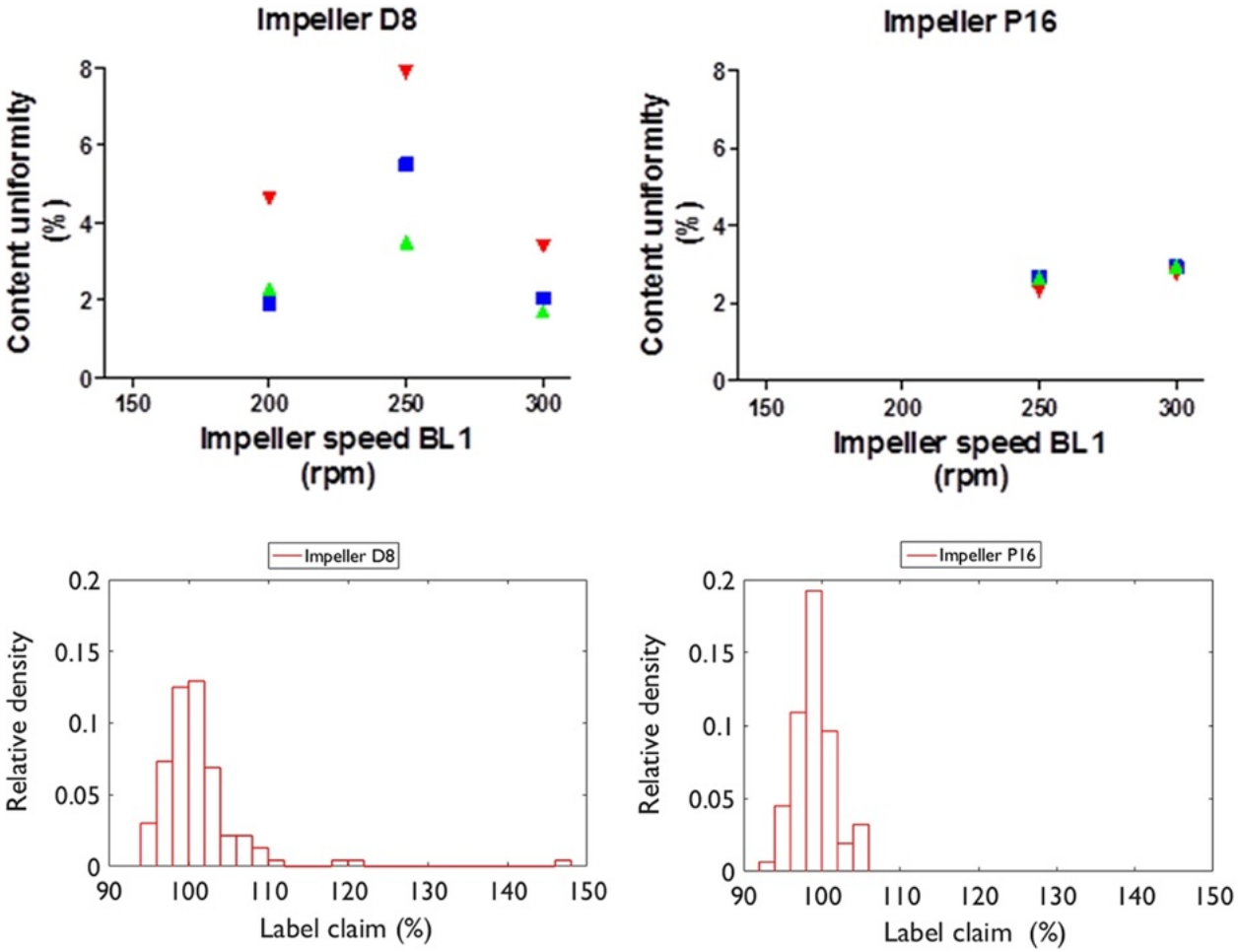


Figure 2.11: Tablet uniformity corresponding to the blade configurations seen in Figure 2.10 (D8 and P16); Upper graphs: content uniformity as a function of impeller speed and mass rate (green triangle = 24 kg/h, blue square = 30 kg/h, red triangle = 36 kg/h). Lower graphs: relative density distribution based on the target API dosage at the centre point of the experimental design (250 rpm and 30 kg/h). Gathered with permission from Van Snick et al. [32].

Gao et al. [97] developed a two-blade (periodic) section of a continuous horizontal mixer (see Figure 2.12), and evaluated mixing performance using a monodisperse DEM simulation of the blender. Gao et al. [97] subjected four different simulated powders (classified as: control, lower density, larger particle size, and cohesive) to the same tests, and mapped the axial conveying efficiency in fill level-rpm space. This conveying efficiency was quantified by normalising the mean axial velocity of particles with the rotor speed and effectively giving the mean distance conveyed per revolution. The powders were subjected to various fill levels (from 25–75%) and a range of rpms (50–250). Figure 2.13 shows that the relationship between normalised axial speed, and fill level/rotational speed was very different for the cohesive simulation: axial velocity is lower, when compared to the control and to the other powder types, especially at low speeds (50–125 rpm) with a moderate-to-high fill level (50–75%). In addition, the cohesive particles achieved a max velocity of only 38 mm/revolution, the lowest of the four samples [97]. These results are in agreement with the discussion gained from the work of Portillo et al. [79] work.

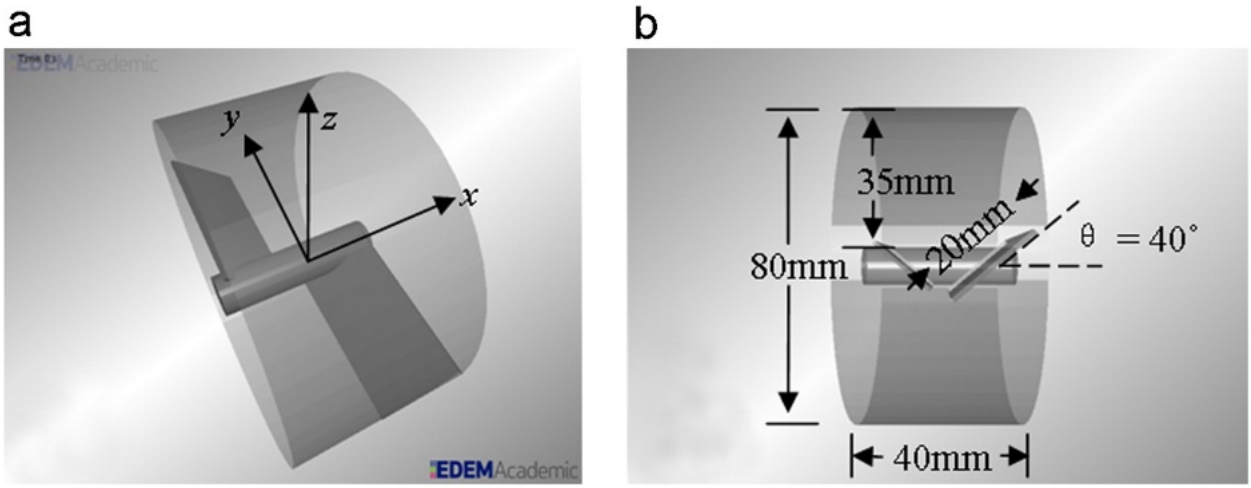


Figure 2.12: Periodic section of a continuous blender including two blades (**a**) Isometric View, (**b**) Side profile view with dimensions. Gathered with permission from Gao et al. [97].

It is worth noting that, for all non-cohesive powders used in Gao et al.'s work, when

going from high to moderate fill levels (i.e., from 75% to 40%) at 100 rpm, normalised axial velocity increases. Cohesion is still shown to have an effect at higher rpms, demonstrated by the increased distance between the contours. This finding corroborates with the rpm-cohesion-significance result from Portillo et al. [79], clearly showing that the relative effect of cohesion will depend on operating conditions (speed and fill/mass rate), and not necessarily in a predictable way, reinforcing the need for more work in this area. This finding, surrounding the three non-cohesive powders, was further supported by the work of Sarkar and Wassgren [98], where the normalised axial velocity presented the same trend, despite different geometry, particle properties, and operating conditions.

Gao et al. [97] also mapped the continuous blending rate (k_c), which is the ratio of the normalised mean axial velocity to the time-dependent RSD decay rate, where k_c essentially details the ratio between the axial (macro) and radial (micro) behaviour of the system. The results obtained were a similar contour plot to Figure 2.13, but in terms of k_c. Across the different particle properties, it was shown that high RPM and low fill produced the greatest k_c. Moreover, there was little difference seen in k_c at $<$125 rpm irrespective of fill level. For rpm $>$ 125: going from high-to-low fill showed a sluggish increase in k_c, as the space between contours and colour changes progressed slowly. This highlights that cohesion does not only affect the axial aspect of the mixing process, but also contributes to the hampering of radial mixing. Finally, Gao et al. [97] suggest further investigation on segregating materials, which would prompt several questions on a constituent's experience within the bi-or-polydisperse system. Particularly, it is worth considering what might be the best excipients to pair with different levels of cohesive materials, in order to best aid their macro- and micro-mixing. This has the potential to result in a CDC formulation, of the same drug, differing from their original batch formulation. Different excipient(s) may offer a significantly improved CDC performance, without impacting the tablet's therapeutic efficacy.

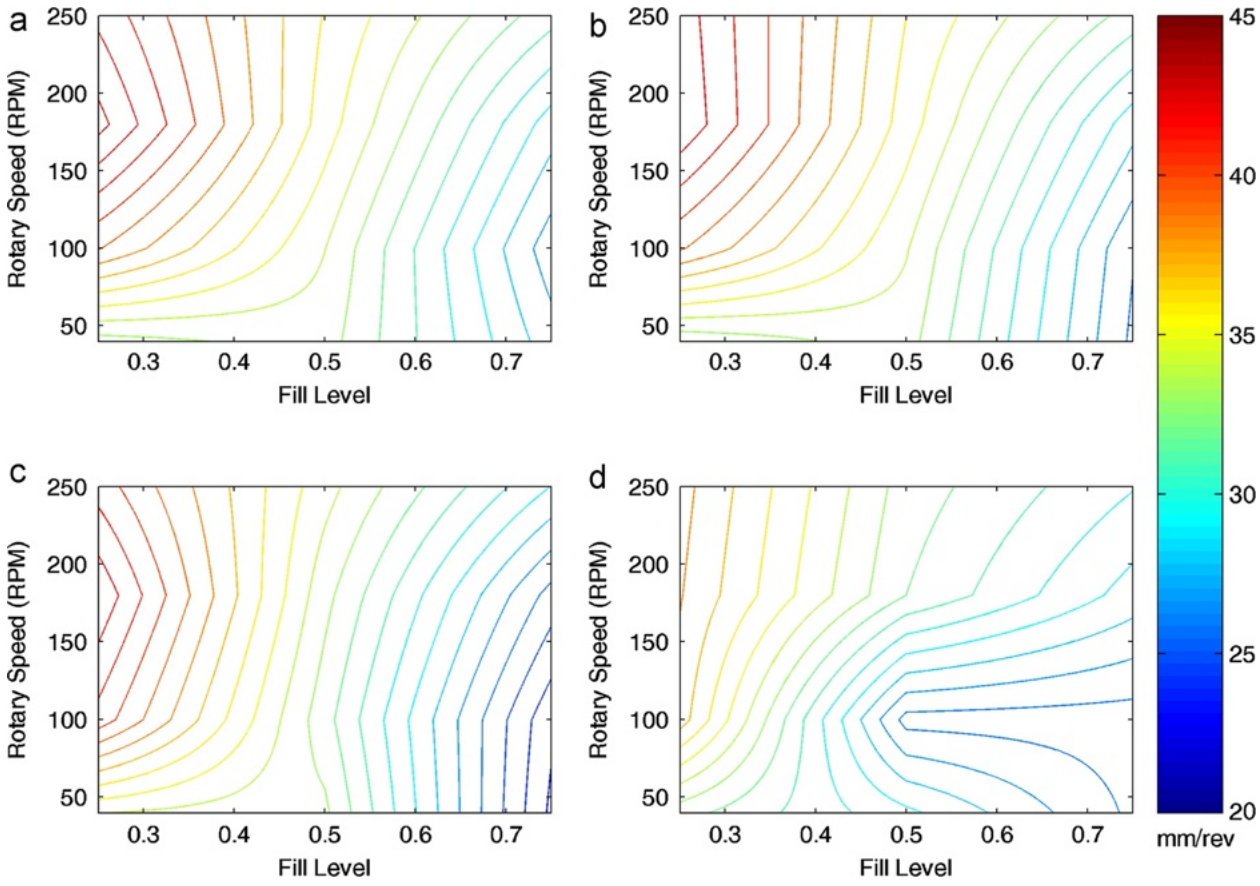


Figure 2.13: Contour plots of normalized mean axial velocity: (**a**) control, (**b**) lower density, (**c**) larger particle size, and (**d**) cohesive particles. Gathered with permission from Gao et al. [97].

Tomita et al. [99] utilised an atypical blending set-up, operating with both an impeller and a scraper in a horizontal mixer (see Figure 2.14). The inclusion of the scraper allowed for the control of the mean residence time in a manner that—unlike the previously-discussed systems—was quasi-independent of the magnitude of the impeller's agitation. In this system, the rpm of the axial impeller was driven separately to the ribbon-shaped scraper, which circumscribed the internal wall of the blender. Figure 2.14B shows the RTD curves of spiked acetaminophen using different scraper rpm speeds, whilst running at a feed rate of 10 kg/s and constant axial agitator speed of 3000 rpm. There is a considerable difference in the RTD

performance between the slowest (5 rpm), and highest (50 rpm) scraper speed, which delivered a mean residence time of 84.3 s and 12.1 s, respectively. The mixer provides a method of achieving higher micro-mixing whilst managing the macro-mixing through either increasing or decreasing the mean residence time. A similar result could be achieved with both the horizontal, or incline, blender through the alteration of either the angle of inclination, and/or the quantity of blades, blade angle, and/or blade positions. These design choices are, however, less practical to implement within a feedback loop or control strategy—though the incline angle of a blender may conceivably be varied dynamically.

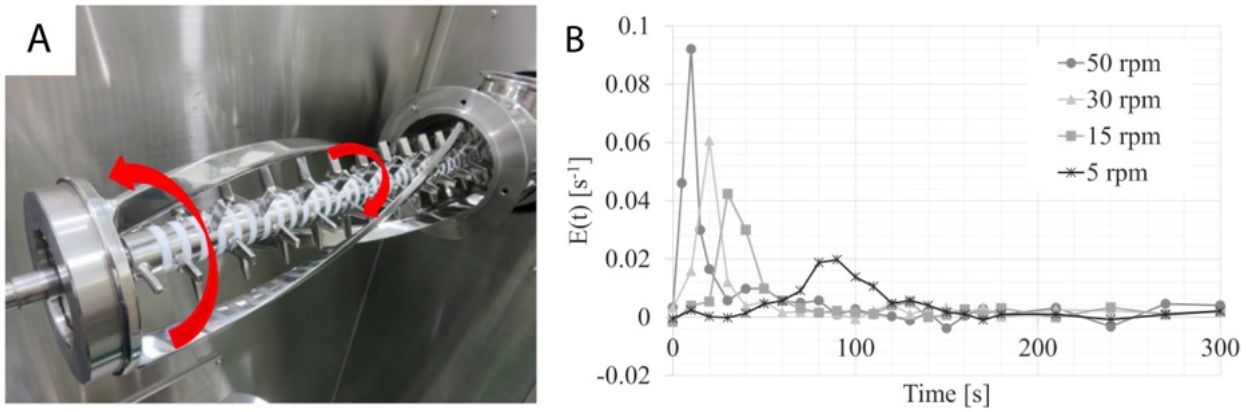


Figure 2.14: (**A**) Impeller and scraper continuous mixer with arrows detailing rotation direction, (**B**) APAP RTD spike response. Adapted from Tomita et al. [99].

Despite the advantages of an incline blender from a high-shear perspective, practical considerations must be made when attempting to maximise mixing capabilities. For example, the use of two units in series (horizontal blender and co-mill), as shown in Vanarase et al. [24], would allow independent, de-coupled, control in real-time. This reduces the risk that the process would leave a state of control, as each unit would have the capacity to compensate for the other. Conversely, if the incline blender is the only unit responsible for delivering both micro and macro-mixing, given it has the capacity to do so, it is likely the domain of control will be smaller when compared to the two units in series. This is because the process

parameters controlling the micro-mixing also control the macro-mixing, and so there is a smaller window for advanced process control to operate within to ensure the mixing balance is maintained. This, therefore, showcases the strength of Tomita et al's [99] blending unit, as it possesses the ability to independently influence the macro and micro aspects of mixing, in real-time, using process control.

Palmer et al. [76] evaluated fill level and content uniformity across a range of processing parameters in an inclined ($+15^{\circ}$) continuous blender. These processing parameters include: throughput, number of mixing blades, and agitator RPM. The study then explored the same parameters, using the same formulation, with different grades of API (APAP)—see Table 2.1. The result is the proposed exponential decay model (see Figure 2.15), and micro-mixing model (see Figure. 2.16), which uses both the Peclet Number (Pe, see Equation (2.4)) and the strain (ϵ, see Equation (2.3)). In addition, Figure 2.17, showcases a series of contour plots describing the effect of processing parameters on the fill level, for each APAP formulation. The study explored a range of Froude numbers (Fr) between 1.5, and 13.4 (for 150 and 450 rpm, respectively).

Table 2.1: Material properties of the APAP grades used in Palmer et al. [76].

Material	**FFC**	**Bulk Density** ($\mathbf{g\ cm^{-3}}$)	**Tapped Density** ($\mathbf{g\ cm^{-3}}$)	**Hausner Ratio**	**Carr's Index**
Micronized APAP	1.4	0.19	0.30	1.58	36.67
Powdered APAP	1.9	0.31	0.53	1.71	41.51
Special Granular APAP	19.4	0.73	0.83	1.14	12.05

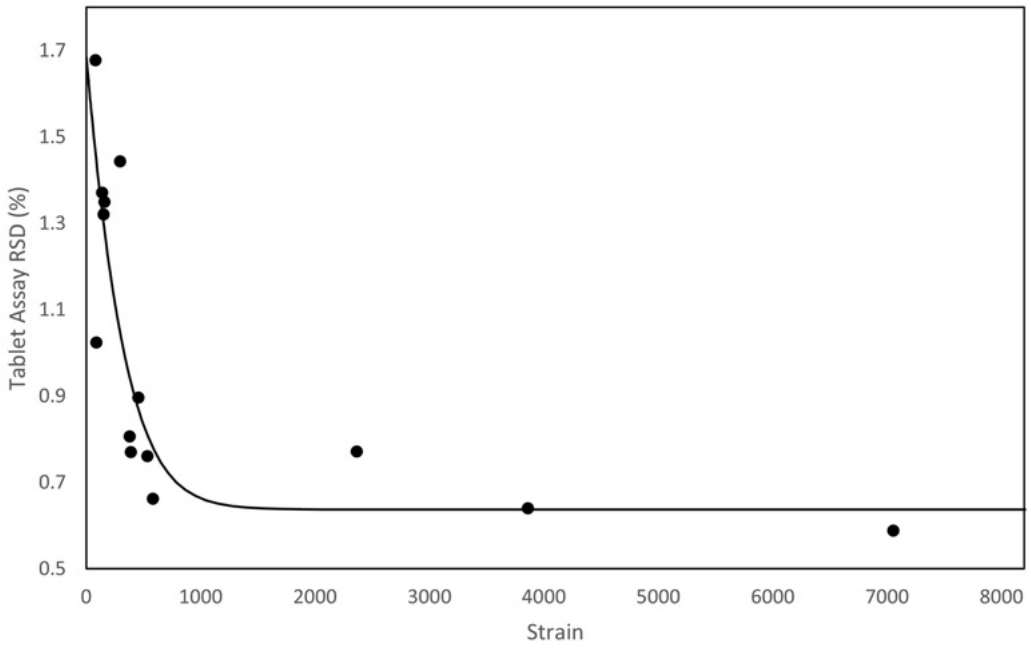


Figure 2.15: Tablet assay RSD plotted against Strain (see Equation (2.3)), an exponential decay model is fitted to the data. Gathered with permission from Palmer et al. [76].

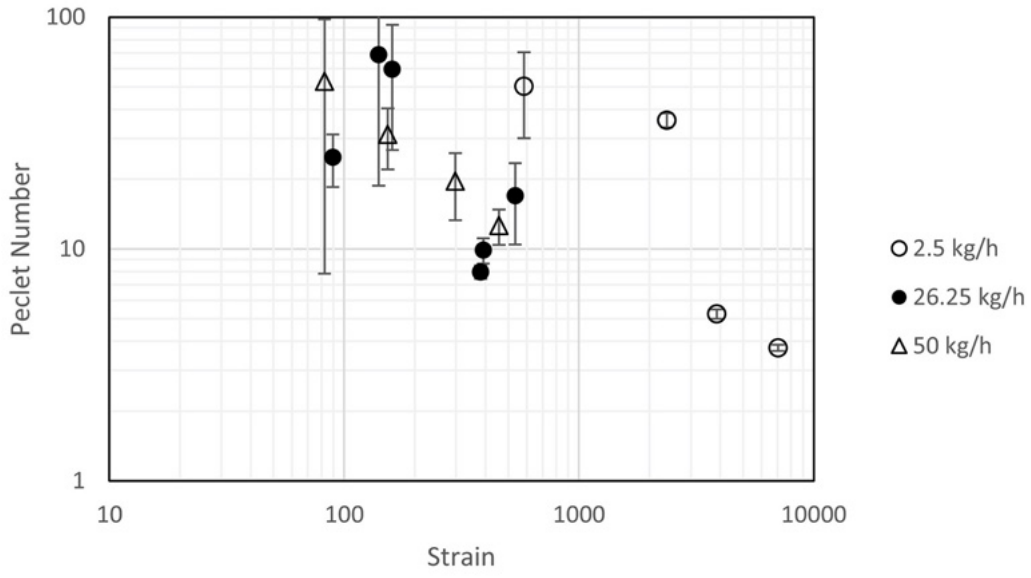


Figure 2.16: Peclet Number (Pe) and Strain relationship plotted on a log–log graph, grouped by throughput. Gathered with permission from Palmer et al. [76].

Comparing the bulk characteristics in Table 2.1, Micronized APAP (mAPAP) has closer bulk characteristics to Powdered APAP (pAPAP), but shows a unique shape contour in Figure 2.17. Despite pAPAP and Special Granular APAP (sgAPAP) being opposed in flowability indices, they present similar contour shapes. This indicates a similar fill-level, and therefore bulk powder response, to the number of radial mixing blades (see Figure 2.10) across a range of RPMs. For the mAPAP, however, increasing the number of radial mixing blades has more impact on the fill level at lower RPMs, and this impact reduces with increasing RPM. Van Snick et al. [32], discussed the necessity of sufficient mass hold-up (fill level) to attain good levels of macro mixing. The combination of these two studies suggests (i) that it is critical to determine the fill level landscape for the desired formulation to achieve and maintain sufficient mixing, and (ii) that different highly cohesive powders would be expected to exhibit different complex behaviours. What is more, using the mAPAP contour from Palmer et al. [76], considerations have to be made regarding what variables can be controlled in real-time. Since the radial mixing blades cannot be changed in real-time, it could be inferred from Figure 2.17, that using the highest number of mixing blades would be more optimum, as it would allow the system to have the largest range of fill levels.

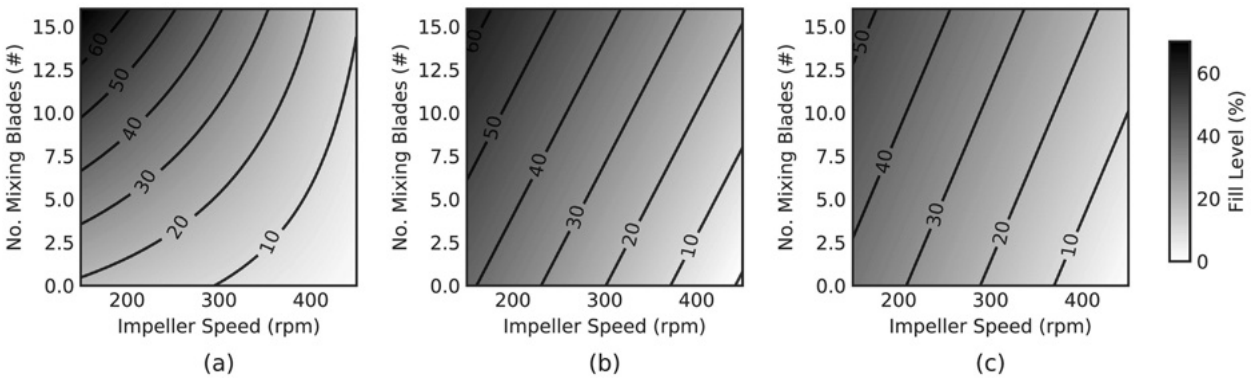


Figure 2.17: Contour plots mapping the impeller speed, number of mixing blades, and fill level at a throughput of 26.25 kg/h (**a**) Micronized APAP, (**b**) powder APAP, (**c**) special granular APAP. Gathered with permission from Palmer et al. [76].

Furthermore, Figure 2.15, from Palmer et al. [76], models the exponential decay of content uniformity RSD with increasing Strain (Strain, Equation (2.3)). Strain is a confounded variable for this system (an incline ($+15^{o}$) linear blender), as increasing the RPM decreases the mean residence time, meaning that the number of blade passes also affects the mean residence time [93, 76]. Thus, strain is dependent on the throughput, RPM, and the powder's material properties, making it essential to understand how the powder responds to processing parameters. Understanding in this area can be gleaned from the work of Portillo et al. [93, 79], Gao et al. [91], and Lopez et al. [48] regarding powder velocity, fill level, and resultant changes in residence time due to cohesion. More cohesive powders would be subject to longer residence times, but lower relative velocities. Therefore, more cohesive powders should be more resistant to increasing RPM in turn reducing cohesion's effectiveness; Figure 2.17 demonstrates the added complexity. Ultimately, strain is a great, yet elusive, measure of effective work done to the powder. The model shows there is an optimum amount of strain required (around 1500) to attain a high-quality blend.

Lastly, Palmer et al. [76] shows a linear log–log relationship between Peclet Number (Pe) and strain, see Figure 2.16. Pe is a dimensionless number describing the ratio between advective and diffusive mixing in the system (see Equation (2.4)). To give an example, a high Peclet number would be expected to produce a narrow RTD. The model, at higher throughputs (and therefore, higher residence masses), showed reduced scattering and more linear behaviour, implying that the model may be favoured in predicting systems with high residence mass, whilst also implicitly suggesting that systems with low residence mass may present unstable micro-mixing capability and therefore may be unfavourable. Despite this, across all throughputs, it was seen that with reducing strain, the Peclet number increased.

$$Strain = \epsilon = MRT * \omega \tag{2.3}$$

where MRT is the mean residence time and ω is the rotation rate of the agitator.

$$Peclet\ Number = Pe = \frac{advective\ transport}{diffusive\ transport} = \frac{uL}{D} \tag{2.4}$$

where u is the flow velocity, L is the characteristic length and D is the mass diffusion coefficient.

$$Froude\ Number = Fr = \frac{centripetal\ force}{gravitational\ force} = \frac{\omega^2 R}{g} \tag{2.5}$$

where ω is the blade rotation rate, and R is the geometrically relevant length-scale—i.e., the radial distance from the centre axis to the tip of a blade.

While, as outlined above, strain is considered beneficial for powder mixing, it has also been shown that powders that experience high levels of strain (number of blade passes) are also more likely to be subject to triboelectric charging [100]. Naturally, the effect will present some interest in how electrostatics influence/interact with powder cohesion. Karner and Urbanetz [100] investigated the influence of pharmaceutical mixing in a batch mixer and found that particle size, the fraction of fine particles, and mixing volume were significantly impacting the charging behaviour of the powder, stating that small particles were more prone to generate higher charge density. How these findings would translate to a continuous blender represents a potentially interesting and valuable line of inquiry.

Beretta et al. [36, 37] performed a two-part study on the triboelectric effect of charging powder via. powder transport in twin-screw feeding. This was followed by a study using relative humidity (RH) to subdue the electrostatic effect. Given that it is typical to maintain a RH between 30–60% in ISO-graded GMP environments [101] and that additional air moisture can increase the presence of liquid bridging, promoting cohesion [50], it becomes difficult to assess purely on the grounds of cohesion. The downside of controlling relative humidity is that it becomes difficult and expensive to maintain HVAC systems, especially as temperature and humidity fluctuate across the year. There are other options to consider, such as silication, outlined by Lumay et al. study [50], which was shown to be capable of

electrostatic dissipation and localised relative humidity control. Therefore, the use of silicates becomes a much cheaper and simpler option, despite what relative humidity may offer. However, this assumption is limited by current knowledge and awareness of the author(s) at the time of composing this review—novel literature may render this assumption moot.

Beretta et al. [36, 37] stated that the charging forces are primarily recruited through particle–particle friction, while particle–wall friction did not directly contribute to charging. In addition, the authors made considerations for impacts on powder mixing; interestingly, the discussion touched on utilising these static forces to aid the mixing process [36]. Huang et al. [23] provide evidence of this, as dry powder coating is seen in a high-shear co-mill. Huang et al. [23] investigated the effect of dry powder coating of different APIs and excipients and found that the coating of fine colloidal silica improved both bulk density and FFC performance. SEM images displaying the silica coating are shown in Figure 2.18. Therefore, charge- or cohesion-based coating could provide an avenue to attain what Fan et al. [84] (see Figure 2.7) would describe as perfect ordered mixtures.

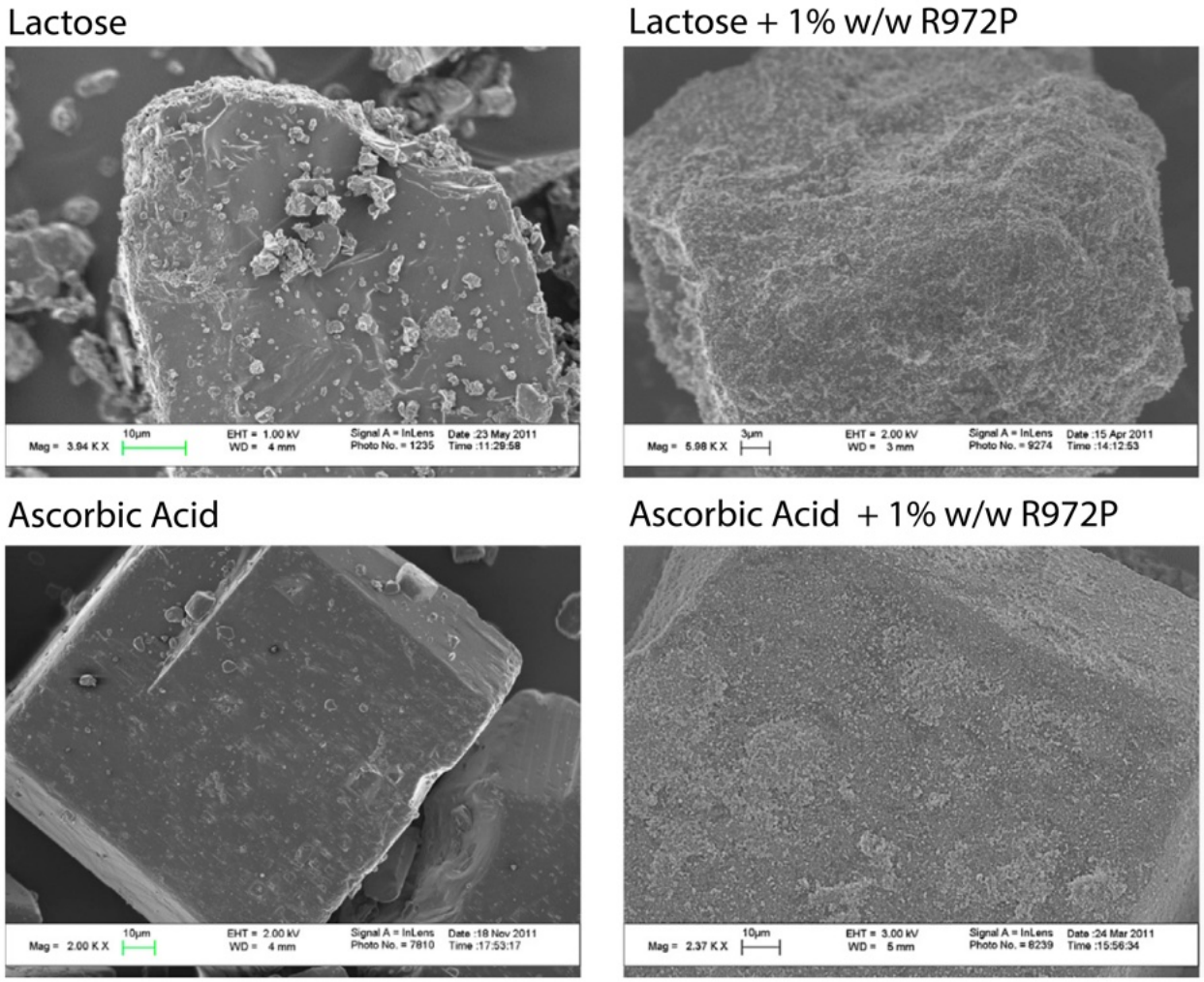


Figure 2.18: SEM images showing the surface coatings of **Top**: excipient (lactose) and **bottom**: API (Ascorbic Acid). **Left**: Non-coated and **Right**: 1% w/w Aerosil® R972 colloidal silica coating. Gathered with permission from Huang et al. [23].

Lastly, alternative silicates—such as magnesium aluminosilicates (MAS)—have been trialled in some flowability studies; demonstrating an increase in flowability, without a constraint on mixing time and intensities, which is a limitation of several glidants [102]. Such materials could be used in place of the more traditionally used MPS grades for processes which may operate with different materials or mixing regimes.

Blending Summary

The scope of this topic is multidimensional, and therefore increasingly difficult to surmise without reducing the complexity of the situation; despite this, several trends—and avenues for future work—have emerged throughout this review.

Firstly, and perhaps most obviously, the literature strongly suggests that, regardless of differences between continuous blenders, cohesion provides a barrier to dispersion, and thus a barrier to achieving micro-mixing [79, 91], which therefore decreases the quality of the mix. Cohesion has also been shown to exhibit complex behaviour at higher fill levels and lower rpms [91, 79, 76], where the particle–particle contacts are expected to be at their highest.

There is a common theme across the literature emphasizing the need to devise solutions to mitigate the effects of cohesion through the optimisation of processing parameters [76, 32, 90, 34, 103]. The literature suggests multiple manners in which this may be achieved, for example through alterations in system or agitator geometry, agitator rotation rate, feed rate, and various other factors. The differences in geometry for each blending system, however, means that each system has its own approach to solving the cohesion problem, thus making it difficult to generalise findings, and methodology, when attempting to understand the mechanisms and behaviour which explicitly govern cohesive blending. This is then exacerbated when considering that different formulations respond differently under the same conditions. An important task for future research is to define common parameters—e.g., dimensionless numbers—which can successfully generalise previous findings.

In the literature to date, several variables have been determined to affect the influence of cohesion on mixing. These include the Froude number (Fr, Equation (2.5)) or rpm, the magnitude of powder cohesivity, and the fill level of the blender. It has also been widely suggested that, due to cohesive particle–particle contact, a given system will require either a

higher shear or more frequent agitation to break apart the additional cohesive forces. Strain (ϵ, Equation (2.3)) is defined as the mean residence time multiplied by the rotation rate of the agitator (RPM), and is a measure used to quantify the amount of work the agitator does per unit of space-time (τ) [76, 90, 32, 83]. This quantity has been suggested as a valuable indicator of the degree of shear in a system and thus of blending success [76, 90, 32, 83].

It has also been suggested that cohesion loses its significance, and complex behaviour, when rpm increases, implying that by running a continuous blender at high RPM, one may improve (micro-)mixing. However, the work of Van Snick et al. [32] suggested the need for a sufficiently large mass hold-up in order to ensure good macro-mixing. However, these seemingly contradictory requirements can potentially be reconciled by ensuring that RPM is high enough to minimise cohesion's effect, thus improving micro-mixing, whilst altering the system's geometry (or other system-specific variables) to ensure a suitable amount of hold-up mass is retained, thus retaining good macro-mixing.

Regarding future work, it would be interesting to see where the lines of significance lie for each of the three cohesion-dependent variables and their interactions. Such a study would most likely have to be conducted via DEM and should follow the suggestions left by Gao et al. [91]. In general, there is potentially significant value to be found in using numerical modelling methods such as DEM to address a number of the experimental observations discussed in this section.

A Perspective on Continuously Blending Cohesive Species

A final thought on continuous blending; is that the tablet's powder formulation could be thought of as an emulsion, whereby work (in the form of strain) is given by the blender to shear through existing API clusters, reducing their size, and promoting the distribution and circulation of the new, finer API clusters around the bulk mass. The cycle then continues,

by imparting even-more work and further distributing the API clusters. The remainder of the tablet's formulation (which is mostly excipient) should, therefore, promote and stabilise the small API clusters, ensuring that they are maintained before they receive more work. Similarly, emulsions require thickeners and surface active agents to develop and maintain immiscible fluids [104]. Formulation development for CDC processes could look to use the same methodology, namely, through the exploitation of dry powder coating [23] and electrostatic charging [100]. However, considerations have to be made to ensure that, if the API is coated, it does not affect the therapeutic efficacy of the tablet.

Chapter Three

Business Impact: AstraZeneca, Oral Product Development

3.1 Introduction: Continuous Blending Equipment

Continuous blending in essence follows a similar method (in terms of mass transfer) to a Continuous Stirred Tank Reactor (CSTR), albeit mixing powder within the tank's volume, rather than fluid. Thus, principles in the realm of mixing, such as residence time, influence of impeller geometry, and dead zones, are readily translated (conceptually) into the space.

It is important to recognise that the selection of fixed parameters[1] can significantly affect the performance of mixing processes. These parameters often depend on the options provided by the equipment manufacturers. Naturally, in any market, manufacturing equipment evolves to incorporate improved geometries, materials, and methods to enhance manufacturing efficiency. Consequently, competition within the industry has led to various geometrical innovations, most notably in the angle of the blender's inclination. The literature

[1]In this context, 'fixed' explicitly refers to process parameters that are selected before operation and cannot be changed during operation, such as tank volume and impeller geometry.

discussing the influence of these parameters on the mixing of cohesive species is presented in Chapter 2.2.3.

Therefore, the strategic investment of AstraZeneca has led to the purchase of CDC-50 from GEA (Düsseldorf, Germany); it uses a 15° inclination from the inlet to the outlet, with an idealised throughput of 50 kilogrammes an hour of powder. This investment is situated within AstraZeneca's Gothenburg (Sweden) GMP facility. At the beginning of the project, there was a significant need for the equipment to meet the scheduling requirements for both product development activities and clinical supply for various projects in the portfolio. This project saw the introduction of MACH-1, a Good Laboratory Standard (GLS) suite of equipment to assist early development work, enabling the GMP facility to focus on later development tasks, such as clinical supply. The achievement of this achievement successfully fulfils the first objective of the thesis.

3.2 Business Criticality: The Role of MACH-1

3.2.1 What is the MACH-1?

The MACH-1, or **M**acclesfield's **A**ccelerated **C**DC **H**ub, is a suite of Good Laboratory Standards (GLS) equipment assembled to perform early-stage product development experiments. Data collected from instrument trials are used to calibrate and validate process modelling platforms, thereby guiding the determination of optimal processing parameters, which also inform the required parameters for the GMP CDC-50 in Sweden.

The GLS test bench includes the following equipment:

1. Two Loss-in-Weight (LIW) feeders: the first, a 'GZD 200.22' powder feeder from Ger-

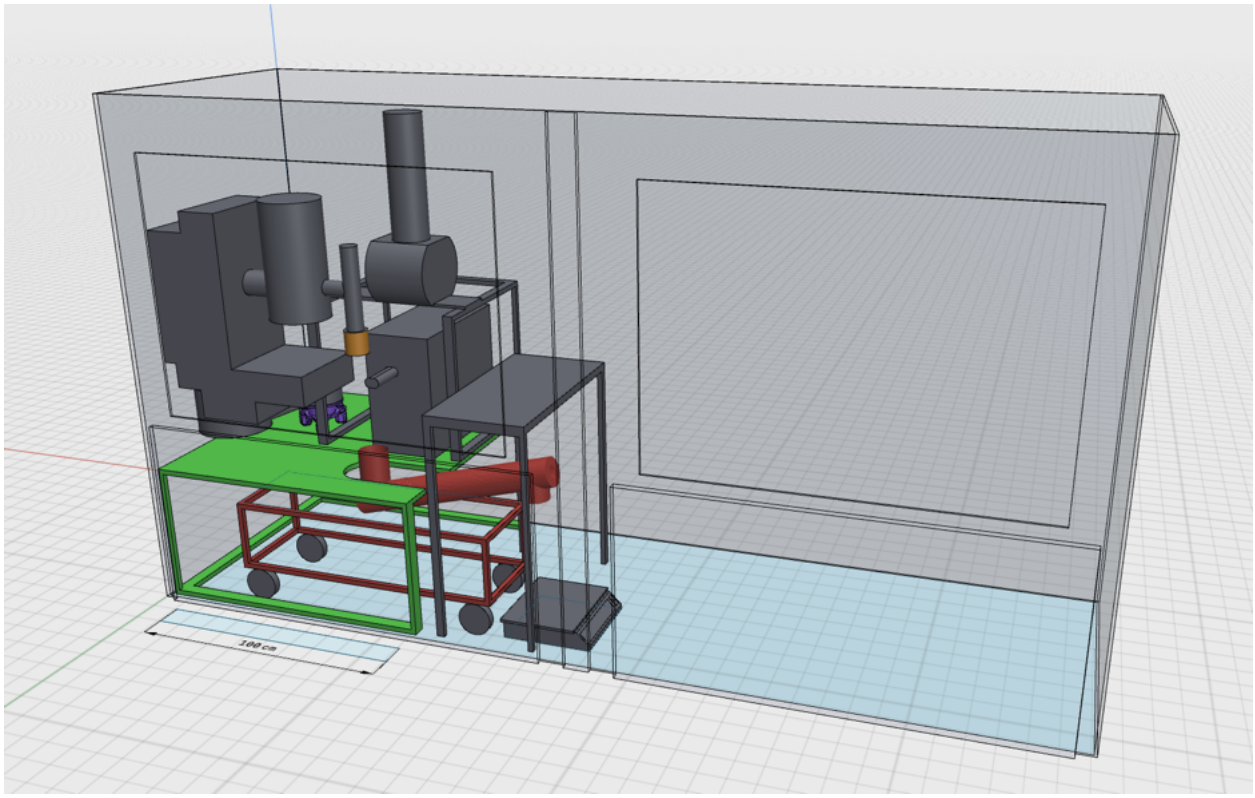


Figure 3.1: Simplified Computer-Aided Design (CAD) drawing of the MACH-1 equipment arranged within the powder booth, equipment and arrangement are to scale. The set scale can be seen by the 1-meter scale bar (of the 10 consecutive 10cm squares) outside the powder booth.

icke (Regensdorf, Switzerland), and the second, a 'Compact feeder' from GEA (Düsseldorf, Germany). Both have a variety of screw types and pitches, as well as their respective proprietary attachments.

2. A prototype of an 'incline linear powder blender', which is the predecessor of the commercially available CDB-1 Incline Linear Blender from GEA (Düsseldorf, Germany).

3. A Mettler Toledo (Greifensee, Switzerland) XS64000LX Balance, using Mettler Toledo's proprietary LabX software for data logging.

4. An in-house-fabricated manifold for the outlet with PAT probe port named the 'JSS' sampler.

This modular configuration can provide valuable information on the precision and uniformity of the feeding and blending processes, making it beneficial for exploratory and validation analyses. A CAD drawing (seen in Figure 3.1) displays the assembly organised within the powder booth ready for operation; furthermore, a colour-labelled drawing can be seen in Figure. 3.2 which describes by colour the different unit operations seen in the MACH-1 assembly.

3.2.2 The Role of MACH-1

This section, while brief for confidentiality reasons, aims to outline the significant work carried out for this project by the Oral Product Development, Pharmaceutical Technology, and Development Teams at AstraZeneca UK. The concept of scaling up batch equipment is not new and has been explored for many years. The goal of the MACH-1 suite aligns with this traditional approach: to collect valuable data that inform the manufacturing process, improve production efficiency, and minimise material use. Nevertheless, continuous manufacturing, such as CDC, represents a relatively new area of focus, particularly the scale-up of

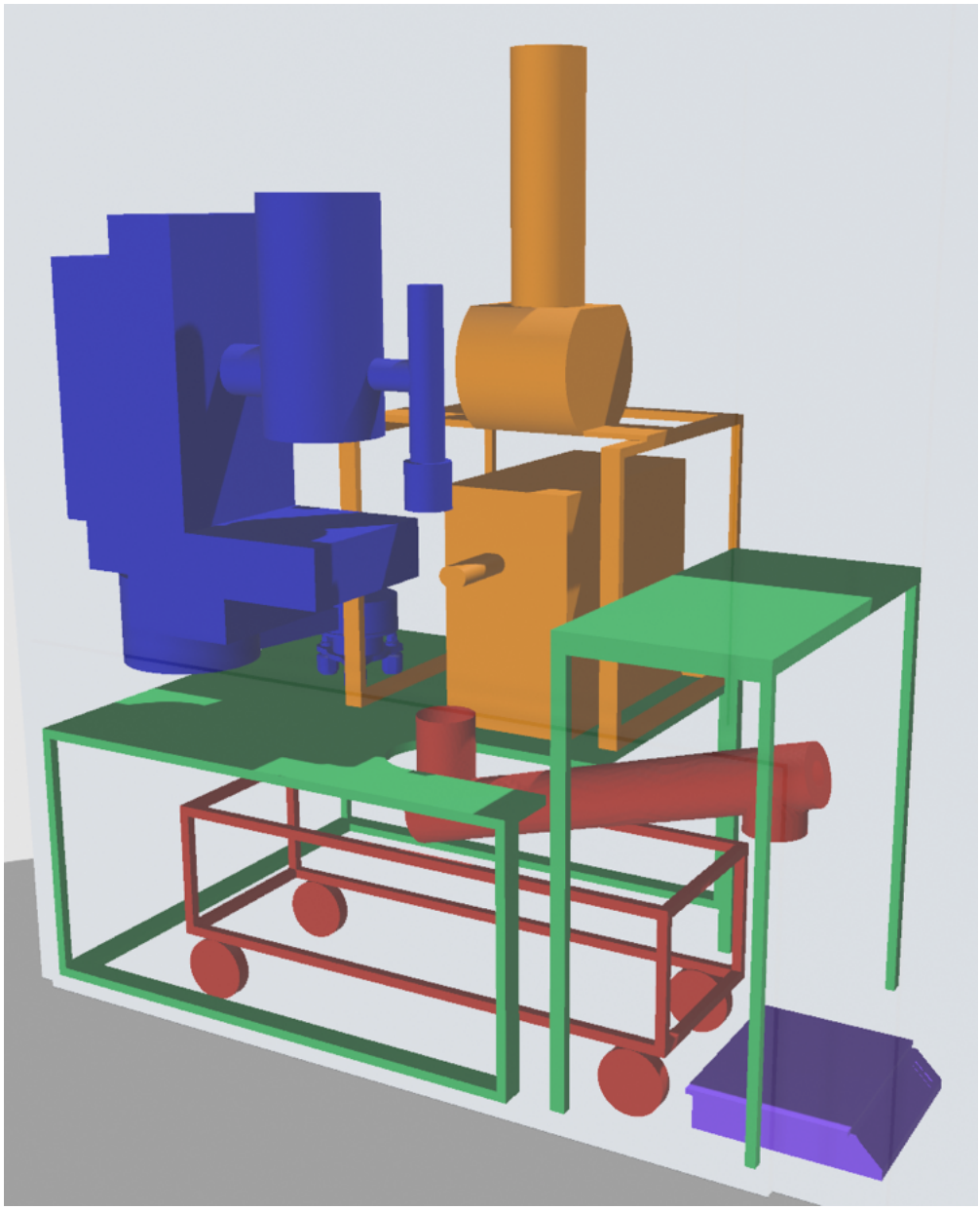


Figure 3.2: Colour labelled Simplified CAD Drawing of the MACH-1 equipment. Colours correspond to the following equipment: blue, Gericke LIW powder feeder; gold, GEA LIW powder feeder; green, fabricated stainless steel frames/trolleys; red, GEA CDB-1 prototype blender; purple, Mettler Toledo catch scale.

such processes, necessitating a deep dive into the expertise required to enable this capability effectively.

In this project, a prototype of the CDB-1 blender was acquired from GEA. For context, the CDB-1 functions as the initial blender in a sequence of two (CDB-1, which supplies CDB-2) within the GEA CDC-50 equipment train. The equipment was subsequently adapted in-house to improve alignment with the GMP CDC-50 (in Sweden) and to meet the specific requirements of the experimental work. These modifications are detailed in more detail in Chapter 3.2.3 and revisited in Chapters 4 and 5.

The primary objective of MACH-1, along with the data gathered from this prototype and other additional equipment, was to accelerate the early stages of product development, thus reducing waste. This approach allows for conducting experiments that deliver faster results at a lower cost, which in turn enhances the overall development process. The modularity of MACH-1 and its dedicated use for GLS activities offers a unique opportunity to deepen our understanding of the blending process. A notable example of its application is discussed in Chapter 4, where the blender was used off-site for experiments using a novel measurement technique to gain insight into the mechanics of mixing by tracking particle trajectories under various conditions.

These empirical findings are particularly valuable at crucial stages of evaluating manufacturing techniques for specific pharmaceutical candidates. In addition, the device serves to conduct verification tests for existing medicines. For example, if a new supplier is explored for a formulation component, one can verify whether this change affects manufacturability in a CDC setup. This is especially critical during periods of supply chain volatility, where external factors such as global disruptions and the variability introduced by contract manufacturers are concerns. Furthermore, streamlined experiments designed to measure performance also offer insights into other variables, such as batch variability of supplied ma-

terials or environmental conditions such as relative humidity, which could be significant for manufacturing in different global locations.

In essence, the MACH-1 equipment is instrumental in enhancing the development process and mitigating risks during the development phase. The insights from MACH-1 experiments enable the Digital Department to refine, calibrate, and validate digital models, thereby informing processing parameters for feeding and blending operations during future GMP trials.

Although GMP trials will still be mandatory to gain a thorough understanding of various operational states, they require significantly more material and time; therefore, the number of trials should be minimised. In contrast, MACH-1 presents an efficient, cost-effective, and simpler approach to progressing from the early stages of product development to the regulatory submission of a manufacturing method for continuous direct compression.

3.2.3 Required Modifications for the Prototype Blender

When the prototype blender arrived, it was important to confirm that the data it produced truly mirrored that of the GMP blender situated in Göteborg, Sweden. First, a review was carried out to assess the safety and appropriateness of using the blender and its auxiliary equipment within the laboratory setup in Macclesfield, UK. Following this review, it was identified that a few modifications were needed, primarily to enhance safety and additionally to ensure the blender could accurately mimic the GMP outcomes.

The subsequent section provides a brief overview of the design and safety modifications essential to the functionality of the equipment.

1. **Mechanical adjustments/connections:** The outlet flange was adapted to accom-

modate a 3-inch triclamp ferrule, allowing easy attachment of a fixed coarse mesh to prevent unwanted manual interference. Additionally, this ferrule allowed for the connection of a containment bag (collecting the powder from the outlet) and the JSS manifold used for PAT probes. In addition, stainless steel funnels and caps were installed at key entry and exit points. These versatile fittings served multiple functions: they ensured that the vessel maintained adequate airflow during containment; they blocked unauthorised manual interference; and they directed the material flow to the proper locations, both before and after blending.

2. **Motor upgrade:** The original 3GVA082002-ASB AC motor from ABB (Zürich, Switzerland) was replaced with an RX67-DRN90S4-IE3 AC motor from SEW (Bruchsal, Germany). This upgraded motor provides increased power, ensuring greater reliability in maintaining the desired RPM during operation due to its higher torque.

3. **Feedback PID loop for constant RPM delivery:** By combining a proximity sensor (which monitors rotations via a sensor on the impeller shaft) with a variable frequency drive, variable power is applied to maintain a constant RPM. Consistent RPM is essential to ensure that the blender runs at the desired speed. Moreover, this setup, along with higher torque values, enhances the control of the impeller to achieve a steady state.

These modifications were driven by two primary objectives: first, to improve containment and reduce dust generation, and secondly, to enhance the reliability and accuracy of operation—the latter effectively addressed by the motor upgrade and control loop. However, the former objective is particularly critical because of the potential processing of highly potent substances by the equipment, necessitating the minimisation or elimination of exposure for personnel handling or processing the materials. Furthermore, it is crucial to prevent any local build-up (even within the powder booth) or surface coating in areas not properly

grounded for static dissipation. The blender itself was equipped with a suitable ATEX rating (ATmospheres EXplosibles) to process such materials, and hence the modifications made were aimed at enhancing experimental practices and mitigating risks within the available facilities in accordance with the UK's Health and Safety Executive (HSE) ATEX [105] and DSEAR (Dangerous Substances and Explosive Atmospheres Regulations) [106] regulations and guidelines.

3.3 MACH-1 Integration

The execution of the MACH-1 and its integration into Oral Product Development proceeds as follows:

The strategy for operating MACH-1 equipment involved placing it in a powder air booth to prevent airborne dust, ensuring safety for operators and observers. Mechanical enhancements included specialised manifolds and a bagged collection system at the discharge point, creating a self-contained set-up that reduces dust in the workspace. To maintain the airflow of the blender while ensuring containment, all external openings were designed with a minimum diameter of 5 cm and equipped with a sock filter.

The equipment was subsequently installed on mobile frames specifically designed for easy removal or positioning, individually or in groups. This setup not only improves operational safety, but also simplifies cleaning. As illustrated in Figure3.1, the frames are engineered to mitigate vibrations that could affect the load cells of the LIW feeders, thus ensuring precise processing within a confined workspace. The principal frame design substantially obstructs the vertical cross-sectional area below the feeders, effectively isolating the blender from the feeding units and protecting the blender's motor from dust during powder management, while still allowing unrestricted air circulation (from the booth) around

the feeders to effectively capture airborne particles. In addition, secondary containment is achieved using rigid transparent plastic containers for powder storage, preventing spills or breaches.

The second phase involved refining best practices for work methods, cleaning procedures, and data management. After conducting several hundred experiments with the MACH-1 using low-risk non-active powder materials, these practices were digitised into visual standard operating procedures. This step ensured that operational methods were fully developed and optimised to reduce human error before progressing to finer powders and eventually to active compounds.

A subsequent phase involved a comprehensive safety review of the equipment utilising a safe active substance to measure exposure levels during its use and subsequent cleaning. The operators donned protective equipment, including personal powered respirators and Tyvek® coveralls with overshoes. The concentration of the substance, measured in Parts Per Million (PPM) outside the containment area, was found to be negligible during both the operational and cleaning phases, suggesting minimal and acceptable exposure risk. This successful exercise confirmed compliance with AstraZeneca's safety criteria, establishing that the equipment is suitable for managing materials up to Operational Exposure Band (OEB) 5 when following the Standard Operating Procedure (SOP). However, for compounds within OEB 3-5, operation requires a superuser following a detailed risk assessment to ensure adherence to safety protocols.

In the fourth stage, data validation involved blind replication of experiments to compare the results. The data matched within an acceptable variance, convincing the leading engineers in the product development department of the MACH-1's value as an initial testing bench, aligning with the GMP CDC setup.

The fifth and final stage was the training of the personnel and the full integration of

MACH-1 into business as usual operations. This knowledge transfer began with presentations across sub-departments and the introduction of the equipment to project teams, followed by a scheduling system for equipment use. As interest grew, prospective users shadowed experiments before receiving 1-to-1 training. Feedback from these sessions informed the training materials, resulting in the development of an interactive SOP on Tulip Software (Boston, United States) for experimental methods, assembly/disassembly and cleaning, thus completing the integration and knowledge transfer process regarding the equipment.

3.4 The Impact of the MACH-1

In Q2 2024, the MACH-1 facility was used for three drug projects and is scheduled to be used for new projects that advance through the product development pipeline. Below are some examples of experiments that each project could carry out to gather data on the project journey through its early CDC evaluation or process optimisation stages.

- **Process Development:** Identify, and prove, that the blending parameters (e.g. mixing blade configuration and impeller RPM) are fit for purpose to deliver the desired uniformity of content with the desired formulation.
- **Method Development:** The development of PAT model(s), *via.* the use of inline sensors, which can evaluate the uniformity of the formulation content at the outlet of the blender. The resultant model can be imported to the complete CDC-50 rig for validation, which accelerates the PAT method process. Accordingly, a study by Alam et al. [107], where a Near Infra Red (NIR) method (for a tablet press feed frame) was developed on a bench-top version of the system and directly translated (and validated) to a full-scale continuous manufacturing line.

- **Optimisation:** Evaluate the combination of processing parameters that aid in providing a more accurate and reliable powder feed rate of a constituent powder to the blender, in addition to its accompanying top-up strategy.

3.4.1 MACH-1 Enabled Experimentation, Modelling & Simulation

Traditionally, experimental campaigns for process optimisation rely on a multi-run Design of Experiments (DoE) approach often involving 12 or more trials [108], plus validation runs. Given the system has 3 primary process parameters to use, and an expectation to see non-linearity in the trending, either a CCD (central composite design) or a BBD (box-Behnken design) would be suggested; the former requires a minimum of 15-19 runs and the latter 13-15 runs, both depending on the number of centre point repeats done. This can be time-consuming and expensive, especially when dealing with highly complex Active Pharmaceutical Ingredients (APIs) that can cost upward of £10,000 per kg [109]. Concerns about cost and the availability of materials are typical at this stage of development, necessitating a first-time-right strategy for determining the parameter ranges used in the DoE. The MACH-1 workflow, especially when supported by the web-based AI/ML tool, can reduce the number of experiments needed through *in-silico* experimentation, thus shrinking development costs and environmental impact.

Key Assumptions

- **API per Experiment:** For a blending study, it would be common to use 1 to 1.5 kg of API. This is defined by the downstream needs of clinical and biopharmaceutical applications.
- **Design of Experiments (DoE):** A DoE that evaluates the nonlinear behaviour of

three factors for process optimisation typically involves 12 or more experiments. Three to five additional validation runs (on the GMP equipment) are often performed to verify reproducibility and robustness [108].

- **API Manufacturing Cost:** Hill et al. (2018) [109] explored the expenses involved in producing generic APIs in various regions. The study highlights that the creation of complex small molecule Active Pharmaceutical Ingredients (API), influenced by strict quality requirements and intricate chemical processes, incurs costs ranging from $1 to over $ 100,000 per kg. Furthermore, Hill et al. (2016) [110] detailed the feasible pricing of four generic tyrosine kinase inhibitors, which are used in cancer treatment. These medications have price ranges from $347 to $4671 per kg. This pricing is feasible for generic drugs, which face intense competition, prompting extensive process optimisation that reduces production, manufacturing, and supply chain costs. Hence, considering the cost variations due to the size, complexity, manufacturing scale, and the development stage of the API synthesis, this evaluation employs a conservative cost estimate of £10,000 per kg.

- **API Requirement per Experiment:** Each blending run requires approximately 1–1.5 kg of API. Material recovery at early-stage development is often infeasible, so used API is typically non-recoverable.

- **Carbon Footprint of API:** An article by Witte et al. (2024) in McKinsey & Company [111] examined the decarbonisation of API manufacturing, delving into associated costs and regulatory mandates. The authors noted that the carbon footprints for the environmental factors of the API vary between 50 and 1000 kg, CO_2 per kg, which are affected by the complexity of the synthetic route, the intensity of the mass of the process, as well as the efficiency of the supply chain and the operational efficiency.

Comparison: Without vs. With MACH-1

Without MACH-1:

- *High experimental burden:* A typical 3-factor DoE investigating nonlinear conditions run would require around 15 experiments; all of which would have needed to take place on a GMP asset.
- *Elevated cost:* Each experiment would require between 1–1.5 kg of API, some of which can be recovered for specific development tasks, but the majority are lost, leading to substantial material consumption costs. The magnitude of API is high because the system needs to reach steady state, resulting in losses start-up and shut–down, as well as loss of material due to cleaning, or material at the outlet not content uniformity specification.
- *Greater environmental footprint:* Excessive experiments within a GMP facility translate to higher power and material requirements for the same effective experimentation, resulting in higher carbon emissions.
- *Higher opportunity costs:* The GMP equipment experienced operational bottlenecks, as it served both clinical and developmental purposes. With a significant focus on helping clinical manufacturers, only essential development tasks were performed.

With MACH-1:

- *Reduced experimental burden:* The MACH-1 boasts only a single blender within the modular equipment suite, resulting in reduced time to achieve steady state and decreased mass retention. Combined with accessible AI/ML tools, users can forecast the region of interest, aiding engineers in model validation instead of constructing a surface

model for process parameters, thereby achieving a 60–70% reduction in experimentation.

- *Cost savings:* Fewer runs significantly reduce API usage, potentially saving around £100k per campaign.
- *Lower environmental impact:* Reducing redundant experiments reduces the consumption of raw materials, such as APIs and cleaning solvents, thus curbing carbon emissions. Furthermore, there is a decrease in facilities needed for GLS equipment in contrast to those required for GMP.
- *Faster insights:* Accelerated development schedules and faster design modifications, which aids in setting the initial parameters for the GMP facility. Furthermore, utilising a modular GLS system, as opposed to the GMP system, offers greater adaptability, permitting us to relocate the equipment to different locations for new insights, such as those obtained from the Positron Emission Particle Tracking experiments mentioned in Chapter 4.

Cost Calculations

(a) Cost per Experiment:

$$\begin{aligned}\text{Material required per experiment} &= 1.25\,\text{kg} \times £10{,}000\,(\text{per kg}) \\ &= £12{,}500 \quad .\end{aligned}$$

(b) Total Initial Cost for DoE (No MACH-1):

$$\begin{aligned}\text{Total DoE Cost} &= (12\,\text{experiments} + 3\,\text{validation runs}) \times £12{,}500 \\ &= £187{,}000 \quad .\end{aligned}$$

Estimated Savings (With MACH-1)

(a) Reduced Number of Experiments: By leveraging the AI-driven insights from Chapter 5, the number of runs can be reduced by 60—- 70%. This is done by replacing *in vitro* experimentation with *in silico* experimentation, from which a series of validation experiments can be formed on the basis of the surface plot response to the formulation's quality under a range of processing conditions.

$$\begin{aligned}\text{High Confidence} &= 1\,\text{Investigatory Experiment(s)} + 3\,\text{Validation Experiment(s)} \\ &= 4\,\text{Total Experiments} \\ &= 73\,\%\,\text{Reduction}\end{aligned}$$

$$\begin{aligned}\text{Low Confidence} &= 3\,\text{Investigatory Experiment(s)} + 3\,\text{Validation Experiment(s)} \\ &= 6\,\text{Total Experiments} \\ &= 60\,\%\,\text{Reduction}\end{aligned}$$

Initially, scenarios may start with a strong level of confidence before transitioning to areas with less certainty. This sequential experimentation is used to validate the model's surface, particularly as the formulation and process settings deviate from the training data to which the model was exposed. For additional information on the model and its training data, refer to Chapter 5.

(b) Associated Cost Reduction: Assuming a baseline of 60% reduction in costs while excluding expenses related to power, non-API materials, preparation, execution, cleaning, and skilled labour costs.

$$\text{Savings} = £187{,}000 \times 0.60 = £112{,}000 \quad .$$

(c) Environmental Impact Reduction: Following the same exclusions of expenses and following the median value between the ranges 50 and 1000 kg, CO_2 per kg, land the value 0.525 T, CO_2 per kg.

$$\begin{aligned} \text{API Saved} &\approx 9\,\text{runs} \times 1.25\,\text{kg/run} \\ &= 11.25\,\text{kg of API saved (approx.)} \\ \text{Emissions Reduction} &\approx 11.25\,\text{kg} \times 0.525\,\text{T}\,CO_2\text{e/kg} \\ &= 5.91\,\text{T}\,CO_2\text{e (approx.)} \end{aligned}$$

3.4.2 Model Democratization

As modelling techniques advance in sophistication and complexity, the knowledge gap between technical experts and Subject Matter Experts (SMEs) has widened. Bridging this divide has become increasingly critical, particularly as innovation requires the input of SMEs across a broad spectrum of disciplines. Simplification, therefore, emerges as a key enabler in this journey. It is vital to ensure that individuals with moderate expertise in modelling, but deep domain-specific knowledge, can leverage these tools effectively without relying on technical specialists.

The democratisation of modelling seeks to address this challenge by making models user-friendly, widely accessible, and easily interpretable. The term "democratisation" encapsulates the aspiration to ensure advanced modelling capabilities are accessible to a broader

audience, enabling a more inclusive approach to problem-solving. Marco Iansiti and Satya Nadella (2022) [112] emphasise this concept as a crucial aspect of digital transformation. Their article in the Harvard Business Review illustrates how intuitive tools can empower organisations to harness the diverse expertise within their teams, yielding substantial benefits through enhanced collaboration and innovation.

In this chapter, a practical illustration of model democratisation is explored, with further details provided in Chapter 5. At AstraZeneca, the trained model (discussed in Chapter 5) was hosted on the company's secure intranet, ensuring accessibility while maintaining data security. Users could interact with the model *via* a hyperlink that directed them to a dedicated website. This interface facilitated input through user-friendly mechanisms such as value entry boxes, slider bars, and dropdown menus, providing a seamless experience even for non-specialists.

The model instantly outputs a generated graph, predicting the performance quality space based on the entered parameters. This interactive functionality allowed users to input experimental values or hypothetical scenarios and adjust one (or more) variables to evaluate the sensitivity of the operating space. This real-time feedback enabled users to navigate the operating space dynamically, cultivating both quantitative understanding and intuitive grasp of the behaviour of the system. This capability proved particularly valuable in assessing the impact of processing parameters on formulation quality and vice versa.

The immediacy and flexibility of being able to simply interface with complex modelling were instrumental in empowering users to explore and interpret results independently. This not only reduced the reliance on modelling specialists, but also fostered a deeper engagement with the modelling process. For more information regarding the specific technical details of the model and its inputs/outputs, see Chapter 5. Moreover, this section within this chapter is *specifically* placed in this chapter to highlight the broader implications for organisational

impact.

3.5 Closing Remarks

The impact of this project can be summarised through two interrelated dimensions. Firstly, the foundation of the GLS equipment, operating parallel to the GMP facility, addressed an urgent need for additional experimental capacity. This modular suite of equipment was later divided into project-specific work packages and integrated into AstraZeneca's established workflows for oral product development. Beyond its on-site utility, the equipment also proved invaluable in supporting novel mechanistic studies conducted off-site, as detailed in Chapter 4.

Secondly, the GLS equipment was augmented with a digital layer: a democratised Artificial Neural Network (ANN) model. This model evaluates the performance of the blender against specific formulation properties, as discussed in detail in Chapter 5. By embedding this digital capability, the project exemplifies how user-centric design in modelling interfaces can facilitate wider accessibility and operational efficiency. The ability to interact with such a model in real time allowed users to evaluate performance and optimise formulation quality independently, reducing the dependency on technical specialists.

Quantitative outcomes of these innovations include:

- Reduced experimental burden: Cut the total number of experiments by up to 60–70%, resulting in significant savings on high-cost APIs.
- Cost efficiency: Lowered overall development costs by an estimated £100k per campaign, with individual cases reaching savings of £112k.

- Environmental sustainability: Reduced material consumption and carbon emissions by nearly 6 tonnes of CO_2, excluding auxiliary and operational environmental costs.
- Accelerated timelines: Transitioned from traditional *in-vitro* experimentation to rapid *in-silico* studies, reducing timelines from days to minutes while improving early-stage process knowledge.

These advancements align seamlessly with AstraZeneca's commitment to sustainability, innovation, and cost efficiency. The MACH-1 suite serves as a compelling example of how the industry can approach early-stage drug development through modular process design, leveraging digital transformation to meet both scientific and organisational objectives. The project not only emphasises the power of democratized modelling but also demonstrates its broader implications for fostering sustainable and cost-effective pharmaceutical development.

Chapter Four

Application of Positron Emission Particle Tracking (PEPT) for the Evaluation of Powder Behaviour in an Incline Linear Blender for Continuous Direct Compression (CDC)

4.1 Preface

This experimental work was conceived as one of the first substantial investigatory tasks of the thesis, designed to establish a foundation for later chapters. The focus was to develop an understanding of the fundamental transport behaviour inside the blender, with the expectation that such insight would simplify the treatment of more complex topics by providing a benchmark dataset and a unique measurement technique to which subsequent analyses could be referred.

The core insights obtained in this stage are presented in Chapter 3 and provide the basis for the next chapter (Chapter 5).

<The following chapter reproduces a research article published in ***Elsevier****'s International Journal of Pharmaceutics (Impact Factor = 5.8, available at https://doi.org/10.1016/j.ijpharm.2023.123361), for which the candidate acted as lead investigator, lead author, experimentalist, and editor.>*

4.2 Abstract

Positron Emission Particle Tracking (PEPT) is a non-invasive measurement technique which offers the ability to track the motion of individual particles with high temporal and spatial resolution and thus build up an understanding of the bulk behaviour of a system from its microscopic (particle level) dynamics. Using this measurement technique, we have developed a series of novel metrics to better understand the behaviours of powders during the steady-state operation of a continuous blender system. Results are presented on the response of particle motion to processing parameters (mixing blade configuration and RPM), quantifying motion in terms of predicted mixing performance.

It was found that both increasing the rpm and increasing hold-up mass (by selecting fewer transport blades and more mixing blades) provided improved mixing conditions. Interestingly, under specific conditions, there is evidence of convection-like mixing occurring at the interface of the transport and mixing region. This suggests the existence of a potential 'folding region' in which the powder is transported up the barrel (and away from the powder bulk bed) before being reconstituted back into the bulk mass.

4.3 Introduction

In the pharmaceutical industry, the shift from batch to continuous manufacture (CM) carries the potential to significantly reduce both manufacturing cost and product variation [113, 114, 115, 116], thus ultimately reducing the cost to the end user, the patient. This mutually beneficial outcome is being pursued by the entire pharmaceutical industry and the authorities are active in parenting the development of these methods (e.g., ICH guidelines [117, 118, 19]), requiring that the introduction of new technologies is sufficiently understood to ensure no risk is passed on to the recipient of these therapeutic products [31, 115, 19].

Therefore, it is paramount that understanding is demonstrated in the form of consistent manufacture (i.e. process design and control strategy) and rigorous models to transition from batch to continuous direct compression [114, 119, 115]. Furthermore, when considering both the complexity of the task and limited of experience manufacturing CM therapeutic products, it highlights that the journey to developing this knowledge is both challenging and costly [120]. Reviews by Wahlich 2021 [19] and Tężyk et al 2015 [120] both surmise these challenges in greater depth. Wahlich stated that– at the time the review was submitted (June 2021)– only seven CM products were on the market, and of those seven products, they were owned by four companies. As is evident from the above, from both a scientific, regulatory, and commercial standpoint, improved understanding of continuous process equipment is vital to ensuring that the rollout of continuous manufacture can continue in a manner which is both rapid *and* low-risk. The provision of new imaging capabilities stands to play a crucial role in facilitating this understanding.

The continuous direct compression (CDC) process for solid dosage forms (tablets), offers the simplest route to CM by using a minimal number of unit operations to continuously produce tablets. However, our understanding of how powders respond to mixing process conditions is limited. Excellent examples of work have been conducted by several researchers

providing an initial understanding of how bulk powders respond to mixing processes across units with different designs and orientations [79, 24, 32, 76, 99].

The seminal use of PEPT on small-scale continuous blenders was performed by Portillo et al [79], and the findings are discussed later. Vanarase et al. [24] studied the effect operating conditions had on a horizontal continuous blender through the use of RTD measurements. Van Snick et, al. [32] comprehensively investigated several factors which contribute to end-to-end CDC performance. Where blending is concerned (using a 15° incline blender), Van Snick et, al. demonstrated the influence of blade configuration on mass hold-up and its resultant effect on processing accuracy and consistency - in the form of content uniformity. Palmer et al. [76] then furthered this by mapping the processing response of three paracetamol formulations and produced a strain micromixing model - which demonstrated an exponential decay between content uniformity (attained from tablet assays) and strain (effectively defined as the number of blade passes). While Tomita et, al. [99] demonstrated the independent control of micro and macro mixing by using a different blender system the CTS-MG100 (Powrex Corporation, Hyogo, Japan), which utilised both a paddle impeller and a circumscribing scraper.

Despite providing considerable insight into mixing processes within CDC, the aforementioned studies nonetheless provide little direct insight into the internal dynamics of the mixing process, due in large part to the optically-opaque nature of the systems studied. Positron Emission Particle Tracking (PEPT) is a technique that uses highly-penetrating gamma radiation to image particulate systems' full, three-dimensional dynamics, including metal-walled industrial process equipment. PEPT is able to track the motion of individual particles through a given system of interest and use these individual traces to build up the understanding of the bulk behaviour of the system, taking a 'micro-up' approach, rather than the typical 'macro-down' approach. Moreover, the spatial-temporal data can be used to calculate a multitude of metrics which are not possible from commonly applied PAT methods,

such as NIR, and therefore, PEPT serves as a great tool for investigatory work. Full details of the PEPT technique may be found in references [121, 122].

PEPT has already been used, in the previous work of Portillo et, al. [79], to investigate the effect of RPM and blender inclination on 3 powder species using a small-scale linear blender not dissimilar to that studied here. In their study, it was determined that an inclined blender produced longer residence times and greater mixing potential; the powders travelled similar path lengths but the more cohesive the powder the longer residence time; increasing RPM decreased residence time (lending to poorer macro mixing conditions) but increased radial dispersion- thus increasing the potential mixing quality [79].

An alternative method through which insight may be gained into the internal dynamics of mixing processes is the discrete element method (DEM). DEM, like PEPT, offers a method of understanding the behaviour of not only the bulk but the individual particles within a particulate system. Past studies of such systems have investigated the effect of blade revolution rate (RPM) on axial and radial dispersion [82, 97] as well as the influence on blade angle on powder transport and mixing [123, 124, 125, 97, 126].

DEM offers two pragmatic advantages over PEPT, namely a comparatively low financial cost (due to PEPT's requirement for high energy and materials costs in the production of tracers [122]) and more ready availability (there exist at present only a handful of active PEPT facilities in the world). However, DEM simulations (depending on the number of particles simulated) will typically take significantly longer than PEPT experiments and, unlike PEPT, DEM simulations may provide misleading results without rigorous calibration and validation. The necessary calibration and validation thereof is typically complex, time-intensive and lacking a standardised 'best practice', meaning that in many cases such simulations can only be trusted to provide at best qualitative information [127, 128]. Nonetheless, through careful comparison with detailed experimental data such as that extracted via PEPT

or other three-dimensional imaging techniques, near-quantitative accuracy may be achieved [129].

This research presents the first application of Positron Emission Particle Tracking (PEPT) on a commercially representative, manufacturing-scale continuous blender, following the precedent set by Portillo et al.[79]. This approach utilizes industry-relevant geometries, blade configurations, and RPM ranges. Drawing from the discussions of Gao et al.[125] and Van Snick et al.[32], our goal is to critically analyze how these variables influence the mixing conditions within pharmaceutical blending systems. This focus, however, is directed towards the micro-behaviour of the powder at the crucial interface between the transport and mixing blade sections of the blender, a region thought to significantly affect the mixing process. In this study, local factors and their impacts on *mixing conditions* within the immediate environment are specifically investigated, rather than evaluating the overall, global mixing performance. The results obtained from this research will provide meaningful context for our findings and contribute to a broader discussion on *mixing conditions* and regime-like behaviour in similar continuous mixer systems.

4.4 Equipment, Materials and Methods

4.4.1 Equipment

Continuous Blender: GEA, CDB-1 Prototype

Experiments were performed using a prototype of the GEA CDB-1 continuous blender (GEA; Frankfurt, Germany). The blender's mixing volume is angled at a 15-degree incline from the inlet to the outlet so as to increase the total hold-up mass as compared to an equivalent, horizontal system. The internal diameter of the blender is 118 mm and the mixing volume

of the blender is 9.3L. The blender has the same mixing dimensions as its commercial counterpart but is more modular in its assembly. The blender's axial shaft has 28 collars, each of which accepts two blades which can either be at 45 degrees to the axis (push blades) or 90 degrees to the axis ((radial) mixing blades). The mixing configuration is set up such that each collar is offset from the preceding collar by 60 degrees thus the progress of the mixing blade(s) moves as a helix along the shaft. The helix rotation provides positive movement in the direction of flow. The two configurations used for this experiment are '8H' (8 mixing blades) and 16H (16 mixing blades), meaning that the mixing section covers roughly 25 and 50 per cent of the shaft, respectively. Schematic representations of the two blade configurations explored can be seen in Fig.4.3. The system is controlled using a variable frequency drive allowing the user to manually control the RPM. The rotation rate was measured using a CT6/LSR laser tachometer (Compact Instruments, Bolton, UK) with a contrasting marker on the drive shaft. The rotation rate of the shaft is measured and the drive frequency is adjusted accordingly.

Twin Screw Feeder: Coperion, KTron-20

For all experiments, particles were fed into the blender using a KTron-20 Feeder (Coperion; Stuttgart, Germany) with concave screws. The feeder was calibrated prior to use, ensuring a consistent volumetric feed over a range of hopper fill levels and screw RPMs. All experiments used a volumetric feed rate equivalent to 15kghr^{-1}. This feed rate was the highest feed rate which provided a consistent mass flow rate. Due to the age of the feeder, and therefore the settings available, only volumetric feeding was possible. The calibration gave confidence in operating volumetrically over the full range of hopper fill levels. This is primarily attributed to the free-flowing nature of the powder. Consequently, the feed rate remained accurate and stable across all experiments.

PEPT Detector: ADAC, PET Scanner

Data were acquired from the experimental system using an ADAC Forté dual-headed gamma camera. The camera offers a peak acquisition rate of approximately 100 kHz [130] and, with modern algorithms [131], can compute the three-dimensional position of a tracer particle with sub-millimetre accuracy more than 100 times per second. Full details of the Forté can be found in references [130, 132].

4.4.2 Materials

Bulk & Tracer Material: 1mm MCC

A coarse microcrystalline cellulose (MCC), Vivapur 1000 (JRS Pharma; Rosenberg, Germany), was selected as both the bulk material and the tracer for this experiment. The primary advantage of this material is its narrow particle size distribution and average particle diameter of 1.2mm; this large particle size provides a greater surface area which is desirable for improved radioactive labelling tracer performance. The large size of the particles also reduces the total number of particles within the system, thus making our results more viable as a calibration/validation data set for future DEM simulations. Furthermore, the selected powder is a pharmaceutical-grade material and is free-flowing [133]; which would be representative of a low-dose API formulation, as many excipient formulations prioritise flowability for improved manufacturability [134, 25].

Lastly, the tracer was created via the surface adsorption of the positron-emitting radioisotope Fluorine-18 (^{18}F). Details of this procedure, known as 'indirect activation' can be found in reference [131].

4.4.3 Experimental Set-Up

Since the blender is commercial scale, with a length of 0.85m, the blender does not fit fully within the maximum 0.55m field of view (FoV) of the detector. With the 15-degree inclination of the blender, the total length that fits within the FoV is 0.57m or 67% of the blender's length. For the purposes of the present study, imaging of the interface between the mixing blade zone and the former transport section is of primary interest. This volume is expected to contain more than 80% of the residence mass; supported by the comprehensive DEM work of Zheng et al. [133], which showcases analysis of a simulation calibrated for the same blending volume and powder- Vivapur 1000. This will enable the specified FoV to capture most of the trajectory of the tracers in the initial section of the barrel, as well as the boundary between the transport and mixing zones.

Thus, the inlet of the blender was positioned at the start of the FoV with the interface of the smaller mixing blade zone (8H) being captured by the end of the FoV. The finalised FoV was 0.5m (in the length axis), and the interface was prioritised within the FoV (which spanned from 0.22m to 0.42m). The region of interest for calculation is shown with greater clarity with the following: Fig.4.2.

The blender sits, fastened, within the middle section of a two-tiered extruded aluminium frame. The upper section of the frame accommodates the feeder, which is bolted in place (see Fig.4.1). The aluminium frame, and therefore the blender, is kept stationary within the detector heads of the ADAC for all experiments. The ADAC detector head separation is then narrowed in the width axis ensuring the highest possible geometric efficiency (i.e. the largest fraction of gamma-rays detected) and thus in turn the maximal data rate and location accuracy [131, 132].



Figure 4.1: Picture of the Experimental Set-up; supporting frame holding the blender and feeder in the ADAC detector's FoV

4.4.4 Experimental Design

Two variables were investigated: blade revolution rate (RPM) and the number of mixing blades (#MB).

Increasing the number of mixing blades has been previously shown to increase the overall fill level (residence mass) of such a mixer system, while increasing RPM has been shown to reduce the fill level [32, 76]. By varying both of these parameters, a range of system fill levels can be explored, thereby providing insight into the behaviour of powder under strongly varying conditions.

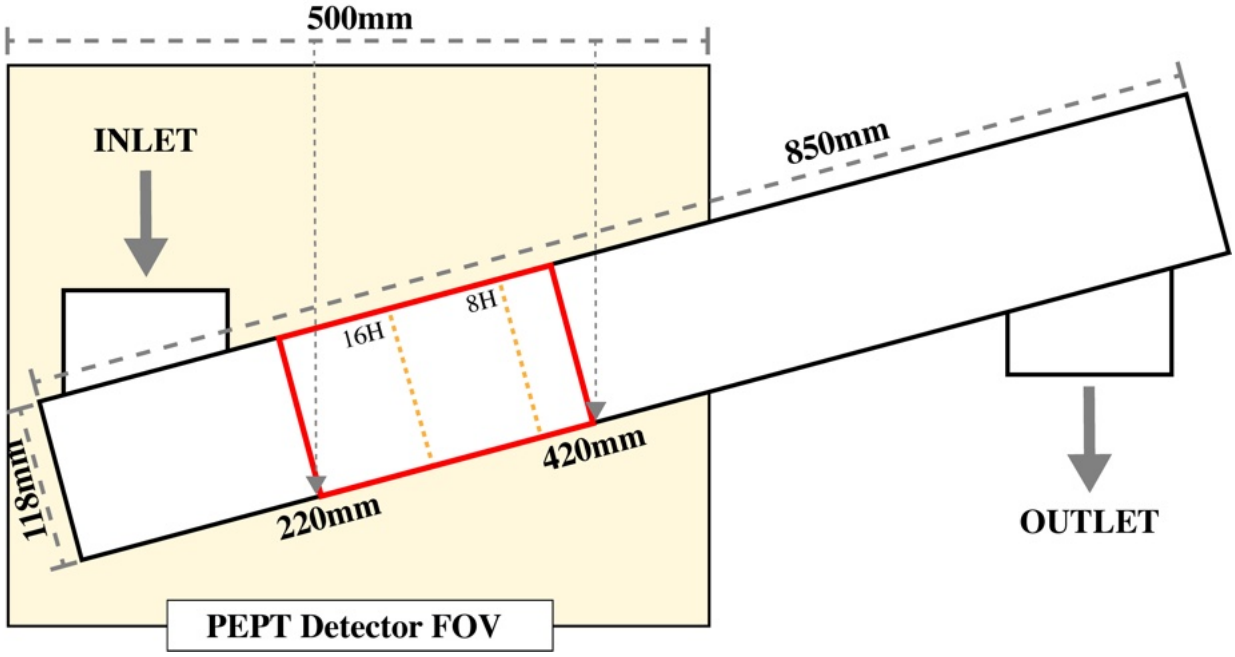


Figure 4.2: Schematic of the Experimental Set-up; showing the blender, and the dimensions, within the ADAC detector's FoV. The Region of Interest (RoI) is indicated by the red box.

It was found that the combination of low speed and reduced transport resulted in high material hold up, and consequently the torque required exceeded that deliverable by the motor. For this reason, the lowest speed used for 16H is 225rpm. This, coupled with the limited amount of time available to perform the PEPT experiments, means the analysis includes only the following data sets: 150 RPM at 8H, 375 RPM at 8H, 225 RPM at 16H, 300 RPM at 16H, and 375 RPM at 16H.

4.4.5 Experimental Method

The blade configuration is set to the desired configuration and installed into the blender. The blender is subsequently turned on and set to the desired RPM whilst filling. The MCC is then added to the feeder and set to run at 15kg/hr. While the blender is filling, using both the variable frequency drive and the tachometer, the frequency is adjusted until both remain

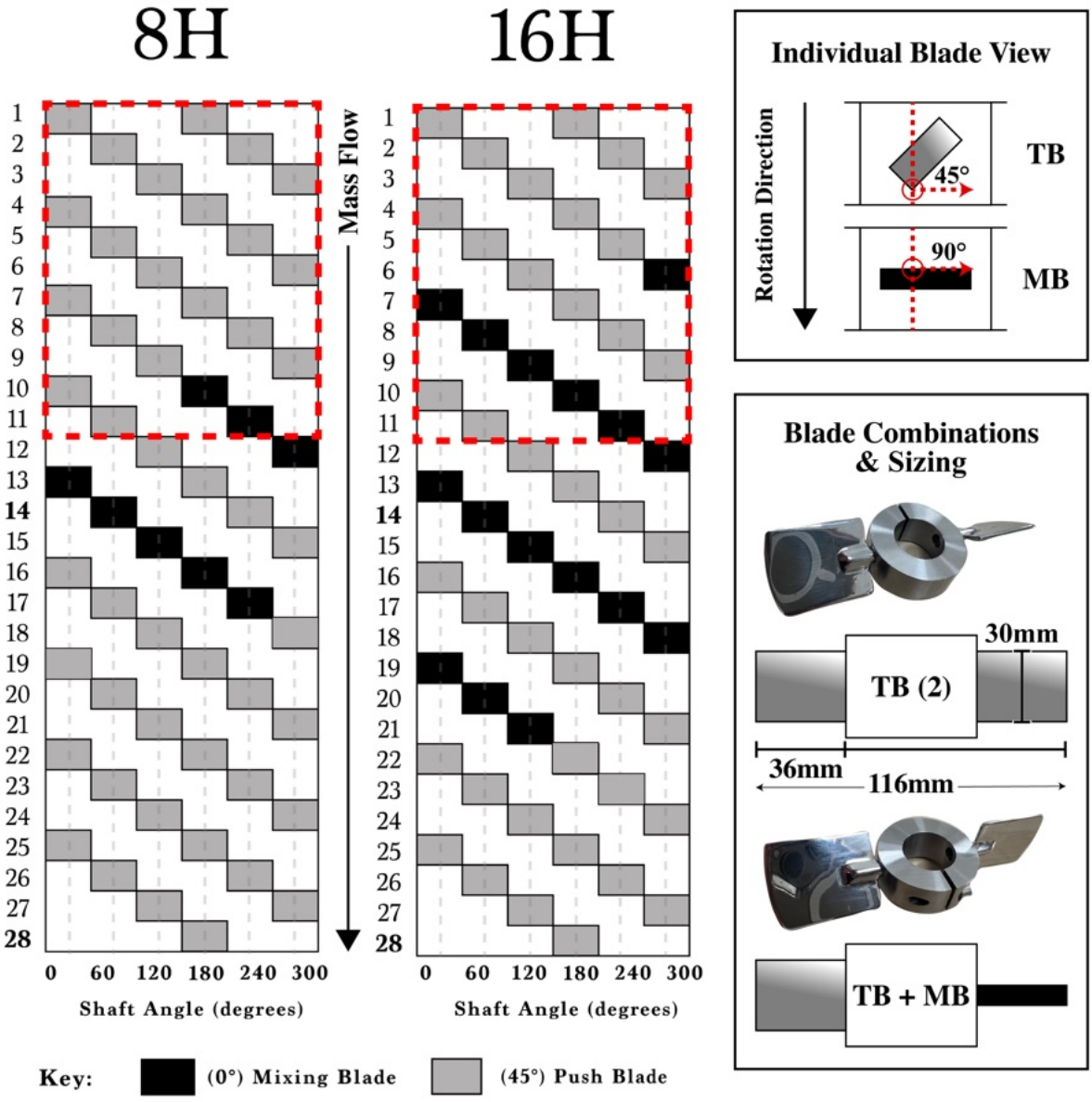


Figure 4.3: Blade dimensions and angle arrangement for the 8H and 16H configurations. The red dashed-line box indicates the FoV of the detector.

constant. When the torque (and therefore rpm) remains constant, there is an equal amount of mass entering and exiting the system, effectively stating the system is at steady state due to the constant load on the blades. To ensure the system was at steady state; the system was monitored for a further 5-minute period, in which the rpm was regularly monitored for

consistency.

Once at steady state, the tracer is then directly inserted into the neck of the feeder, bypassing the hopper, and enters the blender. A bucket collects the powder output of the blender and is returned to the hopper of the feeder when the tracer is detected in the bucket. This is repeated to gather a sensible number of passes through the system. The data is then processed using the method in the following section (Section 4.4.6). Finally, the residence mass (hold-up mass) of each experiment was estimated by weighing the powder remaining in the system at the end of the trial.

4.4.6 Analysis

Extracting and cleaning individual trajectories

In order to acquire data with the maximum spatial resolution, tracers are passed through the system one at a time. Though PEPT is capable of tracking multiple tracers simultaneously [135, 136], doing so reduces the accuracy with which each individual particle may be located, meaning that single-particle tracking provides optimal data [131]. In order to build up adequate statistics, therefore, for each set of system parameters, a single tracer is repeatedly passed through the system. By exploiting the principle of ergodicity, data acquired from a series of individual transits of the tracer particle through the mixer (for brevity referred to throughout this paper as 'trajectories') may be combined and suitably averaged so as to provide data representative of the system as a whole [137].

As the detector does not encompass the complete system, there is a possibility that during the tracer's full pass through the system, the tracer may leave and re-enter the field of view, thus potentially being erroneously considered as multiple individual trajectories, creating small, fragmented data sets towards the extremes of the Field of View (FOV)

which, if incorporated into statistical analyses, may adversely bias results. Accordingly, filtering measures were put in place to uphold the integrity of those tracers which have truly re-entered due to back-mixing and expelling the erroneous traces. As such, methods were developed to algorithmically remove such fragmented data sets in pre-processing by Firstly, any data sets possessing an overall location error above a given threshold – as expected to be produced by tracers outside the field of view – were eliminated. Secondly, any trajectories containing < 120 contiguous data points – implying only a partial transit – were eliminated. Thirdly, only trajectories containing data points spanning at least the central 200 mm (50%) of the system's field of view were included in our analyses, capturing the interface between transport and mixing blade zone.

Once all erroneous data sets had been eliminated, the remaining trajectories in each experiment were then subjected to a series of 'post-processing' analyses. Due to the sparsity of the data acquired – an inevitable consequence of the complexity of the system and the limited experimental time available – in addition to conventional PEPT outputs such as occupancy and velocity fields, a number of novel metrics were developed specifically for this project. These metrics are described in the following sections.

Novel Analyses

Traversal Classification During preliminary analysis, it was observed that the observed particle trajectories could be reasonably classified into three primary 'blender traversal modes':

1. Centrifuging: particles remain at the outer edge of the blender, resulting in bulk rotation about the unit's central axis with minimal transport along the radial direction. This is not to be confused with centrifuging observed in rotating drums where the

powder bed attaches to the wall as a solid body with no relative movement between particles. In this case, the particles are held at the wall by action of the rotating blade.

2. Axial traversal: particles pass through the blender with minimal motion in either the radial or azimuthal directions, resulting in relatively short, straight trajectories.

3. Random motion: particles are actively entrained between the blades, resulting in stochastic axial and radial motion (i.e. a random trajectory).

This novel analysis has been included in the present work as the different behaviours are expected to represent different mixing mechanisms and different mixing efficiencies. Further work is required to explore this, but it is certainly arguable that the random motion mode would lead to effective mixing while that of the axial traversal mode would be quite poor, hence undesirable in pharmaceutical blending applications. The centrifugal mode is less clear cut; it requires knowledge of the motion of the particles relative to the blade and hence the relative extents of the blade pushing the bed of particles (convective motion, poor mixing) versus shearing through (dispersive motion, good mixing). Identifying the prevalence of these behaviours for different processing conditions can thus play a role in the optimisation of said conditions.

To ensure rigour, an algorithmic approach has been taken to the classification of trajectories. In order to classify a given trajectory, the following considerations are applied:

1. The PEPT tracer locations are rotated by $-15°$ and centred such that the main blender body lies horizontally, with the X-axis passing through the centre of the shaft.

2. Each trajectory's points are converted to cylindrical coordinates, with the longitudinal (shaft) axis corresponding to the Cartesian X-axis, such that the YZ coordinates are transformed into a radial distance r and an azimuthal angle θ.

3. In perfect centrifugal motion, the distribution of azimuthal angles will be uniform between $[-\pi, \pi]$ and hence their standard deviation will be $\sigma_\theta = \pi/\sqrt{3}$, while the radial position r will be equal to the blender radius. Empirically-defined thresholds are used, such that if $\sigma_\theta < 0.75\pi/\sqrt{3}$ and the 25th percentile of a tracer pass' radial distances is greater than half the blender radius $P_{25\%}(r) > R/2$, the trajectory is classified as centrifuging.

4. Axial motion corresponds to minimal blade entrainment, such that the tracer radially explores a small area of the pipe. The plane orthogonal to the main axis of flow is extracted by converting each trajectory point's coordinates into principal component space (PCA, using the eigenvectors of their covariance matrix) and extracting the coordinates of the two least important axes X_2 and X_3 (note that the most important axis X_1 corresponds to the main flow direction); the area spanned by the 5-th to 95-th percentiles $A = (P_{95\%}(X_2) - P_{5\%}(X_2))(P_{95\%}(X_3) - P_{5\%}(X_3))$ robustly approximates the radial side of an oriented bounding box containing the trajectory's points, without outliers - and hence the radially-explored area. As the principal components X_2 and X_3 still have physical units, their dimensions can be compared with that of the blender. If the computed area A is smaller than a blender octant $A < \pi R^2/8$, the trajectory is classified as an axial traversal. This (axial) classification is supplemented graphically by Fig. 4.4.

5. Finally, all remaining trajectories are considered to undergo random mixing.

In other fields of study, for example in rotating drum systems, the classification of particle motion provides a valuable tool for the inference of mixing quality and other important parameters [138]. It is hoped that these classifications may prove similarly valuable in the pharmaceutical mixing field.

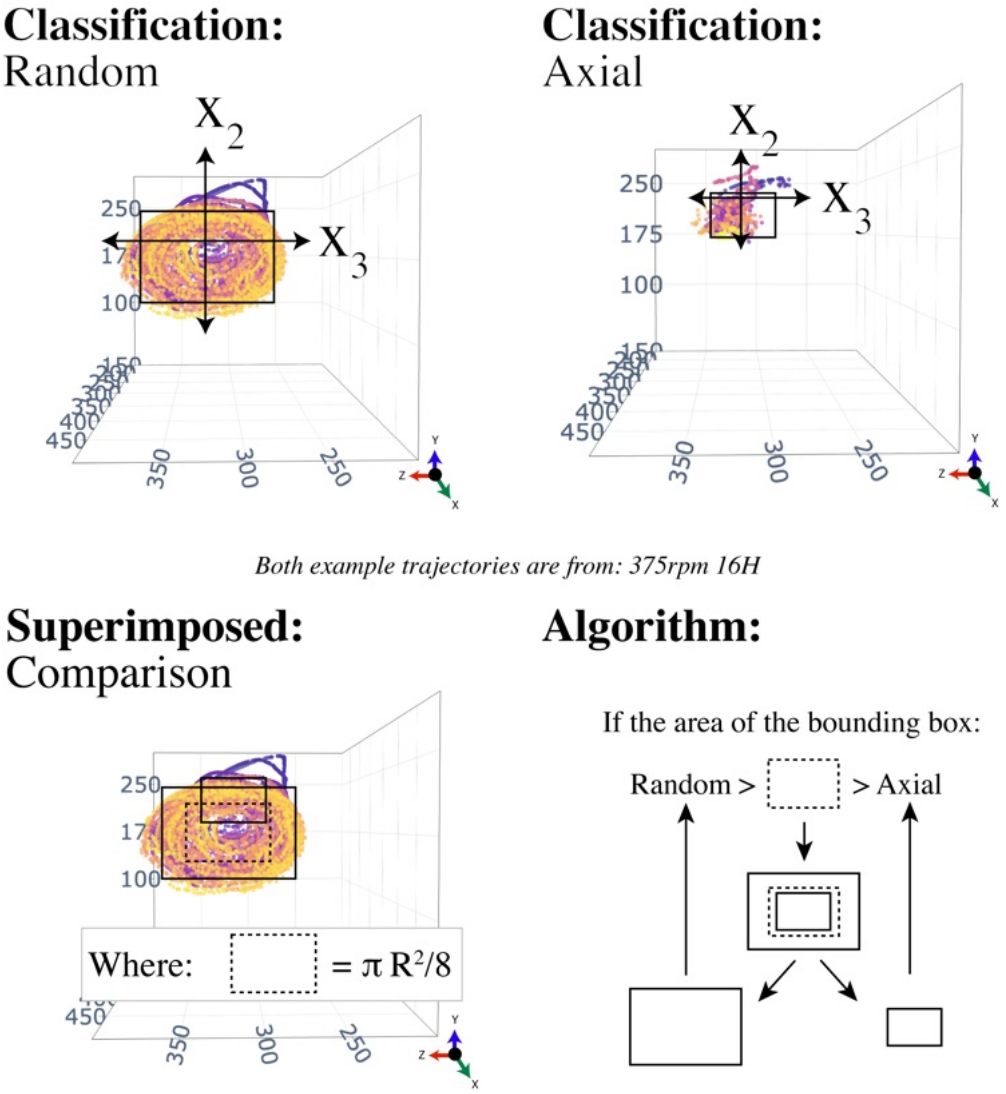


Figure 4.4: Graphical supplementation of the axial classification calculation. The units of the 3D scatter plots are in millimetres. Overlayed examples are not to scale.

Lagrangian Micromixing As more industrial systems are imaged using Lagrangian techniques offering rich three-dimensional information of their internal dynamics, new mixing measures must be developed beyond the classical approaches in chemical engineering. A novel method for quantifying the radial movement of flow specifically targeted to moving frames of reference (i.e. Lagrangian data) has been developed, providing richer information regarding the 'microscopic' mixing [94] of tracer particles. The algorithmic steps are as

follows (supplemented by Fig.4.5):

1. Take a cross-sectional slice through the blender at length L_1 (axial position) along it and record each tracer's location as it passes through the slice.

2. On this slice, compute the radial distances from each trajectory to the pipe centre $(r_1^{L_1}, r_2^{L_1}, ..., r_N^{L_1})$ for N tracer passes.

3. Take a second cross-sectional slice at a later length L_2 along the blender and similarly compute the new radial distances $(r_1^{L_2}, r_2^{L_2}, ..., r_N^{L_2})$.

4. Compute the *radial deviations* due to micromixing $(r_1^{L_2} - r_1^{L_1}, r_2^{L_2} - r_2^{L_1}, ..., r_N^{L_2} - r_N^{L_1})$.

5. Quantify the distribution of radial deviations through its mean, standard deviation, skewness and kurtosis.

6. Move the second slice, L_2, to a new position further along the blender and repeat steps 3-5, keeping track of the radial deviations' statistics as tracers pass through the mixing region.

This method is robust to both axial and centrifuging types of trajectories, as: if tracers follow laminar-like straight trajectories, the mean radial deviation will be zero; if tracers follow the (centrifugal) bulk rotation, it will again be zero. This way, only *true micromixing* is captured by the Lagrangian Micromixing metric. Specifically, a larger mean value corresponds to stronger micromixing, with the standard deviation representing the mixing uniformity. A larger skewness (i.e. a longer right tail on the distribution) indicates that only a few tracers are mixed well; finally, a negative kurtosis suggests the presence of a small number of mixing outliers.

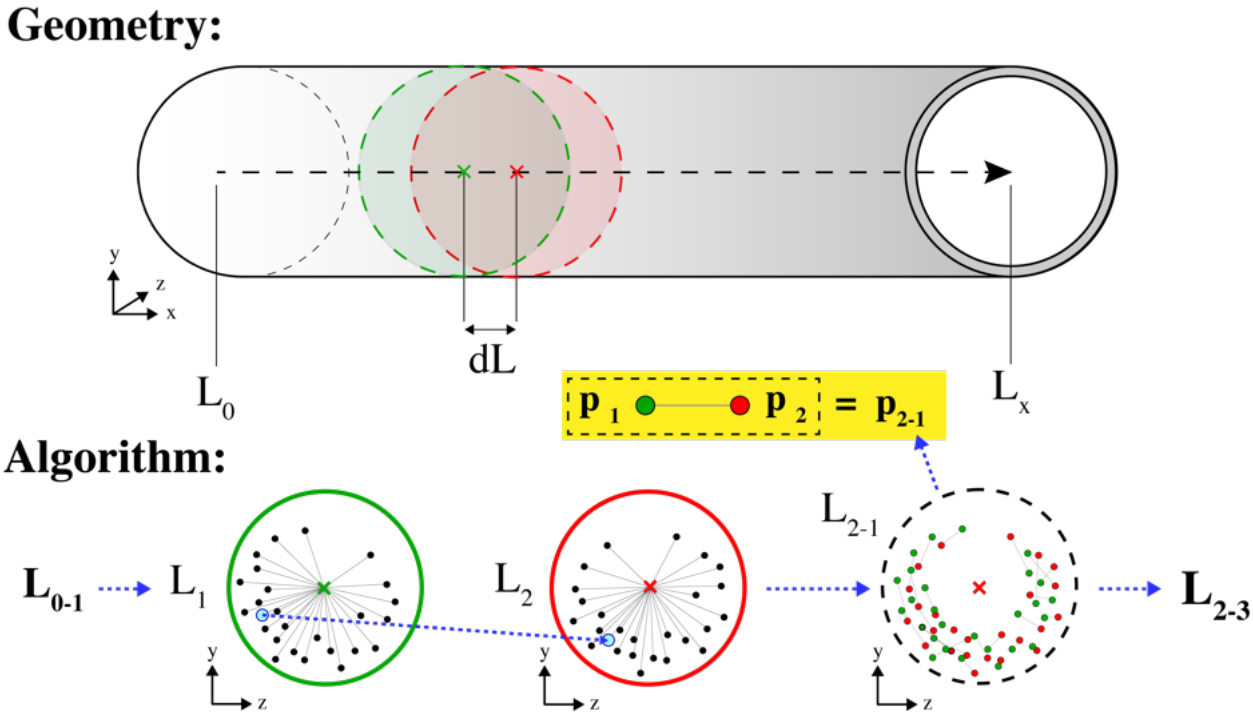


Figure 4.5: Graphical Representation of the Lagrangian micromixing metric discussed in section.4.4.6

Auto-Correlation Auto-correlation within PEPT has been generalised from the molecular dynamics' velocity auto-correlation function (VACF) [139], defined as the ensemble average - across N trajectory passes - of the dot product of a vector quantity (e.g. velocity $V = (v_x, v_y, v_z)^T$) measured at an initial time t_0 and the same vector quantity measured at a later time t_i:

$$\mathrm{VACF}(t_i) = \frac{\sum_N (V(t_0) \cdot V(t_i))}{N} \tag{4.1}$$

The time can be substituted with any 'signal' S that has a lag added to it, e.g. position along the blender, in which case it represents the correlation C of a vector quantity $\vec{Q}$ as tracers traverse the mixing region:

$$C(S_i) = \frac{\sum_N (\vec{Q}(S_0) \cdot \vec{Q}(S_i))}{N} \tag{4.2}$$

High auto-correlation indicates that tracers strongly follow a trend, while zero auto-correlation represents unpredictable, or randomly-distributed values; for example, as tracers are being mixed along the blender, their coordinates (x, y, z) are expected to become less correlated and hence C to decay to zero.

While *velocity* auto-correlations have been previously applied in PEPT studies of *batch* systems [140, 141], the present work develops a new formulation for continuous systems, and generalises the algorithm to allow the auto-correlation of arbitrary parameters to be computed. All algorithms described in this section are freely available through the authors' open-source `pept` library (see https://github.com/uob-positron-imaging-centre/pept).

Classical Analyses

In addition to the novel analyses defined above, data were also obtained in the form of spatial residence time distribution (otherwise described as temporal occupancy) and velocity profiles, providing further insight into transport and mixing within the system, and the dependence thereof on process conditions. The methodology for attaining these standard measurements can be found in references [121, 122].

4.5 Results & Discussion

In order to improve CDC processes, it is vital to develop a better understanding of the processes underlying both the micro- and macro-mixing of powders, thereby enabling their prediction and, ultimately, control. While previous studies have elucidated correlations

between the 'input' process parameters and the bulk response of the system, the use of PEPT in the current study offers insight into the system's microscopic response. This not only offers a direct insight into the micro-mixing behaviours of the system studied but also carries the potential to provide a greater mechanistic understanding of the previously-observed macroscopic behaviours.

In the following section, the analysis methods described in Section 4.4.6 are applied to provide both Lagrangian and Eulerian data, offering insight—both direct and indirect—into the mixing dynamics of the incline blender system and their variation with key system parameters.

4.5.1 Traversal Classification

Table 4.1: Tracer classification based on the definitions provided in section 4.4.6, followed with the number of trajectories collected.

Blender Parameters	8H		16H		
	150	375	225	300	375
Froude No.	1.5	9.3	3.4	5.9	9.3
Axial	48%	4%	18%	25%	20%
Centrifugal	0%	73%	0%	2%	10%
Random	52%	23%	82%	73%	70%
n-trajectories	23	271	66	51	93

Table 4.1 (and Fig. 4.6 graphically) show, for each combination of blade rotation rate and mixing blade number explored, the percentage of recorded trajectories classified as 'centrifuging', 'axial traversal' or 'random motion' based on the criteria described in section 4.4.6. As noted previously, random motion is expected to be desirable in terms of mixing,

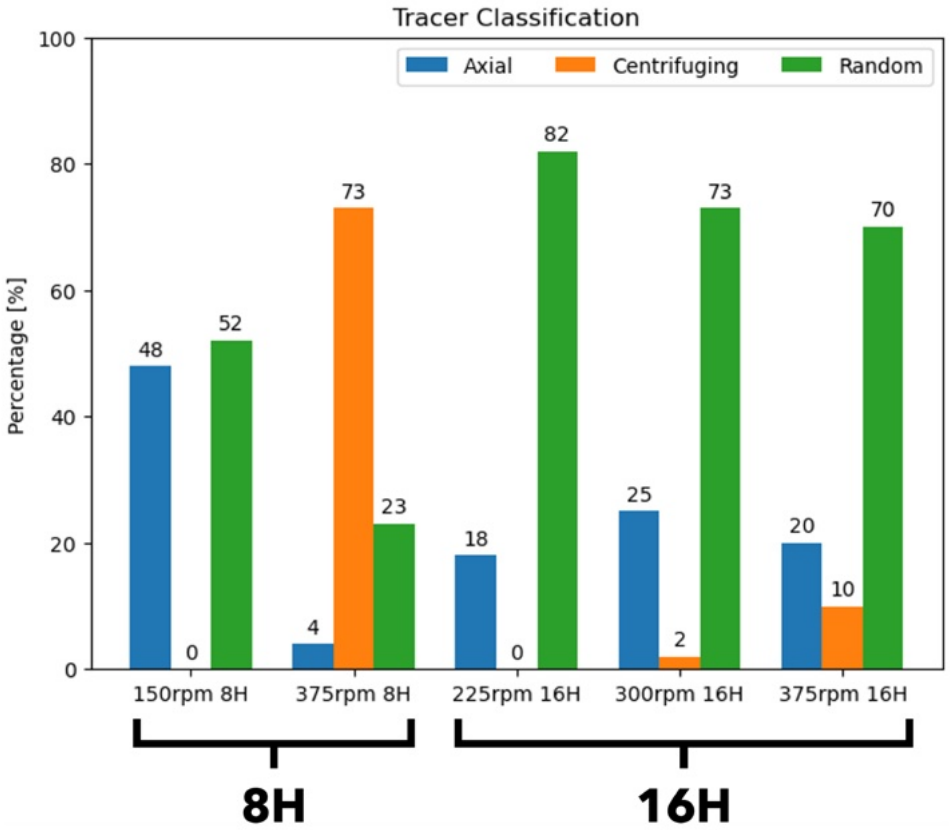


Figure 4.6: Graphical Representation of Table. 4.1 discussed in section.4.5.1

while both axial traversal and centrifuging trajectories, which limit transport in one or more directions, are expected to be detrimental. Classified example trajectories can be seen in Fig. 4.7

As might be intuitively expected, there is a clear positive correlation between the percentage of centrifuging trajectories and the blade RPM, and thus the Froude number, which in this context is defined as:

$$Fr = \frac{\omega^2 R}{g}$$

where ω is the blade rotation rate in radians per second, and R is a relevant length-scale,

here the radial length of a blade – i.e. the distance from the centre axis of the system to the tip of a given blade.

Interestingly, at equivalent blade rotation rates, the percentage of centrifugal trajectories is significantly reduced for the 16H case as compared to the 8H case, strongly suggesting that the presence of (more) mixing blades acts to suppress this undesirable transport modality.

The relationship between the system parameters and the recorded number of axial traversal-type trajectories is less clear-cut. For an 8H configuration, the data emphatically show that a low rotation rate produces a large number of such trajectories; and that this number is significantly reduced at higher rotation rates. However, this positive reduction is more than outweighed by the substantial increase in centrifugal trajectories. For the 16H case, the number of axial trajectories remains constant, to within experimental error margins, for all RPM tested.

Finally, consideration of the prevalence of (desirable) 'random' trajectories shows that an increased number of mixing blades is preferable, with the overall fraction of such trajectories higher for all 16H cases than for either 8H case explored. Within the 16H cases, there appears to be a weak negative correlation between blade RPM and the percentage of 'good' trajectories. As such, based on considerations of mixing alone, a lower RPM seems desirable. However, considering the comparatively weak relationship observed, when considering also throughput, a faster rotation rate may in fact be desirable.

4.5.2 Lagrangian Micromixing

As described in section 4.4.6, the Lagrangian Micromixing metric provides information regarding the overall strength of micromixing, illustrated by the mean 'Deviation' values pre-

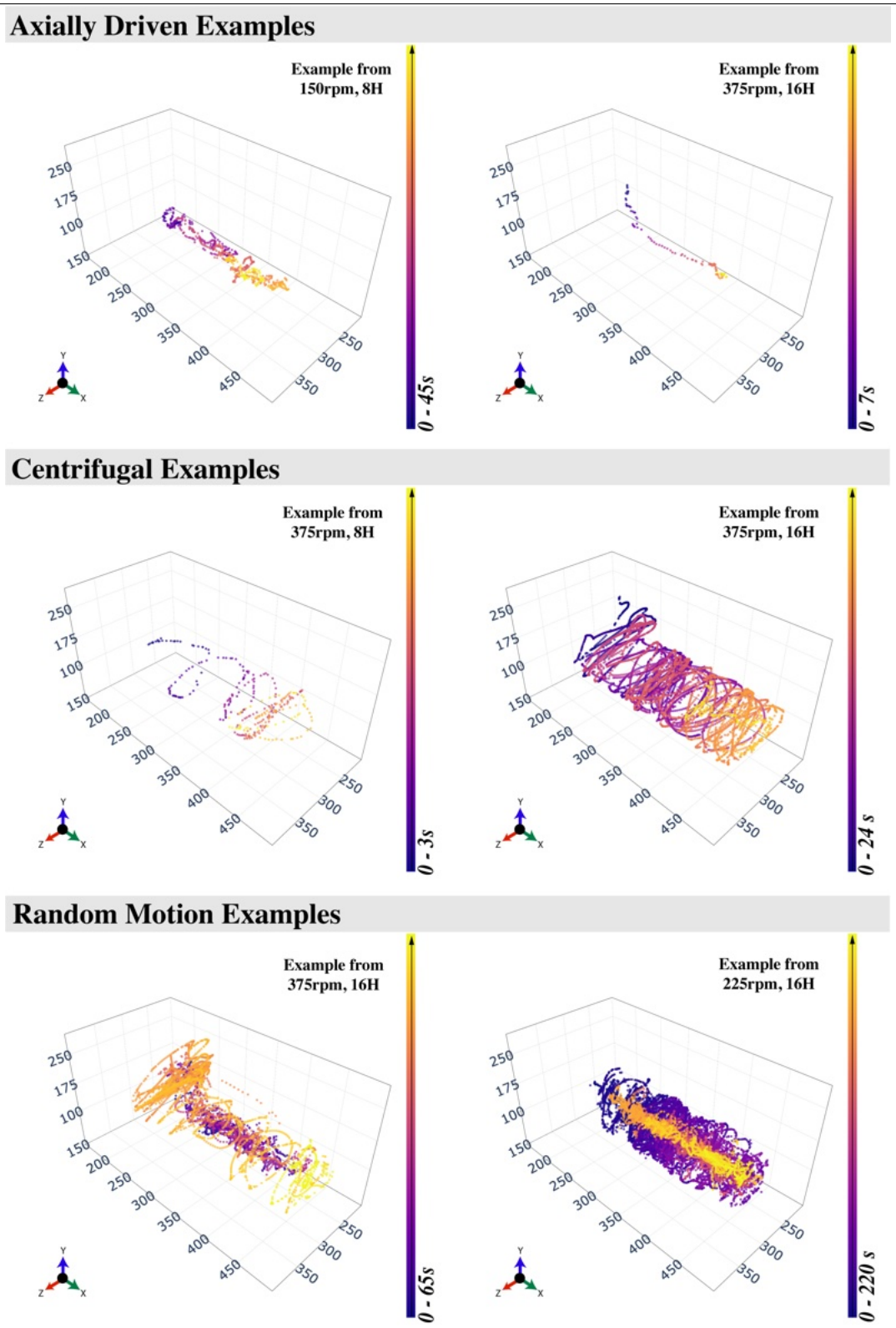


Figure 4.7: Example tracers plotted in 3D (with units mm), where each trace is labelled by its corresponding classification, RPM and blade configuration. While the colour bar indicates the time in seconds.

sented in Fig. 4.8, as well as the uniformity with which mixing is achieved across different regions of the system, illustrated by the standard deviation thereof. As such, strong and consistent mixing is represented in Fig. 4.8 by a large mean with a wide distribution. This method would be categorised as a distance-based method within Bhalode and Ierapetritou's review on continuous solid-based mixing indices [142]; which comprehensively showcases a plethora of useful comparable mixing indices across a range of publications.

The data presented in Fig. 4.8 strongly indicate that the 375 RPM, 16H case provides both the strongest and most uniform micromixing, showing also – as one may intuitively expect – an increase in the micromixing parameter within and immediately adjacent to the mixing blade zone (MBZ). Curiously, this uptick in micromixing within the MBZ is not clearly observable within the other data sets. From the figure, it can also be seen that the poorest mixing performance is observed for the 150 RPM, 8H case.

The system with the greater number of mixing blades and the highest RPM (i.e. more energy imparted to the system) results in the highest value for the micromixing parameter (an indication of the speed at which particles are expected to diverge from one another), while that with the fewer blades and the lowest RPM yields the lowest value, again makes physical sense on a fundamental level. The existence of a correlation between RPM and the micromixing of particles has been previously demonstrated (for a horizontal system) by the numerical simulations of Sarkar & Wassgren 2009 [98], who investigated the variation of a dimensionless radial-plane dispersion index as a function of the Froude number and mixer volume-fill. For lower (< 0.5) fill fractions, a positive correlation was observed between the dispersive index and the blade revolution rate, though at higher fill levels the inverse was observed. As a result of the relatively low feed rate, a comparatively low average fill height was achieved in the system, and the results are broadly in line with the expectations of prior work.

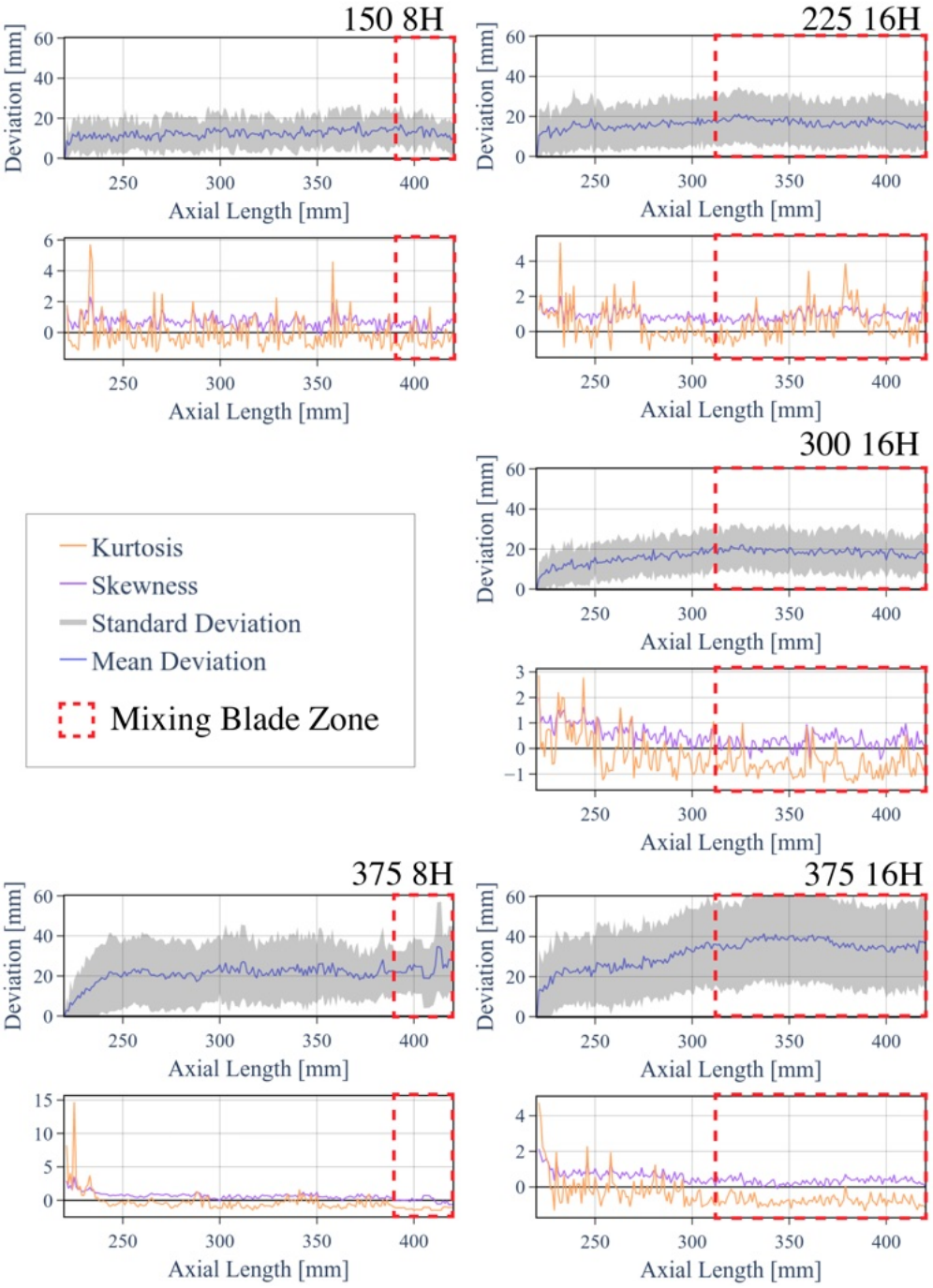


Figure 4.8: Lagrangian micro mixing along the axis between: Point 1, 220mm and Point 2, 420mm. The Mixing Blade Zone (MBZ) starts at 310mm and 390mm for the 16H and 8H configurations respectively.

Furthermore, by abstracting Sarkar & Wassgren's [98] findings for this inclined system (compared to their horizontal system), it would be sensible to map this similar behaviour to the blender – i.e. considering an environment in which the fill level (and therefore, the radial-plane dispersion) would vary down the length of the barrel. By Sarkar & Wassgren's [98] measures, the 8H at 375 RPM should show the greatest radial-plane dispersion index and therefore the greatest mixing performance, as it would have the lowest fill with the highest Froude.

Conversely, the results of Van Snick et al. [32] – who use a blender with the same geometry as this study – show that configurations with fewer mixing blades and thus lower residence mass provide poorer mixing outcomes than configurations which hold greater residence mass. The results from the lagrangian micromixing (Fig. 4.8) align well with Van Snick et al's findings- but also suggest that there is further complexity associated with the interaction between fill level (residence mass) and Froude number RPM. It should be noted the differences in inclination between the two studies (0° and +15°, from the horizontal respectively), however, the pure comparison between fill level and RPM on the dispersion performance, contradict one another. Highlighting the fact that the underpinning behaviour is still poorly understood. Employing methodologies like the lagrangian micro mixing help elucidate both the local behaviour and regional behaviour along the length of the barrel– effectively describing radial dispersion as a function of conditions experienced along the axial length.

4.5.3 Auto-Correlation

The autocorrelation functions presented in Fig. 4.9 illustrate the rate at which the radial positions of particles become decorrelated from their initial values as a function of the distance, x, travelled along the blender axis. A value of $C_r(x) = 0$ thus indicates chaotic,

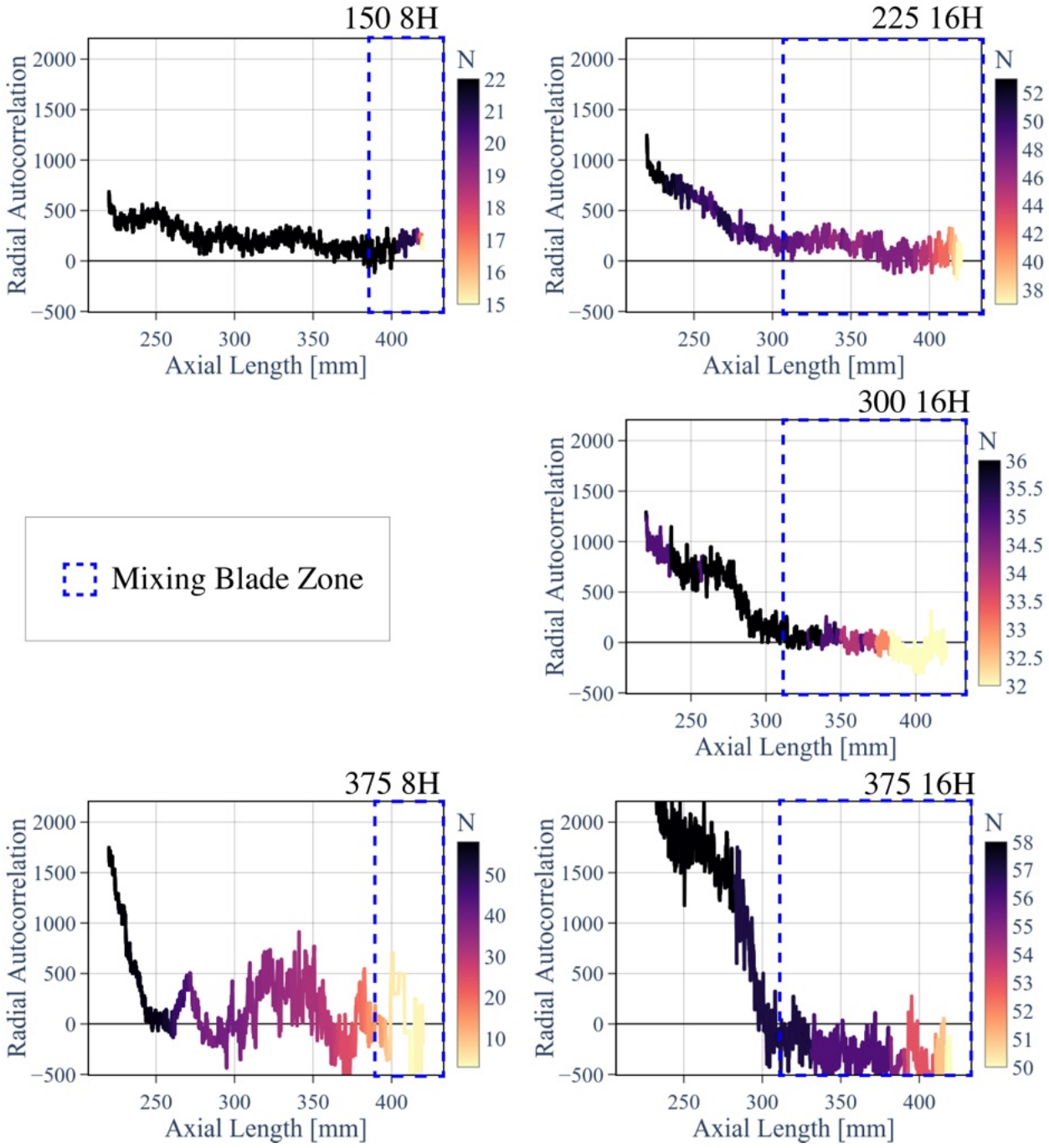


Figure 4.9: Auto-Correlation ($C_r(x)$) of the [y, z] radial plane as a function of [x] the axis length. Detailing predictability of the radial position along the barrel. $AC = 0$ shows no predictability between the radial and axial plane, suggesting a high level of radial dispersion. N is the number of traces in the AC calculation, and therefore an indicator of confidence.

history-independent behaviour [143], making it a valuable proxy measurement for mixing.

For all cases investigated, a general decrease in $C_r(x)$ is observed as the distance from the inlet increases, indicating an increase in mixing. For the 16H cases in particular, $C_r(x)$ decreases to approximately zero within the mixing blade zone, indicating the presence of strong, chaotic mixing in this region, as might be inherently expected.

Cross-comparison of the autocorrelation data shown in Fig. 4.9 with the residence time profiles presented in Fig. 4.10 shows that this behaviour coincides with a distinct peak in occupancy indicative of a 'pile-up' of material at the interface between the 'push-blade' zone and the mixing blade zone which is not present in the other data sets. The presence of this additional mass hold-up suggests a region of back-mixing or 'folding' as the fast-moving particles from the push-blade region meet the slower-moving MBZ, thus creating in essence an extended 'effective mixing region'.

The folding region' is shown by the 16H blade configuration at 300RPM and 375RPM, identified by the combination of key 'signatures' in both the autocorrelation (AC)(Fig. 4.9) and the spatial residence time (Fig. 4.10) at axial length 290mm. Specifically, in the presence of a folding region a sharp drop in the radial correlation is expected, combined with a significant increase in hold-up before the mixing blade interface. The simultaneous expression of these phenomena describes a behaviour in which axial transport is converted into the radially promoted section, resulting in the powder undergoing an increase in dispersive radial mixing, as well as an increased probability of slipping back down the barrel. This provides a remixing effect in the axial direction, mimicking the behaviour observed in a rotating tumbler [138]. The tumbling and reconstitution of powder within a rotating-drum mixer, or the convective remixing inside a bubbling fluidized bed, are both known for their ability to promote micro- and macro-mixing [94] and, as such, a similar effect can reasonably be expected here.

In the case of the 225 RPM, 16H system, this 'folding region' is seemingly absent, likely due to a reduced differential in the transport rate between the push-blade and mixing-blade zones at lower RPM. In this instance, $C_r(x)$ does not reach 0 until well within the MBZ. Such a zone is also absent from both 8H cases.

Unlike the 16H cases, which show a generally monotonic decrease in $C_r(x)$ with x, the 8H data sets – in particular the 375 RPM, 8H case – show an autocorrelation function which oscillates on a relatively large length scale, indicating that the particles – or at least a subset thereof – retain some degree of 'memory' of their initial conditions even after they have travelled a significant distance through the system [144]. This observation aligns with the earlier finding (Section 4.5.1) that the 150 RPM, 8H and 375 RPM, 8H cases elicit, respectively, a large number of axial traversal and centrifuging trajectory modes.

Finally, it is worth noting that calculating the autocorrelations for both a constant initial position with varying lag (as presented in Fig. 4.9) and a constant lag with varied initial position produced similar results, indicating the robustness of the observations.

4.5.4 Axial Spatial Residence Time Distribution

The spatial residence time profiles presented in Fig. 4.10 illustrate the relative fraction of time spent by tracers, on average, within different axial regions of the system. As described in Section 4.5.3, the higher-RPM 16H case shows a tendency to produce a hold-up region at the interface of the push-blade and mixing zones, whereas such a region is absent in the lower-RPM case.

In the 8H cases studied, no hold-up region is observed for either blade rotation rate, and – unlike the 16H cases – the difference in residence between the push-blade zone and mixing-blade zone is stark, in particular for the 375 RPM case, where the minimal occupancy

in the former region indicates an extremely rapid transit therein. This observation once again ties in well with previous observations (sections 4.5.1 and 4.5.3) suggesting a tendency for tracers to take a direct path through the system (either axially or centrifugally) rather than experiencing any significant back-mixing.

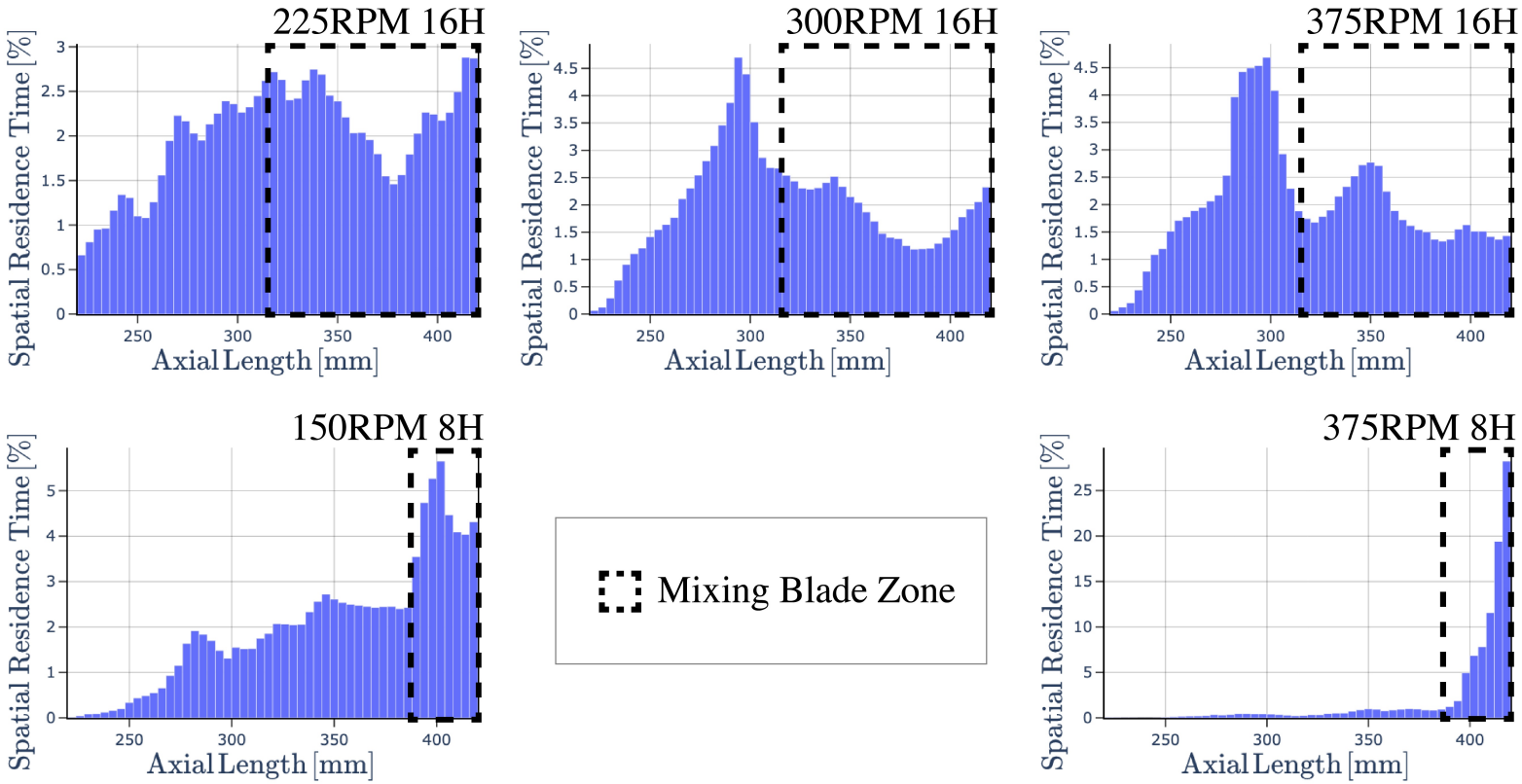


Figure 4.10: Spatial Residence Time plots, normalised by the area under the graph, for the various speeds and their given blade configuration. The region of interest for the calculation spans between 220mm to 420mm. A black dashed line denotes the Mixing Blade Zone and corresponds to where the mixing zone starts along the axial length (mm), the zones start at 310mm and 390mm for the 16H and 8H respectively. To remove any erroneous tracers, a filter was applied to the calculation excluding points which had; traces shorter than 200mm, min velocity of 0.01m/s, max velocity of 3m/s, and points with relative error $>95^{th}$ percentile.

These distributions are expected to change significantly, depending on the bulk material's characteristics and processing conditions. Moreover, it would be interesting to investigate whether the spatial residence time distribution remains the same for materials operating with equal strain; where strain is described as the number of blade passes multiplied by the mean residence time. If true, it would show evidence of mixing being influenced by regime-like behaviour within the blender- which may be a parameter to optimise.

4.6 Conclusion

In this study, positron emission particle tracking (PEPT) was used to investigate the underpinning particle-level (microscopic) behaviours of a simple pharmaceutical powder in a commercial-scale incline linear blender. Data were obtained for a variety of blade rotation rates and two distinct blade configurations, including either 8 or 16 'mixing blades (orientated, as their name implies, to encourage mixing) with the remainder of the system occupied by 'push blades' (oriented to encourage transport).

Leveraging the unique capabilities of PEPT to extract Lagrangian information from particulate systems with high temporal and spatial resolution, a series of novel metrics was developed to probe and quantify the powder's dynamic response to differing process parameters in an incline linear blender.

Firstly, a set of algorithms was established through which the trajectories of particles through the system could be classified as either 'random motion' (desirable for mixing) or 'centrifuging' or 'axial' motion (less desirable). Knowledge of the existence of these less-desirable modes, not previously documented in the literature, may prove valuable to industrial users of continuous blenders, who will naturally aim to avoid the process conditions that give rise to them.

The results show that the '8H' systems – those possessing a lower number of mixing blades – exhibited a larger number of less-desirable transit modes than the '16H' systems, with a shift from axial to centrifuging motion as the blade rotation rate increased. For the 16 mixing blade case, a similar increase in the percentage of centrifugal trajectories was observed, though this apparent shift is less statistically significant.

Secondly, a 'Lagrangian Micromixing' metric was introduced, similar in interpretation to the more conventional 'dispersion' metric used in prior PEPT studies [145, 121] but capable of handling sparse, discontinuous data in rotating reference frames. The data obtained using this metric suggest that the 16 mixing blade system at the highest tested blade rotation rate exhibited the strongest (micro)mixing conditions, with the 8H case at the lowest RPM producing the weakest (micro)mixing conditions.

Finally, a generalisable PEPT auto-correlation function suitable for continuous systems was developed. As the autocorrelation function can be meaningfully interpreted as a measure of order and thus, by definition, an indicator of the presence of chaos, it provides another valuable predictor of mixing. This parameter once again indicates that improved mixing conditions may be achieved with more mixing blades and at a higher RPM. These data, combined with additional data in the form of spatial residence time distributions, show the existence of a high-hold-up 'folding region' at the interface of the push-blade and mixing blade regions, creating in essence an extended mixing zone. This folding region was observed only for the 16-blade configuration at relatively high ($\gtrsim$ 300 RPM) blade rotation rates.

Overall, the results suggest that – for the range of parameters tested – improved mixing conditions may be achieved through the combination of more mixing blades and higher RPM. The positive influence of high blade rotation rate in particular is a potentially valuable finding for the field, as it reduces the need for a compromise between mixing quality and throughput. Nonetheless, these data were acquired only using a comparatively simple,

non-cohesive powder, and a relatively low feed rate and (thus) fill fraction. Further work should be performed using additional materials and feed rates in order to assess the generality of these results.

It is important to note that more mixing or improved mixing conditions may not always have a positive effect. In the case of powder lubrication with, for example, magnesium stearate, over-zealous mixing may lead to over-lubricated tablets, which then result in reduced tablet tensile strength [146] and slower disintegration/dissolution rates [147]. Therefore, processing parameters such as the 8H (at high speed) may be better suited for a given formulation and specific use case.

In addition to the insights gained directly from the results, the detailed three-dimensional data obtained provide a valuable calibration/validation data set for future DEM models of continuous blender systems [128].

Chapter Five

Using AI/ML to Predict Blending Performance and Process Sensitivity for Continuous Direct Compression (CDC)

5.1 Preface

This chapter describes the experimentation and development of Artificial Intelligence / Machine Learning models to provide a digital layer over the MACH-1 capability. This chapter builds on Chapter 3, which details the development and structure of the equipment. The primary business objective is to take advantage of the physical and digital together, as described in this article, to minimise the risk and experimentation involved in the OSD development stages.

A tool was created and provided via an easy-to-use Graphical User Interface (GUI) on the intranet to enable distributed departmental access, referred to as the model **democraticisation**. For further information on model democratisation, see Chapter 3.4.2.

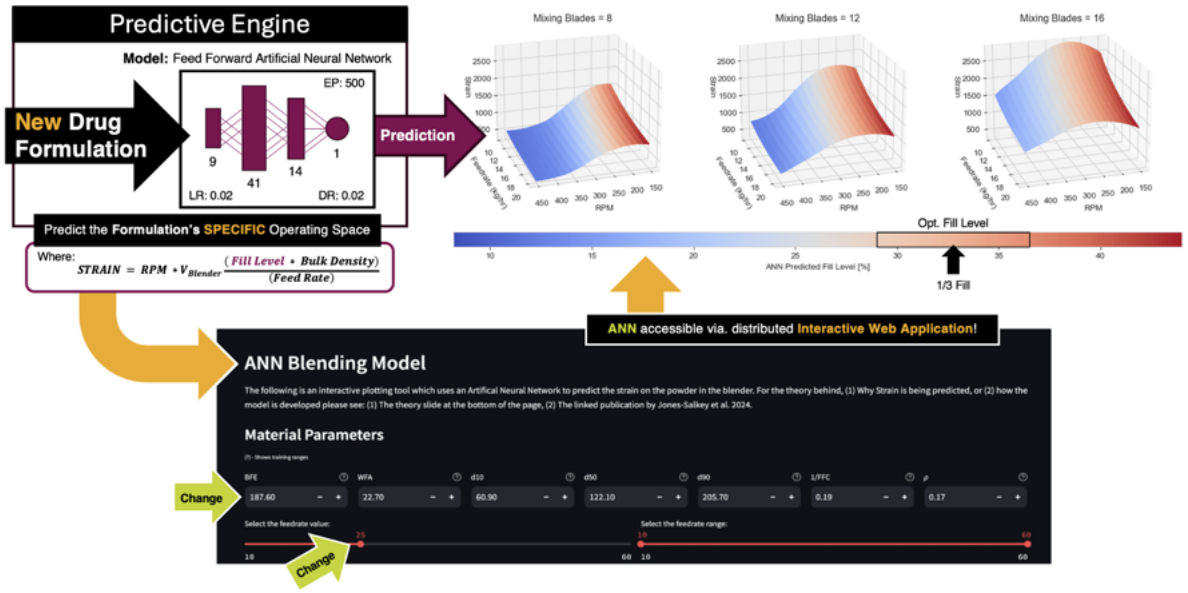


Figure 5.1: Demonstration of using the Web-Based Artificial Neural Network Application.

<The following chapter reproduces a research article published in ***Elsevier****'s International Journal of Pharmaceutics (Impact Factor = 5.8, available at https://doi.org/10.1016/j.ijpharm.2024.123796). The candidate served as lead investigator, lead author, experimentalist and editor of the paper.>*

5.1.1 Preface: Model Democratisation & Re-training/parameterisation

In addition, a supporting script was supplied to the department which automates the re-training and parameterisation of the three most important parameters in the ANN: Learning Rate, Dropout Rate, and Layer Width (of Hidden Layers 1 and 2) [64]. Meaning, an approved scientist in the department can update the training data file, run the script, and then copy the saved files for the retrained model over to the intranet (by replacing the existing ones) and redeploy the application. Similar to Chapter 3, this aims to streamline and simplify work without sacrificing functionality or adaptability.

5.2 Introduction

A significant volume of research on continuous powder blending has focused on understanding how processing parameters affect performance using metrics such as residence time distributions and dispersion. [83, 24, 148, 32, 149], while other – typically simulation-based – studied have demonstrated the differences that particle properties have on processing efficacy [82, 97, 91, 98, 150, 103]. However, there is little work mapping physical experimental bulk powder characteristics to processing conditions in the blender. The only research done to the researchers' knowledge lay with that of Bekaert et al. [90, 151], who investigated blend properties in a horizontal blender and the development of an empirical predictive model in an incline blender.

With the advent of readily-available, open-source Artificial Intelligence and Machine Learning tools, this study looks to leverage these methodologies to propose a novel framework to approach new pharmaceutical development projects. These methods allow the deconvolution of material properties and processing parameters by mapping processing outcomes to powder characteristics and processing parameters. This, in turn, allows for the prediction of key process outputs, such as the fill level within the blender and (thus) the strain experienced by the formulation, which has been shown to be a good predictor for blending performance [83, 25, 90].

The utilisation of the three different models in the study ideally highlights the individual strengths of using each of the specific modelling methods. Random Forest Regression (RFR) can 'pull the logic' from the data by providing insights into feature importance and parameter relationships. Individual 'trees' extracted from the model may also provide useful guidance to system operators. PyTorch's Artificial Neural Networks (ANN), on the other hand, fit highly complex nonlinear functions to the data to enable accurate and reliable predictions of the data surface, though are somewhat more of a 'black box', offering only

limited physical insight regarding the outputs they produce. Finally, M^2E^3D was used, a tool that utilises evolutionary AI and symbolic regression to transform complex systems into simple equations [152, 153]; the methodology of the tool is discussed further in Section 5.5.5 and accessible on GitHub: https://github.com/uob-positron-imaging-centre/MED.

Ultimately, by using these tools, this study unveils a correlation between fill level and optimum strain, which holds true for varied processing and material properties. The discussion focuses on how this relation develops by relating it to current literature and exploring space-time optimisation and optimum Peclet Numbers in specific regime-like behaviour. The study then discusses the use of such tools in an industrial setting by touching on how best to use this mapping ability to inform decisions to mitigate risk whilst navigating the complexities of drug project development.

5.3 Equipment

5.3.1 Prototype GEA, CDB-1, Linear Blender

A prototype of the commercially available GEA CDB-1 Linear Blender (GEA, Dusseldorf, Germany) was used for these experiments. The blender, made of stainless steel (316L), has an internal radius of 59mm and a volume of 8.2L at a 15° incline to the horizontal. The equipment is driven by a motor paired with a proximity sensor (to measure the rotation of the impeller's shaft) and feed-back controlled variable frequency drive - allowing RPM to be set and maintained.

The shaft of the mixer has 28 removable collars each with two paddle blades the orientations of which can be adjusted from 0° (parallel to shaft axis) to 90°(orthogonal to shaft). Resulting in the ability, with the adjustable paddle blades, to simply change the

angle and position of the collars to create a blade configuration. In this study, the 'number of mixing blades' refers to the helical organisation of 90° (to the axis) radial mixing blades from the centre of the mixer out towards the ends of the blender. In effect, the mixing blades are aligned in a helix along the shaft with 60° rotation between adjacent collars; thus increasing the number of mixing blades increases the size of the mixing zone. Ultimately, allowing the categorical variable (of a set configuration) to be considered continuous (as the number of blades varies the size of the mixing zone). The remaining blades in the configuration are aligned in transport orientation, at 45° to the axis. Fig 5.2 displays these orientations and their positions in the configurations investigated; 8 mixing blades (8H) and 16 mixing blades (16H). These configurations are the same as the two configurations used in the PEPT study reported by Jones-Salkey et al [154].

Each blade configuration is examined across five blender speeds: 150rpm, 225rpm, 300rpm, 375rpm and 450rpm. This choice allows the investigation across the full range of relevant blending speeds, exhibited by the CDB-1. Palmer et al. [76] investigated in increments of 150rpm, demonstrating a significant difference in mixing performance. In this work, the increments were reduced to 75 rpm to provide better resolution and more reliable model fitting. Each configuration was run with every material at feed rates of 10 kg/hr and 20 kg/hr. Additionally, 3 materials (which are very commonly used filler excipients) run at 26.25kg/hr and 50kg/hr.

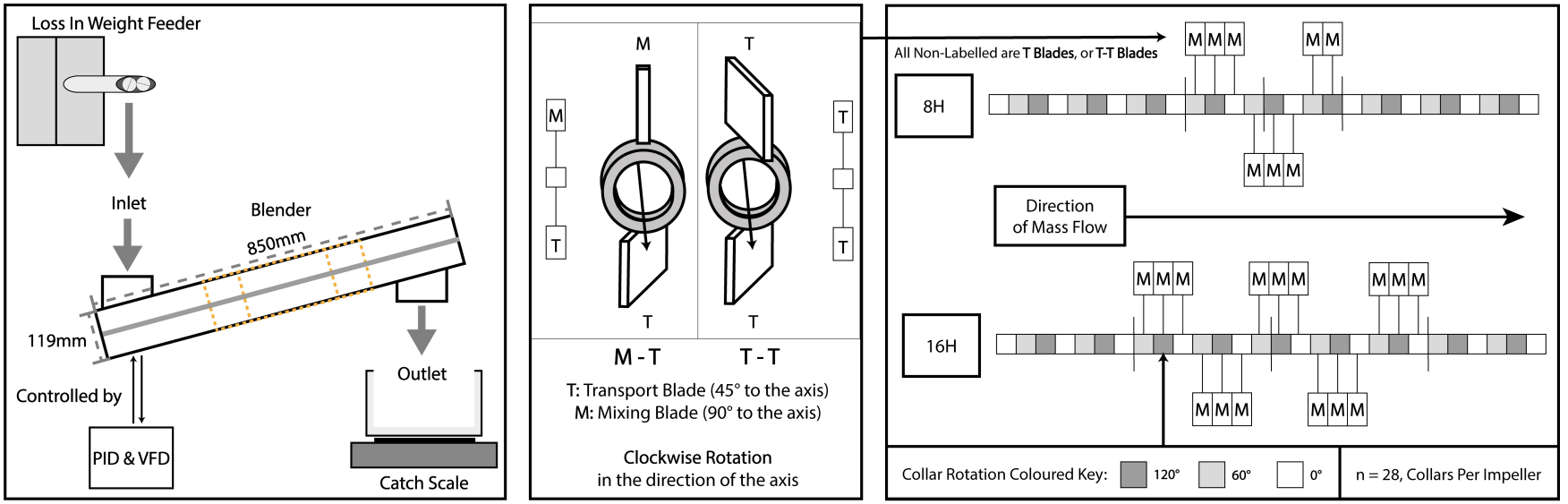


Figure 5.2: The above figure graphically describes the Experimental Set-Up, Blade Arrangement, and Impeller configuration used for the experiments

5.3.2 GEA, Compact Powder Feeder

The powder is fed to the blender using a Loss-In-Weight (LIW) GEA Compact Feeder (GEA, Dusseldorf, Germany). The LIW feeder holds roughly 2L of material and can operate in gravimetric (constant mass/time) and volumetric (constant screw speed, effectively constant volume/time) modes. Furthermore, the feeder is accompanied by a combination of a top-up ball valve, with varying volume inserts, and a 10L chute facilitating automatic system refills.

Gravimetric feeding operates by controlling screw speed to maintain a constant mass/time. Thus, a target feed rate can be maintained in the presence of powder flow disturbances, which may occur due to transient disturbances within the hopper or during powder transfer into the conveying screw volume. Therefore, gravimetric operation should be prioritised and the system's mechanical components should be configured to comfortably achieve the desired mass/time setpoint.

The calibration for the feeder is discussed in the following method section 5.5.1. The calibration allows for each experiment to have the highest gravimetric feeding up-time, meaning the feeding of each powder is as accurate and reliable as possible.

5.3.3 Mettler Toledo, Catch Scale

The XS64000LX Mettler Toledo Balance (Mettler Toledo, Greifensee, Switzerland) was used to monitor the mass flow rate at the blender's outlet, recording mass (g) over time (s). Real-time response from the catch scale is used to monitor the mass flow rate from the outlet to ensure the system is operating at steady-state and to determine the residence mass at the end of the run. The scale is linked to Mettler Toledo's LabX software which records the mass at a frequency of 2Hz, saving it to an output file. The position of the balance, relative to the system, can be seen in Fig. 5.2. The fill level is then calculated from the residence mass and

the bulk density of that powder, the calculation is discussed in the following section 5.5.3.

5.4 Materials & Characterisation

5.4.1 Material List

Nine commonly used commercial excipients were used in this study, comprising: Avicel PH-101, Microcrystalline Cellulose, abbreviated to 'PH-101' (DuPont, Cork, Ireland), Avicel PH-102, Microcrystalline Cellulose, abbreviated to 'PH-102' (DuPont, Cork, Ireland), Avicel PH-105, Microcrystalline Cellulose, abbreviated to 'PH-105' (DuPont, Cork, Ireland), Vivapur 350, Microcrystalline Cellulose, abbreviated to 'VP350' (JRS Pharma, Rosenberg, Germany), Fast Flo 316, Lactose Monohydrate, abbreviated to 'FF316' (Kerry, Tralee, Ireland), Pharmatose 110M, Lactose Monohydrate, abbreviated to 'PH110M' (DFE Pharma, Veghel, Holland), Pharmatose 200M, Lactose Monohydrate, abbreviated to 'PH200M' (DFE Pharma, Veghel, Holland), Pharmatose 450M, Lactose Monohydrate, abbreviated to 'PH450M' (DFE Pharma, Veghel, Holland), A-Tab, Dicalcium Phosphate Anhydrous, abbreviated to 'A-Tab' (Innophos, New Jersey, USA), and Pearlitol 200SD, Mannitol, abbreviated to 'PT200SD' (Roquette, Lestrem, France). In addition, the formulation utilises two additional materials: Powdered Paracetamol, abbreviated to 'pAPAP' (Mallinckrodt, USA) and Gycolys, Sodium starch glycolate (SSG), abbreviated to 'Gycolys' (Roquette, Lestrem, France). Furthermore, the drug surrogate formulation (F) in Table 5.1, is made up of 4 materials at the following weight percentages: Powdered Paracetamol (27% *w/w*), Avicel PH-102 (41% *w/w*), DCPA A-TAB (27% *w/w*), and Glycolys (5% *w/w*).

The materials list was selected according to use in commercial formulations and their relation to one another, with the intention of filling the characterisation space occupied

by typical formulations. The first step was to select the more common formulation materials (i.e. PH102, 316FF and P200M), which had innately different material properties. Secondly, alternative grades of the same material were selected to evaluate the differences between the grades, allowing us to evaluate the effect of particle size distribution on both bulk characteristics and ultimate process outcomes. Lastly, after evaluating the characterisation space, additional materials were selected that either filled the characterisation spaces (e.g. PT200SD), provided an extreme value (e.g. VP350), or would be considered a good filler excipient for CDC formulations (e.g. ATAB), resulting in the final material list for the experiments.

Despite the powder (Vivapur 1000) investigated in Chapter 4 being excluded here, the mechanistic insights remain relevant. The microcrystalline cellulose used in the PEPT experiments is a free-flowing excipient, with flowability and intrinsic bulk density comparable to coarse MCC grades, and most notably to its finer grade equivalent, Vivapur 350, which is included in the modelling dataset. The larger particle size of Vivapur 1000 places it outside the domain of typical formulation excipients and could bias model training, providing the rationale for its omission and inclusion of Vivapur 350. Nevertheless, both experimental and numerical studies have shown that Vivapur 1000 is a suitable surrogate for other free-flowing excipients. Hu et al. demonstrated, through combined PEPT measurements and DEM simulations, that Vivapur 1000 exhibits reproducible flow and dispersion behaviour characteristic of low-cohesion powders [**hu2025dem**], while Zheng et al. employed it in GPU-enhanced DEM studies, where its high flowability and stable residence time distribution enabled robust calibration and validation of continuous blending models [**zheng2022dem**].

In Chapter 4, this free-flowing behaviour was shown to promote predictable transport through the blender and to enable clear differentiation of particle trajectories under varying impeller speeds and blade configurations. As Vivapur 350 and similar excipients exhibit analogous flow characteristics, the transport and mixing mechanisms revealed in Chapter 4

Table 5.1: Characterisation results for the ten materials and the surrogate formulation.

#) Material	Grade	Abbreviation	Basic Flowability Energy (BFE) [mJ]	Bulk Density [kg/L]	WFA @ 2kPa, 0.4Ra	1/FFC @ 2kPa	d10 [μm]	d50 [μm]	d90 [μm]
1) MCC	Avicel PH-101	PH101	202	0.35	13.4	0.26	26.3	69.4	142
2) MCC	Avicel PH-102	PH102	191	0.35	15.2	0.15	33.1	113	240
3) MCC	Avicel PH-105	PH105	81.9	0.37	49.4	0.47	7	21	49
4) MCC	Vivapur 350	VP350	124	0.86	3.87	0.01	377	432	509
5) Lactose	Pharmatose 110M	P110M	119	0.73	10.2	0.14	78.9	153	219
6) Lactose	Pharmatose 200M	P200M	128	0.60	44.5	0.31	21.8	57.8	122
7) Lactose	Pharmatose 450M	P450M	100	0.47	11.4	0.63	3	21	56
8) Lactose	Lactose FF316	316FF	274	0.61	36.5	0.08	39.8	92.9	173
9) Mannitol	Pearlitol 200SD	PT200SD	297	0.54	14.5	0.03	40.3	143	238
10) DCPA	DCPA A-Tab	ATAB	253	0.74	16.3	0.02	48.2	168	305
F) Formulation	Surrogate	—	242	0.58	11.6	0.12	23	123	257

can therefore be considered transferable. This provides complementary validation that the data-driven modelling approaches presented in this chapter capture physically meaningful blending behaviour rather than artefacts of a specific material system.

5.4.2 Material Characterisation & Methods

The powders in Section 5.4.1 were subjected to a series of powder characterisation tests to determine intrinsic properties and flow behaviour. These are described below and the results are given in Table 5.1. All characterisation measurements were repeated in triplicate, from which the mean value is used.

Basic Flowability Energy (BFE) was measured using the Freeman FT4 Powder Rheometer (FT4, Freeman Technology, Tewkesbury, UK). BFE is, effectively, a measure describing the energy required for a stainless steel blade to initiate and sustain the bulk flow of a powder. Powders in the FT4 rheometer are exposed to a comparatively similar form of excitation to those in the CDB-1, suggesting that this measurement method may provide useful predictors of the powders' behaviours in the blender. For more information on the measurement technique see Freeman [155] and for evaluation of the dynamics within the environment see Hare et al [156]. In the present work, each powder went under four conditioning cycles and

four test cycles.

Bulk density was measured using a 50ml glass measuring cylinder and scale, where the powder was loosely deposited into the cylinder amounting to the maximum (50ml) line. The powder mass is recorded and the bulk density is calculated (weight/volume). The samples were prepped by shaking the 250ml holding vessel, ensuring the powder was not consolidated prior to pouring the powder into the measuring cylinder. Pouring the powder from the holding vessel, the cylinder is then filled to the measuring cylinder's 50ml volume mark, the mass is recorded and used to calculate the bulk density. After each measurement, the powder was returned to the holding vessel before shaking the powder and taking another measurement. Furthermore, there was no manual intervention, agitation or extraction of powder while filling the cylinder- if the volume was not correctly poured the first time, the measurement was removed and repeated. Lastly, the bulk densities were all measured at the same time, negating the influence of humidity when comparing the results to one another.

Flow Function Coefficient (FFC, (using a consolidation pressure of 2 kPa) and Wall Friction Angle (WFA (0.4 Ra @ 2 kPa)) are two measurements describing powder cohesion and powder adhesion, respectively, characterised using the Schulze Ring Shear Tester (Dr. Dietmar Schulze, Wittenburg, Germany). For additional information on FFC and WFA see both Schwedes and Schulze [157] and Schulze [158]. Additionally, the FFC values were transformed into their reciprocal to linearize the measurement sensitivity. This is because it is difficult to discern differences between high values of FFC compared to low values of FFC.

Particle Size Distribution (PSD) was obtained from dynamic image analysis using the QICPIC Rodos (Sympatec GmbH, Clausthal-Zellerfeld, Germany), resulting in d10, d50 and d90 measurements. The Rodos powder disperser was set to 0.6 bar pressure and the M5 lens was used for all measurements.

It shows that the materials demonstrate a wide range of material properties (seen in

Table 5.1), spanning those that would be appropriate for a typical pharmaceutical formulation [134], offering a variation of suitably significant magnitude to successfully monitor their impact. The BFE can be varied from 81.9 to 297.2 mJ; Bulk Density from 0.346 to 0.86 kg/L; WFA from 3.87 to 49.4°; 1/FFC from 0.01 to 0.47; d10 from 3 to 367 µm; d50 from 21 to 432 µm; d90 from 49 to 509 µm.

VP350 has the highest bulk density, FFC and particle size distribution, and lowest WFA, whereas, Avicel PH-105 has the lowest BFE, lowest bulk density, and smallest particle size distribution, with the highest WFA. This is a rather striking result since both of these materials are different grades of the same material (MCC).

The characterisation techniques used in this study were selected based on their fulfilment of one or more of the following criteria: First, they closely resemble the processing environment – for example, the basic flowability energy, BFE, which directly involves the motion of a rotating impeller through a non-compacted particulate medium. Second, they are extensively used in literature to describe a particular behaviour – for example the FFC, which is widely considered to be an accurate measurement technique for quantifying powder cohesion. Third, they are simple and/or widely accessible measurements that succinctly detail bulk powder behaviour, such as bulk density. Furthermore, the fewer measurement techniques required for an accurate prediction, the lower the number of material characterisation experiments needed to make that prediction; as such, parameters were deliberately chosen to encode a considerable amount of information about the system into a single parameter. The result is a set of measurements which can be performed with relative speed and ease, and require minimal use of proprietary equipment.

It is worth noting that, while a simple poured bulk density measurement was sufficient for the comparatively free-flowing powders and formulations examined in this study, the use of the FT4's conditioned bulk density measurement may be preferable when investigating

more cohesive powders, as it provides a more reproducible and representative measurement. For the materials tested, both methods yielded equivalent results.

5.5 Methods

5.5.1 Feeder Calibration

Before the feeder is used to take a measurement, it must be calibrated to ensure the system configuration can accurately dose the desired gravimetric (mass/time) feed rate. Therefore, duplicate/triplicate calibration runs are used to determine the feed factor profile and the hopper top-up strategy.

Feed factor is defined as the mass delivered (from the feeder spout) per screw revolution (g/rev). Due to the differences in the physical properties of the materials used, the loading of the conveying screw and behaviour within the hopper will vary with each material, so each one must be calibrated prior to each investigation.

The feed factor profile is gained through GEA's calibration method, which effectively measures the feed factors whilst emptying the hopper from full with volumetric feeding. The hopper is separated into 10% fill level intervals (F_n), the mass fill of the hopper is then divided into 10 slices in the vertical direction, and the average feed factor within each of those intervals is stored against that hopper fill level. The resultant profile (see Fig. 5.3) provides insight into the stability of powder dosing, at constant screw speed, with the expectation that free-flowing powders will have minimal change in feed factor across the full range of fill levels. Had a material being discharged suffered from disturbances to feeding, changes to either the gear ratio or screw type/pitch would have been tested to ensure a more consistent feed. Fortunately, the calibration was assessed for all materials and found that the same

gearbox ratio of 63:1 and a pair of conveying screws with a concave pitch of 10 mm width were appropriate for all tests.

Lastly, the feed factors are also used to define the stable operating region for the hopper fill level for triggering a hopper top-up event. This was done by plotting mean feed factors from F_9 (full hopper) to F_0 (empty hopper)(100% into 10% intervals, respectively) and identifying the most stable region during discharge. From this, the time and volume of the top-up event were defined, for each material; this event was to be initiated during the stable period of the volumetric emptying and the volume of top-up was selected to be the total volume dispensed over the identified stable region. This was then validated and optimised to ensure the automatic refills occurred with the largest proportion of gravimetric feeding to volumetric feeding. For three different grades of the same powder, the refill window is indicated by red dashed lines in Fig. 5.3.

This methodology ensures that the system operates with the utmost accuracy and reliability. The stable operating region, describes the operating window that is most resistant to feeding variance under volumetric operation, signifying that the feeding is the least sensitive to the fill level within the hopper. This is because the powder above compresses the powder below, as explained in Engisch and Muzzio 2015 [30]. This means that during a top-up event, when the feeder switches from gravimetric to volumetric, the feeder will show a consistent and accurate feed in grams per revolution, which is indicated by the aforementioned feed factor profile.

5.5.2 Residence Mass (RM) Measurements

Residence mass (RM) is defined as the mass of powder within the blender's mixing volume during steady-state operation. Several studies have highlighted its importance for improving

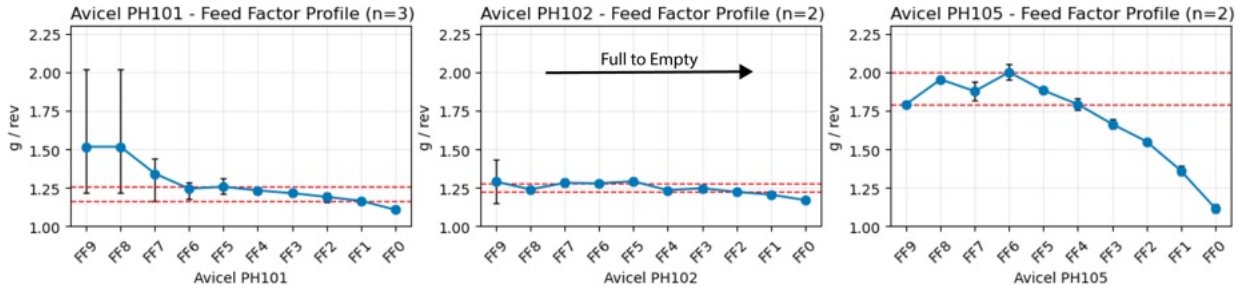


Figure 5.3: Three example feed factor profiles, showcasing the profiles for the three different grades of the same material, Avicel (MCC). Error bars indicate the range of values from the duplicate/triplicate calibration runs (indicated by $n =$ in the graph's title). The red dashed lines indicate the feed factor at which the top-up occurred. The following windows were used for the three powders: FF1 to FF4 (0.8L top-up) for Avicel 101, FF2 to FF6 (0.8L top-up) for Avicel 102, and FF4 to FF6 (0.4L top-up) for Avicel 105

the macromixing potential of pharmaceutical blenders [159, 79, 32]. RM is particularly useful because it can be measured directly, without sensors, detectors, or imaging devices. Its real value lies in its sensitivity to both processing parameters and material properties. For example, increasing RPM reduces RM (Section 5.6.1) and enables calculation of the Mean Residence Time (MRT, Equation 5.1). Together, RM, RPM, and MRT form the basis for evaluating strain (Equation 5.3, Section 5.5.3).

$$\text{MRT (s)} = \frac{\text{Residence Mass (g)}}{\text{Feed Rate (g/s)}} \tag{5.1}$$

Each run begins by setting the blender to the target RPM. Once at speed, the LabX software records the powder mass exiting the blender via the catch scale. Simultaneously, the GEA Compact Feeder communicates with TwinCAT 2 (Beckhoff, Henley-on-Thames, UK), exchanging operational data such as hopper weight, screw speed, and gravimetric mode. Once both dispensing and receiving data are recording, the feeder is set to dispense gravimetrically at the desired setpoint.

The powder is delivered into the blender until steady state is achieved, confirmed when the feeder's mass flow matches the catch scale's. During this period, RPM is controlled by a feedback loop from the proximity sensor and variable frequency drive. At steady state, all equipment is stopped simultaneously, and the RM within the blender is measured.

To measure RM efficiently, the blender is run at 450 RPM without powder input. The powder mass emptied to the catch scale is recorded (Fig. 5.4). As 450 RPM does not fully empty the blender, the residual mass was quantified (by manual extraction) and confirmed to be independent of speed history. This residual was determined after a sequence of runs (150–450 RPM) and treated as an offset, which was then added to the "450 RPM empty" values across all feed rates and blade configurations.

Mass removal during emptying is inherently time-dependent, particularly at 450 RPM. Therefore, the mass discharged over time was recorded until stable, and an inverse log curve was fitted to extrapolate the mass at $t = \infty$ (Fig. 5.4). This standardised approach ensured consistency, with only minor differences (a few grams) across runs.

While Residence Mass (RM) underpins the experiment, the response is better represented as **fill level (%)**, defined as the volume fraction of powder occupying the blender at steady state and calculated by normalising RM with blender volume (and bulk density) (Eq. 5.2). Expressing the results as fill level, rather than RM, provides a more transferable target for prediction, enabling like-for-like comparisons across materials, scales, and geometries. Beyond this normalisation, fill level has direct relevance to blending performance: it governs the flow regime within the blender, where low fills promote free-fall and poor exchange, high fills restrict motion and localise shear, and intermediate fills promote turnover and redistribution. These regimes are recognised to influence mixing efficiency and the likelihood of achieving homogeneity [160].

Effectively, fill level, as a composite measure, integrates material properties, process

parameters, and blender geometry, while serving as a practical proxy for bulk motion behaviour. Furthermore, as it is a function of RM it also provides access to MRT relating to a key descriptor for mass transfer, and therefore mixing performance. Consequently, fill level is adopted as the predictive target in this work and is used in place of RM when evaluating process parameters and identifying optimal operating regimes (Section 5.7.2).

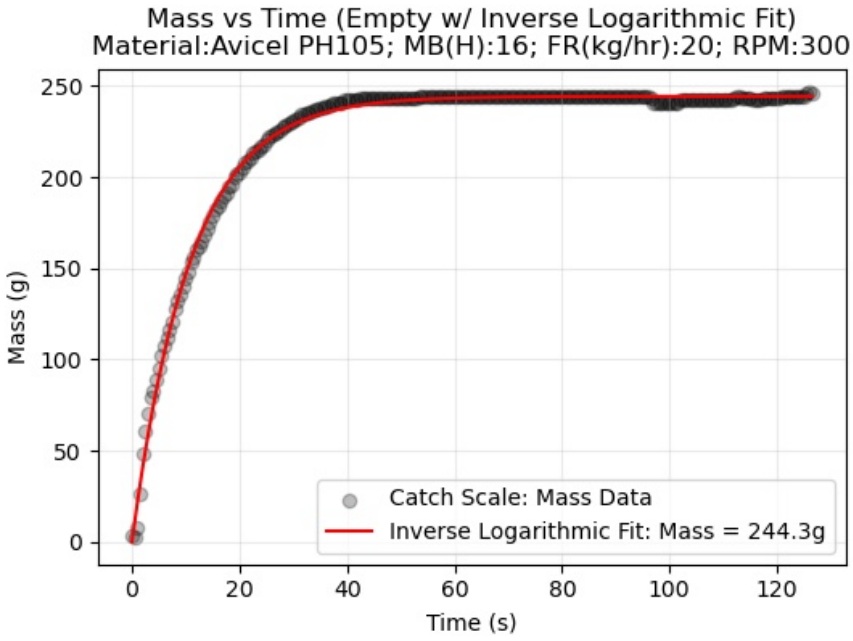


Figure 5.4: Example of a '450 RPM Empty', where the offset (remaining mass in the blender) would then be added to the asymptote collected from the curve fitting to gain the final residence mass at steady state.

5.5.3 Calculations

Fill Level

Fill level [%], is defined as the percentage volume the powder occupies within the mixing volume.

$$\text{Fill Level } (\%) = \frac{\left(\text{Residence Mass}/\text{Bulk Density}\right)}{\text{Mixer Volume}} \tag{5.2}$$

Strain

Strain (ω) can be considered as a measure of 'work done' to the powder. In the case of a continuous blender, it can be defined as the mean number of blade passes the powder flux would experience [83].

$$\text{Strain } (\omega) = \frac{FL \times \rho \times v_{blender}}{\dot{m}} \times \text{RPM} \tag{5.3}$$

The influence of the mixing blades is implicitly expressed in this equation due to how the mixing blades alter the fill volume and thus the mean residence time of the powder at a steady state.

where RPM is the rotation rate of the agitator in rotations per minute; ṁ is the feed rate in kg/hr; FL is the fill level (as a fraction) of the powder at steady state; $v_{blender}$ is the volume of the blender in m^3; and ρ is the bulk density of the powder in kg/m^3.

5.5.4 Predictive Modelling

The predictive modelling in this work draws on three complementary families of supervised learning algorithms to interrogate the same dataset from different angles. Random Forest regression, introduced by Breiman [63], combines many decision trees to produce accurate predictions while providing measures of variable importance that reveal which factors drive system performance. Feed-forward artificial neural networks are employed to capture complex, nonlinear relationships; these models follow the principles outlined in Goodfel-

low, Bengio and Courville's *Deep Learning* [64] and have proven effective at approximating intricate functions when sufficient data are available. To bridge empirical modelling and mechanistic insight, we also use symbolic regression, which automatically discovers analytical expressions that relate inputs to outputs; the approach pioneered by Schmidt and Lipson demonstrates how genetic-programming-based symbolic regression can extract interpretable equations from experimental data [65]. By integrating these ensemble-based, data-driven and equation-discovery paradigms, the analysis balances predictive accuracy with interpretability and lays a robust foundation for the results presented in this chapter.

Random Forest Regression

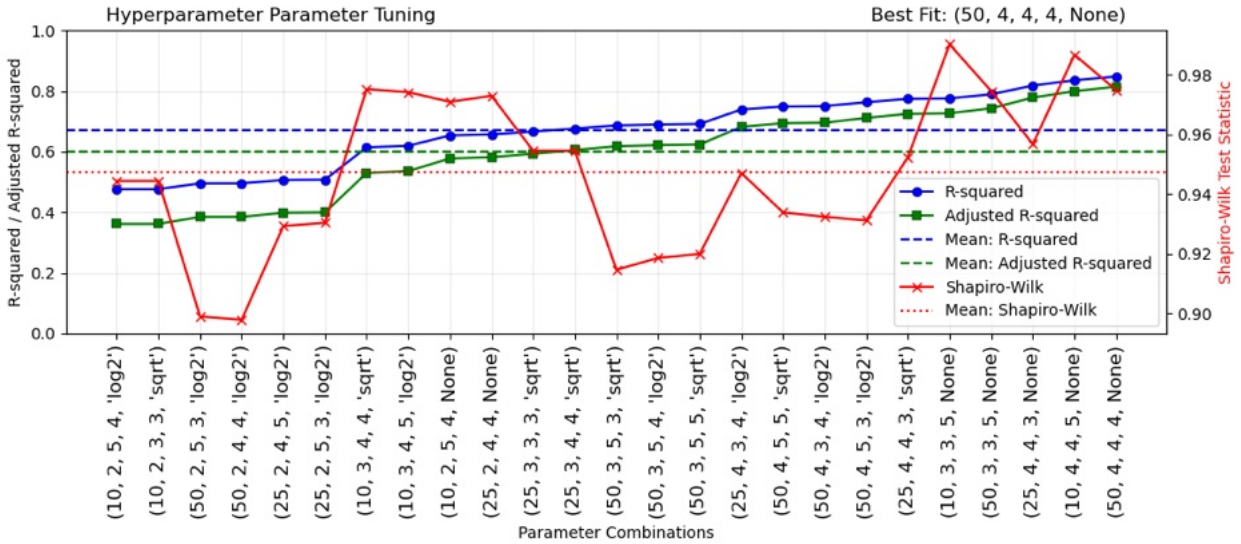


Figure 5.5: Random Forest Regression (RFR) Model Parameter Tuning. Results were ordered from worst (left) to best (right) r^2 value, with the secondary axis plotting the assessment of the residual's normal distribution using the Shapiro-Wilk Test (SWT)– higher SWT scores indicate a normal distribution. The x-axis shows the combination of the following 5 hyperparameters (in respective order): number of estimators, maximum depth, minimum number of samples to split, minimum number of samples for a leaf and maximum features.

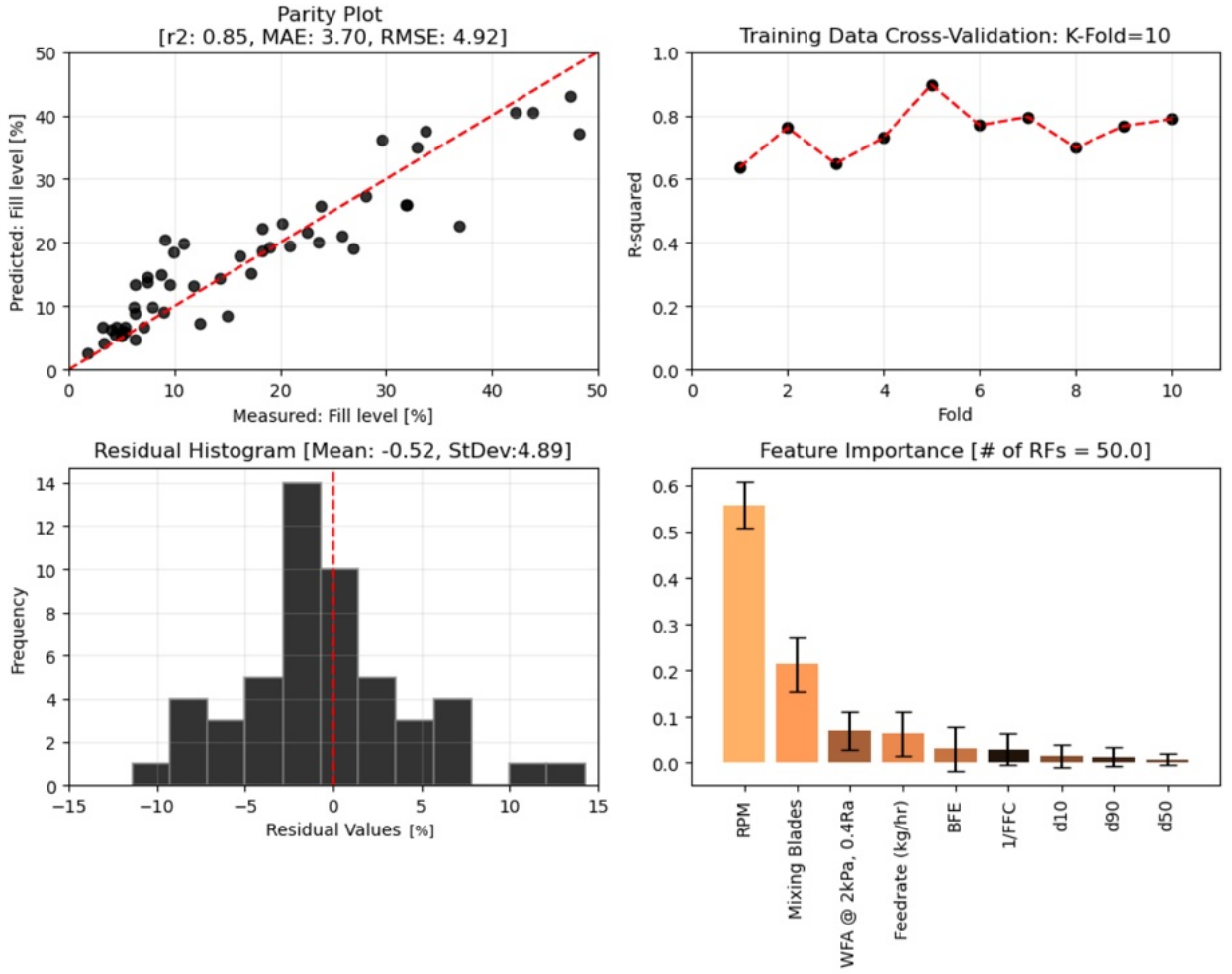


Figure 5.6: Random Forest Regression (RFR) Model Performance. The top left graph shows a parity plot of the measured vs predicted fill level. Top right, training data (only) k-fold cross-validation. Bottom left, RFR's residual histogram. Finally, the bottom right shows the Feature Importance (FI) of each of the parameters on the RFR's predictive capability, higher indicates more importance. The error bars show the standard deviation of the FI across the $n = 20$ generated estimators.

Despite the numerous insightful findings drawn from various studies using methods such as Partial Least Squares (PLS), [31, 161, 24, 90] the method presents a few key constraints. For instance, PLS is inherently linear and tends to obscure the intricate interplay of variables behind its principal components. In contrast, Random Forest Regression (RFR)

offers the ability to capture nonlinear relationships, providing a descriptive, 'logic-like' portrayal of the variables' interaction. When the primary focus is comprehending the system from both a material and processing perspective, it is crucial to understand these interactions and their resulting sensitivities.

RFR is a machine learning algorithm that combines the predictions of multiple decision trees to produce a more accurate and robust model. In this context, x represents an individual input data point (or a set of feature values) for which an output is to be predicted, while y is the actual output or response value corresponding to that input. Hence, for each instance of x, the goal is to predict its corresponding y value. This process can be depicted as multiple trees each making a prediction for a single x, followed by the aggregation of those predictions to obtain $\hat{y}(x)$.

In this formulation, $\hat{y}(x)$ denotes the predicted value for the dependent variable based on the input x, aggregating the insights from all n decision trees. Mathematically, given n decision trees, the prediction of RFR for an instance x is given by:

$$\hat{y}(x) = \frac{1}{n} \sum_{i=1}^{n} T_i(x) \tag{5.4}$$

In the context of the equation, $T_i(x)$ represents the prediction of the ith tree. Each tree is sculpted using bootstrapped data subsets, a technique where random samples are drawn with replacements from the original dataset, allowing some observations to be repeated in each sample. At every decision point, whether it's a split or a branching, a random selection of features (variables) is integrated to ensure that the trees are decorrelated and there is reduced inter-tree correlation. This inherent randomness can be observed in both the data samples and feature subsets. These techniques enhance the model's generalisation potential, making it more robust and accurate.

To train the model, the entire dataset was randomly split into a train:test split of 80:20 (203:51, datapoints respectively) and training data passed into the tuning stage of modelling. The RFR model was tuned by training approximately 240 models with different combinations of 'sensible' hyperparameter values: the number of estimators, max depth range, minimum samples to split, minimum samples for leaf, and maximum features range (for additional information on RFR see Sci-Kit's documentation: https://scikit-learn.org/stable/modules/generated/sklearn.ensemble.RandomForestRegressor.html).

To clarify the function of the aforementioned (RFR) hyperparameters, the following explanation(s) is provided:

- **Number of Estimators**: Specifies the total number of decision trees within the forest. Increasing the number of trees can improve the model's performance, but there's a threshold beyond which accuracy gains are marginal, trading-off for an increased computational cost.
- **Max Depth Range**: Designates the maximum depth or levels each tree can achieve. Deeper trees can discern more intricate data relationships but risk overfitting. An optimal depth strikes a balance between bias and variance.
- **Minimum Samples to Split**: Specifies the minimum number of samples required for a decision tree split. Increasing this value can prevent the model from incorporating small patterns that may be noise, which serves as a regularisation technique.
- **Minimum Samples for Leaf**: Specifies the minimum number of samples required to be at a leaf node (end of tree branch). Increasing this value, like the prior hyperparameter, can prevent overfitting and enhance generalisation across training examples.
- **Maximum Features Range**: During optimal split determination, the number of features to consider is specified. Random feature selection for each split promotes tree

decorrelation and model generalization.

In this context, **sensibility** refers to the principle of aligning the complexity of the model with the size and richness of the dataset being modelled. For large and complex datasets, it is appropriate to use more expressive models (e.g. multilayer neural networks with a greater number of parameters) that can capture intricate nonlinear patterns. Conversely, applying the same level of complexity to a relatively small or simple dataset risks overfitting, where the model begins to learn noise rather than meaningful trends, thereby reducing its practical utility. To avoid this, hyperparameters are initially selected within a conservative range considered to be 'sensible', balancing model flexibility against the risk of overfitting. The results obtained from these initial hyperparameter choices then provide feedback for subsequent refinement, ensuring that the final model is both robust and generalisable.

The resultant fitted models were then rank-ordered for r^2 (and adjusted) and plotted alongside the residual's frequency distribution, which is then quantified by the Shapiro-Wilk test (SWT); The Shapiro-Wilk test (SWT) is a statistical analytical test which checks whether a sample comes from a normally distributed population. The null hypothesis (1) assumes that the data is normally distributed, while the alternative hypothesis (0) assumes otherwise. A normal distribution would indicate a lesser propensity for the model to under- or over-predict values, while a narrow distribution indicates lesser error between the measured and predicted values; both a normal and narrow distribution are thus desirable.

The final selected model (Fig. 5.6), which held the following hyperparameter values: number of estimators (50), max depth range (4), minimum samples to split (4), minimum samples for leaf (4), and maximum features range (None), possessed a high r-squared value of 0.85 (showing a good fit) whilst demonstrating a good normal distribution of the residuals (quantified by the SWT, which was 0.97)– see Fig. 5.5. Any additional hyperparameters were held at SciKit Learn's default values.

The RFR model's performance is shown in figure 5.6, by the Parity Plot and Feature Importance graph. The Parity plot is the use of the model to predict the 'test' data, which is not used to train the model and shows a good r^2 fit of 0.848. However, there is considerable spread in places, leading to higher RMSE values– namely the cluster of points that are over-predicting at 10% fill. Furthermore, there is greater variability at the higher fill levels but this is potentially due to increased sparsity of data points at higher percentages. This sparsity at these higher fills, is a feature of the experiment, due to RPM highly dominating the system, irrespective of material or alternative process parameters (discussed in Section 5.6.1); the result is a higher number of points around lower fill levels due to increased RPMs.

The generated data from the full experimental dataset indicates that most operations should be at or below the 35% fill mark. However, further experimentation within these higher fill levels, through both material and process changes (e.g. higher feed rates), would provide the model with greater reasoning, and therefore, the improved capability to predict these fills.

The model was intentionally limited, in terms of accurate predictive capacity, to be able to derive the 'logic' from the system. In this simplified model, only the most important features will be shown, with the most contrasting changes between turning at each feature. This is done in contrast to having fewer samples to split and minimum samples for leaf– which would result in more and longer branches to reach the answer– giving rise to less granular predictions. Accordingly, these trees with higher complexity result in a cumbersome tree with many turns, inevitably resulting in the loss of 'what factors *really* matter'.

Artificial Neural Network (PyTorch)

Artificial Neural Networks (ANN or NN) have demonstrated a great ability to make predictions from data on a wide range of applications. The following ANN model was developed from the guidance provided by Goodfellow et al.'s [64] comprehensive book on machine learning (ML); the book covers foundational elements of ML in detail, with Chapters 5 and 7 playing a pivotal role in this model's creation.

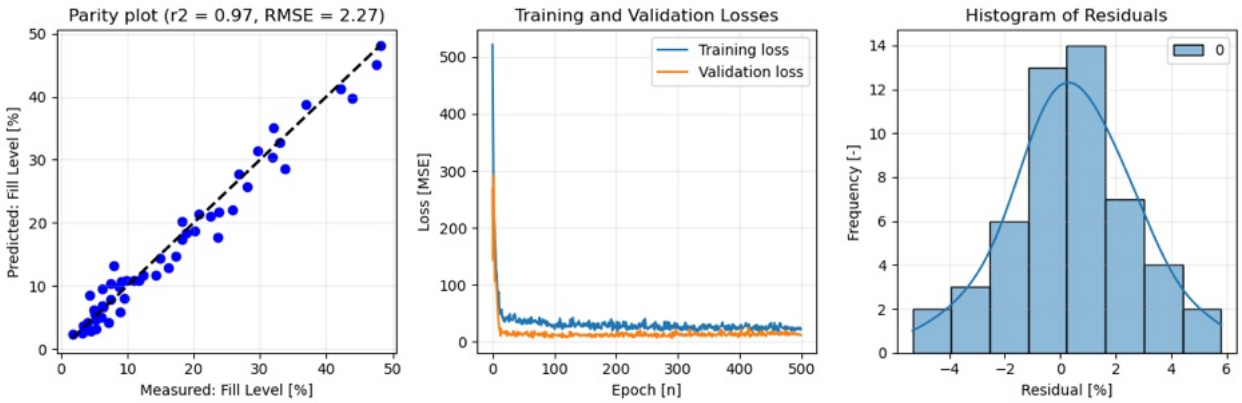


Figure 5.7: ANN training and performance: Left, parity plot of the measured vs. predicted fill level percentage. Centre, training and validation losses (in MSE (Mean Squared Error)) of the model vs. the number of epochs. Right, histogram of the residuals (measured - predicted). The relative root mean squared error was 12%.

ANNs function by propagating input data through layers of artificial neurons. These neurons apply a linear transformation followed by a nonlinear activation function. Mathematically, each layer's output, h, is computed as:

$$h = \sigma(Wx + b) \tag{5.5}$$

In equation 5.5, σ represents the activation function empowering the model to capture intricate relationships between inputs and outputs. The term W stands for the weights, which dictate the significance of each input. The bias b adjusts the neuron's output, while x is the input to the neuron. As data is fed into the network, it undergoes transformations by each layer. The process, known as forward propagation, continues until the final layer produces the network's output or prediction. The connections between neurons, characterized by the weights and biases, determine the strength and nature of the relationships the network captures. However, after a single forward propagation, the network's predictions may not be accurate. This is where *backpropagation* comes into play. Backpropagation is an optimization algorithm used for minimizing the error in the predictions. It works by computing the gradient of the loss function with respect to each weight by the chain rule and iteratively adjusting the weights and biases in the direction that reduces the error. An *epoch* refers to one complete forward and backward pass of all the training examples. By running multiple epochs, the network continues to refine its weights and biases, aiming to enhance its prediction accuracy over time.

ANNs are complex systems that require iteration to configure and fine-tune model performance. The following hyperparameters (used for the model) are detailed and described below:

- **Architecture**: This study employs PyTorch to construct an Artificial Neural Network. Given the dataset's size, this architecture was chosen to be relatively simple to prevent overfitting, which occurs when the model becomes too closely tailored to the training data and performs poorly on unseen data.
  - **Input Layer**: Comprises 9 nodes, corresponding to the number of features in the dataset.
  - **Hidden Layers**: Two hidden layers with 41 and 14 nodes, respectively, were

employed to transform the input data prior to the output layer. As emphasised by Goodfellow et al. [64], network capacity must balance accuracy and generalisation: too few nodes risk underfitting, while too many increase the likelihood of overfitting without regularisation. Initial comparisons of large and small networks showed no benefit to substantially increasing size. Consequently, a configuration of 41 nodes in the first hidden layer was chosen as the basis (half of the input layer squared), with systematic evaluation of alternative sizes (41, 14), (64, 21), and (128, 42) used to assess sensitivity and accuracy within a constrained architecture. The final model parameters were selected on a similar basis to what has been shown in Chapter 5.5.4.

  - **Output Layer**: A single-node layer, providing the final prediction.

- **Hidden Layer Nodes (Linear)**: Each node applies a linear transformation to the data, based on the weights and biases. Using the following equation: $h = \sigma(Wx + b)$. These nodes within the network form the basis of the prediction.

- **Activation Function (ReLU)**: Defined as $\sigma(z) = \max(0, z)$. It introduces non-linearity into the network, allowing the model to understand and represent complex relationships in the data.

- **Dropout Rate (0.0155)**: A regularization method where a fraction of neurons are randomly deactivated during each training iteration. This helps in preventing the model from over-relying on specific neurons and mitigates overfitting.

- **Learning Rate (0.0185)**: Determines the magnitude of adjustments made to the network's weights during training. A smaller learning rate means slower convergence but possibly more precise outcomes, while a larger rate could speed up the training but risk overshooting the optimal solution.

- **Epochs (500)**: Refers to the number of times the entire dataset is presented to the network during training. More epochs can allow for better learning, up to a point, after which overfitting might occur.
- **Batch Size (32)**: The number of data samples processed before the model's internal parameters are updated. Using batches is more memory-efficient than using the entire dataset.
- **Optimizer (ADAM)**: An optimization algorithm that adjusts the weights of the network. ADAM is known for its adaptive properties, where individual learning rates are computed for each parameter.
- **Loss Criterion (Mean Squared Error (MSE))**: Measures the squared differences between the predicted and actual values. The goal during training is to minimize this value.
- **Data Normalization (MinMaxScaler)**: Transforms features to lie in a range between 0 and 1. This ensures that no particular feature dominates the learning process due to its scale, leading to more balanced and efficient training.
- **Other Hyperparameters**: Any parameters not explicitly mentioned were kept at PyTorch's default settings to maintain stability and general best practices in training.

The Python package OpTuna was utilised to methodically search for the best combination of two vital parameters: learning rate and dropout rate. The learning rate determines how quickly the model updates its weights in response to the calculated error, while the dropout rate is a technique where certain neurons are randomly "dropped" or deactivated during training to enhance model robustness. OpTuna's search spanned across 100 combinations, bounded within $1e^{-5}$ to $1e^{-1}$ for the learning rate and 0.0 to 0.5 for the dropout rate.

The performance of the model was gauged through a combination of metrics, visualised in Fig. 5.7.

First, a key indicator of a good model includes a steady decrease in the training and validation loss (centre), indicating that the model is learning, and a close match between these two loss curves, suggesting minimal overfitting. The training loss provides a measure of the model's error on the data it is actively learning from, effectively the loss seen at its current epoch. The validation loss measures the error on a separate subset of data not used during training (unseen data at the current epoch), offering insights into the model's ability to generalise to new, unseen data.

Second, once the model has been trained on the 'training data' (80% of the dataset) the model is asked to predict the remaining 'test' (20%) data, the result is the parity plot (left)– which further validates/indicates the model's ability to predict unseen data. The fit of the model can be quantified by an RMSE of 2.27(%) and a high r^2, which in this case is exceptional with 0.97.

Third, a residual histogram plots the distribution of the actual data minus the predicted data. A narrow and normal distribution here would conclude that the model has minimal bias under or over-predicting across the range of predicted test values. In addition, the frequency distribution of the residuals is greatly improved compared to the RFR's.

Lastly, the developed ANN was investigated using SHAP (SHapley Additive exPlanations) analysis, a method rooted in game theory [162]; further details and documentation can be found at https://github.com/slundberg/shap. Effectively SHAP treats each discrete data point as a player and allows the 'game' to unfold to determine which features are the most 'useful' for predicting the response variable. The resultant is a graph (fig. 5.8) similar to that found in the RFR's Feature Importance (fig. 5.6).

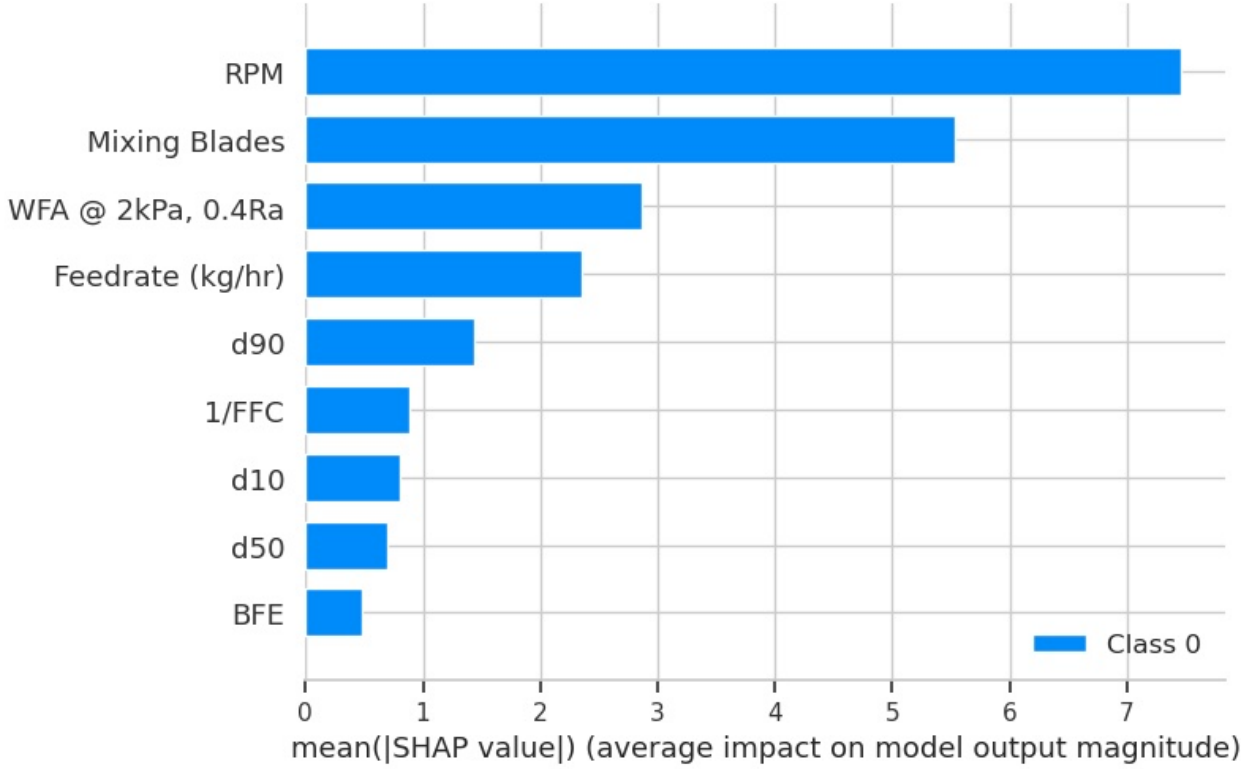


Figure 5.8: ANN SHAP analysis, showing the mean of the modulus SHAP Values. Effectively, the average impact of each of the variables on the output magnitude. This is then ranked-ordered from the most influential feature to the least. The scale quantifies the relative importance of the variables.

The top-performing features match in the same rank order for both models; highlighting the reliability of these factors in the prediction of fill level. The remaining features differ in rank order suggesting the models utilise the remainder of the variables differently. Alternatively, it suggests that the variables (and/or the differences between them) are statistically insignificant compared to the important ones.

5.5.5 Symbolic Regression – M^2E^3D

Multiphase Materials Exploration via Evolutionary Equation Discovery - or M^2E^3D, further abbreviated simply to MED, is a data-driven tool for discovering analytical equations modelling the underpinning physics or correlations of industrial systems that are too complex to be modelled from first principles [152, 153]. The core algorithm of M^2E^3D is its symbolic regression engine, the *SymbolicRegression.jl* library written in the Julia programming language [163, 164], which discovers analytical expressions f mapping given input values X to a measured output $y = f(X)$; the general algorithmic steps are:

1. The user selects the operators available to the symbolic regression engine, including common binary operators (addition, multiplication, etc.) and unary operators (log, sin, etc.) or custom functions - allowing users to incorporate some domain knowledge into the equation search, e.g. if the process outputs are modelled against system geometry, trigonometric functions might be included.

2. The operators, along with inputs and fitting coefficients are combined in a tree to form equations (see Figure 5.9).

3. The free coefficients are fitted against the measured data y and the residuals are computed $f(X) - y$.

4. An evolutionary algorithm is used to minimise both residuals **and equation complexity** (the latter measured simply as the number of branches in the equation tree) - this multi-objective optimisation problem is necessary to discover sensible, physical, interpretable equations rather than overfitted chains of functions.

5. The process of equation generation - fitting - evaluating - evolving is continued until the best-performing equations at each level of complexity are found to stabilise (i.e.

not change between generations) - and hence a Pareto front of equation complexity-accuracy is found.

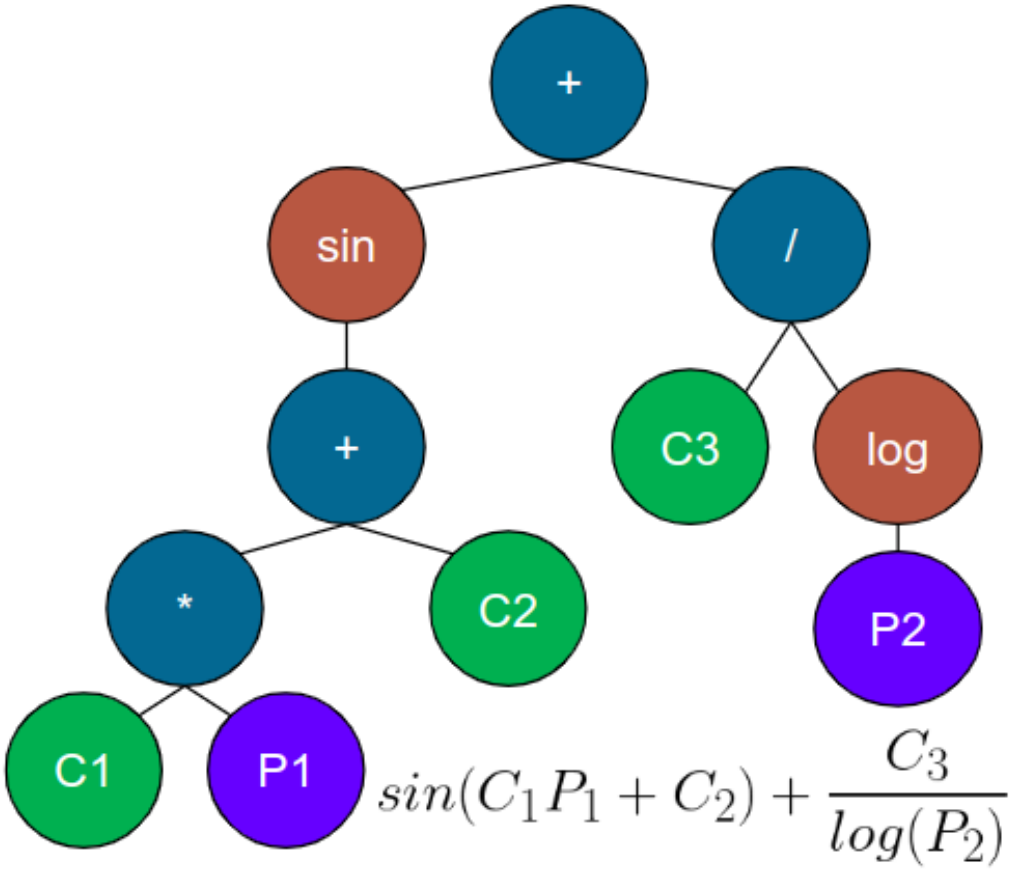


Figure 5.9: M^2E^3D representation of an example analytical model (bottom right), built as a tree with its nodes (circles) representing input parameters (purple), constants which need fitting (green), binary operators (blue) and unary operators (orange).

The main advantages of the technique include:

- **Interpretability**: the equations found give insight into the underlying physics governing the system, while coefficients bear physical units which, again, allow physical interpretation of the correlations found.

- **Robustness against noise**: as equation complexity is also minimised, the most persistent underlying physical terms are identified, naturally removing measurement noise.
- **Requiring few measurements**: if the system is governed by underlying physical laws whose inputs are included in the training data, identifying them requires $O(10)$ data points, which is orders of magnitude lower than what surrogate models and neural networks typically require.
- **Ability to solve the inverse problem**: oftentimes it is not just a predictive model that is desired, but the ability to dynamically change a process input to achieve a fixed output (e.g. fill level); this is possible by rearranging the equations found and can be integrated in continuous on-line process control schemes.
- **Allowing some degree of extrapolation**: unlike virtually all surrogate modelling approaches, if an underlying physical law is identified (e.g. Stokes' law in fluid flow), it can be extrapolated beyond the input training data range to a point (e.g. in the previous example, until turbulence becomes significant).

Both the algorithm and the codebase for M^2E^3D can be found on GitHub: https://github.com/uob-positron-imaging-centre/MED

M^2E^3D has been trained on the same 80:20 train-test split data as the other AI/ML methods and produced an equation (Equation 5.6) whose specific form and interpretation are discussed below. The equation was then used to predict the test data and produced the parity plot shown in Figure. 5.10. It is recognised that there is a single prediction with a negative fill level, this would be considered erroneous and scrapped (since a negative fill level is impossible), but displays the potential limitation of selecting an equation which is not complex enough. M^2E^3D could also be told to use different or more complex operators and re-trained, this may improve the tool's ability to generate more suitable equations– for

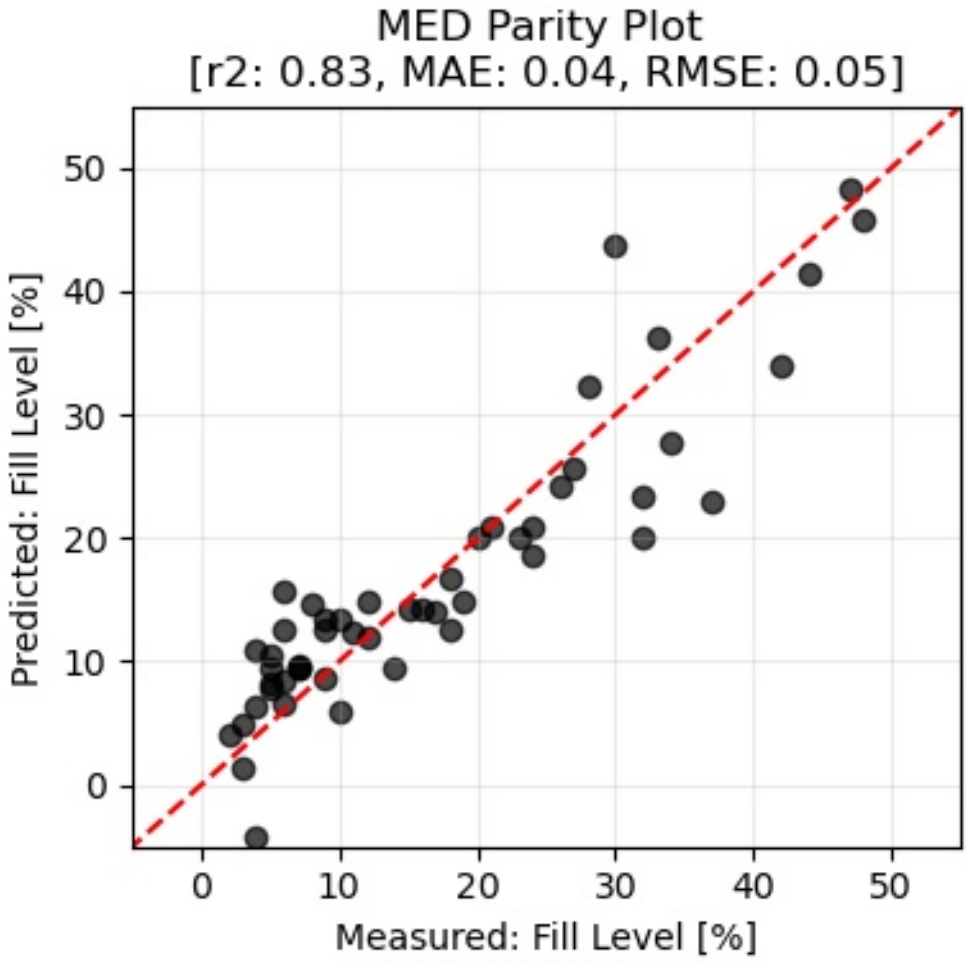


Figure 5.10: M^2E^3D Parity Plot, Measured vs Predicted. With an r-squared of 0.83, a Mean Absolute Error of 0.04 and a Relative Mean Squared Error of 0.05

the training of this model, it was limited to binary operators.

5.6 Results

5.6.1 General Data Trends

The correlation between the response and variables (normalised between +1 and −1) was calculated and plotted as a heat map (5.11). The correlations between the response variable, Fill Level, and the other variables highlight the effect that variables have on the response. For instance, it shows that RPM is highly negatively correlated with Fill Level, whereas Mixing Blades are moderately positively correlated with Fill Level. It is of particular interest how the material properties are related to the Fill Level– but there are no correlations of a moderate magnitude that point to a specific characteristic being a significant influence.

Plotting the fill level against RPM (shown in Figure.5.12) produces a clear, negative linear trend, and in some cases resembles a reverse Sigmoidal curve. The figure. 5.12, shows the fill level response against the three processing parameters: RPM, Mixing Blades, and Feed Rate. As mentioned, RPM dominates the system, reducing the fill level, irrespective of both material properties and mixing blade configuration. A higher feed rate sees a translation upwards, effectively increasing the fill level- but not necessarily changing the shape of the curve- this is seen to have an increased effect for a higher mixing blade configuration (16H). Perhaps this is due to a decrease in axial transport in the centre of the mixing volume, and so there is less direct transport of the powder from the inlet to the outlet. Moreover, increasing the higher mixing blade configuration, resulted in higher fill levels across the rpm range but had a lesser effect at higher RPMs– again suggesting RPM is the most influential parameter on fill level. These observations agree well with prior experimental and numerical studies [93, 79, 83, 32, 76, 133].

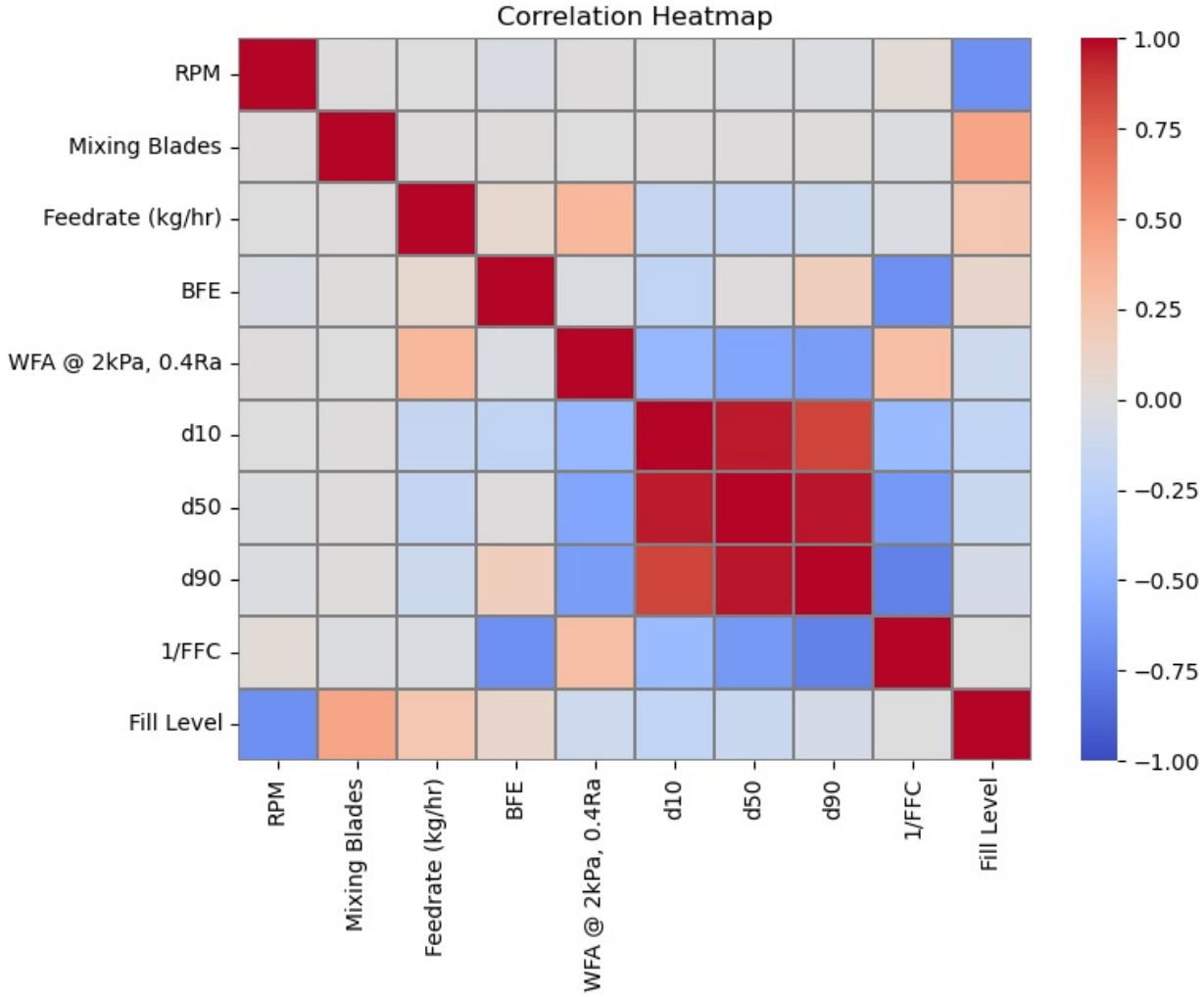


Figure 5.11: Correlation Heatmap (-1 to +1) between Process Parameters, Material Properties and Response Variable (Fill Level). The colour bar indicates the positive correlation (+1, Red) and negative correlation (-1, Blue)

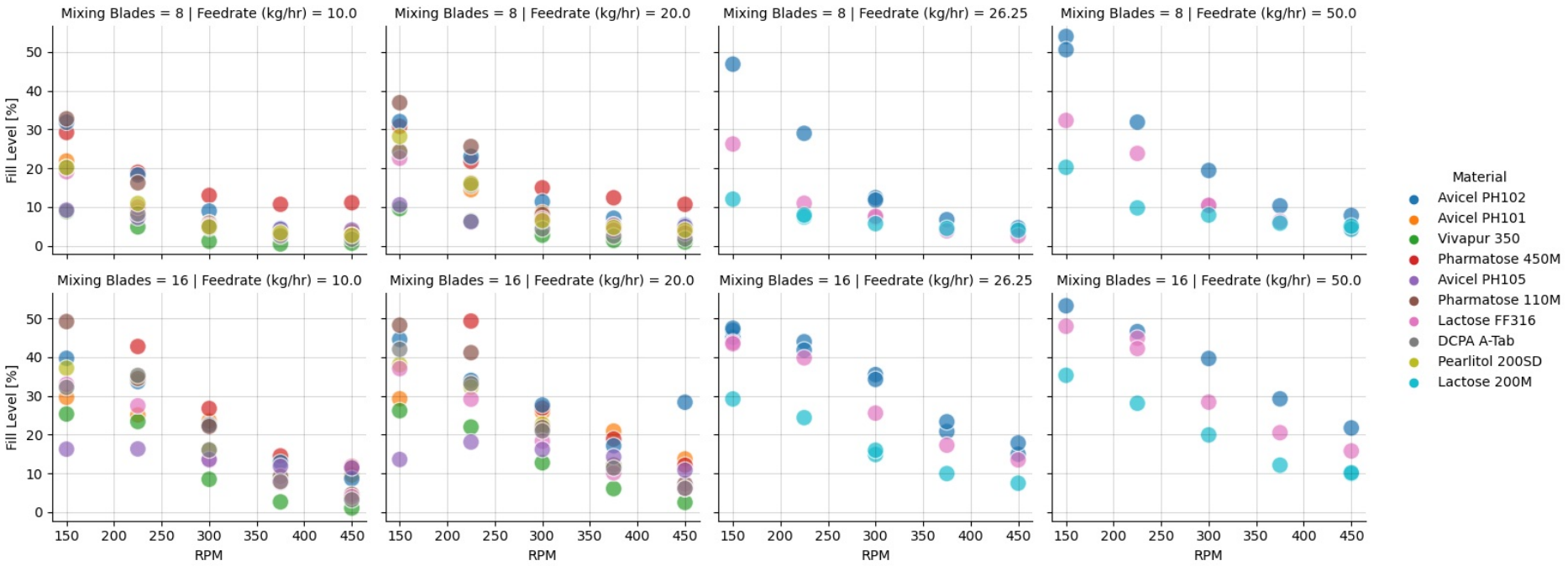


Figure 5.12: Scatter graphs showing the fill level response of the materials used for the experiment with respect to the three processing parameters: RPM, Mixing Blades, and Feedrate (kg/hr)

5.6.2 Model: Random Forest Regression

Evaluating the general data trends with a single material property provides no significant distinction or correlation. This may be due to the difficulty of discerning a true pattern with a single bulk characteristic– as it would be considered too granular. Therefore, their behaviour can be better understood by modelling how these bulk characteristics interact with other material characteristics or process parameters.

The decision tree (35 of 50), seen in Fig. 5.13, showcases an example of the logic output. The tree can be interpreted by moving down the tree from the initial top node. Each node then passes another if statement, questioning *if* the assessed sample possesses values greater or less than what the node is asking, which will decide the following node. The final box (called a *'leaf'*) contains the predicted (value) Fill Level %, for the specific path of logic gates used to reach the leaf.

The results align with Section 5.6.1, insofar as saying that both RPM and Mixing Blades show great significance on the final fill level as these parameters dictate the breadth of the fill levels, sitting at Tier 1 and 2 of the tree. Interestingly, BFE, WFA, d10 and RPM show on the 3rd tier but these are shown to be dependent on the fill level at this point. Furthermore, this is reflected in the initial correlation plot (Fig. 5.11), meaning that at higher fill levels BFE and WFA are shown to be factors to make a further distinction on the fill level.

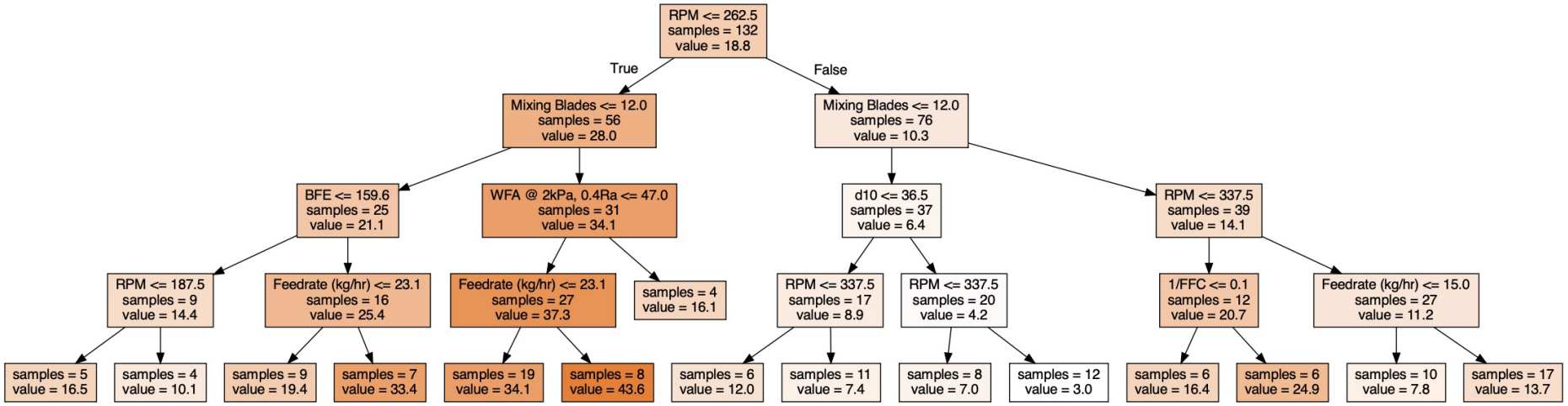


Figure 5.13: Decision Tree (35 of 50) from the Random Forest Regression Model, with darker colours indicating high Fill Level. Samples refer to the number of data points, and value is the mean Fill Level for those samples– in percentage (%)– for that node.

Furthermore, when evaluating the positional importance of a node it is also important to consider the colour of the node– which highlights the mean fill level of all samples at the current node. It is shown at higher fill levels (where motion is likely more frictionally dominated), particle physical properties influence the prediction, demonstrated by the position and colour association of BFE, WFA and FFC. Whereas at lower fill levels (where motion is more likely collisionally dominated) the rotation rate seems to dominate; intuitively described by the increased influence of processing parameters due to the reduction of powder volume and the resultant increase in both the frequency and intensity of particle-wall collision and reduction of particle-particle contacts.

5.6.3 Model: PyTorch ANN Feature analysis & Contour Mapping

The wall friction angle (WFA @ 2kPa, 0.4 Ra) is shown to be the material characteristic with the greatest feature importance in the model, which holds true for both ANN and RFR models. The practical application of understanding this is formulation adjustment. Different excipients can be paired with the existing blend or powder, in order to modify the final powder characteristic.

The result of this allows a quality-by-design approach, as the prediction allows for the understanding of how sensitive a particular property is to processing parameters. This is especially important when building in robustness and early mitigation of risks associated with potential batch-to-batch variation.

This operational sensitivity is best shown in Fig. 5.14, where the two highest-ranking operational parameters have been plotted against the range of WFA values used to train the model. Thus, the sensitivity of the material property can be effectively gauged.

The model shows that the effect of WFA on fill level is, generally, lower at rpms

greater than 300– agreeing with the RFR decision tree (Fig. 5.13). At these RPMs, the fill level is lower, typically ranging from 6-20%, which complements the previous discussion point (from the previous section) on collision-based bulk motion/mixing. The mixing blade configuration comes into play by holding up more mass, promoting a higher fill level. This interaction, which promotes more 'frictional' mixing, results in a more complex interaction between the WFA and the discussed process parameters. This is best demonstrated by the change of shape and colour across the three contour plots.

The application of this knowledge in a practical setting suggests that: if there were (for example) a perturbation from the feeder and thus a slight transient change in the formulation's WFA (due to compositional change), this combination of parameters would provide greater confidence that the fill level (and thus the desired process outcome) will be preserved. This methodology and philosophy build in key quality by design aspects to harmonise formulation development and operational robustness.

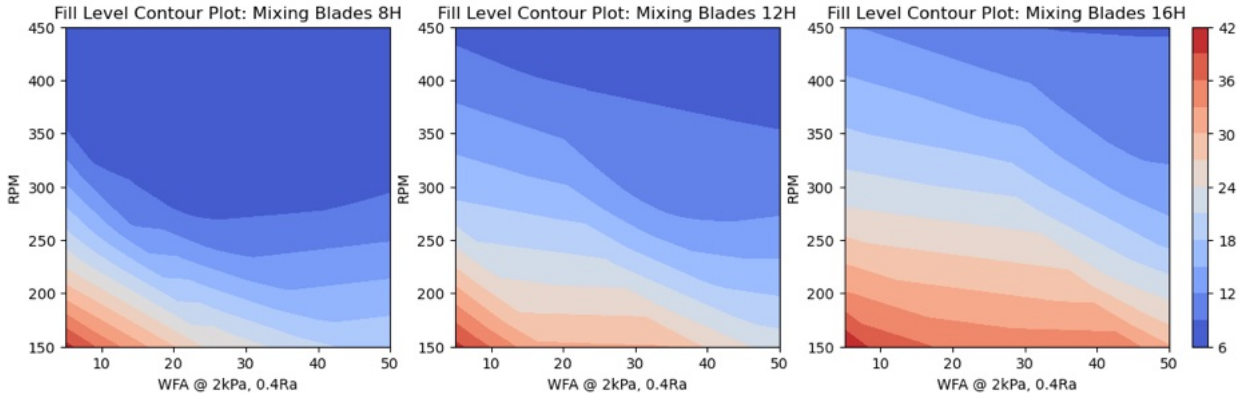


Figure 5.14: Fill Level Contour Plot Prediction using the ANN as a function of RPM and WFA. The (shared) colour bar indicates the fill level in percentage for the 3 plots. The held values for the contour plot are as follows: RPM (150-450), MB (8, 12, 16), Feed Rate (22 kg/hr), BFE (188 mJ), WFA (5-50), d10 (61μm), d50 (122μm), d90 (206μm), 1/FFC (0.189)

$$\text{Fill Level} = 100\Big(\,0.0032\,\text{Feed Rate} - 0.003\,\text{WFA} - 0.0004\,d_{10}\; + \tfrac{4.284\,\text{Mixing Blades}}{\text{RPM}}\Big) \tag{5.6}$$

$$`Predicted = 100 \times (t1 + t2 + t3 + t4)' \tag{5.7}$$

5.6.4 Model: M^2E^3D's Symbolic Regression

While ANNs and random forest regressors can be interrogated to some extent – as has been demonstrated in the preceding sections – they remain, to some extent 'black boxes'. M^2E^3D's methodology (discussed in section 5.5.5), meanwhile, produces complete, closed-form equations to describe the behaviours of the systems to which it is applied. For the present data set, the M^2E^3D equation which provided the highest 'score' was the following:

The linear equation can also be viewed as separate terms (seen in 5.8), where the following terms can be used as descriptors for their relation to the fill level. Furthermore, these equation terms can be evaluated using an ANOVA. To do this, the M^2E^3D Equation's terms were gathered and fit into an OLS (ordinary least squares) model before assessing the statistical significance of each of the terms.

The ANOVA results can be found in Table 5.2. Each term was found to have significance in predicting fill level, which was expected as M^2E^3D ensured that every term was significant. However, by assessing the sum squared variance of the prediction based on each term's sensitivity—quantified as the change in the predicted fill level in response to a standardized perturbation, such as a 1% or 10% increase from the mean value of each term—the relative importance of each term in predicting fill level can be determined.

The rank order is as follows: $t4 >> t1 > t2 > t3$. This indicates that the fourth term is responsible for the largest range of variability in the prediction. These findings align with

$$
\begin{aligned}
&\textit{Where:} \\
&[\textit{Predicted}] \rightarrow \text{Fill Level} \\
&[t1] \rightarrow (0.0032 \times \text{Feed Rate}) \\
&[t2] \rightarrow (-0.003 \times \text{WFA}) \\
&[t3] \rightarrow (-0.0004 \times \text{d10}) \\
&[t4] \rightarrow \left(\frac{4.284 \times \text{Mixing Blades}}{\text{RPM}}\right)
\end{aligned}
\tag{5.8}
$$

the other modelling (in sections 5.6.2 and 5.6.3) methods as they show RPM and Mixing Blades to be the most important features for predicting.

Table 5.2: ANOVA Table for the generated M^2E^3D equation (See Eq. 5.6) based on the split terms (See Eq. 5.7 and Eq. 5.8), showing the sum squared variance (sum_sq), degrees of freedom (df), F-Statistic (F) and P-Statistic (PR(>F))

	sum_sq	df	F	PR(>F)
Term1	0.38	1	7.1e+15	0.00e+00
Term2	0.35	1	6.8e+15	0.00e+00
Term3	0.29	1	6.2e+15	0.00e+00
Term4	2.96	1	2.0e+16	0.00e+00
Residual	0.00	249	nan	nan

5.7 Discussion

5.7.1 Blind Formulation Validation and Model Comparison.

The described models (Sections. 5.6.2, 5.6.3 and 5.6.4) have been developed with the same single excipient data. In this section, the ability of the models to accurately predict the behaviours of a full pharmaceutical blend is tested, despite considerable limitations in their training data. The same experiments were run using a 4-component blend that served as a surrogate for a real drug formulation, in which the active compound of the campaigned drug was replaced with powdered paracetamol, ensuring that the final characteristics of the surrogate blend remained representative of the campaign. The surrogate was validated by ensuring the bulk properties of the surrogate formulation and the true formulation still possessed similar bulk physical characteristics (notably the bulk density and FFC), after the proprietary API was switched out. The bulk characteristic behaviours of this blend were gathered using the same methodology described in Section.5.4.1, and included in the final row of Table.5.1.

The experiments measured the fill level of the surrogate formulation at 3 speeds (250, 350, 450 rpm) at 15kg/hr feed rate and 16 mixing blades. The blend's material characteristics were then measured and used to predict the fill level. The results can be seen in Figure. 5.15. The models were all, to varying degrees of precision, able to predict the fill level of the blend and the variation thereof with RPM. This means that, despite the complexity of a multi-component formulation, there is a correlation between the formulation's characteristics and the resultant fill level. This is an important and potentially exciting finding, as it suggests that the models developed may be used to predict the behaviours of new formulations with no additional training.

The prediction accuracy ranked the model's Mean Absolute Error (MAE) in the

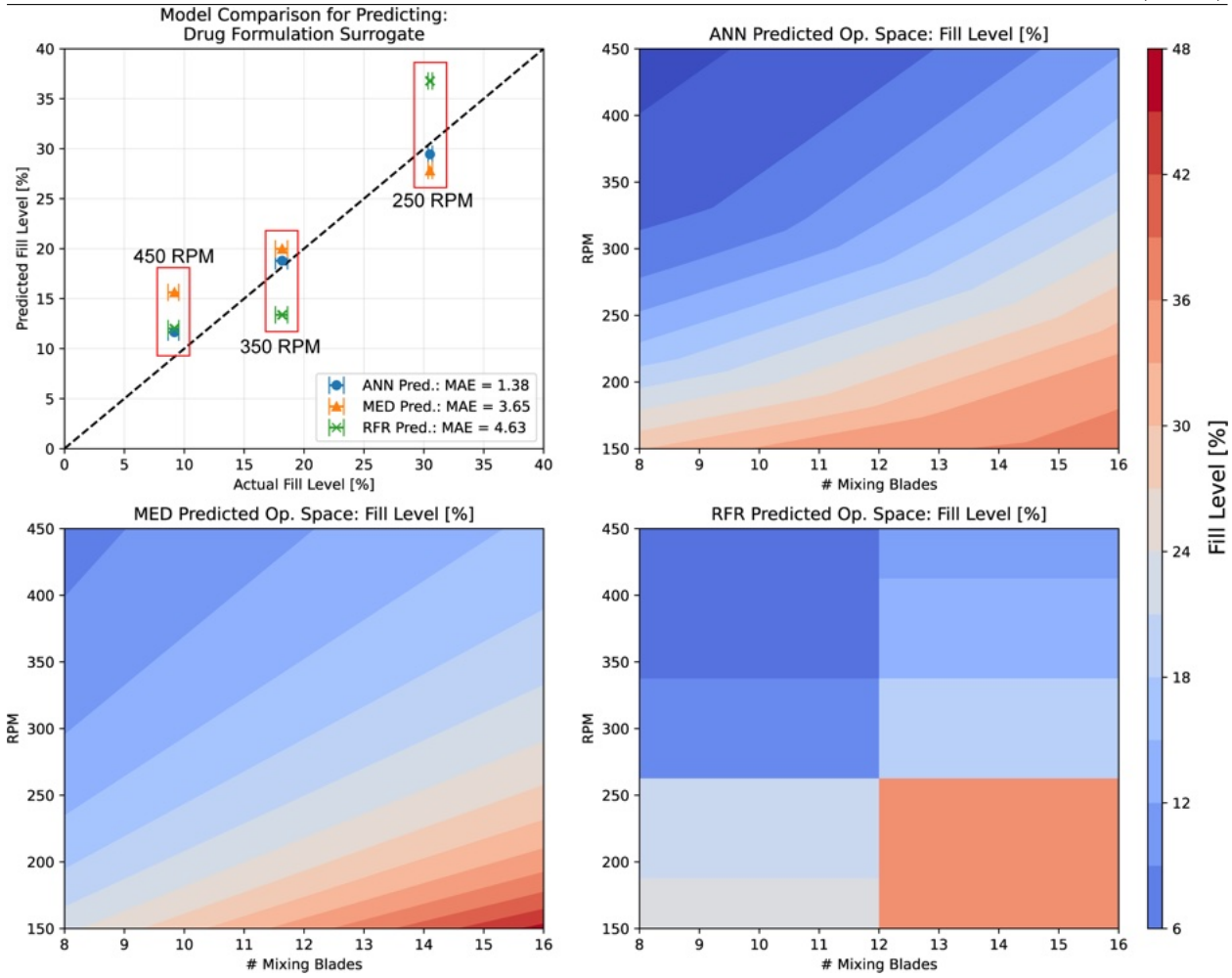


Figure 5.15: Parity Plot between the experimental and predicted fill levels. The parity plot shows the three different models predicting the fill level. Each experiment was repeated 3 times, the mean is shown and the bars indicate the range of values (on the x-axis). Each model demonstrates the operating space between the RPM and mixing blades. The three models are ranked by the MAE (Mean Absolute Error) prediction of the experiment. Subsequently, an example of the design space showing the two most important processing parameters is plotted for each of the models. The model's contour plots are indicated by the graph's title. Furthermore, all contour graphs share the same colour bar and number of gradient steps (12) between the min and max.

following order ANN (1.4), M^2E^3D (3.7), and then RFR (4.6). The contour plots between the ANN and M^2E^3D are similar, displaying similar fills in the same areas. ANN and M^2E^3D differ in terms of linearity, M^2E^3D generally presents a very linear progression of contours– with tighter packing (of boundaries) in the lower corner and wider packing at the maximum. ANN showcases complex shapes and curvature, which has been shown to be advantageous for prediction. RFR, on the other hand, shows almost categorical boundaries. highlighting that despite the granularity of the model, there are some key features which allow for reliable fill level prediction. Ultimately, the following can be said: using each of the predictive methods provides a trade-off between accuracy and conceptual understanding. By using all three tools, however, one can achieve both highly accurate prediction, as well as strong mechanistic insight.

It is important to note that data-driven models exhibit the highest predictive accuracy within the bounds of their training data. While the models demonstrate strong predictive capabilities within the parameter ranges on which they were trained, the same level of accuracy cannot be guaranteed outside this parameter space. Nonetheless, as additional experiments are conducted, the model can be retrained and the predictive confidence boundary correspondingly expanded. Furthermore, if the blender used were not fixed in inclination, it could be another processing variable for the training data. Thus making it possible to evaluate the mixing conditions across a wide set of inclinations, improving applicability for other commercial blenders.

5.7.2 Predicting Mixing Performance

Strain, determined as the number of blade passes through a given powder (calculated using Equation 5.3) has been demonstrated to be a strong predictor of good mixing in several prior publications [83, 93, 76, 24, 133].

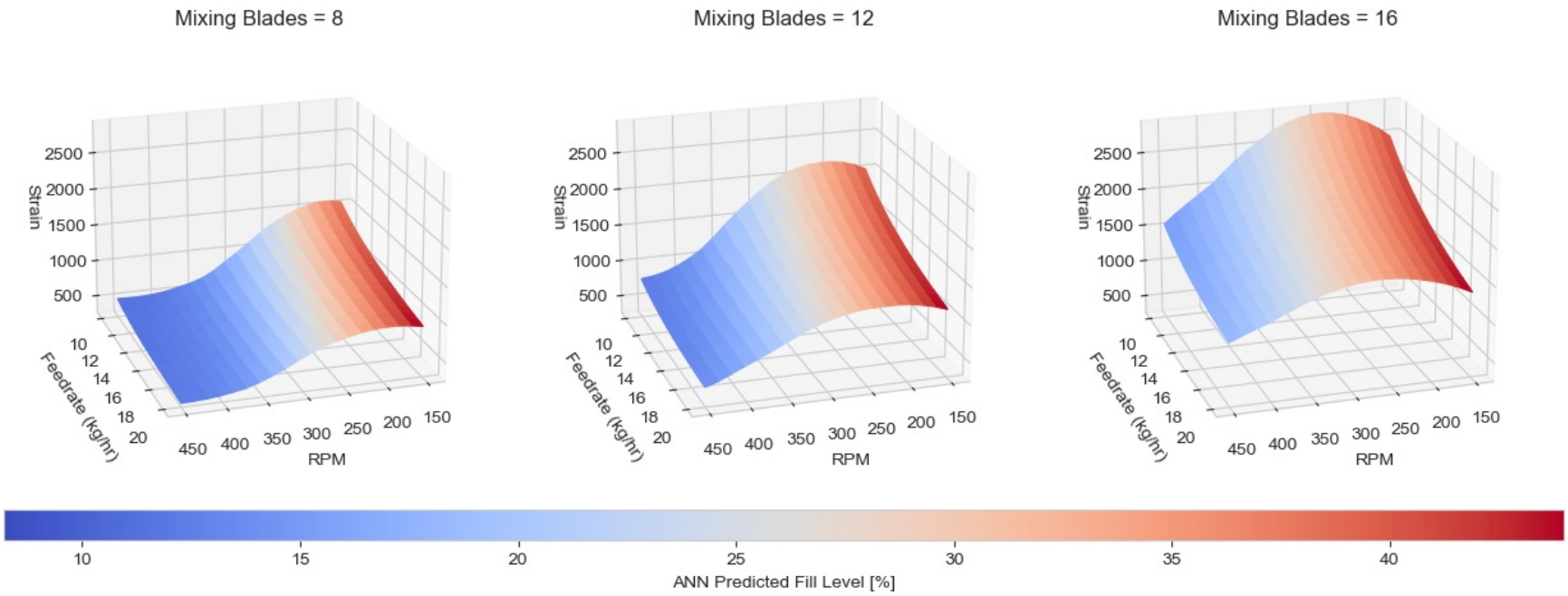


Figure 5.16: Surface plots showing the strain by the three processing parameters for the drug surrogate formulation. The continuous parameters (those that can change during operation) share the same plot as the strain. The colour bar indicates the ANN predicted fill level, the three graphs share the same colour scale– allowing comparison.

Using the validated ANN, a given blend's material properties can be input to calculate the strain from the predicted fill level. The resultant strain values across the range of processing parameters can then be plotted as a set of surface plots in Fig. 5.16. The detailed landscape describes the interaction between the formulation's properties and the range of processing parameters in the context of mixing performance. The surface plots seen in Fig. 5.16 are generated for the surrogate formulation (detailed in Table 5.1). The surface plots are then coloured by the ANN's prediction of the fill level at those same conditions. The fact that the model is able to predict the surrogate accurately (demonstrated in Section. 5.7.1) provides confidence in the surface's shape and position of the colours.

It is immediately interesting to note that, irrespective of processing conditions, the optimum strain seems to consistently be found at or near a fill level of 1/3. The correlation suggests that the material in the blender has reached an idealised balance between the RPM and Mean Residence Time. To speculate on exactly why this occurs; it seems to suggest that the powder is, at this fill level, exhibiting regime-like behaviour which promotes ideal mixing conditions.

To better describe the hypothesis of optimum strain occurring around 1/3 fill level, it is useful to consider similar surrogate systems which show regime-like behaviour. There are two situations that can be conceptually related: rotating drums and fluidised beds.

- **Rotating Drums** utilise a single continuous motion within a batch vessel to mix the granular media within. Thus, when different processing conditions are used, the granular media (e.g. powder) within the drum demonstrate different bulk motion behaviours, which are described as regimes. Increasing the rotating speed of the drum, results in a progressive pulling of the granular media up the side of the drum in the direction of motion, resulting in regimes labelled as (from low to high RPM) rocking, rolling, cascading, cataracting, and centrifuging (to name a few) [138]. The transitions

between these regimes are known to be affected not only by drum RPM, but also fill level – as is the mixing achieved thereby [165]. If mixing is intended for the media, motions which cause high levels of granular dispersion (cascading/cataracting) result in improved mixing. In the context of the incline linear blender, the described 1/3 fill level suggests that this fill may be the balance for adequate powder volume for the powder to mix into (increasing MRT, and therefore macro mixing), whilst providing a sufficient mixing rate (RPM).

- **Vibrofluidised Beds** utilise mechanical agitation in the form of vibration to cause an effective reduction in gravity, invoking fluid-like or even gaseous motion of discrete solid particles [166]. To achieve this, a certain amount of agitation (i.e. a suitably high vibration strength) is necessary for the powder bed to reach fluidisation. Similarly, in the context of the inclined linear blender, the rpm agitator also has a mechanical agitation influence. The suggestion for the incline linear blender is that at a suitably high rpm (Froude Number), the motion of the impeller causes the powder to reach this fluidised state, in which the effects of both gravity and inter-particular cohesion are sufficiently overcome to markedly reduce the resistance to inter-particular mixing.

Thus the hypothesis describes the resulting regimen as a combination of the two situations but in the context of continuous powder blending, where the powder flux receives enough work through agitation, leading to semi-fluidised behaviour. This overcomes the effects of gravity and inter-particulate cohesion of the powder, therefore promoting the local displacement and replacement of powder leading to improved micromixing. When paired with higher 'H' mixing blade configurations (otherwise described as larger mixing zones) there is an increase in axial slippage, which promotes the similarly described re-constitutive behaviour as the cascading regime seen with rotating drums. This, in turn, explains that for a given powder (or formulation), feed rate and blade configuration there is an optimum rpm, at which the powder reaches this regime; which coincides with the blender being 1/3

full. Either side of this apparent optimal fill level leads into contact-dominated mixing (for higher rpms) or friction-dominated mixing (lower rpms)– similar to that outlined by Zheng et al. [133].

However, to attain this regime at a higher strain value- and therefore improved mixing, blade configuration is key, as it will manage the bulk mass- due to its role of promoting both axial and radial transport. In the context of this study, that would be the 16H configuration (when compared to 8H and 12H), which should, by these standards, supply adequate transport at the base (inlet), improved 'slippage' and radial dispersion in the mixing region, and lastly enough transport at the latter part of the barrel to remove sufficiently blended powder. This is supported further by the 'folding region' seen in the Positron Emission Particle Tracking (PEPT) study of Jones-Salkey et al. [154] which describes localised spatial residence time retention of powder in the former part of the barrel, just prior to the mixing zone.

While it is possible that this is a specific feature of the helical mixing blade configuration (H) arrangement, the findings implicitly suggest that alternative blade configurations can form different regime-like behaviour. Nevertheless, in this instance, it would be sensible to offer the use of the H-configuration in order to exploit the described feature. It would be interesting to evaluate alternative configurations, like those discussed in Van Snick et al [32], to see if they present varied regime-like behaviour; and if not, would the configurations they describe present different processing sensitivities to those regimes?

To expand upon the insights from Figure 5.16, let us examine how the proposed theory compares with the broader literature on this subject.

Building on the work of Kushner and Schlack [167], who explored the scaling of blending powdered lubricant in both bin and tubular batch blenders, they highlighted a parameter K that could scale blending across vessel sizes spanning five orders of magnitude,

given a constant Froude number of 0.4. Here, K denotes the 'amount of mixing', which is the product of the 'number of rotations (r)', the 'batch blender's characteristic length scale (L)', and the 'fraction of headspace ($F_{\text{headspace}}$)'.

K can be broken down into two components: 'mixing intensity' ($L \times F_{\text{headspace}}$) and 'mixing duration' (r). Specifically, the characteristic length roughly indicates the mixing region and the headspace gives the powder room to move, facilitating mixing. These combine to show the dispersive potential of each rotation. Meanwhile, the number of rotations conveys the number of times the powder undergoes dispersive rotations. Fortunately, for batch systems, these two components are de-coupled, meaning 'mixing intensity' can be compensated by increasing 'mixing duration', and vice versa.

Transitioning this concept from batch to continuous processes leads to the formulation of the strain equation (strain = rpm $\times$ mean residence time), where rpm and mean residence time encapsulate the mixing intensity and duration, respectively. In continuous systems, however, since the MRT is a function of RPM (assuming a constant feed rate), one cannot independently adjust intensity and duration, emphasising that a balance is required.

Critical to these discussions is the underlying principle that regardless of scaling in batch or varied continuous setups primarily depends on fostering particle-particle interactions—the real catalyst for mixing. This becomes evident in bulk powder flow regimes, especially visible in granular mixing within rotating drums.

Relevant studies by Van Snick et al [32], Palmer et al [76], Bekaert et al [90], and Zheng et al [133] offer deeper insights. The first three emphasize that maximizing strain results in better content uniformity in both horizontal and inclined (15°) linear powder blenders. The latter provides context on regimes.

Interestingly, Bekaert et al. [90], using a horizontal mixer, found no interaction be-

tween the number of blade passes and blend properties, which contrasts the findings of this study. The interpretation is that the inclination of the blender seems to play a pivotal role in powder transport, which is best illustrated by materials showing different fill levels at the same rpm- see Figure 5.12. This highlights the importance of understanding how the material properties interact with the geometrical differences.

Van Snick et al [32] indicated that in the same blender used in this study (15° linear blender), accurate and consistent content uniformity was achieved at intermediate residence mass and an intermediate rpm. This finding was reinforced when comparing two different blade configurations under identical conditions.

Moreover, Palmer et al, [76] demonstrated that after achieving a certain strain, there is only a minimal further increase in blend uniformity, effectively stating that there is an effective 'ideal strain' for a formulation which achieves optimal mixing for a minimal time- and energy-expenditure. Thus, by utilising this tool, the maxima can be predicted and used to work back towards the 'effective' strain. Such insights enable researchers to pinpoint the optimal strain for increased processing efficiency whilst ensuring consistent content uniformity. Furthermore, an additional graph shows a V-shaped dip in the Peclet Number (Pe) plotted against fill level, with the lowest point (of this V-shaped dip) at around 1/3 fill level. Pe number is a ratio which indicates a balance between advective and diffusive transport rates; which could be effectively described as a balance of micro-to-macro mixing. A Pe of one, seems to occur at the fill level that provides the highest strain (demonstrated in Figure 5.16).

Lastly, Zheng et al. [133] utilised calibrated DEM simulations to identify two distinct regimes, which transition at an intermediate RPM of 250. This aligns with the first logic gate in the RFR decision tree shown in Figure 5.13; whilst it is important to note, the model has similarly outlined this RPM across the ten different excipients and remains comparable

to the simulation.

In conclusion, the body of literature, when analysed in tandem with the findings from Figure 5.16, and the related discussions provide a comprehensive rationale of the behaviour being exhibited under these conditions. The significance of this should provide both researchers and industry professionals with an initial look into continuous blending regimens.

5.7.3 Application: Identifying the Strain Window

One potential practical application of these tools could be to adjust the process to compensate for a large disturbance. For example, APC could be used to reduce the RPM, and therefore increase the MRT, in response to a large disturbance. Following the disturbance, the RPM can be returned back to the steady-state set-point.

Referring to Palmer et al [76], the lowest rpm on the APC should match the most suitable point on the exponential decay curve, which could be effectively termed 'Strain Point (ω_P)'. This represents the minimum blade passes needed for desired content uniformity. Given that cohesive species are given an effective shear rate (tip-speed) to sufficiently break particle agglomerates/aggregates. This leads to questions for future research: *"what's the minimum tip speed required for effective blending of cohesive powders"* and *"are two **equal** strain values with different RPMs similar for mixing?"* especially concerning values above or below the specific shear requirement for a formulation.

The predictive toolkit illustrated in Figures 5.14, 5.15, and 5.16 enables the identification of the 'Maximum Strain' (ω_M) for specific processing parameters, which can be verified through subsequent experimentation. Upon confirming the attainment of minimum shear, the focus shifts to optimising the 'Strain Window' (ω_W)—defined as the difference between ω_M and ω_P—as shown in Figure 5.17. Experiments can be directed to maintain

content uniformity around the ideal RPM, as illustrated by points 2 and 3 in the figure. These experimental points establish a strain window from the lowest acceptable strain value to ω_M. Further exploration, as seen at point 4, could widen this window. For a comprehensive understanding of the process limits, additional guided experimentation, towards point n (ω_P), may be performed to identify the threshold of failure.

It is noteworthy that theoretically, the toolkit could streamline experimentation to just three pivotal points. This top-down approach defines a steady-state set-point and establishes bounds for upper and lower RPM ranges. Similarly, it can assess the impact of other variables like feed rate changes on blend properties.

The deployment of these modelling tools is instrumental in developing robust control strategies, offering a nuanced understanding of the process and its operational parameters up to the point of failure. This outlines a safer operating domain, ensuring the product meets

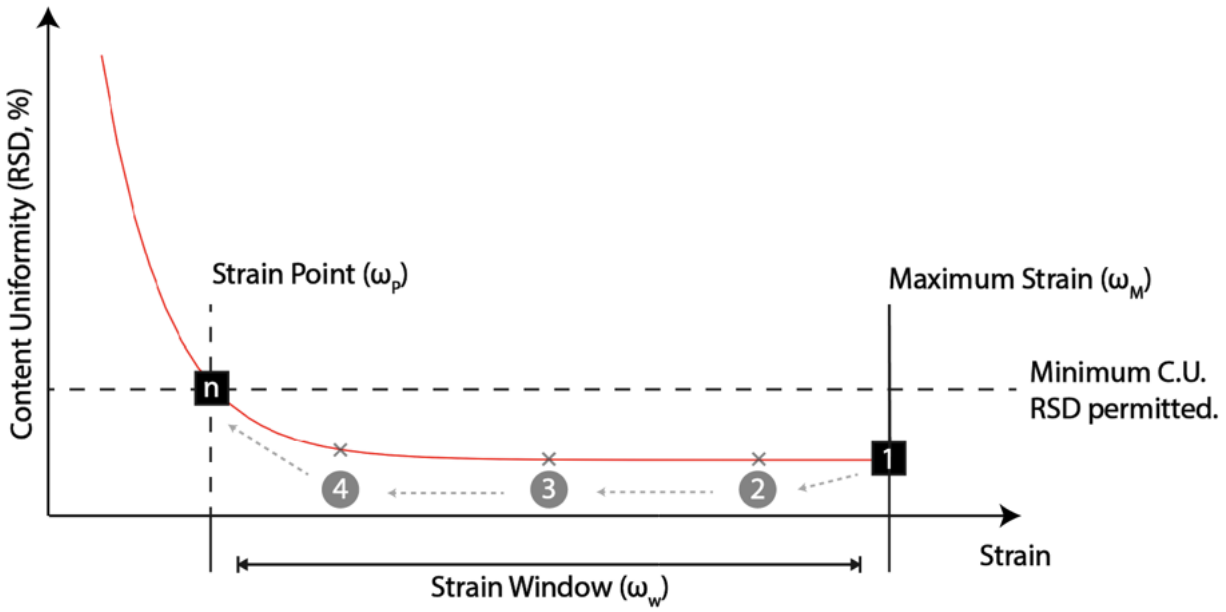


Figure 5.17: Graphical Representation of the Strain Window (ω_W). Points 2, 3, and 4, indicate guided experiments to find the Strain Point (ω_P)– or the expansion of the current Strain Window (ω_W).

critical quality attributes. The use of these tools allows this understanding to be achieved with reduced experimentation, which is particularly important as extensive large-scale experimentation can slow development as well as impact on cost and sustainability. Furthermore, they can verify the consistency of processes or formulations, valuable for modifications like reformulation or changes to processing set-points. This process similarity can be corroborated through a series of validation trials, affirming the model's accurate prediction of the operational landscape.

5.8 Conclusion

This paper presents several machine learning and artificial intelligence models for predicting the performance of a continuous pharmaceutical blender, while also facilitating new insight into its fundamental behaviours.

The methods used include RandomForestRegression (RFR), which extracts logic from the data; a novel symbolic regression and evolutionary AI tool (M^2E^3D), which produces complete, closed-form equations, effectively creating a reduced order model of the data; and Artificial Neural Networks (ANN), which provide more accurate predictions at the expense of a less-interpretable model. All three models independently identified the agitator speed (RPM), the number of mixing blades, the wall friction angle (WFA, 2kPa with 0.4 Ra coupon) and the feed rate (kg/hr) as the most important features for the prediction of fill level, and thus the strain experienced by the powder – an important predictor for mixing. By interrogating the models further, valuable insight into the dynamics and mechanics of the blender was gained through prediction of the operating space.

In terms of pure predictive capability, the ANN demonstrated the greatest strength, both for the single components on which it was trained, as well as in further blind validation,

predicting the behaviour of a 4-component formulation to a high degree of accuracy. Its ability to accurately predict the fill level of a previously unseen formulation, containing an API not included in its training data set, shows considerable promise for such an approach, in the future, to be used as a means of reducing the time and cost currently associated with bringing new drugs to market.

It is worth noting that an interesting correlation has been identified between the maximum strain and the one-third fill level (during steady state) in the prediction of the operating space. This correlation applies regardless of formulation or variable processing parameters, and it represents a crucial set point for blending processes that use a 15-degree incline blender. By achieving this, 1/3 fill level, set point during operation, a balance between advective and diffusive mixing can be attained. It is of further interest if other fill-level, and thus space-time, optimisations exist for other blending platforms and inclinations.

The magnitude of strain can be increased if the process is intensified- in effect simultaneously increasing both RPM and MRT. Yet, since RPM and MRT are coupled, increasing RPM will decrease MRT. Therefore, it is important to consider both the feed rate and the blade configuration. Decreasing the feed rate will increase MRT while decreasing the number of radial mixing blades will decrease MRT.

Given that maximising throughput is often desired, the blade configuration should be adjusted to include more radial mixing blades to retain higher fill levels (at the same RPM) and the RPM should be increased– thus intensifying the process. Similarly, this resolves the issue for highly agglomerated species, where using a higher RPM provides a higher tip speed, which then acts to break the highly agglomerated species. There may be slight differences between the clinical commercial equipment and the prototype (used in this study), however, the fundamental understanding remains the same. To validate this observation, additional runs were performed using various blade configurations, feed rates,

and surrogate formulations (as detailed in Section 5.3.1). These runs were not included in the model training. However, they have shown that the maximum strain is also consistently observed at a fill level of 1/3. In addition, these findings were checked against a backlog of development runs for other formulations using the GMP-compliant CDC-50 from GEA and saw the same relationship of around a 1/3 fill level delivering the highest strain values.

Ultimately, the predictive tools described in this publication can find this optimum range of processing parameters for a newly characterised formulation and then evaluate both the operational and formulation stability of that formulation within the blender. Said tools thus stand to both mitigate risk and reduce wastage of time, energy and materials during product development through prediction of the variability at these early phases, meaning a directed first-time-right approach to experimentation, validation and process establishment, carrying benefits both economic and environmental.

Acknowledgements

Experimental work was carried out as part of an Engineering Doctorate programme funded by EPSRC, United Kingdom through the Centre for Doctoral Training in Formulation Engineering (grant no. EP/L015153/1), and from AstraZeneca plc, United Kingdom. The computations described in this paper were performed using the University of Birmingham's BEAR Cloud service, which provides flexible resource for intensive computational work to the University's research community. See http://www.birmingham.ac.uk/bear for more details.

Chapter Six

Conclusion

6.1 Thesis Conclusion

6.1.1 Industrial Conclusion

The development of complex pharmaceutical products presents significant challenges. Multiple teams typically work in parallel, often with interdependent objectives, while facing the combined pressures of high regulatory standards, market competition, and the requirement to deliver high-quality medicines to patients. Achieving rapid, accurate, and cost-effective development is, therefore, difficult, with progress frequently constrained by trade-offs between these factors. Although this limitation remains true for current best practices, it can be mitigated through innovation. The work described in this thesis addresses a key challenge within AstraZeneca's CDC development process.

This contribution is reflected in three main areas:

1. The establishment of the MACH-1 GLS testing bench (Chapter 3), which enables rapid, modular, and cost-effective at-scale experimentation to inform and de-risk GMP clinical

supply campaigns.

2. The development of standardised ways of working and their integration into the product development pipeline, resulting in a practical playbook for powder feeding and continuous blending (Chapter 3).

3. The creation and deployment of digital tools for predicting processing performance, thereby reducing experimental burden and broadening access to complex modelling approaches. These tools were made possible by the insights gained from Chapter 4, which informed the modelling framework in Chapter 5.

Although each of these outputs could be considered individually, their interdependence is best demonstrated in Chapter 5, where a hybrid model (ML-mechanistic), trained on single-component excipients using data generated from MACH-1, was shown to predict the behaviour of multicomponent formulations. This model is independent of any specific drug project, allowing development teams to establish processing parameters for new formulations without re-building the framework from the ground up. The combined use of non-destructive characterisation methods and *in silico* experimentation further reduces cost and accelerates project timelines.

Ultimately, the Engineering Doctorate (EngD) iCASE programme has enabled the development of novel approaches that contribute to the wider scientific community while simultaneously addressing tangible industrial problems within the UK's largest publicly traded company (at the time of writing, Q3 - Q4 2024).

6.1.2 Technical Conclusion

This impact was delivered through the establishment of the MACH-1 (Chapter 3), where the prototype of a commercial continuous powder blender CDB-1 by GEA (Frankfurt, Germany)

was adjusted to align with the results of the GMP asset in Göteborg, AstraZeneca. Being resourceful was essential, as constraints such as facilities, budget, and lead times resulted in adaptations to the establishment. CAD drawings, 3D printing, liaising with facilities and fabrication teams, and risk assessments were actions taken that allowed the establishment to remain relatively flexible within these constraints. Once the modular GLS equipment was developed, installed and accommodated for business as usual, it, alongside the following chapters, was woven into the product development process. But in the context of this thesis, it enabled all the experimental work described in 4 and 5.

Chapter 4, outlines a key application of a unique and novel measurement technique. These experiments were able to describe and categorise the spatial-temporal pathing of particles in response to processing parameters, fundamentally describing how particles can be influenced through the adjustment of these parameters. Interestingly, a relationship was observed within the blender describing a 'folding zone', a region of powder slippage and turnover due to the combination of the geometrical inclination of the blender and the arrangement of the transport/mixing blades on the impeller. This "folding zone" interacted with the processing parameters, indicating that intermediate agitation rates coupled with a larger number of arranged mixing blades (which push powder azimuthally around the impeller's axis rather than pushing the powder up the length of the barrel) were optimal. This suggests that further studies using techniques such as PEPT or DEM could establish the finding and identify the key drivers of this behaviour, thereby exploiting it to improve mixing conditions. Lastly, the implementation and development of a GLS continuous blending rig allow for the collection of experimental data for the continuous blender, expediting and de-risking development activities. This has been a significant advancement for the department.

The deployed ANN model, featured in Chapter 5, provides a digital layer/twin to the MACH-1 and was developed in parallel with two additional models, all of which were interrogated using various techniques to identify the importance of the features. Interestingly,

the features, most notably in the Random Forest Regression (RFR) model, aligned with the results of other authors (Zheng et al. [133]) in the field. The RFR model specifically demonstrated two distinctive regimes around the 250 rpm mark: contact-dominated mixing and frictional-dominated mixing; further discussion on this can be seen in Chapter 5.7.2.

Importantly, typically for a given feed rate, the void fraction (fill level) and the space-time (e.g., mean residence time, MRT) are not independent: increasing the feed rate simultaneously raises the mass of powder within the blender and reduces the residence time available for mixing. In response, higher rotational speeds (RPM) may be needed to maintain a "peak strain rate" but this in turn can further decrease residence time as material is pushed through the system more quickly. Thus, these parameters, feeding rate, fill level, space-time, and strain rate, are interdependent rather than individually tunable.

Despite this coupling, the findings from this thesis suggest that there is an empirical optimum mixing often where strain rates peak, coinciding (for the blender used in this study) with roughly a one-third fill level. This phenomenon may reflect a blender-specific trade-off between the void fraction and mixing space-time. One way to rationalise this is considering the Péclet (Pe) number; a $\mathrm{Pe} \approx 1$ implies a balance between axial transport (throughput), convective transport, and dispersive (or diffusive) mixing. In practice, each blender design or inclination can change the exact fill level associated with $\mathrm{Pe} \approx 1$, but the principle remains the same: balance feed rate and mixing intensity (RPM) to maintain a zone of maximum strain rate and thus optimise continuous blending performance.

Investigating whether this one-third fill level is similarly optimal in other inclined or geometrically different blenders would help confirm the broader applicability of this relationship. By balancing void fraction, residence time, and mixing intensity, manufacturers can pinpoint and sustain the strain-rate "sweet spot" essential for achieving consistent, high-quality blends under real-world process conditions. Furthermore, it may also be sensible

to alter a given formulation in ways that allow an effective mixing regime over a wider strain window, expanding this “sweet spot" (for example, increasing the flowability of the formulation), particularly when operating at higher feed rates.

6.2 Future Work

The scope of future work is vast and, as a result, it would make sense to focus the scope into areas in which the greatest industrial impact could be seen.

6.2.1 Scaling Over & Technology Transfers

A key challenge for continuous blending remains the transfer of processes across different commercially available platforms. The high capital investment required for equipment has limited most research to specific blender types (highlighted in Section 2.2.3), constraining the ability to translate knowledge between geometries. Building on the mechanistic and modelling insights developed in this thesis, future work should address both scale-up (increasing blender volume and throughput) and scale-over (translating processes across geometries and inclination angles), as these represent critical steps towards flexible and robust manufacturing.

When scaling over, the primary objective is to preserve the fundamental mixing dynamics of the system. This requires identifying scale-independent descriptors that link the variety of geometries across the industry. As highlighted in Chapter 5, strain offers a promising route for parameter optimisation. In addition, future studies should evaluate the Péclet number (in conjunction with strain) as a potential scaling parameter, since it quantifies the balance between convective transport and diffusive dispersion within the blender. Estab-

lishing such dimensionless metrics would enable consistent comparison across platforms and provide a rational basis for technology transfer in continuous blending.

6.2.2 Advanced Drug Formulation

An important direction for future work is the extension of the approaches developed in this thesis to advanced drug formulations. These systems present additional complexity due to the need to balance API properties, excipient functionality, and the requirements of downstream continuous manufacturing. For continuous powder blending, in particular, further work should focus on elucidating the powder–powder interactions that govern mixing performance in complex formulations. Once these properties are understood, the formulation design and selection of process parameters can be aligned accordingly, consistent with a Quality by Design (QbD) philosophy.

Key research priorities include

- **Balancing Trade-Offs:** Investigating how strategies to improve blend uniformity or flow can be implemented without compromising tablet mechanical strength or dissolution performance.
- **Predictive Approaches:** Extending the empirical and modelling frameworks developed in this thesis to accelerate formulation development and support QbD principles.
- **Enhanced PAT:** Applying high-resolution chemometric tools (e.g., Raman or near-infrared spectroscopy) to monitor and correct deviations in real time, with particular emphasis on low-dose and oncology therapeutics where dose accuracy is critical.

These priorities should be pursued with three overarching goals:

- **Manufacturability:** Identifying excipient combinations and process designs that enhance the blending performance and ensure optimal compaction behaviour.
- **Bio-Pharmaceutical Performance:** Selecting excipients that maximise the delivery performance (for example, solubility, release profile).
- **Process Analytical Technology:** Choose and compose formulation components based on distinct PAT signals from the API, optimising PAT technology to detect minimal (or trace) amounts of essential constituents (e.g. API).

Building directly on the mechanistic and modelling insights developed here, such investigations would establish stronger links between formulation design, process behaviour, and product quality, ultimately allowing for more robust continuous manufacturing of advanced medicines.

6.2.3 Improving Upstream Processing — Powder Feeding

As discussed in Chapter 2.2.1, powder feeding is critical to the blending performance. Upstream disturbances (e.g. feed rate fluctuations or density drift) can propagate through the system and impair downstream quality by altering the residence time distribution and local composition at the blender inlet. Although macromixing provides some buffering capacity, a stochastic sequence of feeding perturbations can still bias instantaneous blend composition and reduce overall mixing efficacy. Therefore, robust feeding performance is essential.

Building on the approaches developed in Chapters 4 and 5, future work should (i) identify the mechanisms by which feeder dynamics couples to blender transport and dispersion, and (ii) characterise the interactions between feeder setpoints, powder properties (e.g. PSD, shape, cohesion), and measurable inlet-state variables using high-fidelity models and data-driven methods. Four priorities are proposed:

- **Mechanism-led modelling:** Apply DEM to analyse mass flow stability, screw-pocket filling, and re-filling dynamics for powders with wide size and shape distributions, with the aim of predicting conditions that exacerbate inadvertent segregation. Outputs should be linked to input-state descriptors compatible with RTD and ML frameworks (e.g., mean and variance of instantaneous mass flow and solid fraction).

- **Sensing and control:** Evaluate continuous feeder geometries in conjunction with inline sensors (e.g. load cell analysis, vibration, imaging, NIR/Raman) and feedback or feedforward control strategies to attenuate disturbances before they reach the blender.

- **Generative design:** Employ AI-driven generative design methods to explore auger and impeller geometries that improve the conveyance of cohesive species and minimise pulsation, thus increasing the consistency of mass throughput.

- **Scope boundaries:** Deprioritise "mixing within the feeder" as a development target; feeders should ensure rate stability and outlet-state consistency, while blending equipment should be designed and optimised for mixing.

A further consideration is API attrition within the feeder. Attrition commonly arises late in API synthesis (e.g., during agitated drying in filter-bed, conical, or spherical dryers, whose hoppers are geometrically similar to continuous feeders) and can persist into secondary manufacturing. Although agitation aids mass transfer and moisture homogenisation, it also imposes mechanical stresses that fracture particles, potentially degrading manufacturability and altering critical quality attributes [168, 169, 170, 171]. Considering that CDC often begins immediately after API drying, quantifying and minimising shear within the feeder is warranted. Recommended tasks include: (i) evaluating an operational control strategy around size-distribution drift over extended campaigns; (ii) identifying operating windows and geometric modifications that reduce attrition; and (iii) integrating these findings into process control (advanced process control) to adapt process parameters on the fly to preserve

API attributes, while maintaining throughput and final tablet quality.

In line with these priorities, future work should first focus on DEM-guided design and operation of feeders that handle polydisperse and anisometric powders, as this represents the greatest source of variability at the blender inlet. A second priority is the development of integrated sensor suites and control architectures tailored to continuous feeders, enabling disturbances to be detected and corrected before they propagate downstream. Extending the combined methodology developed in Chapters 4 and 5—mechanism identification, dimensionless descriptors, and predictive modelling - to the feeding stage will provide a systematic understanding of the sensitivities and processes for manipulating complex powders effectively, while building tools which can be leveraged across projects to deliver across the portfolio.

Appendix One

Attached Publication for Chapter 2

Publication Jones-Salkey et al. 2023 [25] has been included below:

<Reference to the author's full first author contribution on sections 'Feeding' and 'Blending' with joint collaborative contributions on the 'Abstract', 'Introduction', 'Summary Table' and 'Conclusions' sections>

pharmaceutics

MDPI

Review

Reviewing the Impact of Powder Cohesion on Continuous Direct Compression (CDC) Performance

Owen Jones-Salkey [1,2,†], Zoe Chu [1,2,*,†], Andrew Ingram [2] and Christopher R. K. Windows-Yule [2]

[1] Oral Product Development, Pharmaceutical Technology & Development, Operations, AstraZeneca, Macclesfield SK10 2NA, UK; oxj807@student.bham.ac.uk
[2] School of Chemical Engineering, University of Birmingham, Birmingham B15 2TT, UK
* Correspondence: zhc906@student.bham.ac.uk
† These authors contributed equally to this work.

Abstract: The pharmaceutical industry is undergoing a paradigm shift towards continuous processing from batch, where continuous direct compression (CDC) is considered to offer the most straightforward implementation amongst powder processes due to the relatively low number of unit operations or handling steps. Due to the nature of continuous processing, the bulk properties of the formulation will require sufficient flowability and tabletability in order to be processed and transported effectively to and from each unit operation. Powder cohesion presents one of the greatest obstacles to the CDC process as it inhibits powder flow. As a result, there have been many studies investigating potential manners in which to overcome the effects of cohesion with, to date, little consideration of how these controls may affect downstream unit operations. The aim of this literature review is to explore and consolidate this literature, considering the impact of powder cohesion and cohesion control measures on the three-unit operations of the CDC process (feeding, mixing, and tabletting). This review will also cover the consequences of implementing such control measures whilst highlighting subject matter which could be of value for future research to better understand how to manage cohesive powders for CDC manufacture.

Keywords: continuous direct compression (CDC); powder cohesion; loss in weight (LIW) feeding; blending; tabletting; continuous manufacture

check for updates

Citation: Jones-Salkey, O.; Chu, Z.; Ingram, A.; Windows-Yule, C.R.K. Reviewing the Impact of Powder Cohesion on Continuous Direct Compression (CDC) Performance. *Pharmaceutics* **2023**, *15*, 1587. https://doi.org/10.3390/pharmaceutics15061587

Academic Editor: Colin Hare

Received: 3 April 2023
Revised: 8 May 2023
Accepted: 10 May 2023
Published: 24 May 2023

Copyright: © 2023 by the authors. Licensee MDPI, Basel, Switzerland. This article is an open access article distributed under the terms and conditions of the Creative Commons Attribution (CC BY) license (https://creativecommons.org/licenses/by/4.0/).

1. Introduction

The pharmaceutical industry is currently undergoing a paradigm shift from batch to continuous processing in order to improve manufacturing efficiency [1]. Continuous direct compression (CDC) (Figure 1) is considered highly efficient because of the reduced number of unit operations involved [2,3]; however, there currently exists only a limited range of formulations for which it is viable. Suitable formulations will generally have low drug load, a need for adequate flowability (as the material has to be transported through the system), and have sufficient tabletability, for the CDC process to work [4].

There are several critical material attributes (CMAs) which impact the flow of pharmaceutical powders and hence the successful formulation of oral solid dosage forms, of which cohesion is thought to be the most significant [5]. Powder cohesion refers to the affinity of particles to adhere to each other. It manifests in the bulk as resistance to powder flow often accompanied by adhesive behaviour, which refers to the tendency of a material to bind to surfaces and other materials [6]. Factors which contribute to cohesion include:

- Liquid bridges (liquid bridges will not be discussed in this literature review as there already exist comprehensive reviews of this topic [7–9]). Our focus in the present work will also be on the *effect* of cohesion in CDC processes rather than the *causes* of cohesion) [10];
- Van der Waals forces [11];

- Electrostatic forces [12];
- Frictional charging during handling [13];
- Particle shape and size [3].

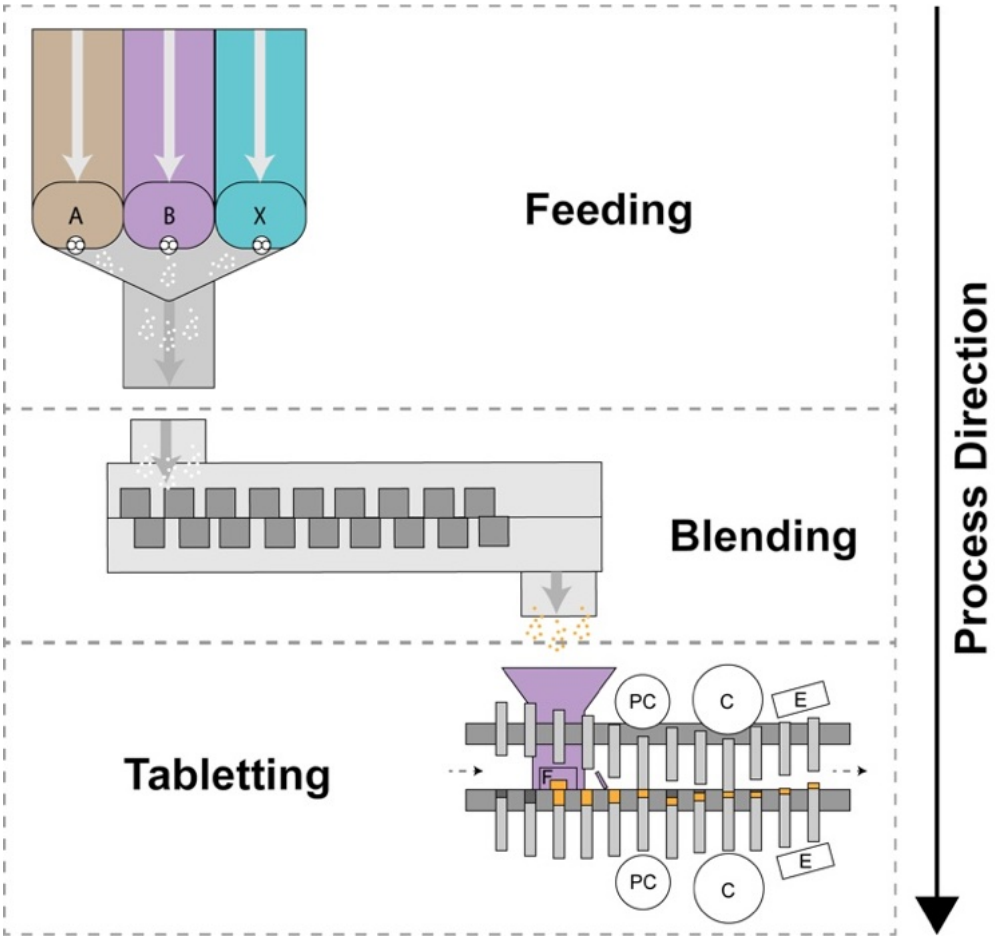


Figure 1. Schematic of the CDC process. Feeding: (where **A**, **B**, & **X**; are example labels of the formulation's constituents) powders are fed into the blending stage. Blending: Shows the constituents entering and being blended by the agitator, before entering the hopper of the rotary tablet press. Tabletting: (where **F**, **PC**, **C**, & **E**; corresponds to the Die Filling, Pre-Compression, Compression and Ejection, respectively) the final formulation fills the die cavity, undergoes compression forces—forming the tablet—before being ejected from the die.

Although humidity is controlled in a GMP environment, moisture is still present in the air and can be adsorbed and or absorbed into the powders, increasing cohesivity [14–16]. This increase in local moisture content in powders results in transient, complex interactions between powder surfaces and water, resulting in higher cohesion and decreased flowability [14–16]. Therefore, for every instance where good flowability is desired, an increase in humidity will have a negative effect. On the other hand, with compaction, there is evidence that some moisture can produce higher-strength tablets. However, too much moisture impacts the tablet strength negatively [17]. Thus, the positive effect of humidity, during tabletting, is largely outweighed by its negative effect across all the other unit operations in the CDC process. Therefore, generally or where suitable, moisture content should be kept to a minimum. In the interest of the review, relative humidity will be discussed when it is the only variable suited to solving an issue, for instance mitigating the triboelectric effect during powder feeding (Section 2). Furthermore, there are additional reviews [8,9] which discuss the influence of humidity on powder cohesion.

Active pharmaceutical ingredients (APIs) are typically the components of tablet formulations that give rise to handling issues, due to their often very high cohesivity, low bulk density, and highly aspherical geometries, in turn resulting in undesirable operating performance for CDC [6,18]. Many APIs are needle-like and very fine (<10 μm) resulting in a high contact area and cohesion (and thus poor flowability), whereas excipients are typically coarser and have a more favourable (spherical) particle shape, leading to better flowability. This difference in flow properties is perhaps unsurprising, as excipients are inactive substances whose purpose is to aid the formulation process by supporting or enhancing the stability and tabletability [19] of a pharmaceutical dosage form; as such, cohesive excipients would be omitted during the experimental design stages [20] as they are much easier to replace than APIs. Based on the above, it is clear that a high concentration of API may heavily affect the processability of powders, rendering the CDC manufacturing route non-viable [21].

In spite of the above, cohesion is not always a negative influence on CDC operations. In some instances, moderate cohesion has been found to aid the proper functioning of a given unit operation. For example, during powder feeding the addition of nano-sized silica was shown to result in reduced adhesion to feeder surfaces and improved powder flow as will be discussed later in this review [6,22]. However, in most cases of high cohesivity, flow is inhibited [23,24], which is problematic for feeding [25], mixing [26] and die filling [27,28]. Conversely, during the tabletting stage, powder cohesivity (specifically interparticle adhesion) is generally desirable, inviting smaller particle sizes and higher surface energy powders [29–36].

There are three main ways in which cohesion can be managed in tablet production:

1. Formulation modification, through the introduction of glidants or lubricants [37].
2. Operational process changes which are documented in many different studies for each unit operation [38].
3. Granulation, which also manages cohesion as poor flowing powder fines are made into coarser more uniform agglomerates. (This is beyond the scope of this literature review as this unit operation is not a part of CDC processes [39]).

However, most literature does not consider how cohesion controls impact downstream unit operations. As far as the authors are aware there are no literature reviews that encompass the mitigation of the effects of cohesion and how those controls may affect certain unit operations. Therefore, the primary aim of this literature review is to explore and consolidate current knowledge concerning the impact of powder cohesion and cohesion control measures on all unit operations in the CDC process (feeding, mixing and compression), discuss the consequences of cohesion control measures implemented, and establish what further studies could be valuably conducted in the future.

2. Powder Feeding

2.1. Feeding Introduction

Powder feeding for CDC processes needs to be accurate and consistent for CDC performance success. Feeding modes are commonly defined by the delivery and maintenance of material, in a given time frame. As such, there are two main categories for feeders: volumetric and gravimetric, which supply material according to volume per unit time, and mass per unit time, respectively [2,22,25,40,41]. Volumetric feeding is often used to understand the characteristics of powder behaviour within the hopper, whereas gravimetric feeding seeks to smooth out any volumetric perturbation through feedback control, arguably resulting in gravimetric being the superior of the two modes for mass delivery [2,22,25,40–42]. Powder feeding is the first unit of operation in the CDC process; thus disturbance or variation from the set point can propagate downstream, fundamentally impacting the tablet quality [25,43].

One of the tasks of the blending stage in ensuring that constituents are well-mixed is to smooth out the perturbations from the feeder. The lower the intensity and frequency of these perturbations, the lower the chance that content uniformity or manufacturability issues

will arise downstream [22,44,45]. Moreover, it should be noted that not all disturbances result in a detrimental impact. It is both dependant on the magnitude and duration of such disturbances—Gyürkés et al. [46] aptly discuss this concept with the use of funnel plots.

Powder cohesion impacts feeding performance by introducing variation through complex bulk behaviour, which results in the variation of flow behaviour [22,25]. This contributes to both the restriction of power into the converting screws, and the resistance to flow within the swept volume of the screws. In addition, these materials are prone to electrostatic charging, causing attraction-repellent behaviour, which can lead to deposits of material residing and adhering to surfaces post-feeding [15,47]. This buildup can migrate into the bulk feeder, dosing it with a spike of material, therefore resulting in a compositional imbalance [15,47]. The following section aims to discuss the work of several publications, exploring the complexity surrounding powder feeding.

2.2. Feeding Discussion

The difficulty associated with powder feeding directly derives from the handling of larger volumes of powder (in the hopper) and converting this into smaller, consistent streams (at the outlet). Essentially, this refers to the driving of powder down a pathway of lowering power-to-powder contact, to instead increase powder-to-wall contact. When there is resistance to this gradient of increasing powder-to-wall interactions, it suggests there is a lack of flowability, which commonly manifests in the form of cohesivity. Though cohesion is ultimately a microscopic process (i.e., it occurs at the scale of particle-particle contacts), at present its effects are predominantly characterised via macroscopic (bulk) measurements [48].

The Flow Function Coefficient (FFC) is a measurement used to quantify the amount of stress required to cause a powder to yield, and is one of several manners in which a powder's 'flowability' may be characterised [49,50]. Gathered from a ring shear tester, for example, the measurement applies a normal consolidation force to a powder bed and measures the tangential force required to cause failure (incipient flow). A yield locus of shear stress vs normal stress is plotted and, applying Mohr–Coulomb failure theory, the major principal yield stresses of consolidated and unconfined material are obtained. FFC is the ratio of these values. The theory and methodology is discussed in various degrees of detail in the following papers: [5,49–51]. Leung et al. [5] performed a comprehensive analysis on 1130 ring shear measurements and effectively surmised that particle friction coefficients are negligible on FFC measurements, suggesting that cohesion is the primary characteristic which influences the measurement. In addition, the authors state that mitigating the effects of cohesion is far more influential than mitigating the frictional aspect(s) of the powder when it comes to improving powder flow, and also suggest that altering interparticle forces is the best approach to take when combating cohesive powders.

Leung et al. [5] demonstrated the effect of introducing 1% w/w of colloidal silicon dioxide into two excipients on FFC, cohesion and angle of internal friction. The first excipient—hypromellose—showed a significant drop in cohesion and an increase in FFC (Figure 2). Meanwhile, the second excipient—dicalcium phosphate anhydrous—showed the inverse behaviour, but to a much lower degree. No significant changes were seen in the angle of internal friction for both materials. Additional work regarding the use of colloidal silicon dioxide nanoparticles for formulation adjustment is seen in [52,53]. The mechanism at work involves the surface coating of SiO_2 nanoparticles, which introduce additional distance, therefore lowering the strength of the van der Waals attraction between the two surfaces of the more cohesive species [5,6,52,53]. Furthermore, Leung et al. state that particles with uneven shapes and rough surfaces may receive little beneficial effect from the SiO_2 surface coating, and therefore minimal improvement in flowability. The SiO_2 will fail to act as a barrier to the contact of the carrier species as it is shown that using SiO_2 as an additive can be detrimental to FFC.

Tran et al. [54], investigated these underpinning mechanisms which govern flow modification through the use of colloidal silica—their findings agree with those of Leung et al. [5].

Tran et al. studied the differences in silica loading for two different excipients using flow characterisation, static image analysis, and particle size distribution. It was found that materials with higher surface area (described as rugged) were able to accommodate higher silica loads, and that the optimal amount of silica loading is dependent on both the surface area and the size of the carrier particle but, most notably, their results discussed the possibility of taking a 'quality by design' approach by determining silicate (glidant) loading by carefully assessing the carrier powder's physical properties.

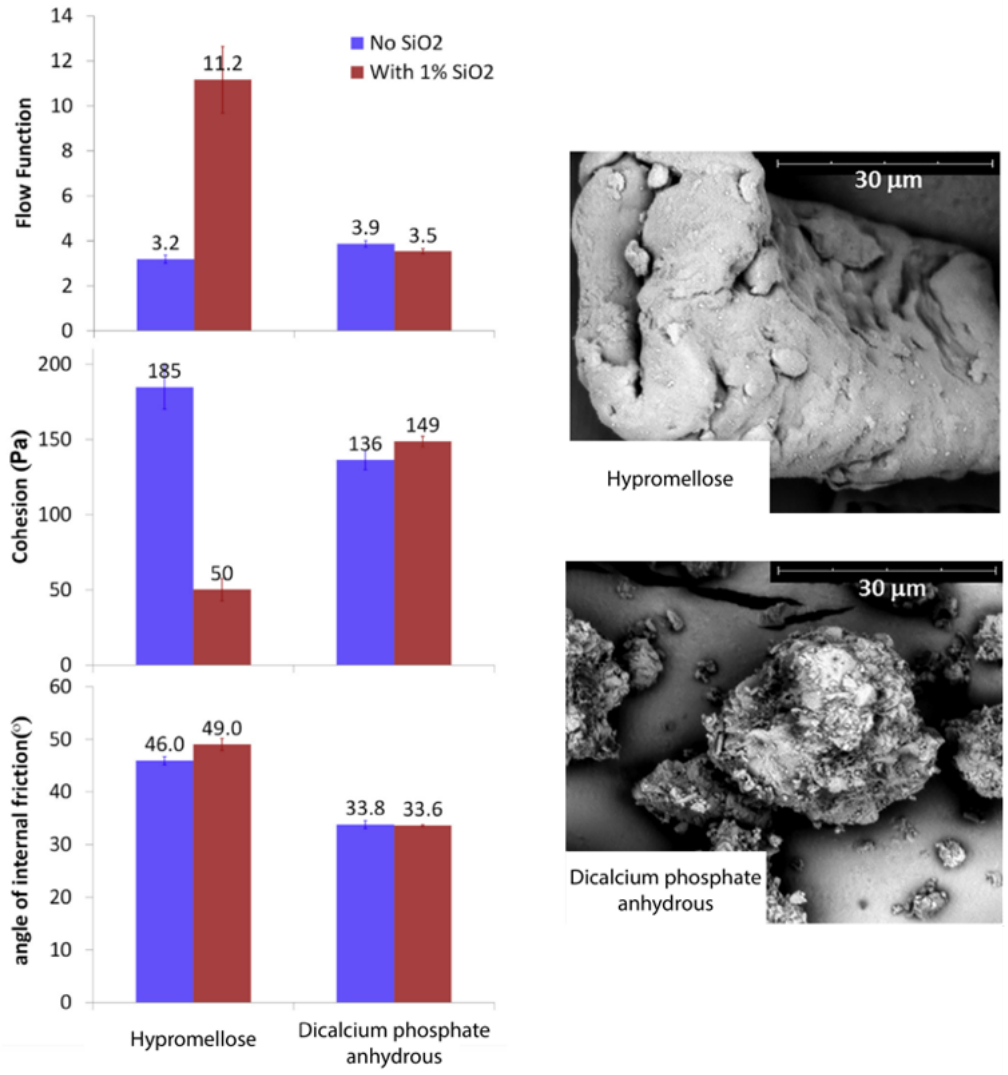


Figure 2. (**Left**): Graphs highlighting the difference in characteristics (Flow Function (FFC), Cohesion, and angle of internal friction) of the two excipients: Hypromellose and Dicalcium Phosphate Anhydrous with and without colloidal silica. (**Right**): Scanning Electron Microscope (SEM) of the two excipients mixed with 1% *w*/*w* colloidal silica. Adapted from Leung et al. [5].

Lopez et al. [55] published a DEM study on the effect of increasing cohesion on feeding performance. The researchers began by calibrating the powder used in the system, first identifying and assigning the physical properties and particle shape of paracetamol, before performing a sensitivity analysis across different adhesive stiffness values (K_{adh}) and conveying impeller rotation rates. When the conveying impeller was kept at a constant rotation rate (10 rad/s), the particles saw an increase in translational velocity in conveying barrel with increasing K_{adh} (ranging from 0 to 0.5). This effect was lesser but present on the interface between the conveying barrel and hopper. On the other hand, keeping K_{adh} at a

constant 0.2, across increasing conveying speeds (10, 20, and 50 rad/s) saw an increase in the overall translational velocity of the particles. Perhaps unsurprisingly, for the range of parameters explored, increasing conveying speed was observed to have a greater influence on particle velocity in the hopper than altering cohesion.

The DEM simulation of Lopez et al. [55] also provides valuable insight into the expected power draw; given the CDC system is continuous, it would mean the process would be running for days, if not weeks, at a time, making this an important consideration. The authors demonstrated the average mass discharged per Watt as a function of the K_{adh} (between 0.1 to 0.5 K_{adh}), which showed an exponential decay with increasing K_{adh} Figure 3. Accordingly, K_{adh} values higher than 0.5 showed arching: a phenomenon which occurs when the cohesive forces between particles are stronger than forces due to gravity. Arching (also referred to as bridging) is a semi-stable instance of particles forming particle–particle structures suspended in a hopper or opening, which are resistant to the displacement of powder beneath them [25]. For additional information on the influence of particle properties on arching, see the following papers: [25,49,56]. Lopez et al. described this behaviour with absolute translational velocity where they revealed instances which lead to inconsistent feeding of the conveying screw, which in turn lead to flow irregularities Figure 3. The authors link this artefact of transient macro behaviour to the micro by stating that inconsistencies in flow result in the improper filling of the screw pitch, giving rise to an inconsistent mass flow rate. This is best demonstrated by the plot of mass per screw pitch vs. K_{adh} shown in Figure 3). Finally, the researchers indicated what future work would be of value, notably suggesting the mapping of the transient cohesive behaviour by altering the particle properties, feeder's geometry and rotational speed.

To build upon the above suggestions, it would be interesting to see the implementation of a DEM study on a more commercially representative feeder, which possesses both a hopper agitator and twin screw conveying elements. Allowing the exploration of concepts such as agitator design and rotation speed to increase barrel/screw filling consistency or the breakage/mitigation of arching. What is more, the research conducted by Leung et al. [5], which discussed the minimal effect of friction in powder flow consistency, could utilise simulation tools such as DEM to more directly support their claims.

Escotet-Espinoza et al. [6] present a publication showcasing the use of silication to improve feeder performance. The researchers began by pre-blending the three different APIs explored with 1% silica, before characterising the bulk behaviour of the pre-and post-silicated API. The APIs (and their silicated counterparts) were then fed through the feeder, whilst a catch scale continuously measured the mass exiting the feeder. The response was then measured over time, with attention being paid to the consistency and accuracy of the feeding process.

Like Leung et al. [5], Escotet-Espinoza et al. [6] also found that the introduction of silica improved flowability by reducing the interparticle cohesion. Feeding improved with the addition of silica, with each of the API case studies showing improved screw speed consistency, a reduction of mass flow RSD (relative standard deviation), a reduction in powder adhesion to the hopper surfaces, and a reduction of remaining mass. This suggests that the addition of silica is hugely advantageous for feeding. The improvement can potentially be attributed to an increase in flowability, allowing the powder to better fill the swept volume of the screws, thus leading to an increase in mass per revolution with the addition of silica. This observation is supported by the work of Lopez et al. [55] which shows that, with a reduction of K_{adh}, there follows an increase in mass per screw pitch. Furthermore, with FFC (as previously discussed) being a strong indicator for powder cohesion, it would suggest that it would be useful to understand this screw-filling behaviour. This conveniently leads to another suggestion to further Lopez et al's work [55], whereby similar DEM studies could be undertaken to understand the effect of additives on feeding and powder conveying. Escotet-Espinoza et al. [6] also describe the material used generating electrostatic charge, which enabled the API to stick to the agitator. However, in the silicated API case study,

there was very low powder adhesion, suggesting that adding silica also suppressed the effects of electrostatic adhesion.

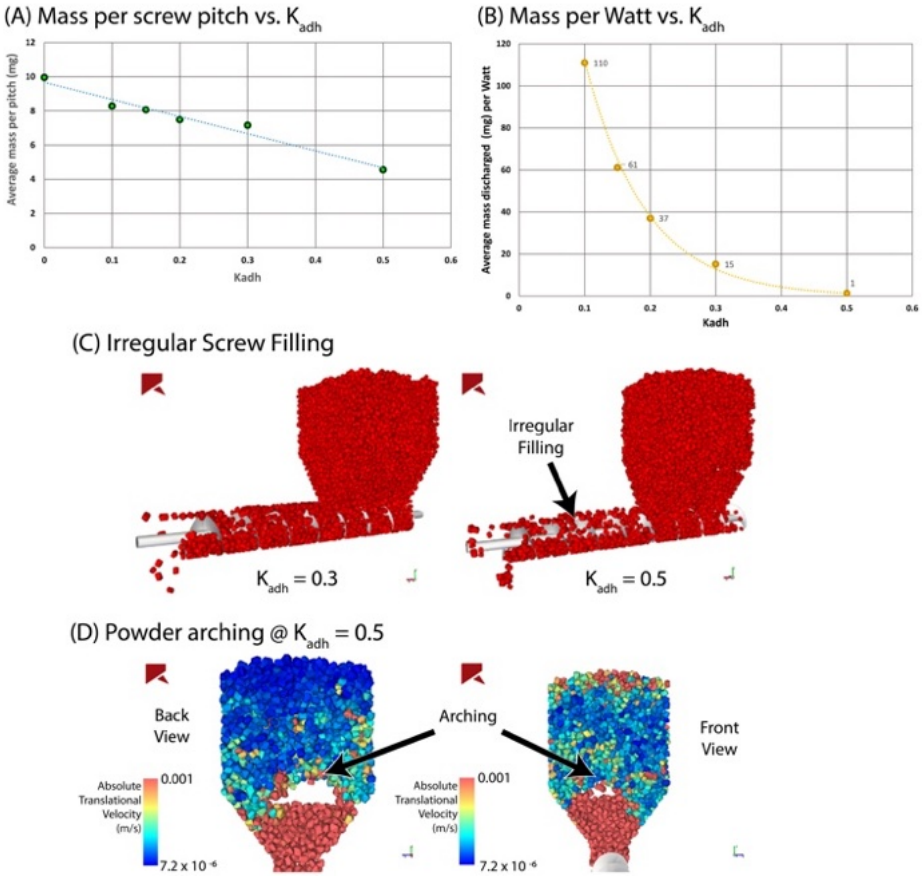


Figure 3. (**A**): Mass per screw pitch as a function of cohesive stiffness (K_{adh}). (**B**): Mass per Watt as a function of cohesive stiffness (K_{adh}). (**D**): Visualisation of the powder arching/bridging within the hopper volume. The images show both the back and front of the hopper from two different simulations using the same K_{adh}. (**C**): Irregular filling of the conveying volume due to cohesive stiffness (K_{adh}). The images compare K_{adh} = 0.3 and K_{adh} = 0.5. Adapted from Lopez et al. [55].

A study by Lumay et al. [57] explicitly investigated the influence and mechanisms of mesoporous silica (MPS) on the electrostatic charge, again finding that the addition of silica species improves powder flow. The experiments differed from those discussed previously in several manners. Firstly, the study differed in the materials and methods used—the authors tested three different grades of silica, varying in particle and pore size, in three common excipients (microcrystalline cellulose, lactose, and maize starch) using a rotating drum. Secondly, the authors applied different experimental analyses: the dynamic effect of silication was evaluated in this case by measuring the cohesive index [58] of materials (with and without MPS) across a range of rotation speeds. Finally, through the use of a standardised charge density measurement technique [59], the charge density of the material blends is shown in the presence of different types and amounts of MPS.

It was found that the MPS with the smallest particle size provided the greatest improvement in flowability. Furthermore, the addition of just 0.5% w/w made a considerable impact on the cohesive index—see Figure 4A. The authors attribute this improvement to the particle size of the MPS, explaining that there would be an increase in effective surface area, which would suggest greater coverage, and thus intervention between, cohesive species.

An additional striking finding of the study was that the addition of silica was also found to change the shear-dependent rheological properties of certain tested materials,

with typically rheopectic materials becoming thixotropic when mixed with a small volume of silica. Specifically, the study evaluated the cohesive index of the powder dynamically by testing the excipients against their 2% *w*/*w* silica counterparts across a range of rotation rates (see Figure 4B). Both materials, maize and lactose, were shown to be more cohesive (thickening) with increasing rotating speed (ranging from 2 rpm to 10 rpm) and in the presence of silica, less cohesive (thinning) with increasing rotating speed. The silicated maize showed a greater decrease in cohesion than the silicated lactose with increasing rotation speed.

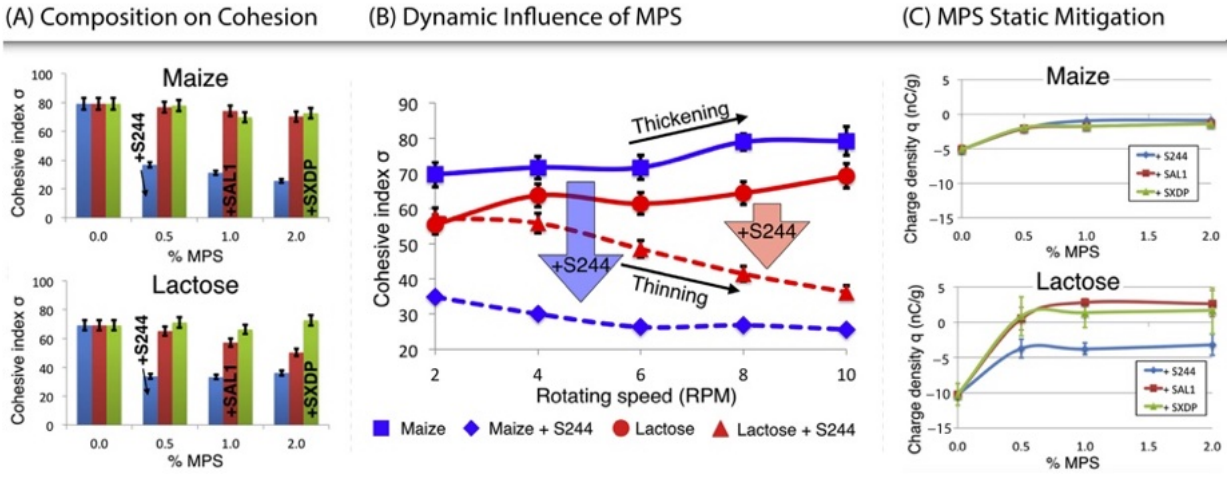


Figure 4. (**A**) Comparing the differences in the dynamic cohesive index (σ) with the addition of different types and weight percentages of Mesoporous Silicates (MPS). (**B**) Dynamic influence of MPS on the cohesive index, demonstrated through plotting the cohesive index over different rotating speeds. (**C**) Comparison of Charge Density (nC/g) in two excipients and resultant performance with the addition of 2% weight silicates. Where: +S244 is Syloid® 244FP, +SAL1 is Syloid® AL–1FP, and +SXDP is Syloid® XDP3050. Adapted from Lumay et al. [57].

Finally, the inclusion of MPS was shown to decrease the static charge density of the powder—see Figure 4C. Across all materials and MPS grades, the addition of 1% (of MPS) saw similar results to the addition of 2—suggesting 1% was sufficient for charge mitigation, with any greater amount being surplus. MPS incorporated into maize saw a decrease in charge after just 0.5% *w*/*w*, with the grade of MPS used making a minimal difference. Conversely, MPS in lactose still produced a decrease in the magnitude of charge density, though different grades responded differently. This suggests there may be some complexity associated with the use of MPS with lactose. It is potentially important to note that Lumay et al. [57] stated that the lactose varied in positive or negative charge on the day, which was dependent on the air's relative humidity. Given the magnitude is roughly the same but the charge differs, if the S244 (Syloid®FP244) was positive it would suggest that the grade of MPS used would have little effect on the charge density and vice versa for SXDP (Syloid®XDP3050). Research by Ramires-Dorronsoro et al. [60] supports this: when completing a similar study—with a different measurement technique—they also witnessed spray-dried lactose exhibiting a positive charge density. Ultimately, this suggests that the use of silica in poorly flowing hygroscopic powders greatly improves the flowability, and decreases the sensitivity to triboelectric charging.

The previously discussed papers showcase the underpinning behaviour of cohesive powders during feeding, and the discussion of silication demonstrates the advantage of understanding the mechanism underlying a powder's cohesive properties. Despite this, when considering CDC in its entirety, the predictive capability is a large part of reducing experimentation and understanding the process. Therefore it is desirable to be able to predict the feeding performance from a few key powder characteristics [42,43,61], one of which is cohesion.

Van Snick et al. [43] and Garcia-Munoz et al. [45] provided some of the first in-depth analysis of the end-to-end CDC process, thus by definition including aspects of feeding. The authors discuss the correlation of bulk density, tapped bulk density and FFC to feeding consistency (Figure 5). The experiments involved the comparison of different materials running volumetrically (at a constant screw speed) from full to empty, whilst measuring the feed factor response over time. The maximum (ff_{max}) and minimum (ff_{min}) feed factors (g/revolution) were then taken and used for further calculation. Feed factors change throughout the hopper fill as powder above the hopper bears down upon the powder below, due to gravity. When the hopper is at low fill, there is not only a reduction of gravitational bulk powder compaction but a potentially inconsistent feed into the conveying volume.

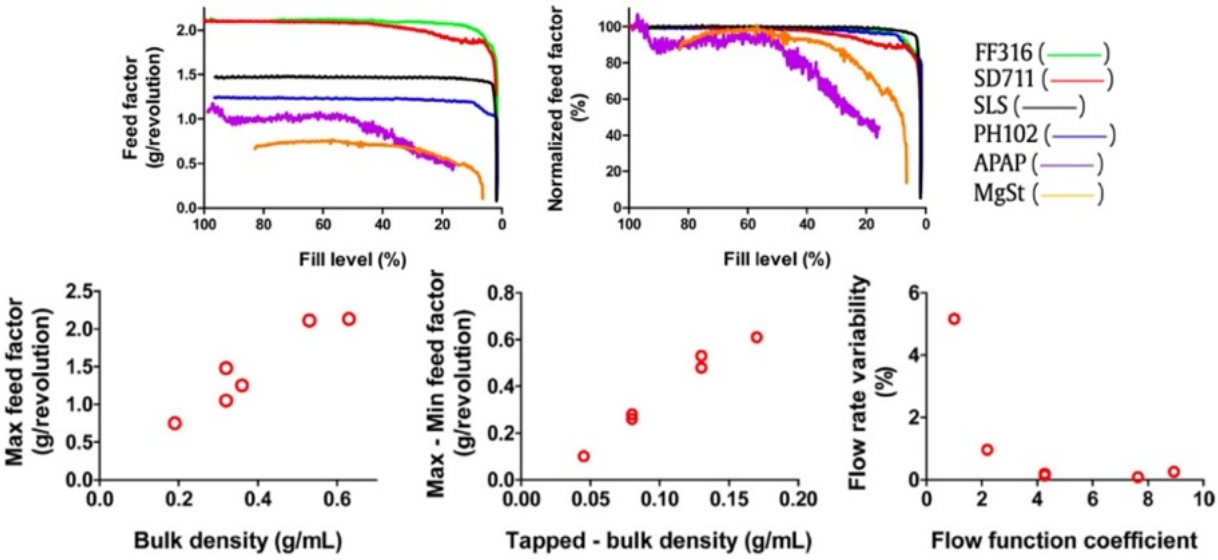


Figure 5. (**Top**): Two graphs detailing the feed factor throughout the volumetric empty, with absolute values (**left**) and normalised values (**right**), the key indicates the material used. Where: FF316 is Lactose Fast Flo® 316, SD711 is Sodium Croscarmellose Ac-Di-Sol® SLS is Sodium Lauryl Sulphate, PH102 is MCC Avicel® PH-102, APAP is Acetaminophen, and MgSt is Magnesium Sterate. (**Bottom**): Three graphs compare feeder performance to bulk characteristics. Adapted from Van Snick et al. [43].

As a result, bulk density increased linearly with max feed factor, tapped bulk density increased linearly with delta feed factor (where delta feed factor is: $ff_{\Delta} = ff_{max} - ff_{min}$), and finally flow rate variability exponentially decayed with increasing FFC. Since both bulk density and FFC are common descriptors for powder cohesion, it then can be used as a proxy to describe behaviour. The study highlighted FFC values greater than 3 would give sub 1% flow rate variability, and that powders with low bulk density and low tapped bulk density are prone to large ff_{Δ}—which suggests instability when processing. Escotet-Espinosa [22,62] also looked into both the influence of powder properties on feed factor and modelling such behaviour using the following (simplified) equation:

$$ff_w = ff_{max} * (ff_{max} - ff_{min}) exp[-\beta * w] \quad (1)$$

where ff_w is the feed factor as a function of $'w'$ the weight, while ff_{max}, ff_{min} and β are the maximum feed factor, minimum feed factor, and a fitting constant based on feeder geometry, respectively.

The ff_{max} and ff_{min} were then plotted in a correlation heat map (Figure 6), relating the responses to a plethora of recorded bulk characteristics. Interestingly, the highest correlation was seen for cBD, conditioned bulk density (g/mL). cBD is akin to tapped bulk density, obtained from the initial standardised conditioning step of a powder rheometer. It involves a blade passing through a volume of powder with a set torque before measuring

the weight of the known volume. Paying attention to the units, it is a given that there is a correlation between the two density measurements, but the interest is with 'compressibility at 15 kPa' which also scored high for ff_{min}, which would be a method for attaining higher bulk density. This suggests that powder that is capable of being compressed, and has a high conditioned bulk density, will deliver a high ff_{min}. Similar studies by Shier et al. [63] and Bekaert et al. [42] similarly look to predict feeder performance using bulk characteristic properties.

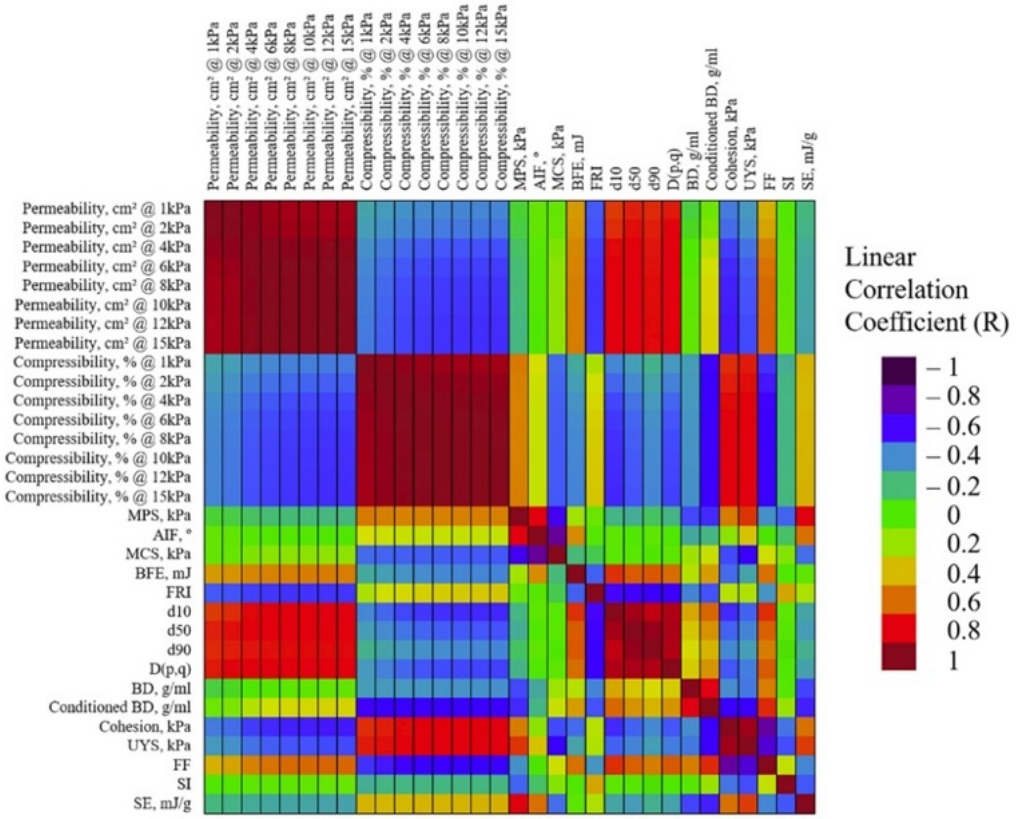


Figure 6. A correlation heat map acquired, with permission, from Escotet-Espinosa [62], detailing the magnitude of linear correlation (R) between bulk powder characteristics and regressed feed factor parameters.

Engisch & Muzzio [41] performed a study on varying hopper refilling conditions on powders with varying cohesiveness and measured the resultant effect on feeding accuracy and consistency. Typical Loss in Weight (LIW) feeder operation is gravimetric, until topping up (or refilling), where the system operates volumetrically to ensure a consistent feed is maintained whilst an influx of mass is registered on the feeder's load cell. This method results in a trade-off between the number of times the system has to enter the 'less accurate' volumetric mode and ensuring the hopper is sufficiently full, such that the feed factor is stable. For an example of the effect of decreasing fill on feed factor, see Figure 5. The conclusion from Engisch & Muzzio is that refilling the feeders with less material, and therefore more frequently, results in better overall performance. This should be kept in mind when paying attention to the duration of time that the system enters volumetric mode and reducing the overall disturbance from the setpoint over the whole duration of running the feeder. Irrespective of the frequency and volume of fill, Engisch & Muzzio state refilling should be gentle as this causes the least disruption to feeding. Furthermore, it is shown that refilling sensitivity is much lower at higher refill levels, Figure 7. Refilling at higher fill levels reduces the maximum set point deviation, time of deviation, and the total amount of mass during deviation.

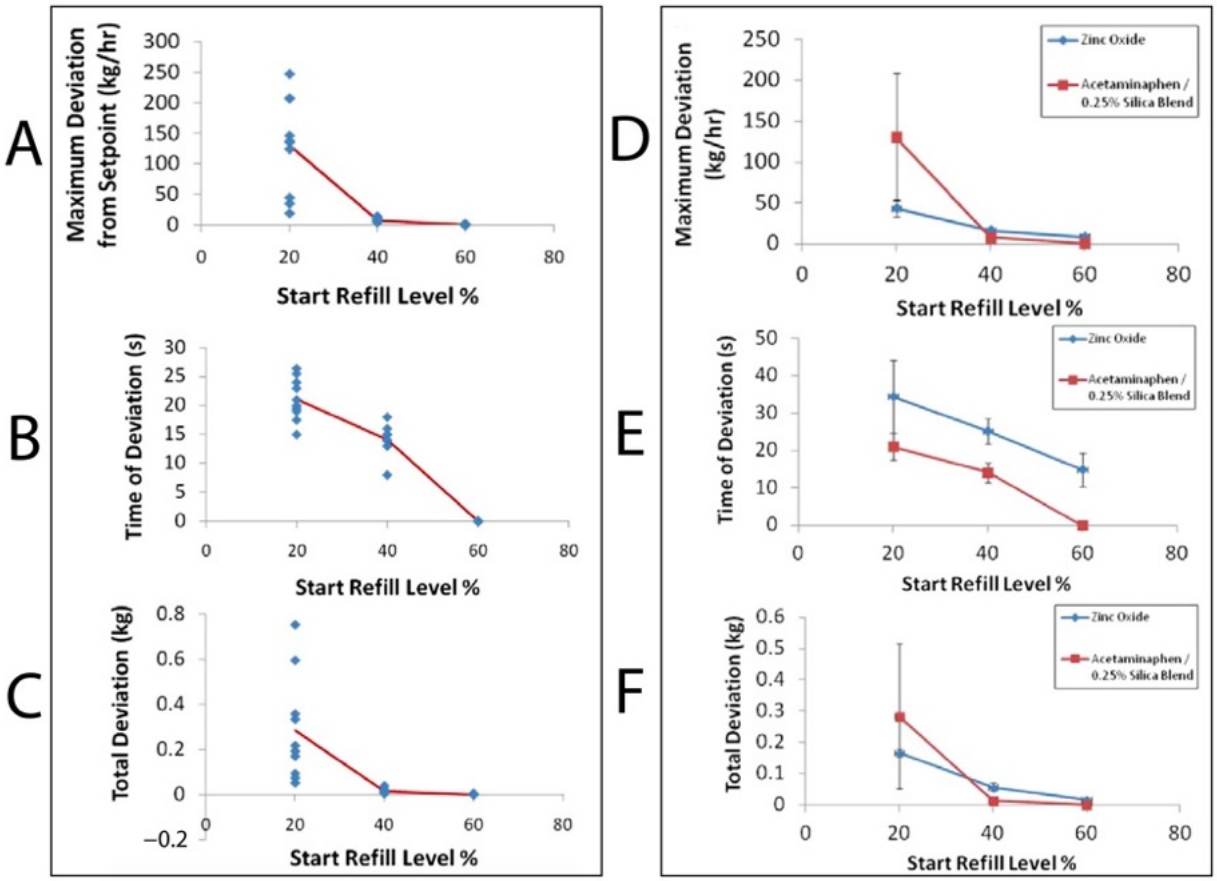


Figure 7. (**A**–**C**) Shows the feeder performance for just semi-fine APAP & 0.25% silica over 3 refill levels, each with 10 manual refills. (**A**) Maximum deviation from setpoint (kg/h), (**B**) Time of deviation (s), and (**C**) Total deviation (kg). (**D**–**F**) Similarly, shows the comparison between zinc oxide powder and semi-fine APAP & 0.25% silica blend. (**D**) Maximum deviation from setpoint (kg/h), (**E**) Time of deviation (s), and (**F**) Total deviation (kg). The deviation is defined as the sum of the surplus powder delivered during refill. Adapted from Engisch & Muzzio [41].

A similar methodology could also be applied to combat cohesive powders through compaction during refilling, by attempting to keep the hopper volume as constant as possible, during their most stable ff_w. To build a theoretical case study, using the APAP being fed volumetrically in Van Snick et al. [43] (Figure 5) and the supporting evidence of refilling stability from Engisch & Muzzio [41], see Figure 7. A top-up of 25–30% of the volume of the hopper could be used and triggered at the 50–60% fill level, refilling to 75–80%. This would occur during the most stable feed factor window, whilst the hopper is already half full. During the window in which powder is dumped into the system, there is a transient influx of powder onto the existing powder bed. This impulse of vertical pressure on the powder would increase powder compression within the bed, increasing the bulk density of the powder local to the conveying screws. Corroboration is seen by adding Escotet-Espinosa's [22] correlation measures, as there is an improvement in the conditioned bulk density, which increases ff_{min} reducing the ff_{Δ}, essentially reducing the feeder inconsistency related to lower fill levels. Albeit this theoretical case study is generalising by not considering phenomena such as disturbances due to air flows during discharging mass, and an increased volume of powder that may be prone to triboelectric charging due to the agitator. DEM studies, such as Lopez et al. [55], open a stage for exploring some of the fundamental behaviours seen in these systems, in particular when looking to evaluate the micro and macro behaviour attributed to conveying inconsistency.

Finally, Yadav et al. conducted a comprehensive study with a loss in weight feeder [64] utilising a range of screw speeds, gear ratios, and screw types, across a range of materials. The result was a PCA model which identified the influence of these processing parameters and how they interacted with the materials' bulk characteristics. The principal components consisted of one comprising the powder's bulk characteristics, a second representing the feeder's processing parameters, and a third representing an interaction component. Most notably, the interaction component related screw free volume (cm^3) to density, particle size (d_{10}, d_{50}, d_{90}), wall friction angle, and Feed Factor. The authors note that a different screw type will have a different screw-free volume, meaning that the comparison between a smaller or larger volume to dispense per revolution must be taken into consideration when evaluating the feed factor. Similar findings are seen with Engisch et al. [2], where their suggestion is the use of both self-cleaning concave screws and the removal of any outlet screens for very cohesive materials.

2.3. Feeding Summary

Cohesion has been shown, across multiple studies, to worsen the flowability of powders, in turn reducing the consistency with which powder flows into the conveying volume [5,43,55]. The transient inconsistency of material flowing into this volume persists and has been shown to result in turn in an inconsistency in the delivered mass powder flow—and therefore a deviation from the desired set point [2,41,55,65]. Thus, it is very important to ensure that powder, despite its cohesive nature, is consistently motivated to enter and be transported through the conveying section of the feeder.

This review outlines just a few examples that have been used so far to reduce the negative influence of cohesion on feeding: reducing interparticle contact between cohesive species [5,57]; reducing the effect of triboelectric charging [57]; refilling the hopper at moderate fill levels [41,65]; and adjusting screw speed and screw type [2,64].

When applying the knowledge gained from Lumay et al. [57] to the work of Escotet-Espinoza et al. [6] and Lopez et al. [55] it would perhaps be sensible to suggest that smaller sized silica nanoparticles would be ideal for improving flowability at this stage of the CDC process. Silica nanoparticles have also been shown to change the blend from shear-thickening to shear-thinning, implying that, when the powder contacts the hopper's agitator or the conveying screws, one might expect a further transient, localised increase in flowability.

Despite silicates holding the much of spotlight for discussion, surrounding improving powder flowability, it should be noted that several alternative materials could be selected. However, every material in question, for flow modification, would need to undergo consideration for its end-to-end impact on the process. Silicates, for instance, have been shown to negatively impact compatibility [66,67] but also improve flowability and therefore improve feeder processing consistency [5,43,55], whereas magnesium stearate has also been shown to increase flowability, but due to its hydrophobicity—coating the surface of the API—would hinder the dissolution of the API within the formulation [68]. This would result in the material being greatly undesirable for any scenario which may involve the intimate blending, or over-mixing, of magnesium stearate with API. However, pre-blending API with other materials such as tricalcium phosphates or microcrystalline cellulose [69,70] propose the ability to improve flow behaviour at a minimised trade-off, and as such, more research should be carried out into both the use (for improving feeding performance) and the end-to-end implications of selecting such materials.

Our review of the literature has also highlighted the benefit of future DEM studies which could be undertaken to better understand the fundamental powder movement that governs powder feeding, in particular using commercially-relevant geometries. Notable areas of study could include modelling the effect of silication; altering, and potentially optimising, agitator and screw design; further investigation of the influence of hopper refill regimes. The development of dynamic DEM simulations could also be used to develop and test various control strategies, both existing and novel. Intuitively, it could be possible to

develop a control proposition for shear thickening powders involving a sudden reduction in RPM followed by a slow build-up of screw speed back to setpoint.

3. Blending

3.1. Blending Introduction

Despite diverse designs available commercially and in the academic literature, continuous blenders can, in general, be reduced to four main components: an inlet, an outlet, a mixing volume, and a mechanism for promoting blending whilst in the volume of the blender. Typically, this last component will be some form of rotating agitator, the geometry of which may differ from mixer to mixer, or even formulation to formulation. Recognising the different types and geometries of mixers that exist within this space is fundamental when evaluating the role of powder mixing in CDC performance, as the features that differentiate one mixer from another can have significant impacts on the behaviour of the powders being blended, and thus may require different measures to handle the blending of cohesive powders.

Achieving good mixing is integral to the performance of any given pharmaceutical tablet; the therapeutic efficacy and mechanical properties of the tablet will suffer without the effective distribution of its constituent materials, ultimately compromising the safety of the product [43,71–75]. Thus, mixing inherently defines the final quality of the formulation (albeit that the final product cannot be delivered without the consistency and accuracy of the upstream and downstream processes [43,45]).

Practically defining whether a formulation is well-mixed is a complex endeavour with issues such as frequency of sampling [71,76,77], location of sampling [71,76,77], and scrutiny (size) of the sample [71,76,77]. However, describing the mechanisms of mixing may be ever-so-slightly easier, and is of more direct relevance to the present work.

The two commonly-defined types of mixing—macro- and micro-mixing—are both essential when looking to create ideal mixtures [71,72,75,78,79]. Macro-mixing is responsible for large, global movements, of material—or bulk transport—allowing the material to flow and circulate around the vessel [71,75,79–82]. Micro-mixing, on the other hand, involves the movement and displacement of material at the particle scale, i.e., the local interactions between particle species [71,79]. Accordingly, micro-mixing achieves the detail of the mixing action due to the mixing happening at the smallest possible scale: the particle–particle level [71,79], whereas macro-mixing serves to smooth out the upstream mass flow rate perturbations, due to the flow and bulk motion of the powder [71,79].

Fan et al. [83], succinctly discuss the evaluation of mixing in terms of cohesive mixtures. Figure 8 and Equation (2) encapsulate the majority of this discussion. It is shown that by increasing the surface force—which is also a function of particle size, and therefore surface area—it is possible to reduce the influence factor defined in Equation (2). A low influence factor means surface forces dominate, and the particle species adhere to the surface of another particle species, creating a perfectly-ordered blend. Small, less dense particles would be the ones to adhere to the more dense 'carrier' particles- due to gravitational forces. Then, if the surface forces are minimal, gravity dominates, and thus the mixture would involve non-cohesive species, following more typical solids mixing criteria.

$$Influence\ Factor = \frac{Gravitational\ Force}{Surface\ Force} \tag{2}$$

Conversely, de-mixing occurs through several mechanisms, such as: segregation, the separation of a formulation into constituent particles of similar properties, for example, size and density [71,76,84]; agglomeration, the formation of particle–particle dense macro-particles, due to interparticle attractive forces [85,86]; and electrostatic repulsion, or attraction, due to inter-particle charge imbalances, which predominantly result from contact-induced electron transfer, as particles move relative to each other and the equipment surfaces [26,87]. The part cohesion plays differs significantly in each of these mechanisms, and can either subdue or exacerbate de-mixing [84]. For instance, electrostatic charges could

be worked into powder, through the triboelectric effect, creating attractive or repulsive forces between different species [26,77]. These interactions underpin much of the following discussion of how cohesion affects the process of mixing and the competition between mixing and de-mixing.

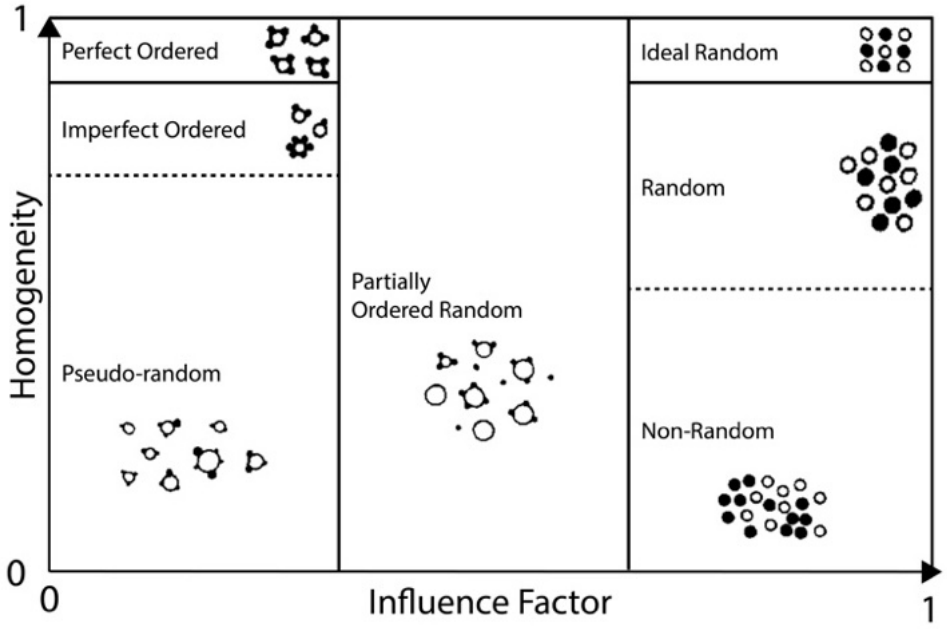


Figure 8. Cohesive mixtures described by homogeneity vs influence factor (Equation (2)). Adapted from Fan et al. [83].

3.2. Blending Discussion

Processing parameters such as agitator RPM, feed rate (throughput), and agitator design, are the primary methods of manipulating powder through a given blending volume [43,75,88]. For example, trends have been identified for improving mixing quality through the use of processing parameters: macro mixing as a function of mean residence time; micro mixing as a function of RPM (agitation); residence time being a function of throughput [43,75,82,89,90]. These examples signify the importance of process parameters on mixing performance. However, the intricacies of powder behaviour in response to these systems are seldom discussed in the wider literature.

As discussed in the preceding section, cohesion can be overcome through the use of formulation additives and/or changes to the process [5,37,57,78]. Additives, such as glidants (e.g., SiO_2), are typically used to make the bulk powder properties easier to deal with, by increasing flowability [5,37,57]. However, additives change the overall formulation composition, which can have detrimental effects on downstream processing-namely tabletting [66,67]. In contrast, process changes (processing parameters) can potentially overcome issues relating to cohesion without altering the formulation's composition [43,75,88]. Utilising these favourable processing parameters is thus the more practical of the two solutions for CDC processes, but the development and transfer of knowledge between different systems appears to be a substantial hurdle. This is largely due to this approach requiring a much deeper understanding of the specific unit operation being used in the study. Therefore, the knowledge gained is often less transferable; each particular set of process parameters may be unique to system geometry, orientation, or method of operation. With this in mind, it is useful to note the use of dimensionless numbers/groups within the discussed research, as it allows greater understanding and application of relative powder behaviour between publications.

Portillo et al. [91] performed trials on an axial continuous blender (see Figure 9)), the axis of which was adjustable between ±30° to the horizontal. The researchers found that

at (+30°) incline there was an increase in mean residence time which led to a decrease in the relative standard deviation (RSD) of Acetaminophen (APAP) concentration in two grades of lactose. This demonstrates the effect of longer mean residence time on macro mixing and a reduction in APAP RSD. The grades of lactose differed in terms of average particle size and size range: Lactose 100 (70–250 µm, average 130 µm) and Lactose 125 (55 µm), whereas APAP (36 µm) remained the same in both tests, and made up 3% *w*/*w* of the mass flow rate. They also discussed that, despite typical behaviour, the smaller (and more cohesive) grade of lactose did not affect mixing performance at either the high or the low rotation speeds. It was observed that while agglomerates were readily formed by the cohesive material, these were relatively weak and agitation from the impeller was sufficient in breaking the clusters up, dispersing the powder.

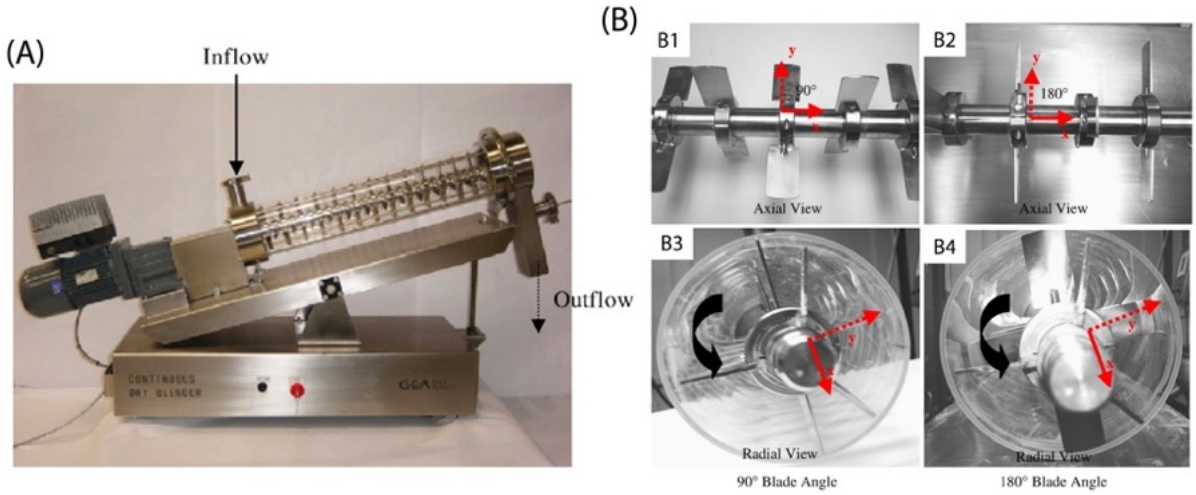


Figure 9. Example linear blender used in Portillo et al. [91]. Profile view of the blender (**A**) view of the agitator shaft and blade angle orientation (**B**).

Later work by the same group [78] discussed the influence of cohesivity on powder behaviour in a different continuous mixer (albeit similar to the blender shown in Figure 9), inclined at +17°. The study used two different grades of lactose, Fast Flo and Edible, which displayed flow indices (measured using a Gravitational Displacement Rheometer) of 24.9 and 34.8 respectively, suggesting them both to be highly flowable powders. In addition, the bulk density tapped density of the Fast Flo Lactose were 0.626 (g/mL) and 0.704 (g/mL), respectively, while the Edible Lactose measured 0.629 (g/mL) and 0.981 (g/mL), respectively. Portillo et al. [78] found that cohesivity negatively impacted axial mixing, becoming a statistically significant factor at higher levels of agitation; thus demonstrating cohesion's effect in resisting the separation or relative movement of particles. In addition, the authors observed that particles with high cohesion experience longer residence times, with similar path lengths, suggesting the particles move at a slower velocity through the blender. This postulates that methods which increase the shear rate, and therefore the relative particle velocity, may combat the effects of cohesion by increasing dispersion [92], and consequently improve micro-mixing. This could also be described as increasing the dynamic granular temperature as a function of the increased shear rate [93,94]. This finding may, at face value, seem to contradict the findings discussed in the previously mentioned study by Lopez et al. [55], in which the translational velocity of the powder going through the conveying portion of the system was observed to be higher with increasing cohesivity. However, despite the *net* velocity being higher, the *relative* velocity (which drives micro-mixing) may nonetheless be lower.

It should be noted that any residence time distribution (RTD) data will be a function of both the volume % of the tracer and the interaction of the tracer within the bulk that it aims to measure. For more detail on RTD behaviour in continuous blenders see

Escotet-Espinoza et al. [61,80], where the authors provide a comprehensive two-part study, analysing the behaviour of tracers with different properties.

Vanarase et al. [89] investigated the blending performance of a horizontal linear blender, both with and without the addition of a co-mill. The authors stated that under optimal macro-mixing conditions, micro-mixing was identified as the limiting factor, leading to poor mixing performance. The inverse was also found for optimum micro-mixing conditions. This highlights the independence of these two types of mixing, and the consequent requirement, to balance a blending system's capability to deliver both sufficient micro and macro mixing.

Interestingly, research by Portillo et al. [91] contains contradictory findings, when compared to Vanarase et al.'s study [89]. They found that using an incline blender increases the overall residence time when compared to a horizontal system—see Figure 10. Thus, for the same residence time as was demonstrated by Vanarase et al. and therefore similar macro behaviour, Portillo et al. showed that the agitator speed could be increased, which in turn provides greater shear, achieving improved micro-mixing conditions with cohesive powders.

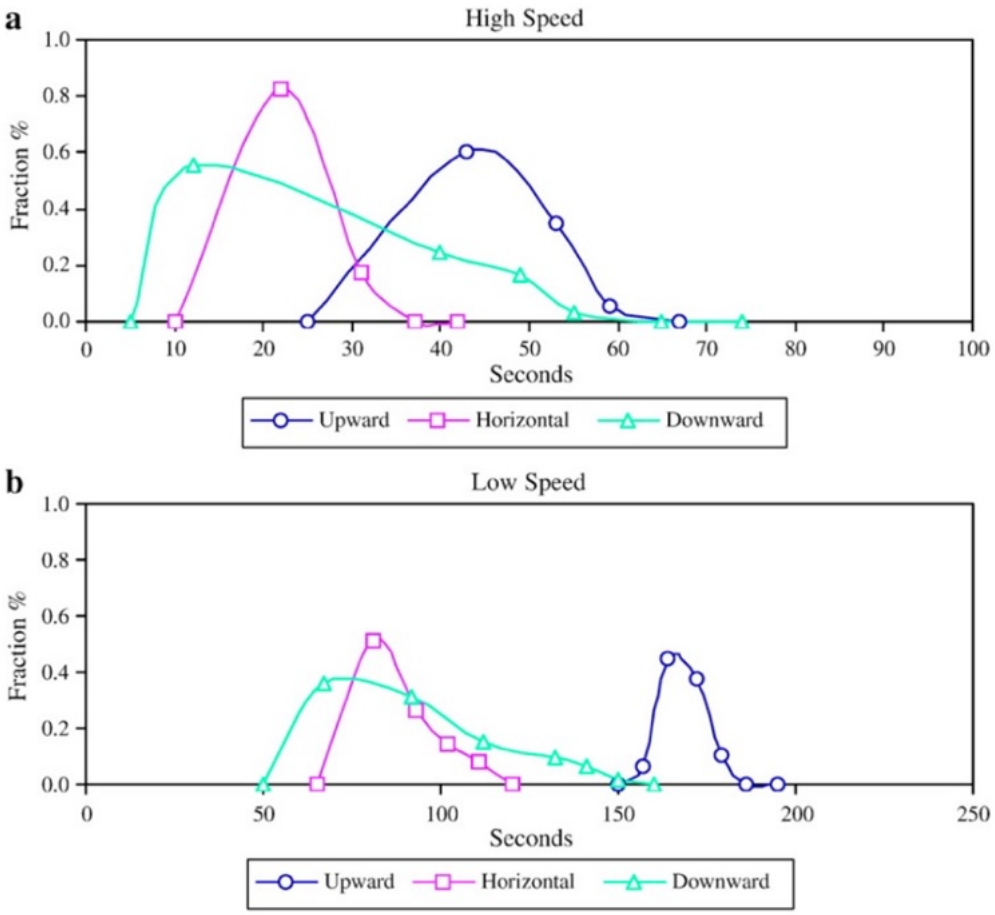


Figure 10. Acetaminophen residence time distribution plots (gathered with permission) from Portillo et al. [91], demonstrating the effect of blender volume inclination and RPM on RTD; (**a**) 78 RPM, (**b**) 16 RPM.

Van Snick et al. [43] investigated the performance of different mixing blade configurations (Figure 11, graphically demonstrates the orientation of blades along the agitator's axis) and found that despite the 'P16' blade configuration not delivering the highest dispersion, it offered the best consistency (see Figure 12). The 'P16' blade config' utilised a series of two sets of transport blades (45º), followed by a set of radial mixing blades (90º). Whereas

the other example—'D8'—delivered the highest powder dispersion, with the downside of higher variability. This is supported by Vanarase et al.'s [89] findings, with both surmising that a balance is required between micro and macro mixing. Based on 'P16's performance, in Van Snick et al. [43], it seems as if the 'D8' configuration provides a surplus of dispersion-lending to poor macro conditions. The authors also attribute the good performance of 'P16' to the increased mass hold-up within the blender's volume, as the mixing blades are shown to increase fill level, and therefore total mass hold-up [43]. Ultimately, the study suggests that varying position, number, and angle of the blades could aid in controlling API within the blending phase, and that different blade configurations may be selected according to the formulations' properties, such that the desired throughput is attained, whilst output variation is minimised.

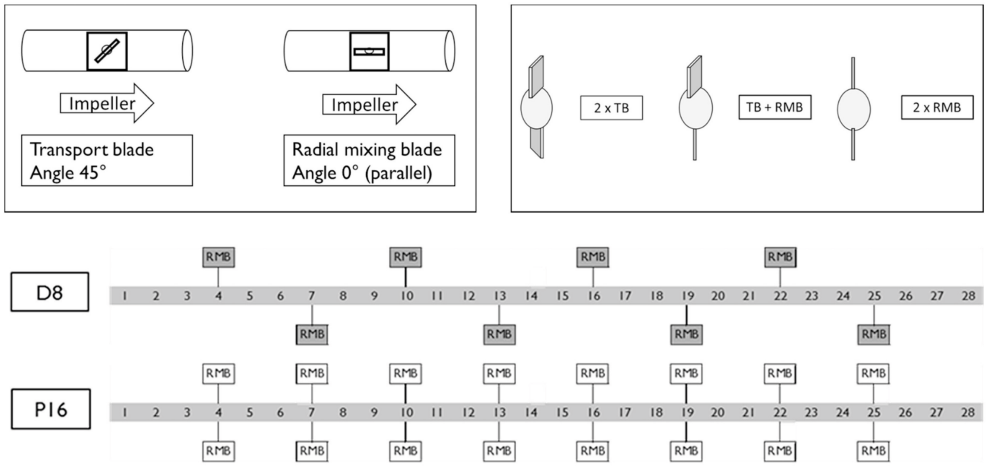


Figure 11. Blade configurations refer to a series of different blade orientations along the agitator's axis. (**Top left**): side-by-side comparison of transport blade and radial mixing blade (RMB). (**Top right**): example of a blade combination that would take a position along the agitator's axis, denoted by a number in the configurations D8 and P16 below. D8 and P16 depict blade configurations; all positions that are not labelled as RMBs are transport blades, and each collar position sees the blade combination rotate 60° clockwise to the direction of the impeller. Adapted from Van Snick et al. [43].

Gao et al. [95] developed a two-blade (periodic) section of a continuous horizontal mixer (see Figure 13), and evaluated mixing performance using a monodisperse DEM simulation of the blender. Gao et al. [95] subjected four different simulated powders (classified as: control, lower density, larger particle size, and cohesive) to the same tests, and mapped the axial conveying efficiency in fill level-rpm space. This conveying efficiency was quantified by normalising the mean axial velocity of particles with the rotor speed and effectively giving the mean distance conveyed per revolution. The powders were subjected to various fill levels (from 25–75%) and a range of rpms (50–250). Figure 14 shows that the relationship between normalised axial speed, and fill level/rotational speed was very different for the cohesive simulation: axial velocity is lower, when compared to the control and to the other powder types, especially at low speeds (50–125 rpm) with a moderate-to-high fill level (50–75%). In addition, the cohesive particles achieved a max velocity of only 38 mm/revolution, the lowest of the four samples [95]. These results are in agreement with the discussion gained from the work of Portillo et al. [78] work.

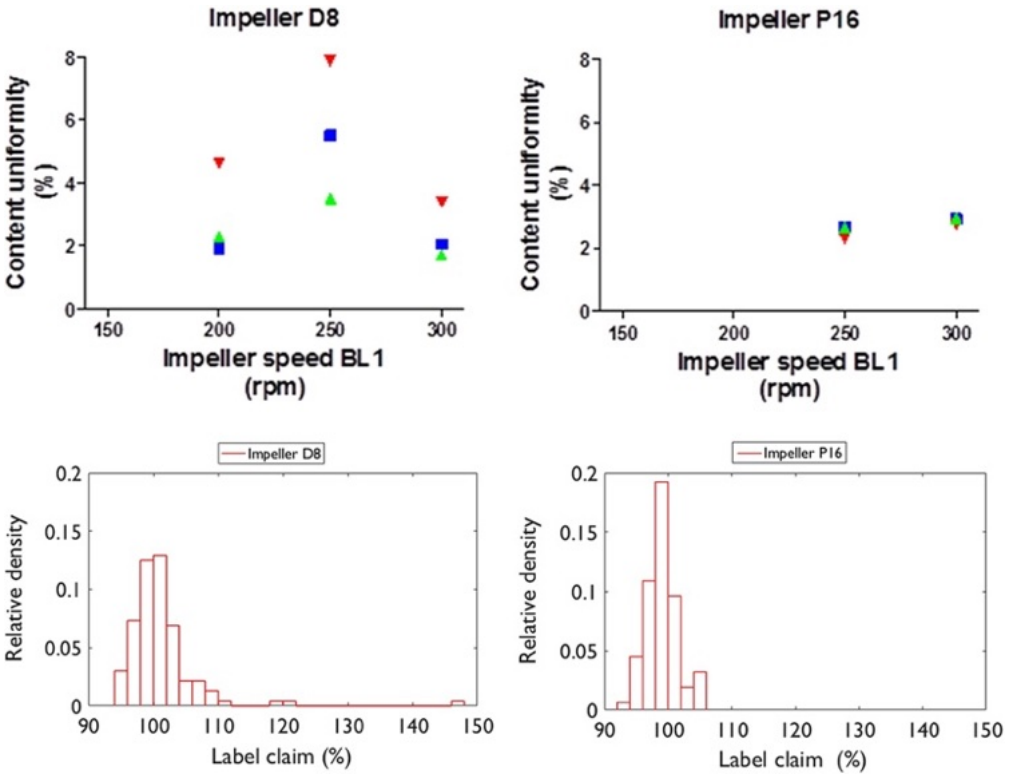


Figure 12. Tablet uniformity corresponding to the blade configurations seen in Figure 11 (D8 and P16); Upper graphs: content uniformity as a function of impeller speed and mass rate (green triangle = 24 kg/h, blue square = 30 kg/h, red triangle = 36 kg/h). Lower graphs: relative density distribution based on the target API dosage at the centre point of the experimental design (250 rpm and 30 kg/h). Gathered with permission from Van Snick et al. [43].

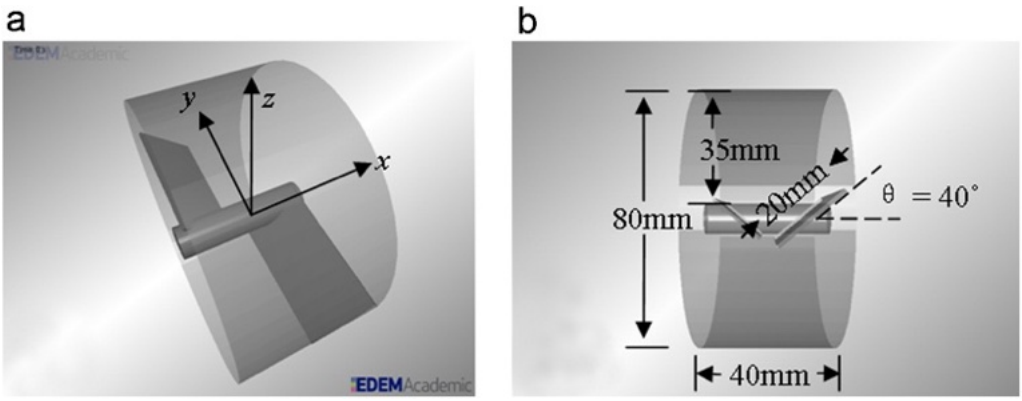


Figure 13. Periodic section of a continuous blender including two blades (**a**) Isometric View, (**b**) Side profile view with dimensions. Gathered with permission from Gao et al. [95].

It is worth noting that, for all non-cohesive powders used in Gao et al.'s work, when going from high to moderate fill levels (i.e., from 75% to 40%) at 100 rpm, normalised axial velocity increases. Cohesion is still shown to have an effect at higher rpms, demonstrated by the increased distance between the contours. This finding corroborates with the rpm-cohesion-significance result from Portillo et al. [78], clearly showing that the relative effect of cohesion will depend on operating conditions (speed and fill/mass rate), and not necessarily in a predictable way, reinforcing the need for more work in this area. This finding, surrounding the three non-cohesive powders, was further supported by the work

of Sarkar and Wassgren [96], where the normalised axial velocity presented the same trend, despite different geometry, particle properties, and operating conditions.

Gao et al. [95] also mapped the continuous blending rate (k_c), which is the ratio of the normalised mean axial velocity to the time-dependent RSD decay rate, where k_c essentially details the ratio between the axial (macro) and radial (micro) behaviour of the system. The results obtained were a similar contour plot to Figure 14, but in terms of k_c. Across the different particle properties, it was shown that high RPM and low fill produced the greatest k_c. Moreover, there was little difference seen in k_c at <125 rpm irrespective of fill level. For rpm > 125: going from high-to-low fill showed a sluggish increase in k_c, as the space between contours and colour changes progressed slowly. This highlights that cohesion does not only affect the axial aspect of the mixing process, but also contributes to the hampering of radial mixing. Finally, Gao et al. [95] suggest further investigation on segregating materials, which would prompt several questions on a constituent's experience within the bi-or-polydisperse system. Particularly, it is worth considering what might be the best excipients to pair with different levels of cohesive materials, in order to best aid their macro- and micro-mixing. This has the potential to result in a CDC formulation, of the same drug, differing from their original batch formulation. Different excipient(s) may offer a significantly improved CDC performance, without impacting the tablet's therapeutic efficacy.

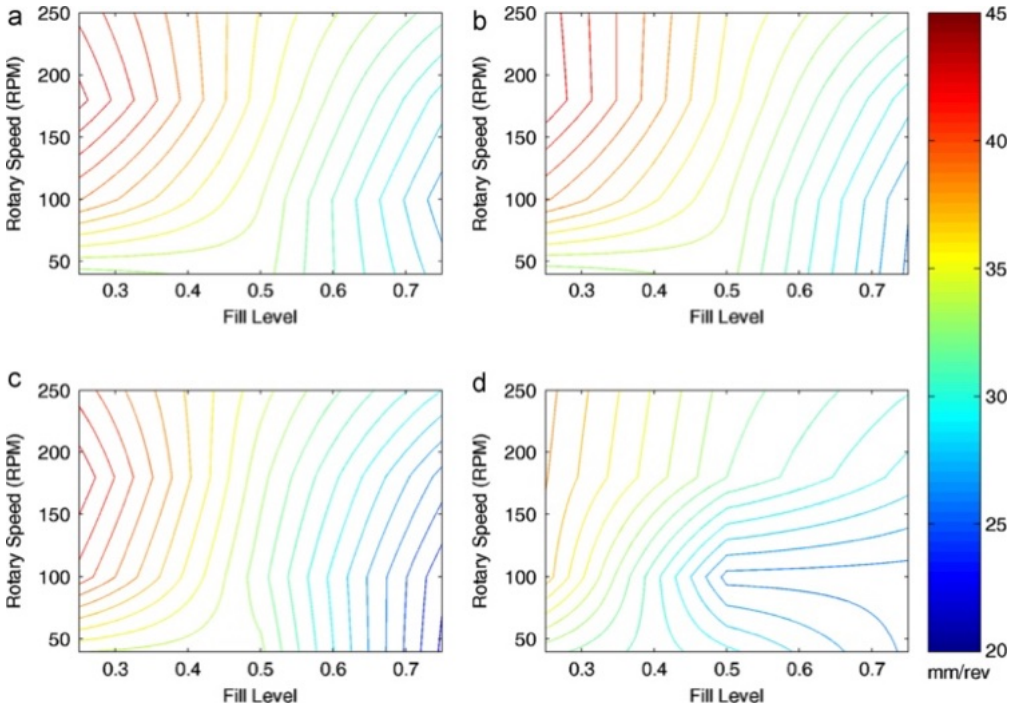


Figure 14. Contour plots of normalized mean axial velocity: (**a**) control, (**b**) lower density, (**c**) larger particle size, and (**d**) cohesive particles. Gathered with permission from Gao et al. [95].

Tomita et al. [97] utilised an atypical blending set-up, operating with both an impeller and a scraper in a horizontal mixer (see Figure 15). The inclusion of the scraper allowed for the control of the mean residence time in a manner that—unlike the previously-discussed systems—was quasi-independent of the magnitude of the impeller's agitation. In this system, the rpm of the axial impeller was driven separately to the ribbon-shaped scraper, which circumscribed the internal wall of the blender. Figure 15B shows the RTD curves of spiked acetaminophen using different scraper rpm speeds, whilst running at a feed rate of 10 kg/s and constant axial agitator speed of 3000 rpm. There is a considerable difference in the RTD performance between the slowest (5 rpm), and highest (50 rpm) scraper speed, which delivered a mean residence time of 84.3 s and 12.1 s, respectively. The mixer provides

a method of achieving higher micro-mixing whilst managing the macro-mixing through either increasing or decreasing the mean residence time. A similar result could be achieved with both the horizontal, or incline, blender through the alteration of either the angle of inclination, and/or the quantity of blades, blade angle, and/or blade positions. These design choices are, however, less practical to implement within a feedback loop or control strategy—though the incline angle of a blender may conceivably be varied dynamically.

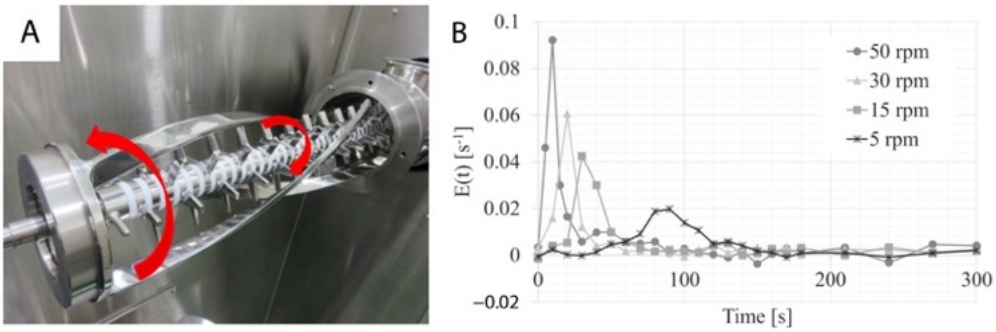


Figure 15. (**A**) Impeller and scraper continuous mixer with arrows detailing rotation direction, (**B**) APAP RTD spike response. Adapted from Tomita et al. [97].

Despite the advantages of an incline blender from a high-shear perspective, practical considerations must be made when attempting to maximise mixing capabilities. For example, the use of two units in series (horizontal blender and co-mill), as shown in Vanarase et al. [89], would allow independent, de-coupled, control in real-time. This reduces the risk that the process would leave a state of control, as each unit would have the capacity to compensate for the other. Conversely, if the incline blender is the only unit responsible for delivering both micro and macro-mixing, given it has the capacity to do so, it is likely the domain of control will be smaller when compared to the two units in series. This is because the process parameters controlling the micro-mixing also control the macro-mixing, and so there is a smaller window for advanced process control to operate within to ensure the mixing balance is maintained. This, therefore, showcases the strength of Tomita et al's [97] blending unit, as it possesses the ability to independently influence the macro and micro aspects of mixing, in real-time, using process control.

Palmer et al. [75] evaluated fill level and content uniformity across a range of processing parameters in an inclined (+15°) continuous blender. These processing parameters include: throughput, number of mixing blades, and agitator RPM. The study then explored the same parameters, using the same formulation, with different grades of API (APAP)—see Table 1. The result is the proposed exponential decay model (see Figure 16), and micro-mixing model (see Figure 17), which uses both the Peclet Number (Pe, see Equation (4)) and the strain (ϵ, see Equation (3)). In addition, Figure 18, showcases a series of contour plots describing the effect of processing parameters on the fill level, for each APAP formulation. The study explored a range of Froude numbers (Fr) between 1.5, and 13.4 (for 150 and 450 rpm, respectively).

Table 1. Material properties of the APAP grades used in Palmer et al. [75].

Material	FFC	Bulk Density (g cm^{-3})	Tapped Density (g cm^{-3})	Hausner Ratio	Carr's Index
Micronized APAP	1.4	0.19	0.30	1.58	36.67
Powdered APAP	1.9	0.31	0.53	1.71	41.51
Special Granular APAP	19.4	0.73	0.83	1.14	12.05

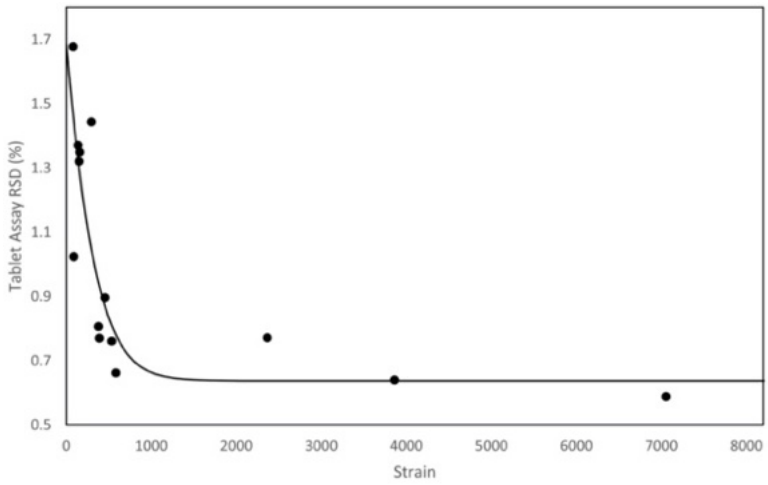


Figure 16. Tablet assay RSD plotted against Strain (see Equation (3)), an exponential decay model is fitted to the data. Gathered with permission from Palmer et al. [75].

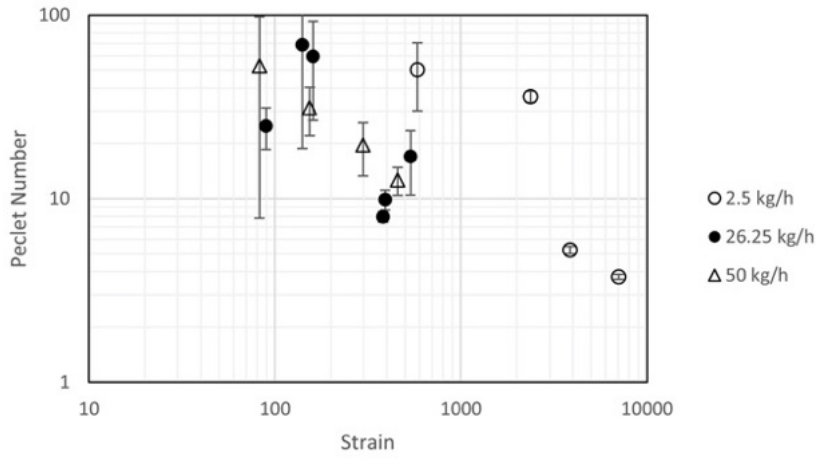


Figure 17. Peclet Number (Pe) and Strain relationship plotted on a log–log graph, grouped by throughput. Gathered with permission from Palmer et al. [75].

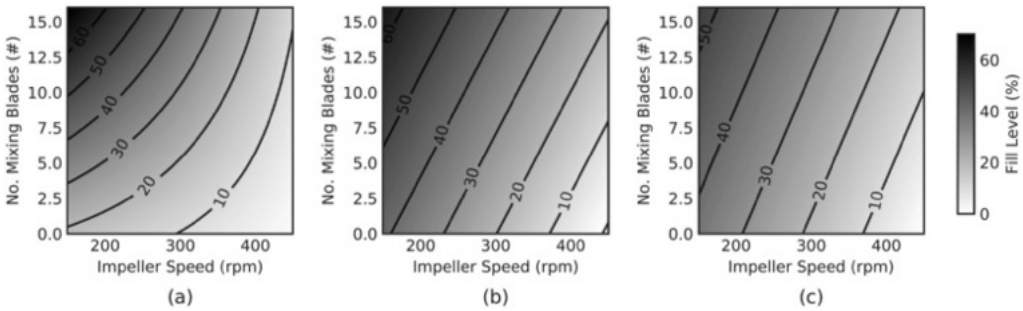


Figure 18. Contour plots mapping the impeller speed, number of mixing blades, and fill level at a throughput of 26.25 kg/h (**a**) Micronized APAP, (**b**) powder APAP, (**c**) special granular APAP. Gathered with permission from Palmer et al. [75].

Comparing the bulk characteristics in Table 1, Micronized APAP (mAPAP) has closer bulk characteristics to Powdered APAP (pAPAP), but shows a unique shape contour in Figure 18. Despite pAPAP and Special Granular APAP (sgAPAP) being opposed in flowability indices, they present similar contour shapes. This indicates a similar fill-level, and therefore bulk powder response, to the number of radial mixing blades (see Figure 11)

across a range of RPMs. For the mAPAP, however, increasing the number of radial mixing blades has more impact on the fill level at lower RPMs, and this impact reduces with increasing RPM. Van Snick et al. [43], discussed the necessity of sufficient mass hold-up (fill level) to attain good levels of macro mixing. The combination of these two studies suggests (i) that it is critical to determine the fill level landscape for the desired formulation to achieve and maintain sufficient mixing, and (ii) that different highly cohesive powders would be expected to exhibit different complex behaviours. What is more, using the mAPAP contour from Palmer et al. [75], considerations have to be made regarding what variables can be controlled in real-time. Since the radial mixing blades cannot be changed in real-time, it could be inferred from Figure 18, that using the highest number of mixing blades would be more optimum, as it would allow the system to have the largest range of fill levels.

Furthermore, Figure 16, from Palmer et al. [75], models the exponential decay of content uniformity RSD with increasing Strain (Strain, Equation (3)). Strain is a confounded variable for this system (an incline (+15º) linear blender), as increasing the RPM decreases the mean residence time, meaning that the number of blade passes also affects the mean residence time [75,91]. Thus, strain is dependent on the throughput, RPM, and the powder's material properties, making it essential to understand how the powder responds to processing parameters. Understanding in this area can be gleaned from the work of Portillo et al. [78,91], Gao et al. [90], and Lopez et al. [55] regarding powder velocity, fill level, and resultant changes in residence time due to cohesion. More cohesive powders would be subject to longer residence times, but lower relative velocities. Therefore, more cohesive powders should be more resistant to increasing RPM in turn reducing cohesion's effectiveness; Figure 18 demonstrates the added complexity. Ultimately, strain is a great, yet elusive, measure of effective work done to the powder. The model shows there is an optimum amount of strain required (around 1500) to attain a high-quality blend.

Lastly, Palmer et al. [75] shows a linear log–log relationship between Peclet Number (Pe) and strain, see Figure 17. Pe is a dimensionless number describing the ratio between advective and diffusive mixing in the system (see Equation (4)). To give an example, a high Peclet number would be expected to produce a narrow RTD. The model, at higher throughputs (and therefore, higher residence masses), showed reduced scattering and more linear behaviour, implying that the model may be favoured in predicting systems with high residence mass, whilst also implicitly suggesting that systems with low residence mass may present unstable micro-mixing capability and therefore may be unfavourable. Despite this, across all throughputs, it was seen that with reducing strain, the Peclet number increased.

$$Strain = \epsilon = MRT * \omega \tag{3}$$

where MRT is the mean residence time and ω is the agitator rotation rate.

$$Peclet\ Number = Pe = \frac{advective\ transport}{diffusive\ transport} = \frac{uL}{D} \tag{4}$$

where u is the flow velocity, L is the characteristic length and D is the mass diffusion coefficient.

$$Froude\ Number = Fr = \frac{centripetal\ force}{gravitational\ force} = \frac{\omega^2 R}{g} \tag{5}$$

where ω is the blade rotation rate, and R is the geometrically relevant length-scale—i.e., the radial distance from the centre axis to the tip of a blade.

While, as outlined above, strain is considered to be beneficial to powder blending, it has also been shown that powders which experience high levels of strain (number of blade passes) are also more likely to be subject to triboelectric charging [13]. Naturally, the effect will present some interest in how electrostatics influence/interact with powder cohesion. Karner and Urbanetz [13] investigated the influence of pharmaceutical mixing in a batch mixer and found that particle size, the fraction of fine particles, and mixing volume were significantly impacting the charging behaviour of the powder, stating that small particles

were more prone to generate higher charge density. How these findings would translate to a continuous blender represents a potentially interesting and valuable line of inquiry.

Beretta et al. [15,47] performed a two-part study on the triboelectric effect of charging powder via. powder transport in twin-screw feeding. This was followed by a study using relative humidity (RH) to subdue the electrostatic effect. Given that it is typical to maintain a RH between 30–60% in ISO-graded GMP environments [16] and that additional air moisture can increase the presence of liquid bridging, promoting cohesion [57], it becomes difficult to assess purely on the grounds of cohesion. The downside of controlling relative humidity is that it becomes difficult and expensive to maintain HVAC systems, especially as temperature and humidity fluctuate across the year. There are other options to consider, such as silication, outlined by Lumay et al's study [57], which was shown to be capable of electrostatic dissipation and localised relative humidity control. Therefore, the use of silicates becomes a much cheaper and simpler option, despite what relative humidity may offer. However, this assumption is limited by current knowledge and awareness of the author(s) at the time of composing this review—novel literature may render this assumption moot.

Beretta et al. [15,47] stated that the charging forces are primarily recruited through particle–particle friction, while particle–wall friction did not directly contribute to charging. In addition, the authors made considerations for impacts on powder mixing; interestingly, the discussion touched on utilising these static forces to aid the mixing process [47]. Huang et al. [70] provide evidence of this, as dry powder coating is seen in a high-shear co-mill. Huang et al. [70] investigated the effect of dry powder coating of different APIs and excipients and found that the coating of fine colloidal silica improved both bulk density and FFC performance. SEM images displaying the silica coating are shown in Figure 19. Therefore, charge- or cohesion-based coating could provide an avenue to attain what Fan et al. [83] (see Figure 8) would describe as perfect ordered mixtures.

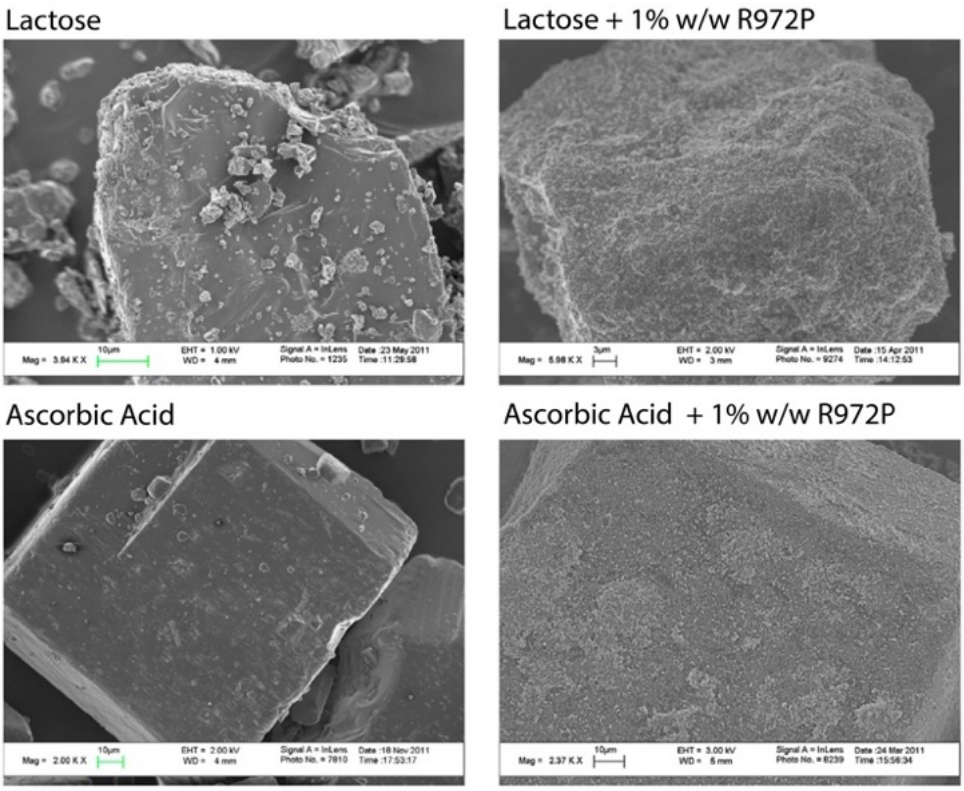


Figure 19. SEM images showing the surface coatings of (**top**): excipient (lactose) and (**bottom**): API (Ascorbic Acid). (**Left**): Non-coated and (**right**): 1% w/w Aerosil® R972 colloidal silica coating. Adapted from Huang et al. [70].

Lastly, alternative silicates—such as magnesium aluminosilicates (MAS)—have been trialled in some flowability studies; demonstrating an increase in flowability, without a constraint on mixing time and intensities, which is a limitation of several glidants [98]. Such materials could be used in place of the more traditionally used MPS grades for processes which may operate with different materials or mixing regimes.

3.3. Blending Summary

The scope of this topic is multidimensional, and therefore increasingly difficult to surmise without reducing the complexity of the situation; despite this, several trends—and avenues for future work—have emerged throughout this review.

Firstly, and perhaps most obviously, the literature strongly suggests that, regardless of differences between continuous blenders, cohesion provides a barrier to dispersion, and thus a barrier to achieving micro-mixing [78,90], which therefore decreases the quality of the mix. Cohesion has also been shown to exhibit complex behaviour at higher fill levels and lower rpms [75,78,90], where the particle–particle contacts are expected to be at their highest.

There is a common theme across the literature emphasizing the need to devise solutions to mitigate the effects of cohesion through the optimisation of processing parameters [43,45,75,88,99]. The literature suggests multiple manners in which this may be achieved, for example through alterations in system or agitator geometry, agitator rotation rate, feed rate, and various other factors. The differences in geometry for each blending system, however, means that each system has its own approach to solving the cohesion problem, thus making it difficult to generalise findings, and methodology, when attempting to understand the mechanisms and behaviour which explicitly govern cohesive blending. This is then exacerbated when considering that different formulations respond differently under the same conditions. An important task for future research is to define common parameters—e.g., dimensionless numbers—which can successfully generalise previous findings.

In the literature to date, several variables have been determined to affect the influence of cohesion on mixing. These include the Froude number (Fr, Equation (5)) or rpm, the magnitude of powder cohesivity, and the fill level of the blender. It has also been widely suggested that, due to cohesive particle–particle contact, a given system will require either a higher shear or more frequent agitation to break apart the additional cohesive forces. Strain (ϵ, Equation (3)) is defined as the mean residence time multiplied by the rotation rate of the agitator (RPM), and is a measure used to quantify the amount of work the agitator does per unit of space-time (τ) [43,75,82,88]. This quantity has been suggested as a valuable indicator of the degree of shear in a system and thus of blending success [43,75,82,88].

It has also been suggested that cohesion loses its significance, and complex behaviour, when rpm increases, implying that by running a continuous blender at high RPM, one may improve (micro-)mixing. However, the work of Van Snick et al. [43] suggested the need for a sufficiently large mass hold-up in order to ensure good macro-mixing. However, these seemingly contradictory requirements can potentially be reconciled by ensuring that RPM is high enough to minimise cohesion's effect, thus improving micro-mixing, whilst altering the system's geometry (or other system-specific variables) to ensure a suitable amount of hold-up mass is retained, thus retaining good macro-mixing.

Regarding future work, it would be interesting to see where the lines of significance lie for each of the three cohesion-dependent variables and their interactions. Such a study would most likely have to be conducted via DEM and should follow the suggestions left by Gao et al. [90]. In general, there is potentially significant value to be found in using numerical modelling methods such as DEM to address a number of the experimental observations discussed in this section.

A Perspective on Continuously Blending Cohesive Species

A final thought on continuous blending; is that the tablet's powder formulation could be thought of as an emulsion, whereby work (in the form of strain) is given by the blender to shear through existing API clusters, reducing their size, and promoting the distribution and circulation of the new, finer API clusters around the bulk mass. The cycle then continues, by imparting even-more work and further distributing the API clusters. The remainder of the tablet's formulation (which is mostly excipient) should, therefore, promote and stabilise the small API clusters, ensuring that they are maintained before they receive more work. Similarly, emulsions require thickeners and surface active agents to develop and maintain immiscible fluids [100]. Formulation development for CDC processes could look to use the same methodology, namely, through the exploitation of dry powder coating [70] and electrostatic charging [13]. However, considerations have to be made to ensure that, if the API is coated, it does not affect the therapeutic efficacy of the tablet.

4. Tabletting

4.1. Tabletting Introduction

The tabletting unit operation consists of three main steps:

- Die filling;
- Compaction;
- Tablet ejection.

The tabletting unit operation starts with the die-filling stage which fills the die with a consistent amount of powder mixture to achieve an adequate fill depth ready for the compaction step while also keeping good drug content uniformity [101,102]. The upper punch then lowers into the die increasing the compressional pressure applied to loose powder in the tabletting die; the powder consolidates as particles rearrange, filling void spaces and finally, as the availability of void spaces reduces, particles deform elastically, and ultimately plastically, before beginning to fragment [21] once the target pressure has been reached the upper die lifts releasing the pressure off the compact. Finally, the lower punch lifts the tablet to the top of the die ejecting the tablet. However, die filling and compaction are strongly influenced by cohesion whereas tablet ejection is not [103]. Qu et al. [103] study showed that additives such as silica which lowered cohesion did not lower ejection stresses effectively. Therefore, as this literature review focuses on cohesion, this section will only discuss die filling and compaction.

4.2. Tabletting Discussion

4.2.1. Die Filling Introduction

As mentioned previously, die filling is a critical process step for tablet manufacture as mass and content uniformity are heavily dependent on the die-filling performance. If the die filling is not consistent, the mass and drug content uniformity is not accurate [104]. This will have an impact in the downstream processes as the quality attributes such as tensile strength and the dissolution profile will be affected [102]. The die-filling process is known to be affected by many bulk powder properties: flowability, cohesion, particle size, and morphology [101,102]. Many studies have shown a good correlation between these bulk powder properties and the die-filling performance [27,28,104]. Normally, dies are filled gravitationally using a shoe-die system where power is dispensed from a feed hopper which is connected to a box-shaped shoe which then moves over the opening of the die and allows powder to flow [38] (Figure 20). However, there are different mechanisms for die filling such as:

- Forced feeders [102] which use moving components (usually paddles) to feed the powder into the die. This is commonly used in turret presses [105] (Figure 20);
- Suction filling is where the lower punch also known as the 'suction punch' moves down creating a negative air pressure gradient promoting powder to move into the

die, promoting the movement of the powder into the die [106] which removes the effect of air entrapment [38,107] (Figure 20).

Similar to Sections 2 and 3, to have a good die-filling performance, the powder will need to have lower cohesive properties [3] These include larger particle size, spherical particle shape powder with lower surface energy. (Lower surface energy will mean that powder will find it more difficult to form strong interparticle bonds [103,108]), which all contribute to improved flowability [27,38,107]. To have content uniformity, the segregation must be kept to a minimum during the die-filling stage so as not to undo the work done during the mixing stage [107,109]. This section will focus on the die fill performance where the mass, segregation and fill depth are important to ensure the compression process will be successful.

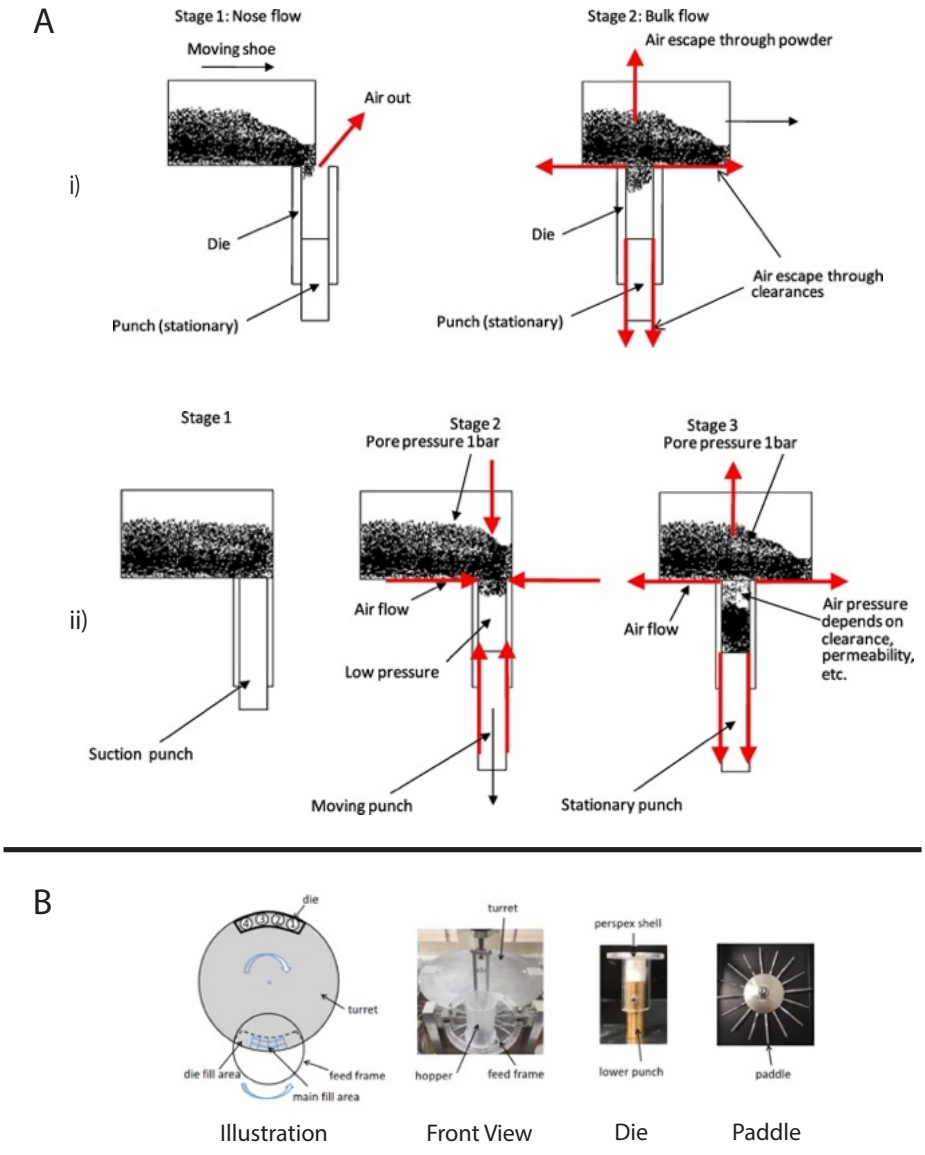


Figure 20. (**A**) Schematic diagram of air flow mechanism in (**i**) gravitational die-filling mechanism (**ii**) suction fill mechanism in a shoe and die system obtained from Mills and Sinka [38]. (**B**) Schematic of a rotary die-filling system, a type of force feeder, typically found in a turret tabletting machine obtained from Tang et al. [105].

4.2.2. Die Filling Discussion

Cohesion has been seen to affect the die-filling performance in many studies as the flowability of the powder is reduced with increasing cohesivity [27,110]. As mentioned previously, CDC processes have fewer unit operations as the granulation step is bypassed. Granulation is where powder fines which have poor flowability are made into agglomerates. The powder fines adhere to one another commonly using a binder fluid (wet granulation) to form a larger multiparticle entity which are also known as granules [111]. The granulation step helps control key attributes such as flowability and the processability of the powder and therefore controls cohesion [112]. However, as the CDC process does not have a granulation step, the tablet formulation will need to have adequate flowability and tabletability [3] which limits the amount of tablet formulation that can be used with the CDC process. However, there are die-filling mechanisms which can improve the die-filling performance of poorer-flowing powders without the granulation step.

Wu [110] established 'critical velocity', which is defined as the maximum velocity which the shoe passes over the die with the die being filled after one pass [27]. The critical velocity is a common way to measure the flowability of the powder. A strong correlation is seen between critical filling velocity and mean particle diameter; specifically, an increase in particle diameter and a decrease in surface energy increases the critical velocity (Figure 21) [101]. This indicates that when the powder is more cohesive, the critical velocity is lower as the flowability is poorer, which means that cohesivity can have a negative impact on die-filling performance and cohesion control measures will be needed.

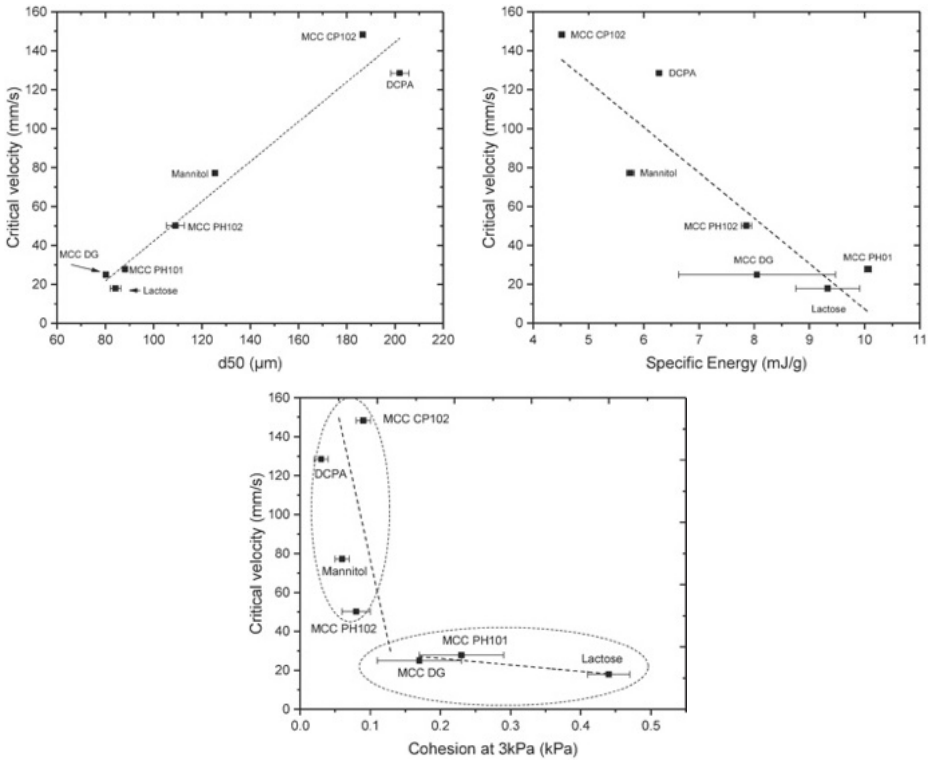


Figure 21. Graphs obtained from Zakhvatayeva et al. [101] showing the change of critical velocity as a function of: average particle size (**top left**), specific energy (**top right**) and cohesion at 3 kPa consolidation stress measured using the FT4 (**bottom**) of a variety of different materials.

The effect of paddle speed in forced feeders was investigated by Goh et al. [107] which saw with a higher paddle speed there was an increase in die fill weight and reduced die variation. However, it was seen in other papers that the paddle speed only had an effect on the weight variability, not the fill weight itself [84] and only affected fair flowing materials such as MCC [113]. Therefore, a higher paddle speed can allow for cohesive powders

to 'flow better' as they can essentially move as a solid block. On the other hand, in the study of Peeters et al. [114], results showed that the paddle speed affected the tensile strength. However, for the formulation with just microcrystalline cellulose, the tensile strength outcome was not affected by paddle speed. The only formulations that were affected were with magnesium stearate that saw a decrease in tensile strength with a higher paddle speed. Lubricants can have a negative effect on the tabletability if excessive shear force and higher levels of mixing occur. This is often referred to as 'over-lubrication' in the literature [115]. Therefore, the decrease in tensile strength is most likely due to these lubrication effects which is promoted with a higher paddle speed [116]. To understand the effects of lubrication in a forced feeder with higher paddle speeds, work should be conducted comparing the tensile strength outcomes of formulations with and without magnesium stearate. However, it should be noted that brittle materials are reported to not be as susceptible to the effects of lubricants as much as plastic materials [117]. Therefore, formulations with majority plastic powders will most likely be affected more heavily than formulations with a majority of brittle powders.

Another method to increase the flowability is by introducing air into the system, as flowing air gives a lubrication effect allowing particles to flow more easily with less resistance, increasing critical velocity [27]. The air prevents the percolation of fine particles, which reduces vertical segregation [118]. However, the presence of air can also create an adverse pressure gradient which resists the motion of particles, and pressure built up can further oppose the flow of the powder [27]. Suction filling has also seen positive effects with overcoming poorly flowable powders [38,106,109,119] and helps with the air entrapment which hinders powder flow as it creates a negative pressure gradient [38,107]. Furthermore, suction fill is generally known to lower the risk of segregation and improve the packing density [38]. This is seen in Figure 22 obtained from the study of Zakhvatayeva et al. [109]. The degree of segregation was measured using a sampling unit which separates the die into five sections; the process was repeated twice. The degree of segregation was calculated using Equation (6) where the segregation index indicates the level of uniformity in the powder blend in the die. Although the conclusion in Zakhvatayeva et al.'s [109] study is that suction filling improves die-filling efficiency and reduces segregation, in Figure 22 it is seen that gravitation filling with a fast die-filling velocity had a lower segregation index compared to suction filling. However, the slow die-filling velocity may not be representative of a real-life scenario in industry. Another interesting observation from Figure 22 is that with acetylsalicylic acid concentration of 10 percent, this had the worst overall segregation index across all cases which was explained as generally lower API concentrations are known to have a higher risk of segregation [120].

$$Segregation\ Index\ = \sum_{i}^{n} \frac{c_i - c_t}{c_t} \tag{6}$$

where c_i is the starting concentration of the blend and c_t is the concentration of the analysed sample.

All these results show that there are promising ways to overcome the effect of particle cohesion on die-filling processes; however, it is often concluded that these results are highly dependent on the particles' material properties [102,107]. Active pharmaceutical ingredients (APIs) are new and complex molecules that will often have unknown material properties [18]. Further studies should measure bulk properties and be able to understand what process parameters need to be utilised during the die-filling stage. APIs are known to be very cohesive and poorly flowing which gives the limitation that formulations for direct compression must have a maximum of 30% drug content [21].

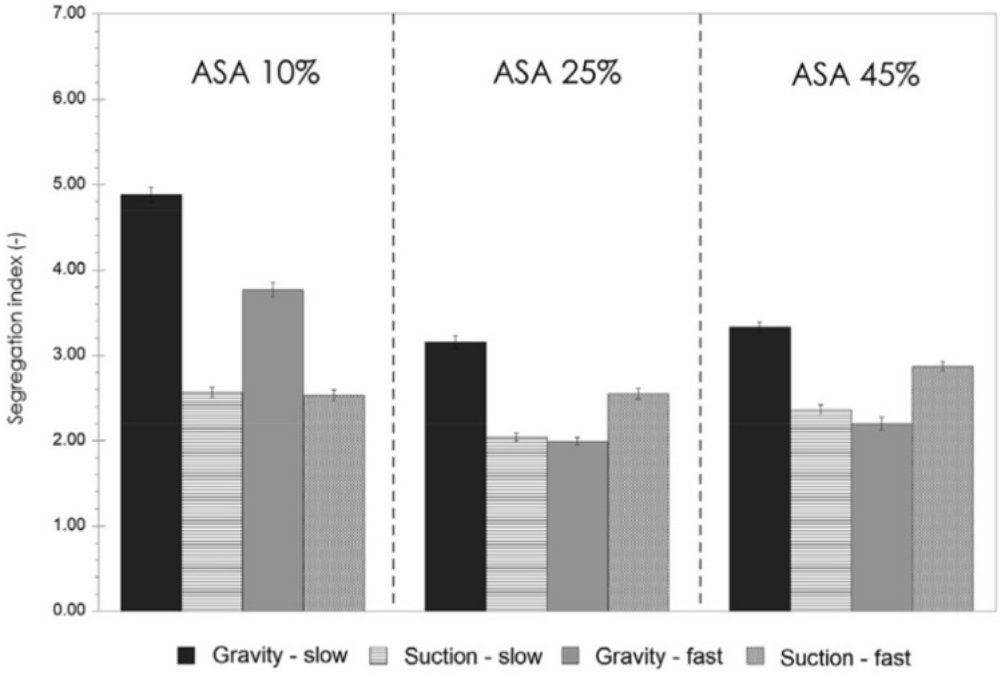


Figure 22. Segregation index of three different blends of Acetylsalicylic acid (ASA) with mannitol using gravity and suction filling where suction filling mostly has a lower segregation index compared to gravity from Zakhvatayeva et al. [109] the fast scenario is where the die-filling velocity is 260 mm/s and slow has a die-filling velocity of 70 mm/s.

A possible method to allow formulations with more than 30% drug content to undergo direct compression is spherical agglomeration/crystallisation, which will improve both processability and tabletability of the API. This is completed by changing the way the API is crystallised by either modifying the solvent addition rate and/or cooling rate [3]. Spherical agglomeration allows the API to crystallise spherically (Figure 23), which increases flowability and therefore lowers cohesion [3]. There are many promising studies using spherical agglomeration/crystallisation such as a study by Chen et al. [18] which saw an increase in flowability and therefore die-filling performance. Furthermore, the tabletability also improved (Figure 23) for the spherical agglomerated/crystallised produced using the quasi-emulsion solvent diffusion (QESD) method. The tensile strength was considerably higher compared to the 'as received' ferulic acid exhibits a needle-like elongated shape (Figure 23f). While spherical agglomeration/crystallisation is beneficial this should not be confused with the negative kind of agglomeration that occurs during secondary manufacture that can have a poor effect on blending, feeding and mixing. It is important to distinguish the two.

On the other hand, there are some disadvantages to spherical agglomeration/crystallisation; for example, solvent selection is a difficult process and may be limiting due to the growing concerns of using more green solvents in industry [121]. This will need to be further researched and optimised in order to be used as a commercial technique [121,122]. Furthermore, the optimisation of process parameters required for the spherical agglomeration/crystallisation method is difficult and will need considerable work to scale up the processes [123]. Therefore, although this technique will help produce many more formulations suitable for direct compression for most drugs to take place, the preparation times at this current state will probably outweigh the benefits of just granulating. However, this technique is very promising and something future research should focus on.

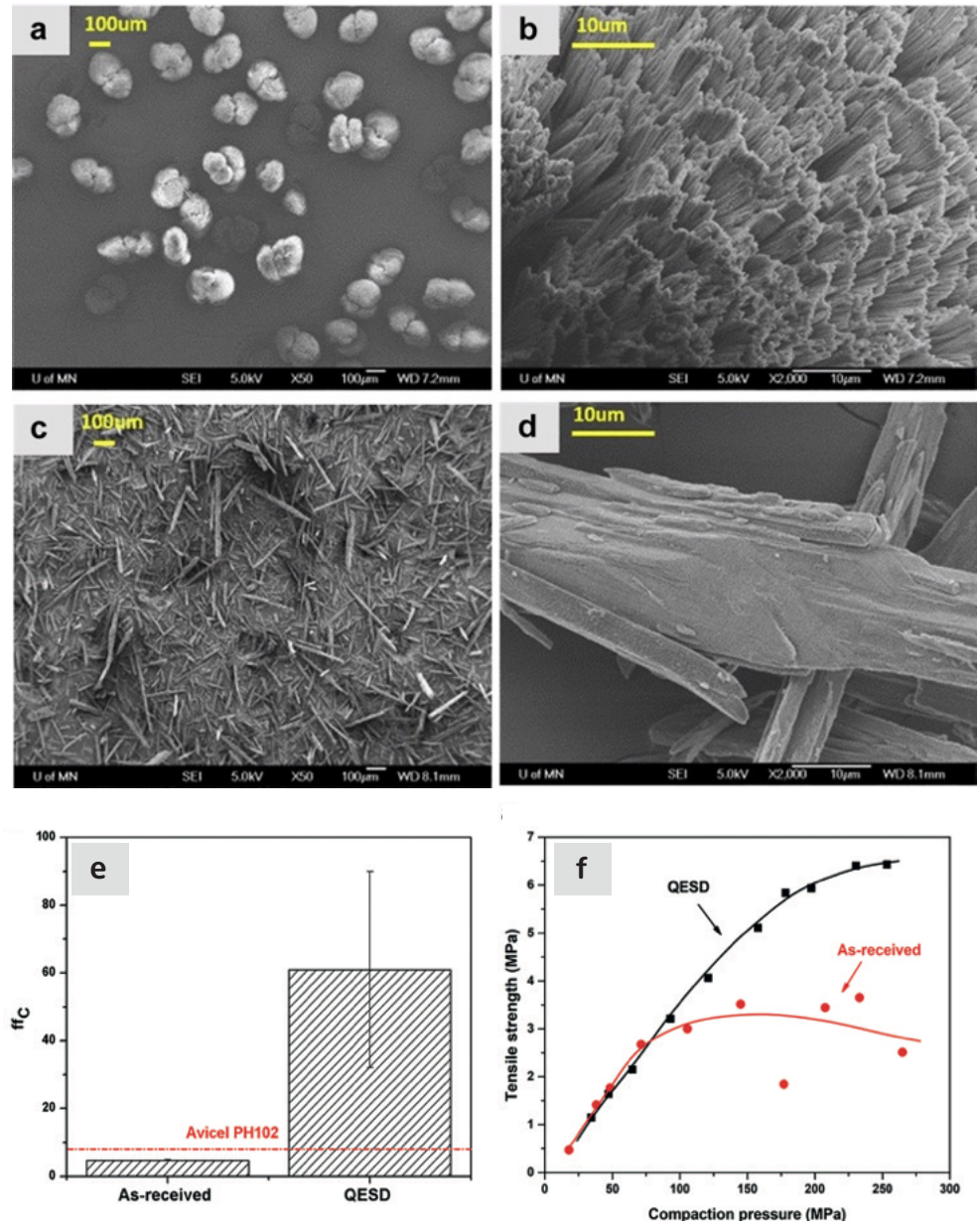


Figure 23. (**a**–**d**): Scanning electron microscope images of ferulic acid (FA) particles (**a**) Quasi-emulsion solvent diffusion (QESD) at 50× magnification, (**b**) QESD powder at 2000× magnification, (**c**) as-received FA powder at 50× magnification, and (**d**) as-received FA powder at 2000× magnification. (**e**,**f**): Figures to show improved tabletability and flowability with spherical agglomerated/crystallised (QESD) ferulic acid obtained from Chen et al. [18].

4.2.3. Compression Introduction

The aim of the compression process is to consolidate the powder mixture consisting of excipients and API into solid and cohesive compacts that can withstand the pressures of coating, packing, and shipping without fracturing. Therefore, the tablets will need to have a high enough tensile strength; however, if the tensile strength is too high this will typically lead to low porosity [30]. If the porosity is too low this could negatively affect the dissolution rate required to deliver the drug to the patient [124]. There are many aspects that contribute to the tablet's strength, such as moisture content [125], compression speed [126], and granulation [127]. However, as this literature review is focusing on the effect of cohesion and assumptions can be made that the tabletting process is completed

under strict humidity controls [100], this section will just be focussing on surface energy and particle size and shape. These three particle properties contribute heavily to the magnitude of cohesion [128]. Although cohesion effects for other process operations in the tabletting manufacturing process are known to have a mostly detrimental effect (see Sections 2 and 3), in contrast, cohesion properties are important to the compression as cohesivity helps produce a strong solid compact. Therefore, it is important to understand how the cohesion properties contribute to the tabletting stage so potential compromises can be taken to help the formulation perform well throughout the manufacturing process.

4.2.4. Compression Discussion

The effect of particle size on powder compaction has been the focus of many papers where it is generally understood that smaller particle sizes form a stronger tablet [29–32,129]. Smaller particles have been found to have a larger specific surface area where interparticle bonding can take place resulting in stronger tablets [130,131]. However, smaller particles are typically more cohesive and have poorer flowability which will affect die filling (Section 4.1).

Particle shape is commonly linked with particle size effects in tabletting and has similar effects on the flowability and cohesivity of the powder [132]. A more irregular shape will exhibit poorer flow properties and be more cohesive compared to regular or spherical-shaped powders [133]. Additionally, irregular-shaped powders have been shown to form a stronger tablet, which was demonstrated by Johansson and Alderborn's [30] study. The authors found that tablets containing irregular shaped MCC granules had a higher tensile strength than spherical-shaped pellets (Figure 24). Both granules exhibited plastic deformation as the dominant deformation mechanism, but at higher pressure, there was some fragmentation/attrition which resulted in a closer pore structure. Šimek et al. [133] investigated the effects of different particle shapes (Figure 24) of a brittle material, paracetamol. Their findings were similar to Johansson and Alderborn's [30], where more irregular shaped paracetamol had increased compressibility shown with the Heckel plot. The Heckel plot is a commonly used equation and plot to help understand the densification of the powder during compaction and allows interpretation of how plastic the powder is which is taken from the yield pressure which is derived from the reciprocal of the linear region gradient of the curve. The lower the yield pressure, the more plastic the material is [134]). Figure 25 compares this to spherical-shaped paracetamol.

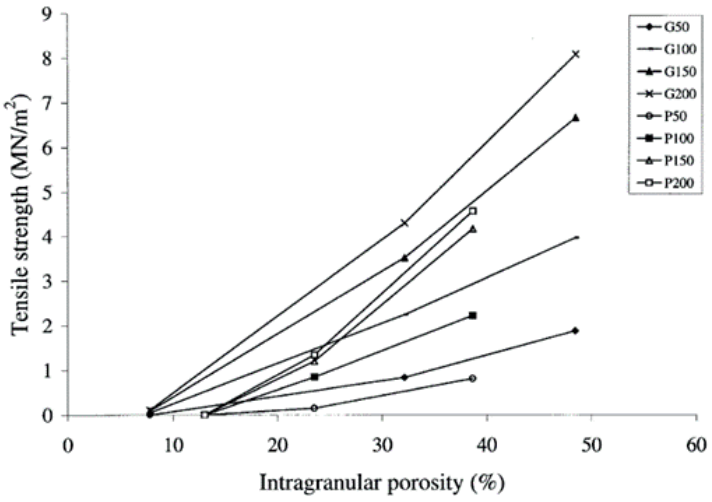


Figure 24. Johansson and Alderborn [30] G = granules (irregular), P = pellets (nearly spherical) the number is the compressional pressure it was compressed to e.g., G200 = granules compressed to 200 MPa.

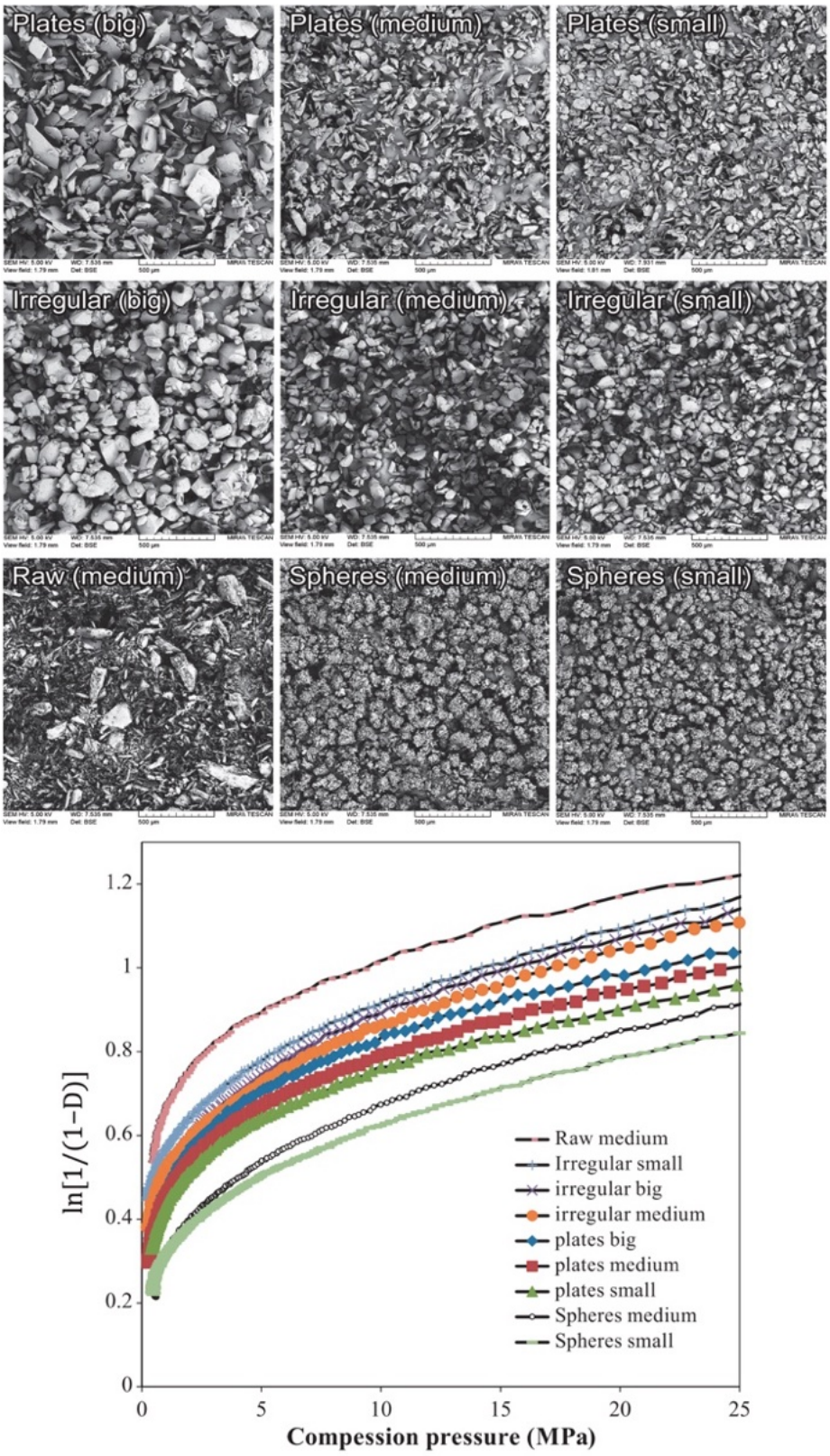


Figure 25. (**Top**): SEM micrographs of the paracetamol samples made (prepared and raw). The prepared samples were dissolved in ethanol and mixed at a set RPM to achieve the modified shapes. (**Bottom**): Heckel plot of different sizes and shapes of paracetamol. Both figures obtained from Šimek et al. [133].

Although the general trends of particle size and shape' effects on tabletting is mentioned in the previous section, there are some conflicting results regarding how they affect the compressibility and therefore tablet strength. This can be differentiated by material properties or the dominating deformation mechanism of the powder. Brittle materials such as lactose and paracetamol deform by fragmentation [135]. In studies, the strength of tablet consisting of brittle materials have been seen to be affected by particle size [29,128,136,137] and shape [138]. Skelbæk-Pedersen et al. [137] found that larger brittle powder particles such as lactose and calcium hydrogen phosphate dehydrate (DCP) fragmented more. In Figure 26, with increasing particle size in DCP and lactose, the peaks are more flatlines for the lines corresponding to the higher compressional pressure which means the particles fragmented into smaller particle sizes more readily. This agrees with De Boer et al. [29] Sun and Grant, [130] and Skelbæk-Pedersen et al. [137]. The more extensive fragmentation allows the void spaces to be filled with the smaller particles which further densifies the powder bed to reduce its negative influence of tensile strength. Nonetheless, smaller particles have higher tensile strength outcomes after compression [130]. Surprisingly, in contrast, Almaya and Aburub [117] found that dibasic calcium phosphate dihydrate did not have a difference with different particle sizes. Suggestions into why this may be occurring will be discussed below.

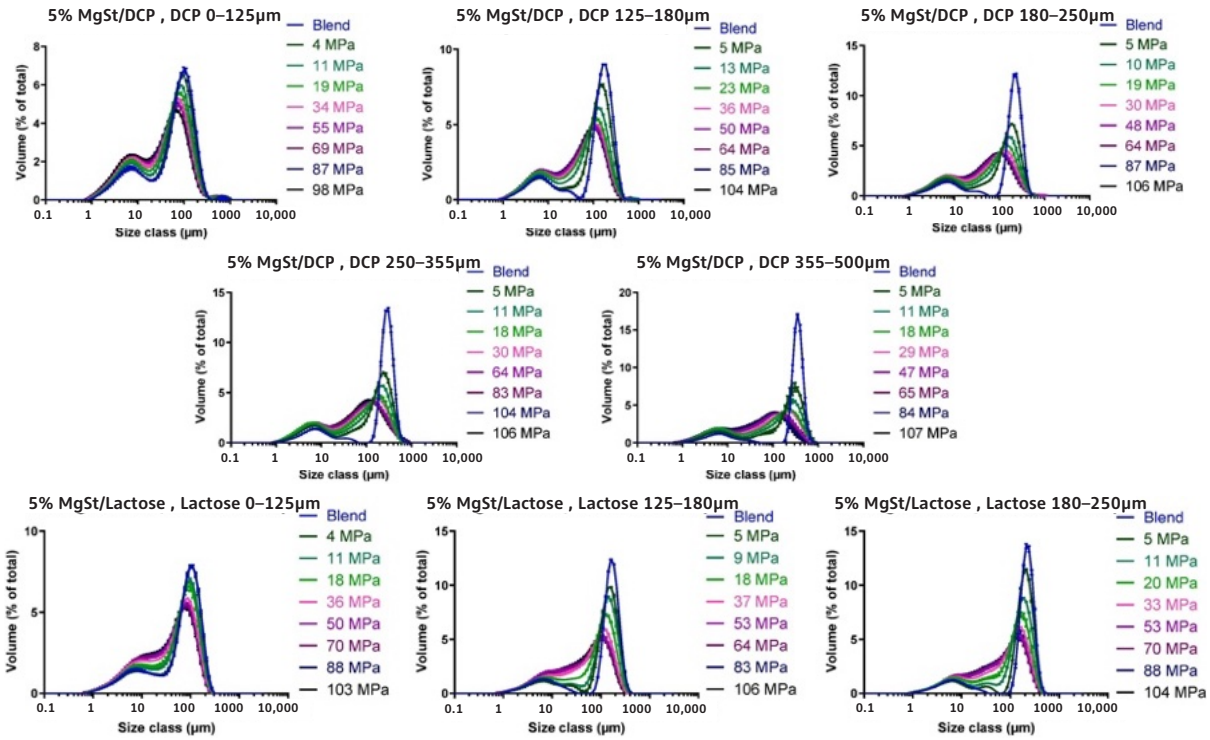


Figure 26. Skelbaek-Pedersen [137] PSD of calcium hydrogen phosphate dihydrate (**top**) and lactose (**bottom**) with different initial particle size distribution in the graph titles. The plots show the change in PSD with increasing levels of compressional pressure.

Plastically deforming powders are known not to be affected by particle size [117,128,136] due to the way they deform. McKenna and McCafferty [128] found that different sizes of microcrystalline cellulose (MCC) did not affect the tensile strength. However, Herting and Kleinebudde [116] found contradicting results that decreasing particle size of MCC and theophylline resulted in higher tensile strength. Wunsch et al. [132] found that there was an increase in tensile strength with decreasing particle size for all materials investigated (MCC and vildagliptin) (Figure 27) However, with vildagliptin, internal defects such as cracks during elastic recovery may have occurred resulting in large error bars. No fundamental

understanding of these differing results is given in the papers, particularly regarding the contradictions with past literature.

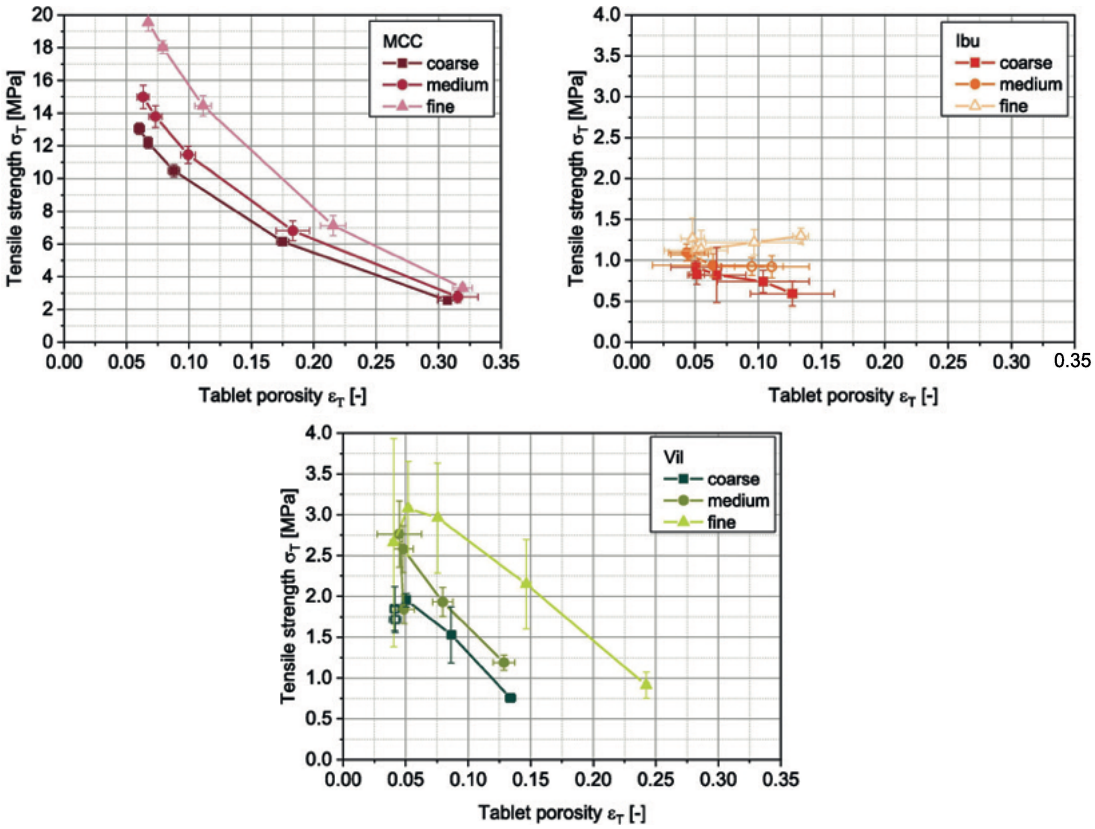


Figure 27. Compactability graphs of coarse, medium and fine grades of MCC, Ibuprofen and vildagliptin showing the change of compactability with particle size, obtained from Wunsch [132].

Despite these contradictions, which need to be further understood, a common conclusion can be made. Many papers agreed that, when the change in particle shape and size saw an increase in tensile strength, this was due to the specific shape or size which resulted in an increase in area of contact between particles under a compressional pressure [29,30,67,130,132]. Wünsch et al. [132] found that the reduction of initial particle size changes the deformation behaviour and therefore the effect of particle size is dependent on the specific material. With increasing initial particle sizes, the specific plastic energy rises but the specific elastic energy and elastic recovery is not affected as much. Therefore, when reducing sizes of materials, this could affect their mechanical response to the exerted compressional pressure. Furthermore, crystal structures may have important information about mechanical properties of the powder which is also seen in Sun and Grant's [130] study which saw two different polymorphs of sulfamerazine exhibit different compaction properties (Figure 28) Similar results were seen in Upadhyay et al.'s [139] study, where it was found that the different polymorphs of ranitidine hydrochloride exhibited different compressibility results. In a later study using the same polymorphs, polymorph I had better tabletability compared to polymorph II at all size fractions [140].

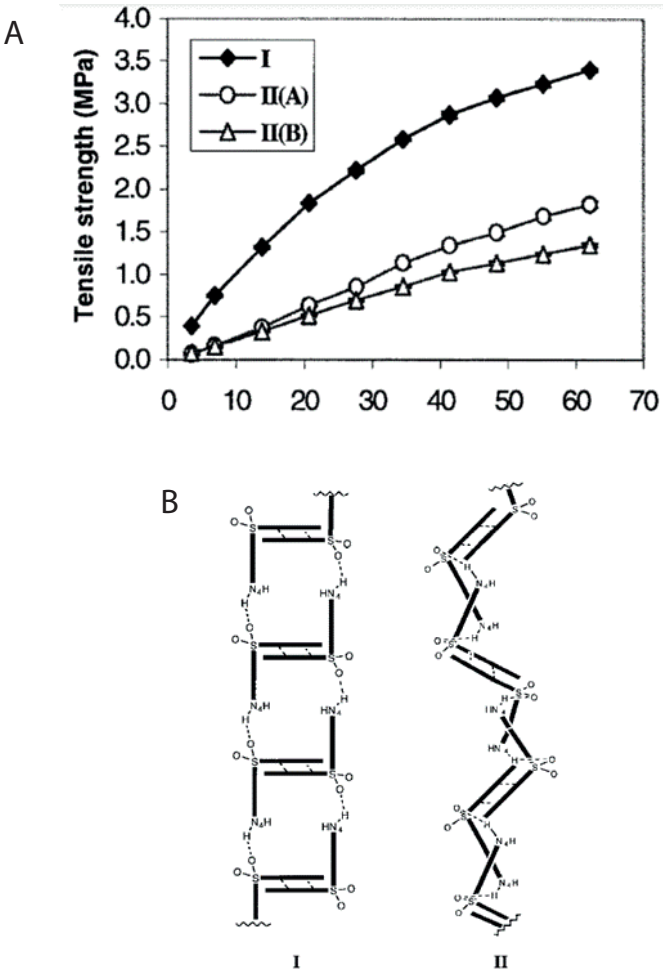


Figure 28. (**A**) Tabletability curves showing the difference of tabletability of three polymorphs of sulfamerazine I, II(A) and II(B). (**B**) Schematic of crystal structure of polymorphs: I and II. Hydrogen bonding are the broken lines. These crystal structure diagrams show that, even though the hydrogen bonding connectivity is the same for both polymorphs, the secondary structures are different. All figures obtained from Sun and Grant [130].

Future studies should pay more attention to crystal structure and understanding the corresponding mechanical properties of the materials being investigated before and after they are processed to a certain particle size which could affect the mechanical properties of the powder. For example, Simek et al. [133] modified their paracetamol samples in ethanol and changed the stirring speed to achieve the desired particle shape (Figure 25). Understanding these discrepancies could allow potential compromises to be made. For example, if a certain material is very cohesive but the particle size is independent of the tabletability properties, a larger particle size could be used to reduce cohesivity while not affecting the tabletability of the tablet formulation.

Surface energy is the excess energy on the surface compared to the bulk [141] which is affected by a number of intermolecular forces such as van der Waals [142]. A more cohesive powder will have a higher surface energy with interparticle bonding that will hinder the powder flow [143]. However, it is well documented that surface energy has a profound effect on producing successful tablets after powder compaction. Many results have suggested higher surface energy leads to stronger bonds forming between powder particles, which form higher tensile strength tablets [33–36]. For example, Wünsch et al. [132] suggested that formation of hydrogen bonds between MCC particles is why there was a considerable

increase of tensile strength compared to ibuprofen and vildagliptin, as seen in Figure 29. However, the way that MCC, ibuprofen and vildagliptin deforms was not considered in this discussion point.

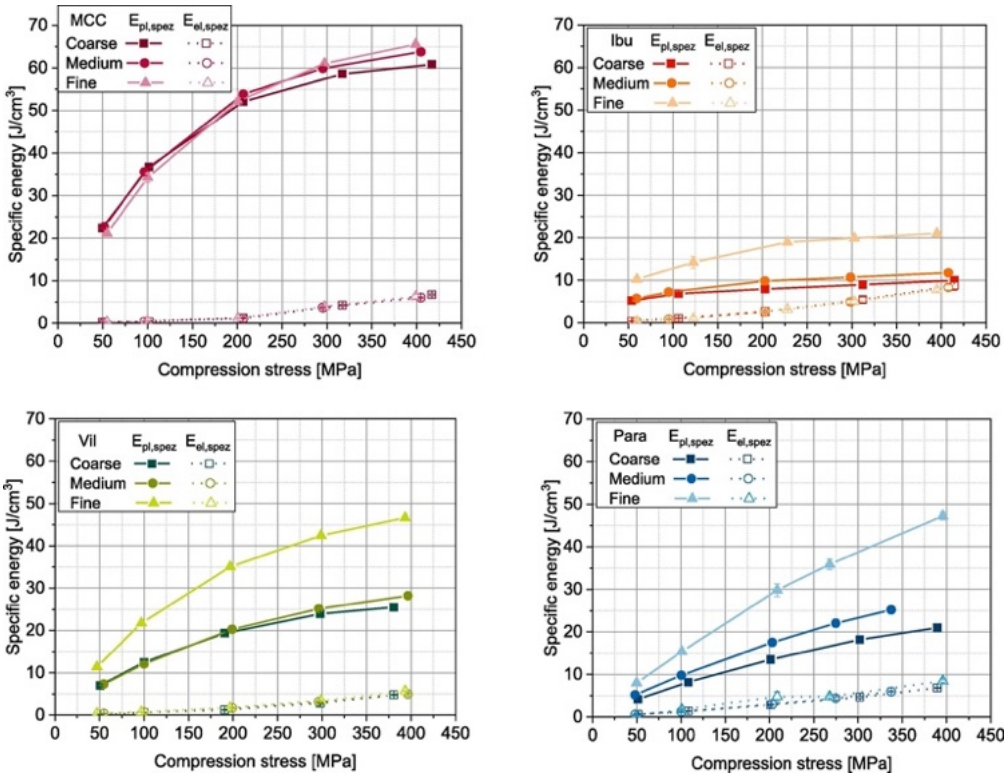


Figure 29. Graphs to show the specific plastic (solid lines) and elastic energies (dotted lines) of fine, medium and coarse grades of MCC, ibuprofen (Ibu) and vildagliptin (Vil) and paracetamol (para) obtained from Wunsch et al. [132] These graphs show that coarse grades have lower specific surface energy across all cases.

To intrinsically measure the effect of surface energy of the powder on the tensile strength is immensely difficult. Fichtner et al. [144] and Chen et al. [145] have attempted to change the surface energy of the powder by dry coating with polysorbate and Aerosil 200 respectively. This showed a decrease in tensile strength with the decrease of surface energy in both studies. However, the effect of changing particle size was not well documented and as previously stated in Section 4.2, depending on the specific material, particle size is another factor that changes the tablet outcome after compression. Ho et al. [146] counteracted this issue by changing the surface energy without changing any other powder particle property by modifying the functional groups on the surface of the powder without disrupting the surface morphology and particle size by silanisation. This treatment profoundly decreased the tensile strength of the tablet as the surface energy was reduced [147].

Another method, which was also mentioned in Section 2.1 to decrease the surface energy of a powder and improve flowability is to add a glidant, which is seen to increase the flowability by reducing cohesion [6]. How these additives affect the tabletability of the powder formulation was looked at in many different studies. Magnesium stearate (MgSt) is known to improve flowability [148]. However, it has a detrimental effect on the tablet strength especially when magnesium stearate is mixed for too long and vigorously. This is an effect which is known as 'over-lubrication' [116,149]. The MgSt is theorised to create a thin hydrophobic layer around powder particles preventing bonding between the powder particles to take place and therefore decreasing the tensile strength [149]. Furthermore, as MgSt is hydrophobic, the powder being 'over-lubcricated' will effect the dissolution [150].

On the other hand, MgSt has excellent lubrication properties and is commonly used in tablet formulation as a lubricant [144] rather than a glidant.

A glidant that is discussed frequently in literature is silicon dioxide. Apeji and Olowosulu [67] used talc and colloidal silica which appears to have had a negative influence on the tensile strength of the tablet. This paper did not have any comparison to a control data without any glidant to compare with. What the previous papers mentioned do not include is whether they are using hydrophobic or hydrophilic silicon dioxide. Kunnath et al. [151] looked at both hydrophilic and hydrophobic nano-silica and their impact on tablet tensile strength and dissolution (Figure 30). The nano-silica was dry coated onto the API with similar methods to those implemented by Chen et al. [145], mentioned previously. This saw an increase in tensile strength for both hydrophilic and hydrophobic nano-silica and did not see an effect on the dissolution profile. The possible explanation of this is that the dry coating of API led to deagglomeration of the powder and increased the total contact area where interparticle bonding can take place. On the other hand, in Mužíková et al.'s [66] study, when colloidal silica (Aerosil 200 and 255) was added, this saw a decrease in tensile strength, therefore the disintegration time also decreased. The max compressional pressure used to produce the tablets was very low (26.37 MPa) compared to what is normally used (200–250 MPa). However, Wunsch [132] found that it is the number of bonds which determine the strength of the tablet, not the bonding strength. Similar to the particle size conclusion, the fundamentals of the mechanical properties and therefore deformation properties of the powder are vital to understand as enhancing the bonding area may be more important than increasing the surface energy. Furthermore, this could mean a compromise can be taken on surface energy which will lower the cohesivity of the powder but would not affect the tablet outcomes if the contact area between particles is sufficient enough to gain the number of bonds needed. This further points to the importance of understanding how the powder deforms and how that effects and governs the contact area between particles [19].

There have been promising results for silicon dioxide alternatives such as magnesium aluminosilicate (MAS) and tricalcium phosphate (TCP). Both of these novel glidants have a positive effect on flowability [98]. However, there is just a single study investigating the tabletability of MAS, and none with TCP; in which, Hentzchel et al. [152] compared the tabletability of MAS with other silicates, when mixed with MCC of different concentrations. MAS was the only silicate that did not decrease in tablet strength, with increasing concentration, which is a positive result. Although the tablet strength is not affected by MAS, a study on how these novel glidants affect the dissolution rate at different concentrations will need to be conducted, as this is a critical quality attribute of the tablet. A study by Khunawattanakul et al. [153] saw the MAS in a tablet film coat increased the dissolution time, suggesting a balance will be required to ensure the right concentration to aid flowability is achieved, without negatively affecting dissolution. Although Tran et al. [98] shows that MAS aids flowability, this will need to be further investigated into whether MAS does have an impact on the feeding and blending parts of the CDC process. As far as the authors are aware there are no extensive studies that analyse the effect of these alternative glidants on these unit operations, essentially showing that additional studies are required to understand the complex interactions between not only CDC processing but the resultant in vivo performance of the tablet. The aforementioned publication Tran et al. [54] takes a perspective of using a range of measurement techniques to inform quantities or types of flow modifiers, practically taking a quality by design approach. A similar methodology could be applied in terms of glidants (namely, MAS) and their subsequent impact on tablet quality CQAs such as tensile strength of binary mixtures with excipients other than MCC.

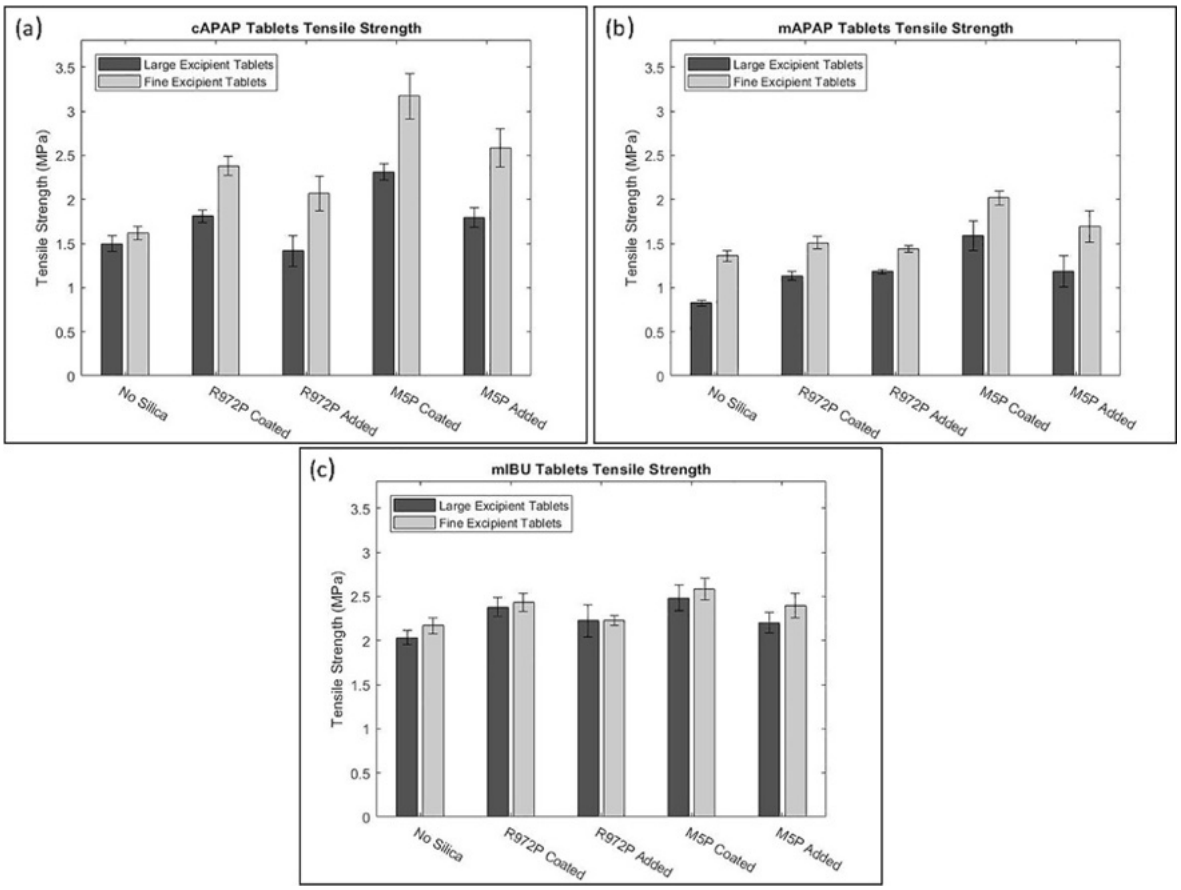


Figure 30. Tensile strength of the tablets made from (**a**) coarse acetaminophen (cAPAP), (**b**) micronised acetaminophen (mAPAP), and (**c**) micronised ibuprofen (mIBU) where Aerosil R972P nano-silica (hydrophobic) and CAB-O-SIL M5P nano silica (hydrophilic) obtained from Kunnath et al. [151].

4.3. Tabletting Summary

In this section, cohesion was split between two main contributing factors, particle size and shape, and surface energy, where smaller particle size and higher surface energy generally resulted in a higher magnitude of cohesion [24]. Although there are some contradictions seen in the particle size section, generally the tabletting process needs a good level of cohesion to be successful. However, spherical agglomeration is a promising technique that can lower the effects of cohesion seemingly without negatively affecting the tabletability [3,122]. More research will need to be conducted to optimise the solvent selection process [123].

Furthermore, both particle size and shape and surface energy research pointed towards the fundamentals of the mechanical properties of the powder. Particle size and shape discrepancies may be due to how the particle size and shapes were manipulated and how the crystal structure and therefore the material properties have changed. Additionally, it was found in Wunsch's et al. [132] paper that it is more the number of bonds rather than the strength of individual bonds that influences the overall tablet strength. Therefore, a higher contact area between particles to allow for a higher number of bonds could be more important than having higher surface energy powders to obtain stronger tablets.

The addition of glidants which increased flowability are seen to have contradicting results from commonly used silicon dioxide discussed in the previous section. On the other hand, promising initial results from modern alternative glidants, such as magnesium aluminosilicate (MAS), showed an increase in flowability and no change in tensile strength of the tablet regardless of concentration [98]. However, more studies need to be completed to scope what kind of an effect MAS has on dissolution and the tensile strength of binary

mixtures with different commonly used excipients with different deformation properties than MCC.

5. Summary Table

Table 2 summarises the effect cohesion has on the unit operation and what control measures are outlined in the discussion. How the control measures from one-unit operation can affect another downstream has yet to be discussed. This section will outline how some cohesion controls that have positive effects on unit operations can promote issues in downstream unit operations in the continuous direct compression line.

The consistency and accuracy of which powders are dispensed from a feeder will directly influence the downstream unit operations [43,45]. Therefore, it is of utmost importance that understanding is gained on how to maintain a consistent feed rate for very cohesive materials [2,41,55]. The use of silica shows great promise, as it seemingly both improves flowability and reduces electrostatic charging, leading to better screw filling and thus resulting in improved feeding consistency [5,47,57]. Lumay et al. [57] also showed silica's ability to influence the thixotropic behaviour; in future work, it would be interesting to see a development on this in the context of LIW feeding. However, the addition of silica has potentially negative effects on tabletting [66,67], while its effect on blending has not been explicitly described. Bridging/arching within the hopper volume has been shown to suffocate the flow of powder into the conveying volume. As a result, both additives and refilling strategy show ideas for reducing the processing variability [2,41,55,65]. Furthermore, using DEM for complex agitator design would further help the development of arching minimisation.

Despite the benefits of silication, attention should be paid to the end-to-end impact of formulation additives. For instance, nano-silicas were seen to have a lesser impact, compared to MPS, on the tablet strength, but greatly improved the flowability [57]. Alternatively, novel glidants, such as magnesium aluminosilicates, show promise in minimising the respective trade-off of improving flowability and affecting the tablet's tensile strength [152].

Blending seeks to intimately mix all of a given formulation's constituents and deliver them to the final, tabletting stage of the process with minimal variation [45,154]. Cohesion, in most cases, serves as a direct barrier to blending, as it provides resistance to intimate mixing [75,78,90]. Thus, higher levels of agitation are required to break apart these cohesive clusters, but systems must devise their own method to balance both the micro and the macro aspects of mixing [43,88]. In addition, complex bulk behaviour occurs when there is a moderate amount of cohesive particle–particle contacts [90]. Thus, it is of interest to develop a greater understanding of the mechanisms which govern this complex bulk behaviour. Moreover, despite the viewpoint to increase RPM to deal with cohesion, it is not understood what these new shear environments look like, and whether they have an impact on tabletability.

Spherical Agglomeration, which was discussed in Section 4.2, is a very promising technique to control the amount of cohesivity APIs add to tablet formulations without compromising tabletability to the same extent as the addition of glidants and lubricants which is beneficial to the whole CDC process. Further work will, however, need to be carried out to improve the efficiency of selecting the right solvent and process parameters [123]. Process parameters especially will need to be focussed on as some parameters are highlighted in studies that may be difficult to scale up. However, there have been good strides looking into the scale-up process and making spherical agglomeration/crystallisation continuous [155,156]. Ensuring the API crystals are not too large will be important to ensure content uniformity within tablets [123].

Table 2. Summary table with all the unit operations discussed in this literature review and their respective cohesion effects and controls. Note: Cohesion compron is denoted with a ◇, future work with ○, considerations △.

Unit Operation		Cohesion Effects Results in …	Cohesion Control or Compromise ◇	Future Work °/Considerations △
Feeding		Inconsistent screw filling	Modifying bulk density and cohesive particle-particle contact through additives, such as Silica [5,47,57]	Understand and be able to modify thixotropic powder ° behaviour
			Increase/Decrease conveying screw speeds [57]	
		Bridging/Arching	Refill Strategy [41,65]	DEM simulations exploring optimum hopper agitator design °
			Agitator Design	
Blending		Reduced micro-mixing	Increase in rpm (Fr) balanced by changes to system geometry to maintain macro [75,78,90]	
		Complex bulk behaviour, which results in poor mixing	Modify the three contributing factors: Fill level, Magnitude of Cohesion, and Froude Number [43,75,88,90]	
			Mechanistic understanding of how these factors interact [90]	
Tabletting	Die filling	Incomplete die fill and weight [102,110]	Spherical agglomeration [3]	Find a more efficient way to find the right solvents °
				Understand how spherical agglomeration will affect other CDC unit operations (feeding and blending) °
				Investigate the possibility of a scale-up method as the will be hard as the process is difficult and time consuming on small scale °
			Paddle speed [107]	Overlubrication can occur if the paddle speed is too high [115]. A compromise will need to be taken to ensure an increase of paddle speed will not effect tablet strength △
			Introduction of air in the system acting like a lubricant [27]	As this can create an adverse pressure gradient which will then resist the motion of particles. Find the ranges when air introduction is beneficial by Quality by Design experiments △
	Compaction	Better tabletability; generally lower particle size and higher surface energy results in stronger tablets but can have bad effects on dissolution if the tablet strength is too high [157]	Nano-silica and other novel glidants (magnesium aluminosilicate) can help promote better flowability and has little to no effect on tablet strength ◇ [151]	Understand the impacts of different types of nano-silica. Magnesium aluminosilicate will need to be tabletted with other common excipients and dissolution testing will to be conducted to assess the limitations°
			Number of bonds is more important than the strength of the bond could be able to compromise lower surface energy/cohesivity if there is sufficient contact area gained during compaction ◇	Understanding crystal structure fundamentally and how that changes material properties. This may be what is causing discrepancies regarding particle size and the tablet strength outcome ° [130]

6. Conclusions

This literature review consolidates the impact of powder cohesion and mitigation for each of the unit processes in CDC, whilst considering the consequences of upstream/downstream processing. For a tablet formulation to be viable for the CDC process, the formulation must possess both suitable flowability *and* tabletability [19,25]. Cohesion is known to cause powders to resist flow [23,24] which has a negative impact on the performance of the feeding [25], mixing [85,87], and die filling [3] unit operations involved in the CDC process whereas, for the compression stage, cohesivity is desired [29,30,33,35].

Understanding the cohesive nature of APIs and excipients and then manipulating them, where possible, is useful for improving the overall performance of the CDC process. The use of additives such as glidants and lubricants may aid the flow of powders, thus improving the feeding [6], mixing [37] and die filling [110] performance; however, these additives can have a negative impact on compaction [29]. Flow variability should be managed (specifically during the feeding stage) as any perturbations will be propagated into successive unit operations [2,158].

Despite the volume of literature in this area, there remain many important open questions and thus valuable future research avenues:

- Silication has benefits similar to glidants and lubricants as it can lower the cohesive behaviour of the powder and therefore increase flowability [6]. However, there are contradictions on whether silication negatively affects tabletability; this will need to be further investigate [67,145]. Alternative glidants, e.g., magnesium aluminosilicates, are a promising option however, more work needs to be carried out to understand the impact on tablet performance.
- Discrete Element Method (DEM) modelling, allowing researchers to create a digital twin(s) of an existing experiment and conduct statistical analysis on the simulated powder behaviour would allow researchers to gather metrics to quantify mixing/feeding performance (as discussed in Escotet-Espinoza et al. [80]) that were not accessible experimentally.
- Utilising triboelectric charging for the blending stage: static surface charge is developed on the surface of particles due to the strain given to the powder during mixing/transport [47], potentially allowing a formulation to be altered to promote attraction/repulsion between constituent species in order to gain a more-ordered well-mixed system.
- Spherical agglomeration/crystallisation can improve the flowability and tabletability of APIs, which is normally the most cohesive component of the tablet formulation [3,18]. However, further work needs to be performed to improve the solvent selection and process parameters to allow for scale-up [123].
- The many discrepancies in the literature regarding the manner in which particle size affects the tabletability of the powder should be comprehensively addressed, as this represents an important gap in the fundamental understanding of powder compression [39,128]. Understanding which types of powders are affected by particle size and which are not could lead to compromises to have larger particle sizes to lower cohesivity and therefore improve flow while not affecting the tabletability.

Author Contributions: Conceptualization, O.J.-S. and Z.C.; formal analysis, O.J.-S. and Z.C.; investigation, O.J.-S. and Z.C.; writing—original draft preparation, O.J.-S. and Z.C.; writing—review and editing, C.R.K.W.-Y. and A.I.; visualization, O.J.-S. and Z.C.; supervision, C.R.K.W.-Y. and A.I.; project administration, C.R.K.W.-Y. and A.I.; funding acquisition, C.R.K.W.-Y. and A.I. All authors have read and agreed to the published version of the manuscript.

Funding: The authors would like to thank the Engineering Doctorate programme funded by EPSRC through the Centre for Doctoral Training in Formulation Engineering (grant no. EP/L015153/1), and from AstraZeneca plc.

Acknowledgments: The authors would like to also thank Adedoyin Yahyi for the initial insight and discussion surrounding powder feeding.

Conflicts of Interest: The authors declare no conflict of interest. The company had no role in the design of the study; in the collection, analyses, or interpretation of data; in the writing of the manuscript, and in the decision to publish the results.

Abbreviations

The following abbreviations are used in this manuscript:

CDC	Continuous Direct Compression
CQAs	Critical Quality Attributes
CMAs	Critical Material Attributes
API	Active Pharmaceutical Ingredient
FFC	Flow Function Coefficient
SEM	Scanning Electron Microscope
DEM	Discrete Element Method
MPS	Mesoporous Sillica
rpm	Revolutions Per Minuite
cBD	Conditioned Bulk Density
LIW	Loss in Weight
APAP	Acetaminophen
RSD	Relative Standard Deviation
PCA	Principle Component Analysis
RTD	Residence Time Distribution
MCC	Microcrystalline Cellulose
MgSt	Magnesium Stearate
MAS	Magnesium Aluminosilicate
TCP	Tricalcium Phosphate
mAPAP	Micronised Acetaminophen
pAPAP	Powdered Acetaminophen
sgAPAP	Special Granular Acetaminophen
RH	Relative Humidity
GMP	Good Manufacturing Practice
HVAC	Heating Ventilation & Air Conditioning
FT4	Freeman Powder Rheometer
QESD	Quasi-emulsion solvent diffusion
DCP	Calcium hydrogen phosphate dehydrate

References

1. Vercruysse, J.; Delaet, U.; Van Assche, I.; Cappuyns, P.; Arata, F.; Caporicci, G.; De Beer, T.; Remon, J.P.; Vervaet, C. Stability and repeatability of a continuous twin screw granulation and drying system. *Eur. J. Pharm. Biopharm.* **2013**, *85*, 1031–1038. [CrossRef] [PubMed]
2. Engisch, W.E.; Muzzio, F.J. Loss-in-Weight Feeding Trials Case Study: Pharmaceutical Formulation. *J. Pharm. Innov.* **2015**, *10*, 56–75. [CrossRef]
3. Chattoraj, S.; Sun, C.C. Crystal and Particle Engineering Strategies for Improving Powder Compression and Flow Properties to Enable Continuous Tablet Manufacturing by Direct Compression. *J. Pharm. Sci.* **2018**, *107*, 968–974. [CrossRef] [PubMed]
4. Liu, L.X.; Marziano, I.; Bentham, A.C.; Litster, J.D.; White, E.T.; Howes, T. Influence of particle size on the direct compression of ibuprofen and its binary mixtures. *Powder Technol.* **2013**, *240*, 66–73. [CrossRef]
5. Leung, L.Y.; Mao, C.; Srivastava, I.; Du, P.; Yang, C.Y. Flow Function of Pharmaceutical Powders Is Predominantly Governed by Cohesion, Not by Friction Coefficients. *J. Pharm. Sci.* **2017**, *106*, 1865–1873. [CrossRef] [PubMed]
6. Escotet-Espinoza, M.S.; Scicolone, J.V.; Moghtadernejad, S.; Sanchez, E.; Cappuyns, P.; Van Assche, I.; Di Pretoro, G.; Ierapetritou, M.; Muzzio, F.J. Improving Feedability of Highly Adhesive Active Pharmaceutical Ingredients by Silication. *J. Pharm. Innov.* **2021**, *16*, 279–292. [CrossRef]
7. Visser, J. Van der Waals and other cohesive forces affecting powder fluidization. *Powder Technol.* **1989**, *58*, 1–10. [CrossRef]
8. Juarez-Enriquez, E.; Olivas, G.I.; Zamudio-Flores, P.B.; Perez-Vega, S.; Salmeron, I.; Ortega-Rivas, E.; Sepulveda, D.R. A review on the influence of water on food powder flowability. *J. Food Process Eng.* **2022**, *45*, e14031. [CrossRef]
9. Zafar, U.; Vivacqua, V.; Calvert, G.; Ghadiri, M.; Cleaver, J.S. A review of bulk powder caking. *Powder Technol.* **2017**, *313*, 389–401. [CrossRef]

10. Wei, Z.; Zhao, Y.P. Growth of liquid bridge in AFM. *J. Phys. D Appl. Phys.* **2007**, *40*, 4368. [CrossRef]
11. Hou, Q.; Dong, K.; Yu, A. DEM study of the flow of cohesive particles in a screw feeder. *Powder Technol.* **2014**, *256*, 529–539. [CrossRef]
12. Allenspach, C.; Timmins, P.; Lumay, G.; Holman, J.; Minko, T. Loss-in-weight feeding, powder flow and electrostatic evaluation for direct compression hydroxypropyl methylcellulose (HPMC) to support continuous manufacturing. *Int. J. Pharm.* **2021**, *596*, 120259. [CrossRef] [PubMed]
13. Karner, S.; Urbanetz, N.A. Arising of electrostatic charge in the mixing process and its influencing factors. *Powder Technol.* **2012**, *226*, 261–268. [CrossRef]
14. Abouzeid, A.Z.M.; Fuerstenau, D.W. Effect of Humidity on Mixing of Particulate Solids. *Ind. Eng. Chem. Process Des. Dev.* **1972**, *11*, 296–301.
15. Beretta, M.; Hörmann, T.R.; Hainz, P.; Hsiao, W.K.; Paudel, A. Investigation into powder tribo–charging of pharmaceuticals. Part II: Sensitivity to relative humidity. *Int. J. Pharm.* **2020**, *591*, 120015. [CrossRef] [PubMed]
16. Haycocks, N.; Goldschmidt, N.A.; Thomsen, U. Temperature & Humidity Requirements in Pharmaceutical Facilities. 2023. Available online: https://ispe.org/pharmaceutical-engineering/september-october-2021/temperature-humidity-requirements-pharmaceutical (accessed on 31 March 2023).
17. Sun, C.C. Mechanism of moisture induced variations in true density and compaction properties of microcrystalline cellulose. *Int. J. Pharm.* **2008**, *346*, 93–101. [CrossRef]
18. Chen, H.; Aburub, A.; Sun, C.C. Direct Compression Tablet Containing 99% Active Ingredient—A Tale of Spherical Crystallization. *J. Pharm. Sci.* **2019**, *108*, 1396–1400. [CrossRef]
19. Sun, C.C. Decoding powder tabletability: Roles of particle adhesion and plasticity. *J. Adhes. Sci. Technol.* **2011**, *25*, 483–499. [CrossRef]
20. Haywood, A.; Glass, B.D. Pharmaceutical excipients—Where do we begin? *Aust. Prescr.* **2011**, *34*, 112–114. [CrossRef]
21. Jivraj, M.; Martini, L.G.; Thomson, C.M. An overview of the different excipients useful for the direct compression of tablets. *Pharm. Sci. Technol. Today* **2000**, *3*, 59–63. [CrossRef]
22. Escotet-Espinoza, M.S. Phenomenological and Residence Time Distribution Models for Unit Operations in a Continuous Pharmaceutical Manufacturing Process. Ph.D. Thesis, Rutgers University-School of Graduate Studies, New Brunswick, NJ, USA, 2018; p. 312.
23. Shah, U.V.; Olusanmi, D.; Narang, A.S.; Hussain, M.A.; Tobyn, M.J.; Hinder, S.J.; Heng, J.Y. Decoupling the contribution of surface energy and surface area on the cohesion of pharmaceutical powders. *Pharm. Res.* **2015**, *32*, 248–259. [CrossRef]
24. Shah, R.B.; Tawakkul, M.A.; Khan, M.A. Comparative evaluation of flow for pharmaceutical powders and granules. *AAPS PharmSciTech* **2008**, *9*, 250–258. [CrossRef] [PubMed]
25. Engisch, W.E.; Muzzio, F.J. Method for characterization of loss-in-weight feeder equipment. *Powder Technol.* **2012**, *228*, 395–403. [CrossRef]
26. Mazumder, M.K.; Sims, R.A.; Biris, A.S.; Srirama, P.K.; Saini, D.; Yurteri, C.U.; Trigwell, S.; De, S.; Sharma, R. Twenty-first century research needs in electrostatic processes applied to industry and medicine. *Chem. Eng. Sci.* **2006**, *61*, 2192–2211. [CrossRef]
27. Wu, C.Y.; Dihoru, L.; Cocks, A.C. The flow of powder into simple and stepped dies. *Powder Technol.* **2003**, *134*, 24–39. [CrossRef]
28. Freeman, R.; Fu, X. Characterisation of power bulk, dynamic flow and shear properties in relation to die filling. *Powder Metall.* **2008**, *51*, 196–201. [CrossRef]
29. De Boer, A.H.; Vromans, H.; Leur, C.F.; Bolhuis, G.K.; Kussendrager, K.D.; Bosch, H. Studies on tableting properties of lactose—Part III. The consolidation behaviour of sieve fractions of crystalline α-lactose monohydrate. *Pharm. Weekbl. Sci. Ed.* **1986**, *8*, 145–150. [CrossRef]
30. Johansson, B.; Alderborn, G. The effect of shape and porosity on the compression behaviour and tablet forming ability of granular materials formed from microcrystalline cellulose. *Eur. J. Pharm. Biopharm.* **2001**, *52*, 347–357. [CrossRef] [PubMed]
31. Chang, S.Y.; Sun, C.C. Insights into the effect of compaction pressure and material properties on interfacial bonding strength of bilayer tablets. *Powder Technol.* **2019**, *354*, 867–876. [CrossRef]
32. Cabiscol, R.; Shi, H.; Wünsch, I.; Magnanimo, V.; Finke, J.H.; Luding, S.; Kwade, A. Effect of particle size on powder compaction and tablet strength using limestone. *Adv. Powder Technol.* **2020**, *31*, 1280–1289. [CrossRef]
33. El Gindy, N.A.; Samaha, M.W. Tensile strength of some pharmaceutical compacts and their relation to surface free energy. *Int. J. Pharm.* **1982**, *13*, 35–46. [CrossRef]
34. Fichtner, F.; Mahlin, D.; Welch, K.; Gaisford, S.; Alderborn, G. Effect of surface energy on powder compactibility. *Pharm. Res.* **2008**, *25*, 2750–2759. [CrossRef] [PubMed]
35. Luangtana-Anan, M.; Fell, J.T. Bonding mechanisms in tabletting. *Int. J. Pharm.* **1990**, *60*, 197–202. [CrossRef]
36. Etzler, F.M.; Pisano, S. Tablet tensile strength: Role of surface free energy. *Adv. Contact Angle Wettability Adhes.* **2015**, *2*, 397–418.
37. Pingali, K.; Mendez, R.; Lewis, D.; Michniak-Kohn, B.; Cuitino, A.; Muzzio, F. Mixing order of glidant and lubricant—Influence on powder and tablet properties. *Int. J. Pharm.* **2011**, *409*, 269–277. [CrossRef]
38. Mills, L.A.; Sinka, I.C. Effect of particle size and density on the die fill of powders. *Eur. J. Pharm. Biopharm.* **2013**, *84*, 642–652. [CrossRef]
39. Herting, M.G.; Kleinebudde, P. Roll compaction/dry granulation: Effect of raw material particle size on granule and tablet properties. *Int. J. Pharm.* **2007**, *338*, 110–118. [CrossRef]

40. Kehlenbeck, V.; Sommer, K. Possibilities to improve the short-term dosing constancy of volumetric feeders. *Powder Technol.* **2003**, *138*, 51–56. [CrossRef]
41. Engisch, W.E.; Muzzio, F.J. Feedrate deviations caused by hopper refill of loss-in-weight feeders. *Powder Technol.* **2015**, *283*, 389–400. [CrossRef]
42. Bekaert, B.; Van Snick, B.; Pandelaere, K.; Dhondt, J.; Di Pretoro, G.; De Beer, T.; Vervaet, C.; Vanhoorne, V. In-depth analysis of the long-term processability of materials during continuous feeding. *Int. J. Pharm.* **2022**, *614*, 121454. [CrossRef]
43. Van Snick, B.; Holman, J.; Vanhoorne, V.; Kumar, A.; De Beer, T.; Remon, J.P.; Vervaet, C. Development of a continuous direct compression platform for low-dose drug products. *Int. J. Pharm.* **2017**, *529*, 329–346. [CrossRef]
44. Simonaho, S.P.; Ketolainen, J.; Ervasti, T.; Toiviainen, M.; Korhonen, O. Continuous manufacturing of tablets with PROMIS-line—Introduction and case studies from continuous feeding, blending and tableting. *Eur. J. Pharm. Sci.* **2016**, *90*, 38–46. [CrossRef]
45. García-Muñoz, S.; Butterbaugh, A.; Leavesley, I.; Manley, L.F.; Slade, D.; Bermingham, S. A flowsheet model for the development of a continuous process for pharmaceutical tablets: An industrial perspective. *AIChE J.* **2018**, *64*, 511–525. [CrossRef]
46. Gyürkés, M.; Madarász, L.; Köte, Á.; Domokos, A.; Mészáros, D.; Beke, K.; Nagy, B.; Marosi, G.; Pataki, H.; Nagy, Z.K.; et al. Process design of continuous powder blending using residence time distribution and feeding models. *Pharmaceutics* **2020**, *12*, 1119. [CrossRef] [PubMed]
47. Beretta, M.; Hörmann, T.R.; Hainz, P.; Hsiao, W.K.; Paudel, A. Investigation into powder tribo-charging of pharmaceuticals. Part I: Process-induced charge via twin-screw feeding. *Int. J. Pharm.* **2020**, *591*, 120014. [CrossRef]
48. Windows-Yule, C.R.; Neveu, A. Calibration of DEM simulations for dynamic particulate systems. *Pap. Phys.* **2022**, *14*, 140010. [CrossRef]
49. Rhodes, M.J. *Introduction to Particle Technology*; John Wiley & Sons: Hoboken, NJ, USA, 2008.
50. Windows-Yule, K.; Nicuşan, L.; Herald, M.T.; Manger, S.; Parker, D. Comparison with other techniques. In *Positron Emission Particle Tracking: A Comprehensive Guide*; IOP Publishing: Bristol, UK, 2022.
51. Thornton, C. *Granular Dynamics, Contact Mechanics and Particle System Simulations: A DEM Study*; Springer's International Publishing: Berlin/Heidelberg, Germany, 2015; Volume 24, pp. 1–195. [CrossRef]
52. Kojima, T.; Elliott, J.A. Effect of silica nanoparticles on the bulk flow properties of fine cohesive powders. *Chem. Eng. Sci.* **2013**, *101*, 315–328. [CrossRef]
53. Meyer, K.; Zimmermann, I. Effect of glidants in binary powder mixtures. *Powder Technol.* **2004**, *139*, 40–54. [CrossRef]
54. Tran, D.T.; Majerová, D.; Veselý, M.; Kulaviak, L.; Ruzicka, M.C.; Zámostný, P. On the mechanism of colloidal silica action to improve flow properties of pharmaceutical excipients. *Int. J. Pharm.* **2019**, *556*, 383–394. . [CrossRef]
55. López, A.; Vivacqua, V.; Hammond, R.; Ghadiri, M. Analysis of screw feeding of faceted particles by discrete element method. *Powder Technol.* **2020**, *367*, 474–486. [CrossRef]
56. Krantz, M.; Zhang, H.; Zhu, J. Characterization of powder flow: Static and dynamic testing. *Powder Technol.* **2009**, *194*, 239–245. [CrossRef]
57. Lumay, G.; Pillitteri, S.; Marck, M.; Monsuur, F.; Pauly, T.; Ribeyre, Q.; Francqui, F.; Vandewalle, N. Influence of mesoporous silica on powder flow and electrostatic properties on short and long term. *J. Drug Deliv. Sci. Technol.* **2019**, *53*, 101192. [CrossRef]
58. Neveu, A.; Francqui, F.; Lumay, G. Measuring powder flow properties in a rotating drum. *Measurement* **2022**, *200*, 111548. [CrossRef]
59. Patel, D.; Francqui, F.; Defrêne, R.J.L.; Neveu, A. Influence of additives on the electrostatic charge build-up of excipients. *Powder Technol.* **2003**, *132*, 192–198. [CrossRef]
60. Ramirez-Dorronsoro, J.C.; Jacko, R.B.; Kildsig, D.O. Chargeability measurements of selected pharmaceutical dry powders to assess their electrostatic charge control capabilities. *AAPS PharmSciTech* **2006**, *7*, 103. [CrossRef] [PubMed]
61. Escotet-Espinoza, M.S.; Moghtadernejad, S.; Oka, S.; Wang, Z.; Wang, Y.; Roman-Ospino, A.; Schäfer, E.; Cappuyns, P.; Van Assche, I.; Futran, M.; et al. Effect of material properties on the residence time distribution (RTD) characterization of powder blending unit operations. Part II of II: Application of models. *Powder Technol.* **2019**, *344*, 525–544. [CrossRef]
62. Escotet-Espinoza, M.S.; Moghtadernejad, S.; Scicolone, J.; Wang, Y.; Pereira, G.; Schäfer, E.; Vigh, T.; Klingeleers, D.; Ierapetritou, M.; Muzzio, F.J. Using a material property library to find surrogate materials for pharmaceutical process development. *Powder Technol.* **2018**, *339*, 659–676. [CrossRef]
63. Shier, A.P.; Kumar, A.; Mercer, A.; Majeed, N.; Doshi, P.; Blackwood, D.O.; Verrier, H.M. Development of a predictive model for gravimetric powder feeding from an API-rich materials properties library. *Int. J. Pharm.* **2022**, *625*, 122071. [CrossRef]
64. Yadav, I.K.; Holman, J.; Meehan, E.; Tahir, F.; Khoo, J.; Taylor, J.; Benedetti, A.; Aderinto, O.; Bajwa, G. Influence of material properties and equipment configuration on loss-in- weight feeder performance for drug product continuous manufacture. *Powder Technol.* **2019**, *348*, 126–137. [CrossRef]
65. De Souter, L.; Waeytens, R.; Van Hauwermeiren, D.; Grymonpré, W.; Bekaert, B.; Nopens, I.; De Beer, T. Elucidation of the powder flow pattern in a twin-screw LIW-feeder for various refill regimes. *Int. J. Pharm.* **2023**, *631*, 122534. [CrossRef]
66. Mužíková, J.; Louženská, M.; Pekárek, T. A study of compression process and properties of tablets with microcrystalline cellulose and colloidal silicon dioxide. *Acta Pol. Pharm.—Drug Res.* **2016**, *73*, 1259–1265.
67. Apeji, Y.E.; Olowosulu, A.K. Quantifying the effect of glidant on the compaction and tableting properties of paracetamol granules. *J. Res. Pharm.* **2020**, *24*, 44–55. [CrossRef]

68. Uzunović, A.; Vranić, E. Effect of magnesium stearate concentration on dissolution properties of ranitidine hydrochloride coated tablets. *Biomol. Biomed.* **2007**, *7*, 279–283. [CrossRef] [PubMed]
69. Bolhuis, G.K.; Anthony Armstrong, N. Excipients for Direct Compaction—An Update. *Pharm. Dev. Technol.* **2006**, *11*, 111–124. [CrossRef]
70. Huang, Z.; Scicolone, J.V.; Gurumuthy, L.; Davé, R.N. Flow and bulk density enhancements of pharmaceutical powders using a conical screen mill: A continuous dry coating device. *Chem. Eng. Sci.* **2015**, *125*, 209–224. [CrossRef]
71. Bridgwater, J. Fundamental powder mixing mechanisms. *Powder Technol.* **1976**, *15*, 215–236. [CrossRef]
72. Cooke, M.H.; Stephens, D.J.; Bridgwater, J. Powder mixing—A literature survey. *Powder Technol.* **1976**, *15*, 1–20. [CrossRef]
73. Laurent, B.; Bridgwater, J. Influence of agitator design on powder flow. *Chem. Eng. Sci.* **2002**, *57*, 3781–3793. [CrossRef]
74. Van Snick, B.; Grymonpré, W.; Dhondt, J.; Pandelaere, K.; Di Pretoro, G.; Remon, J.P.; De Beer, T.; Vervaet, C.; Vanhoorne, V. Impact of blend properties on die filling during tableting. *Int. J. Pharm.* **2018**, *549*, 476–488. [CrossRef]
75. Palmer, J.; Reynolds, G.K.; Tahir, F.; Yadav, I.K.; Meehan, E.; Holman, J.; Bajwa, G. Mapping key process parameters to the performance of a continuous dry powder blender in a continuous direct compression system. *Powder Technol.* **2020**, *362*, 659–670. [CrossRef]
76. Venables, H.J.; Wells, J.I. Powder mixing. *Drug Dev. Ind. Pharm.* **2001**, *27*, 599–612. [CrossRef]
77. Asachi, M.; Nourafkan, E.; Hassanpour, A. A review of current techniques for the evaluation of powder mixing. *Adv. Powder Technol.* **2018**, *29*, 1525–1549. [CrossRef]
78. Portillo, P.M.; Vanarase, A.U.; Ingram, A.; Seville, J.K.; Ierapetritou, M.G.; Muzzio, F.J. Investigation of the effect of impeller rotation rate, powder flow rate, and cohesion on powder flow behavior in a continuous blender using PEPT. *Chem. Eng. Sci.* **2010**, *65*, 5658–5668. [CrossRef]
79. Poux, M.; Fayolle, P.; Bertrand, J.; Bridoux, D.; Bousquet, J. Powder mixing: Some practical rules applied to agitated systems. *Powder Technol.* **1991**, *68*, 213–234. [CrossRef]
80. Sebastian Escotet-Espinoza, M.; Moghtadernejad, S.; Oka, S.; Wang, Y.; Roman-Ospino, A.; Schäfer, E.; Cappuyns, P.; Van Assche, I.; Futran, M.; Ierapetritou, M.; et al. Effect of tracer material properties on the residence time distribution (RTD) of continuous powder blending operations. Part I of II: Experimental evaluation. *Powder Technol.* **2019**, *342*, 744–763. [CrossRef]
81. Gao, Y.; Vanarase, A.; Muzzio, F.; Ierapetritou, M. Characterizing continuous powder mixing using residence time distribution. *Chem. Eng. Sci.* **2011**, *66*, 417–425. [CrossRef]
82. Vanarase, A.U.; Muzzio, F.J. Effect of operating conditions and design parameters in a continuous powder mixer. *Powder Technol.* **2011**, *208*, 26–36. [CrossRef]
83. Fan, L.; Chen, Y.m.; Lai, F. Recent developments in solids mixing. *Powder Technol.* **1990**, *61*, 255–287. [CrossRef]
84. Rosato, A.D.; Windows-Yule, C. *Segregation in Vibrated Granular Systems*; Academic Press: Cambridge, MA, USA, 2020; pp. 197–218.
85. Rennie, P.R.; Chen, X.D.; Hargreaves, C.; MacKereth, A.R. Study of the cohesion of dairy powders. *J. Food Eng.* **1999**, *39*, 277–284. [CrossRef]
86. De Villiers, M.M. Description of the kinetics of the deagglomeration of drug particle agglomerates during powder mixing. *Int. J. Pharm.* **1997**, *151*, 1–6. [CrossRef]
87. Mehrotra, A.; Muzzio, F.J.; Shinbrot, T. Spontaneous separation of charged grains. *Phys. Rev. Lett.* **2007**, *99*, 058001. [CrossRef] [PubMed]
88. Bekaert, B.; Grymonpré, W.; Novikova, A.; Vervaet, C.; Vanhoorne, V. Impact of blend properties and process variables on the blending performance. *Int. J. Pharm.* **2022**, *613*, 121421. [CrossRef] [PubMed]
89. Vanarase, A.U.; Osorio, J.G.; Muzzio, F.J. Effects of powder flow properties and shear environment on the performance of continuous mixing of pharmaceutical powders. *Powder Technol.* **2013**, *246*, 63–72. [CrossRef]
90. Gao, Y.; Ierapetritou, M.; Muzzio, F. Periodic section modeling of convective continuous powder mixing processes. *AIChE J.* **2012**, *58*, 69–78.
91. Portillo, P.M.; Ierapetritou, M.G.; Muzzio, F.J. Characterization of continuous convective powder mixing processes. *Powder Technol.* **2007**, *182*, 368–378. [CrossRef]
92. Werner, D.; Davison, H.; Robinson, E.; Sykes, J.; Seville, J.; Wellings, A.; Bhattacharya, S.; Monsalve, D.S.; Wheldon, T.K.; Windows-Yule, C. Effect of system composition on mixing in binary fluidised beds. *Chem. Eng. Sci.* **2023**, *271*, 118562. [CrossRef]
93. Goldhirsch, I. Introduction to granular temperature. *Powder Technol.* **2008**, *182*, 130–136. . [CrossRef]
94. Ogawa, S. Multitemperature theory of granular materials. In Proceedings of the US-Japan Seminar on Continuum Mechanical and Statistical Approaches in the Mechanics of Granular Materials, Sendai, Japan, 5–9 June 1978; pp. 208–217.
95. Gao, Y.; Muzzio, F.J.; Ierapetritou, M.G. Optimizing continuous powder mixing processes using periodic section modeling. *Chem. Eng. Sci.* **2012**, *80*, 70–80. [CrossRef]
96. Sarkar, A.; Wassgren, C.R. Simulation of a continuous granular mixer: Effect of operating conditions on flow and mixing. *Chem. Eng. Sci.* **2009**, *64*, 2672–2682. [CrossRef]
97. Tomita, Y.; Nagato, T.; Takeuchi, Y.; Takeuchi, H. Control of residence time of pharmaceutical powder in a continuous mixer with impeller and scraper. *Int. J. Pharm.* **2020**, *586*, 119520. [CrossRef]
98. Tran, D.; Komínová, P.; Kulaviak, L.; Zámostnỳ, P. Evaluation of multifunctional magnesium aluminosilicate materials as novel family of glidants in solid dosage products. *Int. J. Pharm.* **2021**, *592*, 120054. [CrossRef] [PubMed]

99. Toson, P.; Siegmann, E.; Trogrlic, M.; Kureck, H.; Khinast, J.; Jajcevic, D.; Doshi, P.; Blackwood, D.; Bonnassieux, A.; Daugherity, P.D.; et al. Detailed modeling and process design of an advanced continuous powder mixer. *Int. J. Pharm.* **2018**, *552*, 288–300. [CrossRef] [PubMed]
100. Kale, D.P.; Zode, S.S.; Bansal, A.K. Challenges in translational development of pharmaceutical cocrystals. *J. Pharm. Sci.* **2017**, *106*, 457–470. [CrossRef] [PubMed]
101. Zakhvatayeva, A.; Zhong, W.; Makroo, H.A.; Hare, C.; Wu, C.Y. An experimental study of die filling of pharmaceutical powders using a rotary die filling system. *Int. J. Pharm.* **2018**, *553*, 84–96. [CrossRef] [PubMed]
102. Schomberg, A.K.; Kwade, A.; Finke, J.H. The challenge of die filling in rotary presses—A systematic study of material properties and process parameters. *Pharmaceutics* **2020**, *12*, 248. [CrossRef] [PubMed]
103. Qu, L.; Stewart, P.J.; Hapgood, K.P.; Lakio, S.; Morton, D.A.; Zhou, Q.T. Single-step coprocessing of cohesive powder via mechanical dry coating for direct tablet compression. *J. Pharm. Sci.* **2017**, *106*, 159–167. [CrossRef] [PubMed]
104. Baserinia, R.; Sinka, I.C. Powder die filling under gravity and suction fill mechanisms. *Int. J. Pharm.* **2019**, *563*, 135–155. [CrossRef] [PubMed]
105. Tang, X.; Zakhvatayeva, A.; Zhang, L.; Wu, Z.F.; Sun, P.; Wu, C.Y. Flow behaviour of pharmaceutical powders during rotary die filling with a paddle feeder. *Int. J. Pharm.* **2020**, *585*, 119547. [CrossRef]
106. Jackson, S.; Sinka, I.C.; Cocks, A.C. The effect of suction during die fill on a rotary tablet press. *Eur. J. Pharm. Biopharm.* **2007**, *65*, 253–256. [CrossRef]
107. Goh, H.P.; Heng, P.W.S.; Liew, C.V. Understanding effects of process parameters and forced feeding on die filling. *Eur. J. Pharm. Sci.* **2018**, *122*, 105–115. [CrossRef]
108. Han, X.; Jallo, L.; To, D.; Ghoroi, C.; Davé, R. Passivation of high-surface-energy sites of milled ibuprofen crystals via dry coating for reduced cohesion and improved flowability. *J. Pharm. Sci.* **2013**, *102*, 2282–2296. [CrossRef]
109. Zakhvatayeva, A.; Hare, C.; Wu, C.Y. Size-induced segregation during die filling. *Int. J. Pharm. X* **2019**, *1*, 100032. [CrossRef] [PubMed]
110. Wu, C.Y. DEM simulations of die filling during pharmaceutical tabletting. *Particuology* **2008**, *6*, 412–418. [CrossRef]
111. Mittal, B. *How to Develop Robust Solid Oral Dosage Forms: From Conception to Post-Approval*; Academic Press: Cambridge, MA, USA, 2016.
112. Bansal, A.K.; Balwani, G.; Sheokand, S. *Critical Material Attributes in Wet Granulation*; Academic Press: Cambridge, MA, USA, 2019; pp. 421–453.
113. Eidevåg, T.; Abrahamsson, P.; Eng, M.; Rasmuson, A. Modeling of dry snow adhesion during normal impact with surfaces. *Powder Technol.* **2020**, *361*, 1081–1092. [CrossRef]
114. Peeters, E.; Beer, T.D.; Vervaet, C.; Remon, J.p.; Peeters, E.; Beer, T.D.; Vervaet, C.; Remon, J.p. Reduction of tablet weight variability by optimizing paddle speed in the forced feeder of a high-speed rotary tablet press forced feeder of a high-speed rotary tablet press. *Drug Dev. Ind. Pharm.* **2015**, *41*, 530–539. [CrossRef] [PubMed]
115. Kushner, J.; Moore, F. Scale-up model describing the impact of lubrication on tablet tensile strength. *Int. J. Pharm.* **2010**, *399*, 19–30. [CrossRef]
116. Mosig, J.; Kleinebudde, P. Critical evaluation of root causes of the reduced compactability after roll compaction/dry granulation. *J. Pharm. Sci.* **2015**, *104*, 1108–1118. [CrossRef] [PubMed]
117. Almaya, A.; Aburub, A. Effect of Particle Size on Compaction of Materials with Different Deformation Mechanisms with and without Lubricants. *Aaps Pharmscitech* **2008**, *9*, 414–418. [CrossRef] [PubMed]
118. Guo, Y.; Wu, C.Y.; Thornton, C. The effects of air and particle density difference on segregation of powder mixtures during die filling. *Chem. Eng. Sci.* **2011**, *66*, 661–673. [CrossRef]
119. Schneider, L.C.; Sinka, I.C.; Cocks, A.C. Characterisation of the flow behaviour of pharmaceutical powders using a model die-shoe filling system. *Powder Technol.* **2007**, *173*, 59–71. [CrossRef]
120. Kukkar, V.; Anand, V.; Kataria, M.; Gera, M.; Choudhury, P.K. Mixing and formulation of low dose drugs: Underlying problems and solutions. *Thai J. Pharm. Sci* **2008**, *32*, 43–58.
121. Byrne, F.P.; Jin, S.; Paggiola, G.; Petchey, T.H.M.; Clark, J.H.; Farmer, T.J.; Hunt, A.J.; Robert McElroy, C.; Sherwood, J. Tools and techniques for solvent selection: Green solvent selection guides. *Sustain. Chem. Process.* **2016**, *4*, 7. [CrossRef]
122. Javadzadeh, Y.; Vazifehasl, Z.; Maleki Dizahj, S.; Mokhtarpor, M. Spherical crystallization of drugs. *Acta Pharm.* **2012**, *62*, 1–14. [CrossRef]
123. Pitt, K.; Peña, R.; Tew, J.D.; Pal, K.; Smith, R.; Nagy, Z.K.; Litster, J.D. Particle design via spherical agglomeration: A critical review of controlling parameters, rate processes and modelling. *Powder Technol.* **2018**, *326*, 327–343. [CrossRef]
124. Quodbach, J.; Kleinebudde, P. A critical review on tablet disintegration. *Pharm. Dev. Technol.* **2016**, *21*, 763–774. [CrossRef]
125. Nicolas, V.; Chambin, O.; Andrès, C.; Rochat-Gonthier, M.H.; Pourcelot, Y. Preformulation: Effect of moisture content on microcrystalline cellulose (Avicel PH-302) and its consequences on packing performances. *Drug Dev. Ind. Pharm.* **1999**, *25*, 1137–1142. [CrossRef]
126. Tye, C.K.; Sun, C.; Amidon, G.E. Evaluation of the effects of tableting speed on the relationships between compaction pressure, tablet tensile strength, and tablet solid fraction. *J. Pharm. Sci.* **2005**, *94*, 465–472. [CrossRef] [PubMed]
127. Osei-Yeboah, F.; Zhang, M.; Feng, Y.; Sun, C.C. A formulation strategy for solving the overgranulation problem in high shear wet granulation. *J. Pharm. Sci.* **2014**, *103*, 2434–2440. [CrossRef]

128. McKenna, A.; McCafferty, D.F. Effect of particle size on the compaction mechanism and tensile strength of tablets. *J. Pharm. Pharmacol.* **1982**, *34*, 347–351. [CrossRef] [PubMed]
129. Hallam, C.N.; Gabbott, I.P. Increasing tensile strength by reducing particle size for extrudate-based tablet formulations. *J. Drug Deliv. Sci. Technol.* **2019**, *52*, 825–830. [CrossRef]
130. Sun, C.; Grant, D.J. Influence of crystal structure on the tableting properties of sulfamerazine polymorphs. *Pharm. Res.* **2001**, *18*, 274–280. [CrossRef] [PubMed]
131. Eriksson, M.; Alderborn, G. The effect of particle fragmentation and deformation on the interparticulate bond formation process during powder compaction. *Pharm. Res.* **1995**, *12*, 1031–1039. [CrossRef] [PubMed]
132. Wünsch, I.; Finke, J.H.; John, E.; Juhnke, M.; Kwade, A. The influence of particle size on the application of compression and compaction models for tableting. *Int. J. Pharm.* **2021**, *599*, 120424. [CrossRef]
133. Šimek, M.; Grünwaldová, V.; Kratochvíl, B. Comparison of compression and material properties of differently shaped and sized paracetamols. *KONA Powder Part J.* **2017**, *2017*, 197–206. [CrossRef]
134. Choi, D.H.; Kim, N.A.; Chu, K.R.; Jung, Y.J.; Yoon, J.h.; Jeong, S.H. Material Properties and Compressibility Using Heckel and Kawakita Equation with Commonly Used Pharmaceutical Excipients. *J. Pharm. Investig.* **2010**, *40*, 237–244. [CrossRef]
135. Prasad, K.V.; Sheen, D.B.; Sherwood, J.N. Fracture property studies of paracetamol single crystals using microindentation techniques. *Pharm. Res.* **2001**, *18*, 867–872. [CrossRef]
136. Roberts, R.; Rowe, R.C. The compaction of pharmaceutical and other model materials—A pragmatic approach. *Chem. Eng. Sci.* **1987**, *42*, 903–911. [CrossRef]
137. Skelbæk-pedersen, A.L.; Vilhelmsen, T.K.; Wallaert, V. Investigation of the e ff ects of particle size on fragmentation during tableting. *Int. J. Pharm.* **2020**, *576*, 118985. [CrossRef]
138. Wong, L.W.; Pilpel, N. The effect of particle shape on the mechanical properties of powders. *Int. J. Pharm.* **1990**, *59*, 145–154. [CrossRef]
139. Upadhyay, P.; Khomane, K.S.; Kumar, L.; Bansal, A.K. Relationship between crystal structure and mechanical properties of ranitidine hydrochloride polymorphs. *CrystEngComm* **2013**, *15*, 3959–3964. [CrossRef]
140. Khomane, K.S.; Bansal, A.K. Effect of particle size on in-die and out-of-die compaction behavior of ranitidine hydrochloride polymorphs. *AAPS PharmSciTech* **2013**, *14*, 1169–1177. [CrossRef] [PubMed]
141. Packham, D.E. Surface energy , surface topography and adhesion. *Int. J. Adhes. Adhes.* **2003**, *23*, 437–448. [CrossRef]
142. Annamalai, M.; Gopinadhan, K.; Han, S.A.; Saha, S.; Park, H.J.; Cho, E.B.; Kumar, B.; Patra, A.; Kim, S.W.; Venkatesan, T. Surface energy and wettability of van der Waals structures. *Nanoscale* **2016**, *8*, 5764–5770. [CrossRef]
143. Li, Q.; Rudolph, V.; Weigl, B.; Earl, A. Interparticle van der Waals force in powder flowability and compactibility. *Int. J. Pharm.* **2004**, *280*, 77–93. [CrossRef]
144. Fichtner, F.; Rasmuson, A.; Alderborn, G. Particle size distribution and evolution in tablet structure during and after compaction. *Int. J. Pharm.* **2005**, *292*, 211–225. [CrossRef] [PubMed]
145. Chen, L.; Ding, X.; He, Z.; Huang, Z.; Kunnath, K.T.; Zheng, K.; Davé, R.N. Surface engineered excipients: I. improved functional properties of fine grade microcrystalline cellulose. *Int. J. Pharm.* **2018**, *536*, 127–137. [CrossRef] [PubMed]
146. Ho, R.; Hinder, S.J.; Watts, J.F.; Dilworth, S.E.; Williams, D.R.; Heng, J.Y. Determination of surface heterogeneity of d-mannitol by sessile drop contact angle and finite concentration inverse gas chromatography. *Int. J. Pharm.* **2010**, *387*, 79–86. [CrossRef] [PubMed]
147. Shinebaum, R. Investigating the Mechanical Properties of Pharmaceutical Excipients in Granule and Tablet Production. Ph.D. Thesis, Univerisity of Birmingham, Edgbaston, UK, 2021.
148. Morin, G.; Briens, L. The effect of lubricants on powder flowability for pharmaceutical application. *AAPS PharmSciTech* **2013**, *14*, 1158–1168. [CrossRef] [PubMed]
149. Lakio, S.; Vajna, B.; Farkas, I.; Salokangas, H.; Marosi, G.; Yliruusi, J. Challenges in detecting magnesium stearate distribution in tablets. *AAPS PharmSciTech* **2013**, *14*, 435–444. [CrossRef] [PubMed]
150. Abe, H.; Otsuka, M. Effects of lubricant-mixing time on prolongation of dissolution time and its prediction by measuring near infrared spectra from tablets. *Drug Dev. Ind. Pharm.* **2012**, *38*, 412–419. [CrossRef]
151. Kunnath, K.; Huang, Z.; Chen, L.; Zheng, K.; Davé, R. Improved properties of fine active pharmaceutical ingredient powder blends and tablets at high drug loading via dry particle coating. *Int. J. Pharm.* **2018**, *543*, 288–299. [CrossRef]
152. Hentzschel, C.M.; Alnaief, M.; Smirnova, I.; Sakmann, A.; Leopold, C.S. Tableting properties of silica aerogel and other silicates. *Drug Dev. Ind. Pharm.* **2012**, *38*, 462–467. [CrossRef]
153. Khunawattanakul, W.; Puttipipatkhachorn, S.; Rades, T.; Pongjanyakul, T. Novel chitosan-magnesium aluminum silicate nanocomposite film coatings for modified-release tablets. *Int. J. Pharm.* **2011**, *407*, 132–141. [CrossRef] [PubMed]
154. Holman, J.; Tantuccio, A.; Palmer, J.; van Doninck, T.; Meyer, R. A very boring 120 h:15 million tablets under a continuous state of control. *Powder Technol.* **2021**, *382*, 208–231. [CrossRef]
155. Tahara, K.; Kono, Y.; Myerson, A.S.; Takeuchi, H. Development of Continuous Spherical Crystallization to Prepare Fenofibrate Agglomerates with Impurity Complexation Using Mixed-Suspension, Mixed-Product Removal Crystallizer. *Cryst. Growth Des.* **2018**, *18*, 6448–6454. [CrossRef]
156. Chen, Y.; Yao, Z.; Tang, S.; Tong, H.; Yanagishima, T.; Tanaka, H.; Tan, P. Morphology selection kinetics of crystallization in a sphere. *Nat. Phys.* **2021**, *17*, 121–127. [CrossRef]

157. Van Snick, B.; Holman, J.; Cunningham, C.; Kumar, A.; Vercruysse, J.; De Beer, T.; Remon, J.P.; Vervaet, C. Continuous direct compression as manufacturing platform for sustained release tablets. *Int. J. Pharm.* **2017**, *519*, 390–407. [CrossRef]
158. Ierapetritou, M.; Muzzio, F.; Reklaitis, G. Perspectives on the continuous manufacturing of powder-based pharmaceutical processes. *AIChE J.* **2016**, *62*, 1846–1862. [CrossRef]

Disclaimer/Publisher's Note: The statements, opinions and data contained in all publications are solely those of the individual author(s) and contributor(s) and not of MDPI and/or the editor(s). MDPI and/or the editor(s) disclaim responsibility for any injury to people or property resulting from any ideas, methods, instructions or products referred to in the content.

Appendix Two

Attached Publication for Chapter 4

Publication Jones-Salkey et al. 2024 [154] has been included below:

International Journal of Pharmaceutics 645 (2023) 123361

Contents lists available at ScienceDirect

International Journal of Pharmaceutics

journal homepage: www.elsevier.com/locate/ijpharm

Application of Positron Emission Particle Tracking (PEPT) for the evaluation of powder behaviour in an incline linear blender for Continuous Direct Compression (CDC)

O. Jones-Salkey [a,c,*], A.L. Nicusan [a,b], C.R.K. Windows-Yule [a,b], A. Ingram [a,b], D. Werner [a,b], S. Clifford [c], G.K. Reynolds [c]

[a] School of Chemical Engineering, University of Birmingham, Edgbaston, Birmingham, UK
[b] School of Physics and Astronomy, University of Birmingham, Edgbaston, Birmingham, UK
[c] Oral Product Development, Pharmaceutical Technology & Development, Operations, AstraZeneca, Macclesfield, UK

ARTICLE INFO

Keywords:
Positron Emission Particle Tracking
PEPT
Continuous Direct Compression
CDC
Pharmaceutical
Formulation
Blending

ABSTRACT

Positron Emission Particle Tracking (PEPT) is a non-invasive measurement technique which offers the ability to track the motion of individual particles with high temporal and spatial resolution, and thus build up an understanding of the bulk behaviour of a system from its microscopic (particle level) dynamics. Using this measurement technique, we have developed a series of novel metrics to better understand the behaviours of powders during the steady-state operation of a continuous blender system. Results are presented concerning the response of particle motion to processing parameters (mixing blade configuration and RPM), quantifying the motion in terms of predicted mixing performance. It was found that both increasing rpm and increasing hold-up mass (by selecting fewer transport blades and more mixing blades) provided improved mixing conditions. Interestingly, under specific conditions, there is evidence of convection-like mixing occurring at the interface of the transport and mixing region. This suggests the existence of a potential 'folding region' whereby powder is transported up the barrel (and away from the powder bulk bed) before being reconstituted back into the bulk mass. The results also provide valuable experimental data for the development, calibration and validation of future Discrete Element Method (DEM) simulations.

1. Introduction

In the pharmaceutical industry, the shift from batch to continuous manufacture (CM) carries the potential to significantly reduce both manufacturing cost and product variation (Burcham et al., 2018; Vanhoorne and Vervaet, 2020; Lee et al., 2015; Roth et al., 2017), thus ultimately reducing the cost to the end user, the patient. This mutually beneficial outcome is being pursued by the entire pharmaceutical industry and the authorities are active in parenting the development of these methods (e.g., ICH guidelines (International Council for Harmonisation of Technical Requirements for Pharmaceuticals for Human Use (ICH), 2023, 2012; Wahlich, 2021)), requiring that the introduction of new technologies is sufficiently understood to ensure no risk is passed on to the recipient of these therapeutic products (Bekaert et al., 2022; Lee et al., 2015; Wahlich, 2021).

Therefore, it is paramount that understanding is demonstrated in the form of consistent manufacture (i.e. process design and control strategy) and rigorous models to transition from batch to continuous direct compression (Vanhoorne and Vervaet, 2020; Pernenkil and Cooney, 2006; Lee et al., 2015). Furthermore, when considering both the complexity of the task and limited of experience manufacturing CM therapeutic products, it highlights that the journey to developing this knowledge is both challenging and costly (Teżyk et al., 2015). Reviews by Wahlich 2021 (Wahlich, 2021) and Teżyk et al. 2015 (Teżyk et al., 2015) both surmise these challenges in greater depth. Wahlich stated that – at the time the review was submitted (June 2021) – only seven CM products were on the market, and of those seven products, they were owned by four companies. As is evident from the above, from both a scientific, regulatory, and commercial standpoint, improved understanding of continuous process equipment is vital to ensuring that the rollout of continuous manufacture can continue in a manner which is both rapid *and* low-risk. The provision of new imaging capabilities stands to play a crucial role in facilitating this understanding.

The continuous direct compression (CDC) process for solid dosage forms (tablets), offers the simplest route to CM by using a minimal number of unit operations to continuously produce tablets. However, our

* Corresponding author at: Oral Product Development, Pharmaceutical Technology & Development, Operations, AstraZeneca, Macclesfield, UK.
E-mail address: owen.jones-salkey1@astrazeneca.com (O. Jones-Salkey).

https://doi.org/10.1016/j.ijpharm.2023.123361
Received 1 May 2023; Received in revised form 11 August 2023; Accepted 31 August 2023
Available online 9 September 2023
0378-5173/© 2023 The Authors. Published by Elsevier B.V. This is an open access article under the CC BY license (http://creativecommons.org/licenses/by/4.0/).

understanding of how powders respond to mixing process conditions is limited. Excellent examples of work have been conducted by several researchers providing an initial understanding of how bulk powders respond to mixing processes across units with different designs and orientations (Portillo et al., 2010; Vanarase et al., 2013; Van Snick et al., 2017; Palmer et al., 2020; Tomita et al., 2020).

The seminal use of PEPT on small-scale continuous blenders was performed by Portillo et al. (2010), and the findings are discussed later. Vanarase et al. (2013) studied the effect operating conditions had on a horizontal continuous blender through the use of RTD measurements. Van Snick et al. (2017) comprehensively investigated several factors which contribute to end-to-end CDC performance. Where blending is concerned (using a 15° incline blender), Van Snick et, al. demonstrated the influence of blade configuration on mass hold-up and its resultant effect on processing accuracy and consistency — in the form of content uniformity. Palmer et al. (2020) then furthered this by mapping the processing response of three paracetamol formulations and produced a strain micromixing model — which demonstrated an exponential decay between content uniformity (attained from tablet assays) and strain (effectively defined as the number of blade passes). While Tomita et al. (2020) demonstrated the independent control of micro and macro mixing by using a different blender system the CTS-MG100 (Powrex Corporation, Hyogo, Japan), which utilised both a paddle impeller and a circumscribing scraper.

Despite providing considerable insight into mixing processes within CDC, the aforementioned studies nonetheless provide little direct insight into the internal dynamics of the mixing process, due in large part to the optically-opaque nature of the systems studied. Positron Emission Particle Tracking (PEPT) is a technique that uses highly-penetrating gamma radiation to image particulate systems' full, three-dimensional dynamics, including metal-walled industrial process equipment. PEPT is able to track the motion of individual particles through a given system of interest and use these individual traces to build up the understanding of the bulk behaviour of the system, taking a 'micro-up' approach, rather than the typical 'macro-down' approach. Moreover, the spatial–temporal data can be used to calculate a multitude of metrics which are not possible from commonly applied PAT methods, such as NIR, and therefore, PEPT serves as a great tool for investigatory work. Full details of the PEPT technique may be found in Windows-Yule et al. (2020, 2022b).

PEPT has already been used, in the previous work of Portillo et al. (2010), to investigate the effect of RPM and blender inclination on 3 powder species using a small-scale linear blender not dissimilar to that studied here. In their study, it was determined that an inclined blender produced longer residence times and greater mixing potential; the powders travelled similar path lengths but the more cohesive the powder the longer residence time; increasing RPM decreased residence time (lending to poorer macro mixing conditions) but increased radial dispersion — thus increasing the potential mixing quality (Portillo et al., 2010).

An alternative method through which insight may be gained into the internal dynamics of mixing processes is the discrete element method (DEM). DEM, like PEPT, offers a method of understanding the behaviour of not only the bulk but the individual particles within a particulate system. Past studies of such systems have investigated the effect of blade revolution rate (RPM) on axial and radial dispersion (Gao et al., 2011b, 2012) as well as the influence on blade angle on powder transport and mixing (Boonkanokwong et al., 2016; Siraj, 2014; Gao et al., 2011a, 2012; Ebrahimi et al., 2018). DEM offers two pragmatic advantages over PEPT, namely a comparatively low financial cost (due to PEPT's requirement for high energy and materials costs in the production of tracers (Windows-Yule et al., 2022b)) and more ready availability (there exist at present only a handful of active PEPT facilities in the world). However, DEM simulations (depending on the number of particles simulated) will typically take significantly longer than PEPT experiments and, unlike PEPT, DEM simulations may provide misleading results without rigorous calibration and validation. The necessary calibration and validation thereof is typically complex, time-intensive and lacking a standardised 'best practice', meaning that in many cases such simulations can only be trusted to provide at best qualitative information (Windows-Yule et al., 2016; Windows-Yule and Neveu, 2022). Nonetheless, through careful comparison with detailed experimental data such as that extracted via PEPT or other three-dimensional imaging techniques, near-quantitative accuracy may be achieved (Che et al., 2023).

In this research, we present the first application of Positron Emission Particle Tracking (PEPT) on a commercially-representative, manufacturing-scale continuous blender, following the precedent set by Portillo et al. (2010). Our approach utilises industry-relevant geometries, blade configurations, and RPM ranges. Drawing from the discussions of Gao et al. (2011a) and Van Snick et al. (2017), our goal is to critically analyse how these variables influence the mixing conditions within pharmaceutical blending systems. Our focus, however, is directed towards the micro-behaviour of the powder at the crucial interface between the transport and mixing blade sections of the blender, a region thought to significantly affect the mixing process. In this study, we specifically investigate local factors and their impacts on the *mixing conditions* within the immediate environment, rather than assessing the overall, global, mixing performance. The results obtained from this research will provide meaningful context for our findings and contribute to a broader discussion on *mixing conditions* and regime-like behaviour in similar continuous mixer systems. Moreover, the collected data will serve as an invaluable resource for the rigorous calibration and validation of future Discrete Element Method (DEM) studies.

2. Equipment, materials and methods

2.1. Equipment

2.1.1. Continuous blender: GEA, CDB-1 prototype

Experiments were performed using a prototype of the GEA CDB-1 continuous blender (GEA; Frankfurt, Germany). The blender's mixing volume is angled at a 15-degree incline from the inlet to the outlet so as to increase the total hold-up mass as compared to an equivalent, horizontal system. The internal diameter of the blender is 118 mm and the mixing volume of the blender is 9.3L. The blender has the same mixing dimensions as its commercial counterpart but is more modular in its assembly. The blender's axial shaft has 28 collars, each of which accepts two blades which can either be at 45 degrees to the axis (push blades) or 90 degrees to the axis ((radial) mixing blades). The mixing configuration is set up such that each collar is offset from the preceding collar by 60 degrees thus the progress of the mixing blade(s) moves as a helix along the shaft. The helix rotation provides positive movement in the direction of flow. The two configurations used for this experiment are '8H' (8 mixing blades) and 16H (16 mixing blades), meaning that the mixing section covers roughly 25 and 50 per cent of the shaft, respectively. Schematic representations of the two blade configurations explored can be seen in Fig. 3. The system is controlled using a variable frequency drive allowing the user to manually control the RPM. The rotation rate was measured using a CT6/LSR laser tachometer (Compact Instruments, Bolton, UK) with a contrasting marker on the drive shaft. The rotation rate of the shaft is measured and the drive frequency is adjusted accordingly.

2.1.2. Twin screw feeder: Coperion, KTron-20

For all experiments, particles were fed into the blender using a KTron-20 Feeder (Coperion; Stuttgart, Germany) with concave screws. The feeder was calibrated prior to use, ensuring a consistent volumetric feed over a range of hopper fill levels and screw RPMs. All experiments used a volumetric feed rate equivalent to 15 $kg\ hr^{-1}$. This feed rate was the highest feed rate which provided a consistent mass flow rate. Due to the age of the feeder, and therefore the settings available,

only volumetric feeding was possible. The calibration gave confidence in operating volumetrically over the full range of hopper fill levels. This is primarily attributed to the free-flowing nature of the powder. Consequently, the feed rate remained accurate and stable across all experiments.

2.1.3. PEPT detector: ADAC, PET scanner

Data were acquired from the experimental system using an ADAC Forté dual-headed gamma camera. The camera offers a peak acquisition rate of approximately 100 kHz Parker et al. (2002) and, with modern algorithms (Windows-Yule et al., 2022a), can compute the three-dimensional position of a tracer particle with sub-millimetre accuracy more than 100 times per second. Full details of the Forté can be found in Parker et al. (2002), Herald et al. (2021).

2.2. Materials

2.2.1. Bulk & tracer material: 1 mm MCC

A coarse microcrystalline cellulose (MCC), Vivapur 1000 (JRS Pharma; Rosenberg, Germany), was selected as both the bulk material and the tracer for this experiment. The primary advantage of this material is its narrow particle size distribution and average particle diameter of 1.2 mm; this large particle size provides a greater surface area which is desirable for improved radioactive labelling tracer performance. The large size of the particles also reduces the total number of particles within the system, thus making our results more viable as a calibration/validation data set for future DEM simulations. Furthermore, the selected powder is a pharmaceutical-grade material and is free-flowing (Zheng et al., 2022); which would be representative of a low-dose API formulation, as many excipient formulations prioritise flowability for improved manufacturability (Megarry et al., 2019; Jones-salkey et al., 2023).

Lastly, the tracer was created via the surface adsorption of the positron-emitting radioisotope Fluorine-18 (^{18}F). Details of this procedure, known as 'indirect activation' can be found in Windows-Yule et al. (2022a).

2.3. Experimental set-up

Since the blender is commercial scale, with a length of 0.85 m, the blender does not fit fully within the maximum 0.55 m field of view (FoV) of the detector. With the 15-degree inclination of the blender, the total length that fits within the FoV is 0.57 m or 67% of the blender's length. For the purposes of the present study, imaging of the interface between the mixing blade zone and the former transport section is of primary interest. This volume is expected to contain more than 80% of the residence mass; supported by the comprehensive DEM work of Zheng et al. (2022), which showcases analysis of a simulation calibrated for the same blending volume and powder — Vivapur 1000.

Thus, the inlet of the blender was positioned at the start of the FoV with the interface of the smaller mixing blade zone (8H) being captured by the end of the FoV. The finalised FoV was 0.5 m (in the length axis), and the interface was prioritised within the FoV (which spanned from 0.22 m to 0.42 m). The region of interest for calculation is shown with greater clarity with the following: Fig. 2.

The blender sits, fastened, within the middle section of a two-tiered extruded aluminium frame. The upper section of the frame accommodates the feeder, which is bolted in place (see Fig. 1). The aluminium frame, and therefore the blender, is kept stationary within the detector heads of the ADAC for all experiments. The ADAC detector head separation is then narrowed in the width axis ensuring the highest possible geometric efficiency (i.e. the largest fraction of gamma-rays detected) and thus in turn the maximal data rate and location accuracy (Windows-Yule et al., 2022a; Herald et al., 2021).



Fig. 1. Picture of the Experimental Set-up; supporting frame holding the blender and feeder in the ADAC detector's FoV.

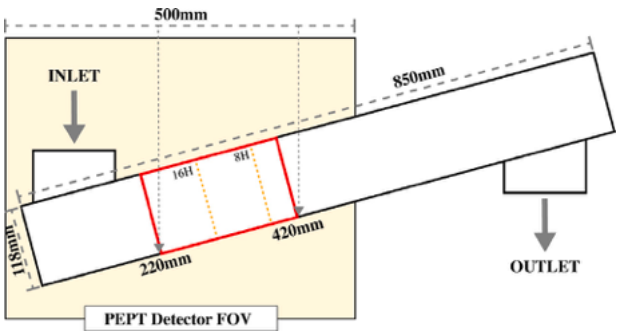


Fig. 2. Schematic of the Experimental Set-up; showing the blender, and the dimensions, within the ADAC detector's FoV. The Region of Interest (RoI) is indicated by the red box.

2.4. Experimental design

In this study, we explore two variables: the blade revolution rate (RPM), and the number of mixing blades (#MB). Increasing the number of mixing blades has been previously shown to increase the overall fill level (residence mass) of such a mixer system, while increasing RPM has been shown to reduce the fill level (Van Snick et al., 2017; Palmer et al., 2020). By varying both of these parameters, we are able to explore a range of system fill levels, and thus gain understanding of the behaviour of powder under strongly varying conditions.

It was found that the combination of low speed and reduced transport resulted in high material hold up, and consequently the torque required exceeded that deliverable by the motor. For this reason, the lowest speed used for 16H is 225rpm. This, coupled with the limited amount of time available to perform the PEPT experiments, means the analysis includes only the following data sets: 150 RPM at 8H, 375 RPM at 8H, 225 RPM at 16H, 300 RPM at 16H, and 375 RPM at 16H.

2.5. Experimental method

The blade configuration is set to the desired configuration and installed into the blender. The blender is subsequently turned on and set to the desired RPM whilst filling. The MCC is then added to the feeder and set to run at 15 kg/hr. While the blender is filling, using both the variable frequency drive and the tachometer, the frequency is adjusted until both remain constant. When the torque (and therefore

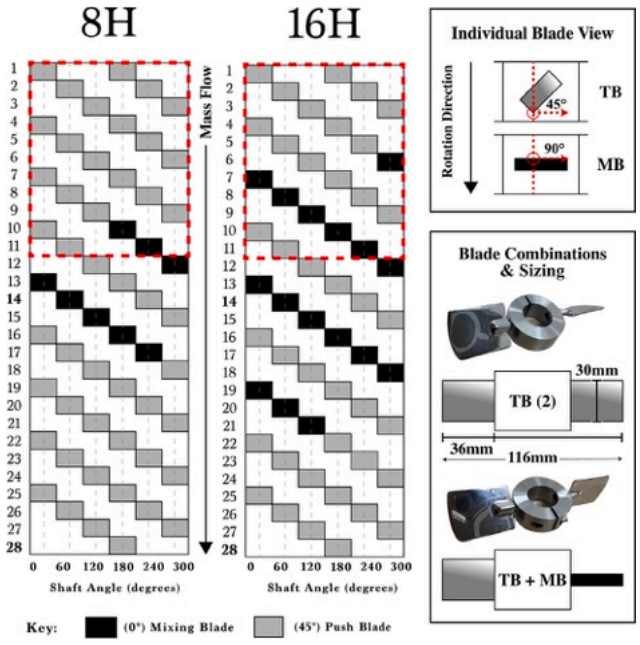


Fig. 3. Blade dimensions and angle arrangement for the 8H and 16H configurations. The red dashed-line box indicates the FoV of the detector.

rpm) remains constant, there is an equal amount of mass entering and exiting the system, effectively stating the system is at steady state due to the constant load on the blades. To ensure the system was at steady state; the system was monitored for a further 5-minute period, in which the rpm was regularly monitored for consistency.

Once at steady state, the tracer is then directly inserted into the neck of the feeder, bypassing the hopper, and enters the blender. A bucket collects the powder output of the blender and is returned to the hopper of the feeder when the tracer is detected in the bucket. This is repeated to gather a sensible number of passes through the system. The data is then processed using the method in the following section (Section 2.6.1). Finally, the residence mass (hold-up mass) of each experiment was estimated by weighing the powder remaining in the system at the end of the trial.

2.6. Analysis

2.6.1. Extracting and cleaning individual trajectories

In order to acquire data with the maximum spatial resolution, tracers are passed through the system one at a time. Though PEPT is capable of tracking multiple tracers simultaneously (Yang et al., 2007; Nicuşan and Windows-Yule, 2020), doing so reduces the accuracy with which each individual particle may be located, meaning that single-particle tracking provides optimal data (Windows-Yule et al., 2022a). In order to build up adequate statistics, therefore, for each set of system parameters, a single tracer is repeatedly passed through the system. By exploiting the principle of ergodicity, data acquired from a series of individual transits of the tracer particle through the mixer (for brevity referred to throughout this paper as 'trajectories') may be combined and suitably averaged so as to provide data representative of the system as a whole (Wildman et al., 2000).

As the detector does not encompass the complete system, there is a possibility that during the tracer's full pass through the system, the tracer may leave and re-enter the field of view, thus potentially being erroneously considered as multiple individual trajectories, creating small, fragmented data sets towards the extremes of the Field of View (FOV) which, if incorporated into statistical analyses, may adversely bias results. Accordingly, filtering measures were put in place to uphold the integrity of those tracers which have truly re-entered due to back-mixing and expelling the erroneous traces. As such, methods were developed to algorithmically remove such fragmented data sets in pre-processing by Firstly, any data sets possessing an overall location error above a given threshold – as expected to be produced by tracers outside the field of view – were eliminated. Secondly, any trajectories containing < 120 contiguous data points – implying only a partial transit – were eliminated. Thirdly, only trajectories containing data points spanning at least the central 200 mm (50%) of the system's field of view were included in our analyses, capturing the interface between transport and mixing blade zone.

Once all erroneous data sets had been eliminated, the remaining trajectories in each experiment were then subjected to a series of 'post-processing' analyses. Due to the sparsity of the data acquired – an inevitable consequence of the complexity of the system and the limited experimental time available – in addition to conventional PEPT outputs such as occupancy and velocity fields, a number of novel metrics were developed specifically for this project. These metrics are described in the following sections.

2.6.2. Novel analyses

Traversal classification. During preliminary analysis, it was observed that the observed particle trajectories could be reasonably classified into three primary 'blender traversal modes':

1. Centrifuging: particles remain at the outer edge of the blender, resulting in bulk rotation about the unit's central axis with minimal transport along the radial direction. This is not to be confused with centrifuging observed in rotating drums where the powder bed attaches to the wall as a solid body with no relative movement between particles. In this case, the particles are held at the wall by action of the rotating blade.
2. Axial traversal: particles pass through the blender with minimal motion in either the radial or azimuthal directions, resulting in relatively short, straight trajectories.
3. Random motion: particles are actively entrained between the blades, resulting in stochastic axial and radial motion (i.e. a random trajectory).

This novel analysis has been included in the present work since we believe that the different behaviours will represent different mixing mechanisms and different mixing efficiencies. Further work is required to explore this, but it is certainly arguable that the random motion mode would lead to effective mixing while that of the axial traversal mode would be quite poor, hence undesirable in pharmaceutical blending applications. The centrifugal mode is less clear cut; it requires knowledge of the motion of the particles relative to the blade and hence the relative extents of the blade pushing the bed of particles (convective motion, poor mixing) versus shearing through (dispersive motion, good mixing). Identifying the prevalence of these behaviours for different processing conditions can thus play a role in the optimisation of said conditions.

To ensure rigour, an algorithmic approach has been taken to the classification of trajectories. In order to classify a given trajectory, the following considerations are applied:

1. The PEPT tracer locations are rotated by $-15°$ and centred such that the main blender body lies horizontally, with the X-axis passing through the centre of the shaft.
2. Each trajectory's points are converted to cylindrical coordinates, with the longitudinal (shaft) axis corresponding to the Cartesian X-axis, such that the YZ coordinates are transformed into a radial distance r and an azimuthal angle θ.
3. In perfect centrifugal motion, the distribution of azimuthal angles will be uniform between $[-\pi, \pi]$ and hence their standard deviation will be $\sigma_\theta = \pi/\sqrt{3}$, while the radial position r will

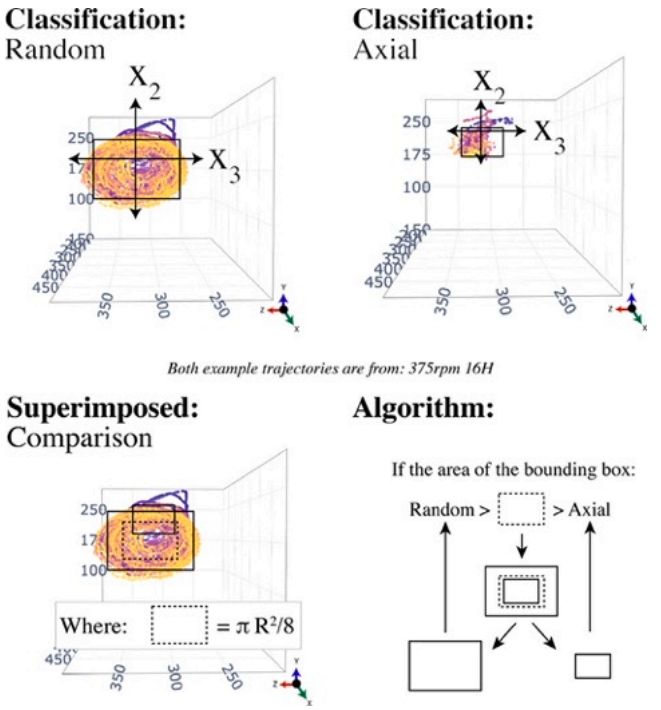


Fig. 4. Graphical supplementation of the axial classification calculation. The units of the 3D scatter plots are in millimetres. Overlayed examples are not to scale.

be equal to the blender radius. Empirically-defined thresholds are used, such that if $\sigma_\theta < {}^{0.75\pi}/_{\sqrt{3}}$ and the 25th percentile of a tracer pass' radial distances is greater than half the blender radius $P_{25\%}(r) > {}^{R}/_{2}$, the trajectory is classified as centrifuging.

4. Axial motion corresponds to minimal blade entrainment, such that the tracer radially explores a small area of the pipe; we extract the plane orthogonal to the main axis of flow by converting each trajectory's points' coordinates into their principal components' space (PCA, using the eigenvectors of their covariance matrix) and extracting the coordinates of the two least important axes X_2 and X_3 (note that the most important axis X_1 corresponds to the main flow direction); the area spanned by the 5th to 95th percentiles $A = (P_{95\%}(X_2) - P_{5\%}(X_2))(P_{95\%}(X_3) - P_{5\%}(X_3))$ robustly approximates the radial side of an oriented bounding box containing the trajectory's points, without outliers — and hence the radially-explored area. As the principal components X_2 and X_3 still have physical units, their dimensions can be compared with that of the blender. If the computed area A is smaller than a blender octant $A < {}^{\pi R^2}/_{8}$, the trajectory is classified as an axial traversal. This (axial) classification is supplemented graphically by Fig. 4.
5. Finally, all remaining trajectories are considered to undergo random mixing.

In other fields of study, for example in rotating drum systems, the classification of particle motion provides a valuable tool for the inference of mixing quality and other important parameters (Morrison et al., 2016). It is hoped that these classifications may prove similarly valuable in the pharmaceutical mixing field.

Lagrangian micromixing. As more industrial systems are imaged using Lagrangian techniques offering rich three-dimensional information of their internal dynamics, new mixing measures must be developed beyond the classical approaches in chemical engineering. A novel method for quantifying the radial movement of flow specifically targeted to

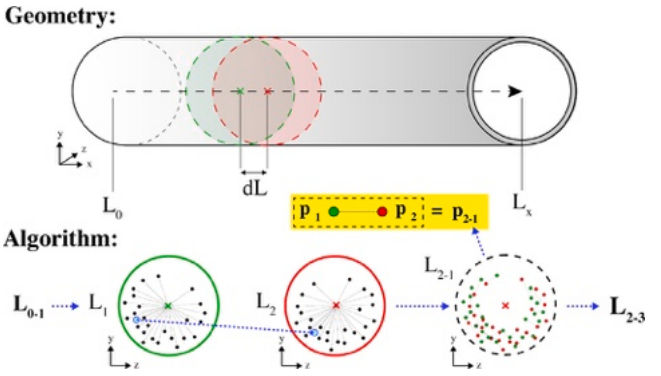


Fig. 5. Graphical Representation of the Lagrangian micromixing metric discussed in Section 2.6.2.

moving frames of reference (i.e. Lagrangian data) has been developed, providing richer information regarding the 'microscopic' mixing (Werner et al., 2023) of tracer particles. The algorithmic steps are as follows (supplemented by Fig. 5):

1. Take a cross-sectional slice through the blender at length L_1 (axial position) along it and record each tracer's location as it passes through the slice.
2. On this slice, compute the radial distances from each trajectory to the pipe centre $(r_1^{L_1}, r_2^{L_1}, \ldots, r_N^{L_1})$ for N tracer passes.
3. Take a second cross-sectional slice at a later length L_2 along the blender and similarly compute the new radial distances $(r_1^{L_2}, r_2^{L_2}, \ldots, r_N^{L_2})$.
4. Compute the *radial deviations* due to micromixing $(r_1^{L_2} - r_1^{L_1}, r_2^{L_2} - r_2^{L_1}, \ldots, r_N^{L_2} - r_N^{L_1})$.
5. Quantify the distribution of radial deviations through its mean, standard deviation, skewness and kurtosis.
6. Move the second slice, L_2, to a new position further along the blender and repeat steps 3–5, keeping track of the radial deviations' statistics as tracers pass through the mixing region.

This method is robust to both axial and centrifuging types of trajectories, as: if tracers follow laminar-like straight trajectories, the mean radial deviation will be zero; if tracers follow the (centrifugal) bulk rotation, it will again be zero. This way, only *true micromixing* is captured by the Lagrangian Micromixing metric. Specifically, a larger mean value corresponds to stronger micromixing, with the standard deviation representing the mixing uniformity. A larger skewness (i.e. a longer right tail on the distribution) indicates that only a few tracers are mixed well; finally, a negative kurtosis suggests the presence of a small number of mixing outliers.

Auto-correlation. Auto-correlation within PEPT has been generalised from the molecular dynamics' velocity auto-correlation function (VACF) (Leimkuhler and Matthews, 2015), defined as the ensemble average – across N trajectory passes – of the dot product of a vector quantity (e.g. velocity $V = (v_x, v_y, v_z)^T$) measured at an initial time t_0 and the same vector quantity measured at a later time t_i:

$$\mathrm{VACF}(t_i) = \frac{\sum_N (V(t_0) \cdot V(t_i))}{N} \tag{1}$$

The time can be substituted with any 'signal' S that has a lag added to it, e.g. position along the blender, in which case it represents the correlation C of a vector quantity $\vec{Q}$ as tracers traverse the mixing region:

$$C(S_i) = \frac{\sum_N (\vec{Q}(S_0) \cdot \vec{Q}(S_i))}{N} \tag{2}$$

Table 1
Tracer classification based on the definitions provided in Section 2.6.2, followed with the number of trajectories collected.

Blender parameters	8H		16H		
	150	375	225	300	375
Froude No.	1.5	9.3	3.4	5.9	9.3
Axial	48%	4%	18%	25%	20%
Centrifugal	0%	73%	0%	2%	10%
Random	52%	23%	82%	73%	70%
n-trajectories	23	271	66	51	93

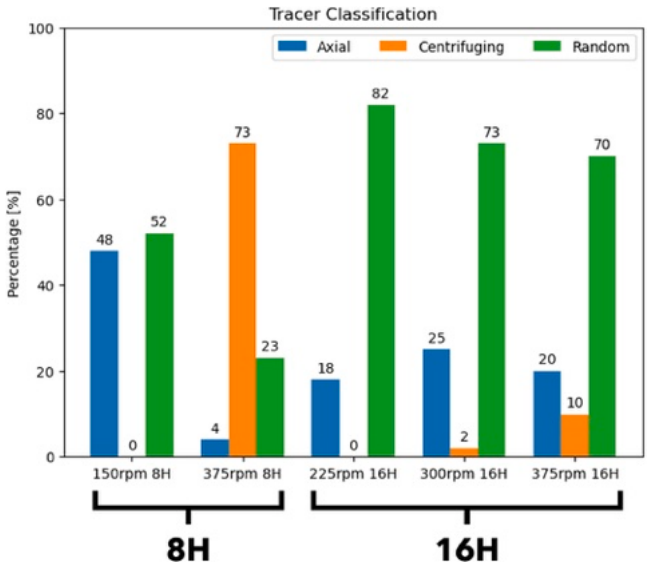


Fig. 6. Graphical Representation of Table 1 discussed in Section 3.1.

High auto-correlation indicates that tracers strongly follow a trend, while zero auto-correlation represents unpredictable, or randomly-distributed values; for example, as tracers are being mixed along the blender, their coordinates (x, y, z) are expected to become less correlated and hence C to decay to zero.

While *velocity* auto-correlations have been previously applied in PEPT studies of *batch* systems (Wildman et al., 2002; Windows-Yule et al., 2014), the present work develops a new formulation for continuous systems, and generalises the algorithm to allow the auto-correlation of arbitrary parameters to be computed.

Algorithm availability. All algorithms described in this section are freely available through the authors' open-source `pept` library (see https://github.com/uob-positron-imaging-centre/pept).

2.6.3. Classical analyses

In addition to the novel analyses defined above, data were also obtained in the form of spatial residence time distribution (otherwise described as temporal occupancy) and velocity profiles, providing further insight into transport and mixing within the system, and the dependence thereof on process conditions.

The methodology for attaining these standard measurements can be found in Windows-Yule et al. (2020, 2022b).

3. Results & discussion

In order to improve CDC processes, it is vital that we are able to better understand – and thus predict and, ultimately, control – processes underlying both the micro- and macro-mixing of powders. While previous studies have elucidated correlations between the 'input' process parameters and the bulk response of the system, the use of PEPT in the current study offers insight into the system's microscopic response. This not only offers a direct insight into the micro-mixing behaviours of the system studied but also carries the potential to provide a greater mechanistic understanding of the previously-observed macroscopic behaviours.

In the following section, we use the analysis methods described in Section 2.6.2 to provide both Lagrangian and Eulerian data providing insight – both direct and indirect – into the mixing dynamics of our incline blender system, and their variation with key system parameters.

3.1. Traversal classification

Table 1 (and Fig. 6 graphically) show, for each combination of blade rotation rate and mixing blade number explored, the percentage of recorded trajectories classified as 'centrifuging', 'axial traversal' or 'random motion' based on the criteria described in Section 2.6.2. As noted previously, random motion is expected to be desirable in terms of mixing, while both axial traversal and centrifuging trajectories, which limit transport in one or more directions, are expected to be detrimental. Classified example trajectories can be seen in Fig. 7

As one may intuitively expect, there is a clear positive correlation between the percentage of centrifuging trajectories and the blade RPM, and thus the Froude number, which for our purposes we define as:

$$\mathrm{Fr} = \frac{\omega^2 R}{g} \tag{3}$$

where ω is the blade rotation rate in radians per second, and R is a relevant length-scale, here the radial length of a blade — i.e. the distance from the centre axis of the system to the tip of a given blade.

Interestingly, at equivalent blade rotation rates, the percentage of centrifugal trajectories is significantly reduced for the 16H case as compared to the 8H case, strongly suggesting that the presence of (more) mixing blades acts to suppress this undesirable transport modality.

The relationship between the system parameters and the recorded number of axial traversal-type trajectories is less clear-cut. For an 8H configuration, the data emphatically show that a low rotation rate produces a large number of such trajectories; and that this number is significantly reduced at higher rotation rates. However, this positive reduction is more than outweighed by the substantial increase in centrifugal trajectories. For the 16H case, the number of axial trajectories remains constant, to within experimental error margins, for all RPM tested.

Finally, if we consider the prevalence of (desirable) 'random' trajectories, we see immediately that an increased number of mixing blades is preferable, with the overall fraction of such trajectories higher for all 16H cases than for either 8H case explored. Within the 16H cases, there appears to be a weak negative correlation between blade RPM and the percentage of 'good' trajectories. As such, based on considerations of mixing alone, a lower RPM seems desirable. However, considering the comparatively weak relationship observed, when considering also throughput, a faster rotation rate may in fact be desirable.

3.2. Lagrangian micromixing

As described in Section 2.6.2, the Lagrangian Micromixing metric provides information regarding the overall strength of micromixing, illustrated by the mean 'Deviation' values presented in Fig. 8, as well as the uniformity with which mixing is achieved across different regions of the system, illustrated by the standard deviation thereof. As such, strong and consistent mixing is represented in Fig. 8 by a large mean with a wide distribution. This method would be categorised as a distance-based method within Bhalode and Ierapetritou's review on continuous solid-based mixing indices (Bhalode and Ierapetritou, 2020); which comprehensively showcases a plethora of useful comparable mixing indices across a range of publications.

The data presented in Fig. 8 strongly indicate that the 375 RPM, 16H case provides both the strongest and most uniform micromixing, showing also – as one may intuitively expect – an increase in the

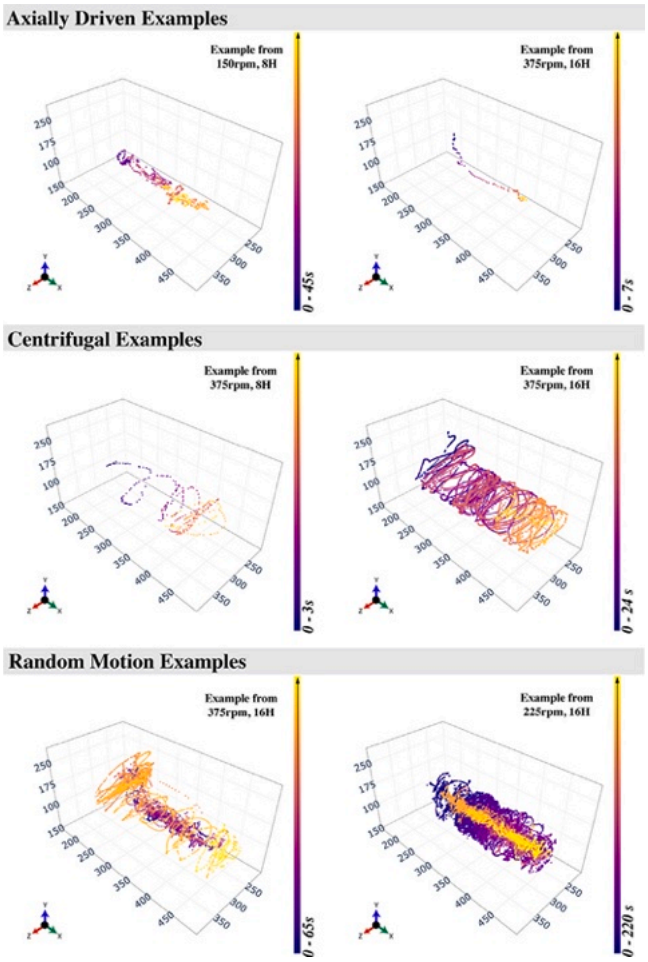


Fig. 7. Example tracers plotted in 3D (with units mm), where each trace is labelled by its corresponding classification, RPM and blade configuration. While the colour bar indicates the time in seconds.

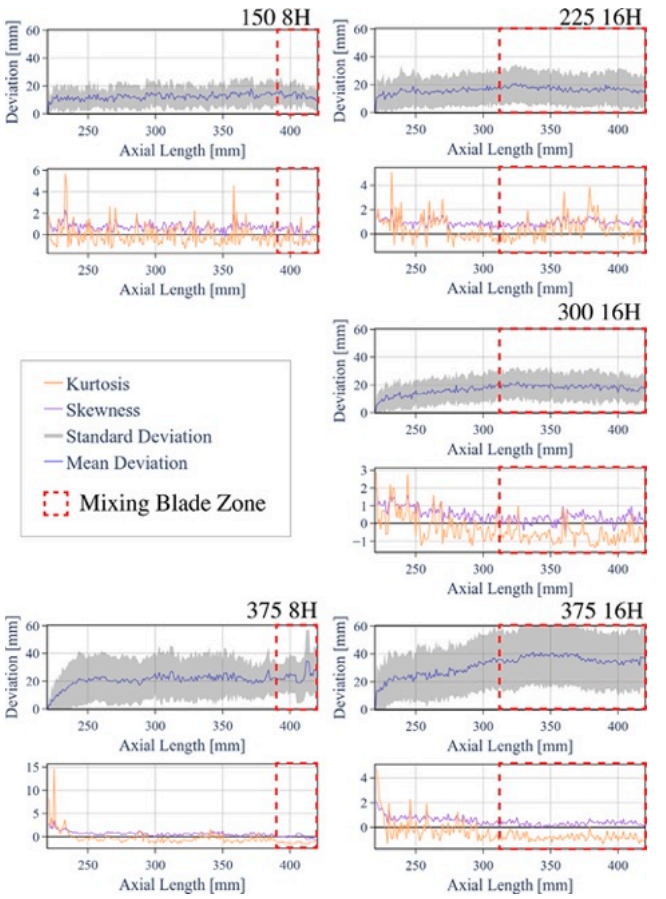


Fig. 8. Lagrangian micro mixing along the axis between: Point 1, 220 mm and Point 2, 420 mm. The Mixing Blade Zone (MBZ) starts at 310 mm and 390 mm for the 16H and 8H configurations respectively.

micromixing parameter within and immediately adjacent to the mixing blade zone (MBZ). Curiously, this uptick in micromixing within the MBZ is not clearly observable within the other data sets. From the figure, we see also that the poorest mixing performance is observed for the 150 RPM, 8H case.

The system with the greater number of mixing blades and the highest RPM (i.e. more energy imparted to the system) results in the highest value for the micromixing parameter (an indication of the speed at which particles are expected to diverge from one another), while that with the fewer blades and the lowest RPM yields the lowest value, again makes physical sense on a fundamental level. The existence of a correlation between RPM and the micromixing of particles has been previously demonstrated (for a horizontal system) by the numerical simulations of Sarkar & Wassgren 2009 (Sarkar and Wassgren, 2009), who investigated the variation of a dimensionless radial-plane dispersion index as a function of the Froude number and mixer volume-fill. For lower (< 0.5) fill fractions, a positive correlation was observed between the dispersive index and the blade revolution rate, though at higher fill levels the inverse was observed. As, due to the relatively low feed-rate of our system, a comparatively low average fill height was achieved in our systems, our results are broadly in line with the expectations of this prior work.

Furthermore, by abstracting Sarkar & Wassgren's (Sarkar and Wassgren, 2009) findings for this inclined system (compared to their horizontal system), it would be sensible to map this similar behaviour to the blender — i.e. considering an environment in which the fill level (and therefore, the radial-plane dispersion) would vary down the length of the barrel. By Sarkar & Wassgren's (Sarkar and Wassgren, 2009) measures, the 8H at 375 RPM should show the greatest radial-plane dispersion index and therefore the greatest mixing performance, as it would have the lowest fill with the highest Froude.

Conversely, the results of Van Snick et al. (2017) – who use a blender with the same geometry as this study – show that configurations with fewer mixing blades and thus lower residence mass provide poorer mixing outcomes than configurations which hold greater residence mass. The results from the lagrangian micromixing (Fig. 8) align well with Van Snick et al.'s findings — but also suggest that there is further complexity associated with the interaction between fill level (residence mass) and Froude number RPM. It should be noted the differences in inclination between the two studies (0° and +15°, from the horizontal respectively), however, the pure comparison between fill level and RPM on the dispersion performance, contradict one another. Highlighting the fact that the underpinning behaviour is still poorly understood. Employing methodologies like the lagrangian micro mixing help elucidate both the local behaviour and regional behaviour along the length of the barrel — effectively describing radial dispersion as a function of conditions experienced along the axial length.

3.3. Auto-correlation

The autocorrelation functions presented in Fig. 9 illustrate the rate at which the radial positions of particles become decorrelated from their initial values as a function of the distance, x, travelled along the blender axis. A value of $C_r(x) = 0$ thus indicates chaotic,

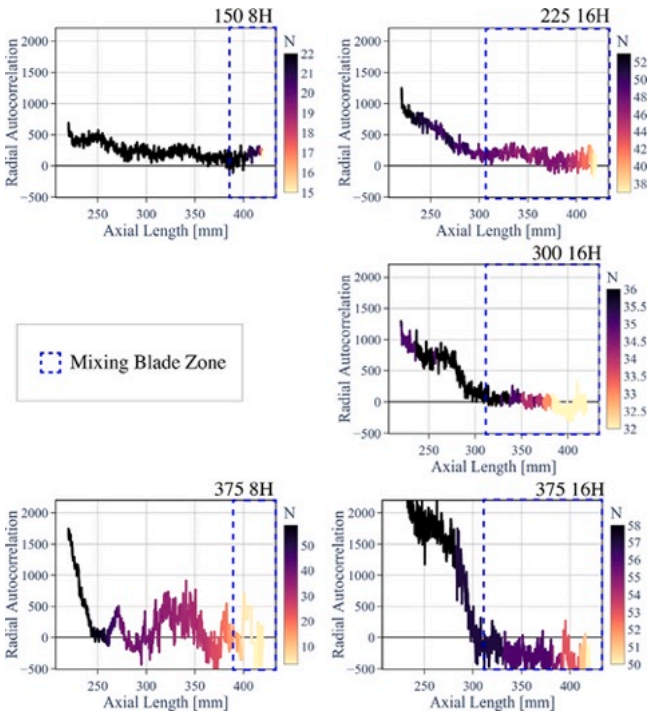


Fig. 9. Auto-Correlation ($C_r(x)$) of the [y, z] radial plane as a function of [x] the axis length. Detailing predictability of the radial position along the barrel. $AC = 0$ shows no predictability between the radial and axial plane, suggesting a high level of radial dispersion. N is the number of traces in the AC calculation, and therefore an indicator of confidence.

history-independent behaviour (Baxter and Olafsen, 2007), making it a valuable proxy measurement for mixing.

For all cases investigated, we see a general decrease in $C_r(x)$ as the distance from the inlet increases, indicating an increase in mixing. For the 16H cases in particular, we note that $C_r(x)$ decreases to approximately zero within the mixing blade zone, indicating the presence of strong, chaotic mixing in this region — as one may inherently expect.

Cross-comparison of the autocorrelation data shown in Fig. 9 with the residence time profiles presented in Fig. 10 shows that this behaviour coincides with a distinct peak in occupancy indicative of a 'pile-up' of material at the interface between the 'push-blade' zone and the mixing blade zone which is not present in the other data sets. The presence of this additional mass hold-up suggests a region of back-mixing or 'folding' as the fast-moving particles from the push-blade region meet the slower-moving MBZ, thus creating in essence an extended 'effective mixing region'.

The 'folding region' is shown by the 16H blade configuration at 300RPM and 375RPM, identified by the combination of key 'signatures' in both the autocorrelation (AC)(Fig. 9) and the spatial residence time (Fig. 10) at axial length 290 mm. Specifically, in the presence of a folding region we expect a sharp drop in the radial correlation combined with a significant increase in hold-up before the mixing blade interface. The simultaneous expression of these describes a behaviour where axial transport is converted into the radially promoted section, resulting in the powder now undergoing an increase in dispersive radial mixing, but also an increase in the probability that the powder will slip back down the barrel, providing also a remixing effect in the axial direction, mimicking the behaviour in a rotating tumbler (Morrison et al., 2016). The tumbling and reconstitution of powder within a rotating-drum mixer, or indeed the convective remixing inside a bubbling fluidised bed, are both known for their ability to promote both micro- and macro-mixing (Werner et al., 2023) and, as such, we may reasonably expect a similar effect here.

In the case of the 225 RPM, 16H system, this 'folding region' is seemingly absent, likely due to a reduced differential in the transport rate between the push-blade and mixing-blade zones at lower RPM. In this instance, $C_r(x)$ does not reach 0 until well within the MBZ. Such a zone is also absent from both 8H cases.

Unlike the 16H cases, which show a generally monotonic decrease in $C_r(x)$ with x, the 8H data sets – in particular the 375 RPM, 8H case – show an autocorrelation function which oscillates on a relatively large length scale, indicating that the particles – or at least a subset thereof – retain some degree of 'memory' of their initial conditions even after they have travelled a significant distance through the system (Campbell, 1997). This observation ties in well with our earlier finding (Section 3.1) that the 150 RPM, 8H and 375 RPM, 8H cases elicit, respectively, a large number of axial traversal and centrifuging trajectory modes.

Finally, it is worth noting that calculating the autocorrelations both for a constant initial position with varying lag (as presented in Fig. 9) and constant lag with varied initial position showed similar results, indicating the robustness of our observations.

3.4. Axial spatial residence time distribution

The spatial residence time profiles presented in Fig. 10 illustrate the relative fraction of time spent by tracers, on average, within different axial regions of the system. We have already described, in Section 3.3, the tendency of the higher-RPM, 16H to produce a hold-up region at the interface of the push-blade and mixing zones, and the absence of such a region in the lower-RPM case.

In the 8H cases studied, no hold-up region is observed for either blade rotation rate, and – unlike the 16H cases – the difference in residence between the push-blade zone and mixing-blade zone is stark, in particular for the 375 RPM case, where the minimal occupancy in the former region indicates an extremely rapid transit therein. This observation once again ties in well with previous observations (Sections 3.1 and 3.3) suggesting a tendency for tracers to take a direct path through the system (either axially or centrifugally) rather than experiencing any significant back-mixing.

We expect these distributions to change significantly, depending on the bulk material's characteristics and processing conditions. Moreover, it would be interesting to investigate whether the spatial residence time distribution remains the same for materials operating with equal strain; where strain is described as the number of blade passes multiplied by the mean residence time. If true, it would show evidence of mixing being influenced by regime-like behaviour within the blender — which may be a parameter to optimise.

4. Conclusion

In this study, we have used positron emission particle tracking (PEPT) to investigate the underpinning particle-level (microscopic) behaviours of a simple pharmaceutical powder in a commercial-scale incline linear blender. Data are obtained for a variety of blade rotation rates and two distinct blade configurations, including either 8 or 16 'mixing blades' (oriented, as their name implies, to encourage mixing) with the remainder of the system occupied by 'push blades' (oriented to encourage transport).

Leveraging the unique capabilities of PEPT to extract Lagrangian information from particulate systems with high temporal and spatial resolution, we have developed a series of novel metrics to probe and quantify the powder's dynamic response to differing process parameters in an incline linear blender.

Firstly, we have developed a set of algorithms through which the trajectories of particles through the system may be classified as either 'random motion' (desirable for mixing) or 'centrifuging' or 'axial' motion (less desirable). Knowledge of the existence of these less-desirable modes, not previously been documented in the literature, may prove

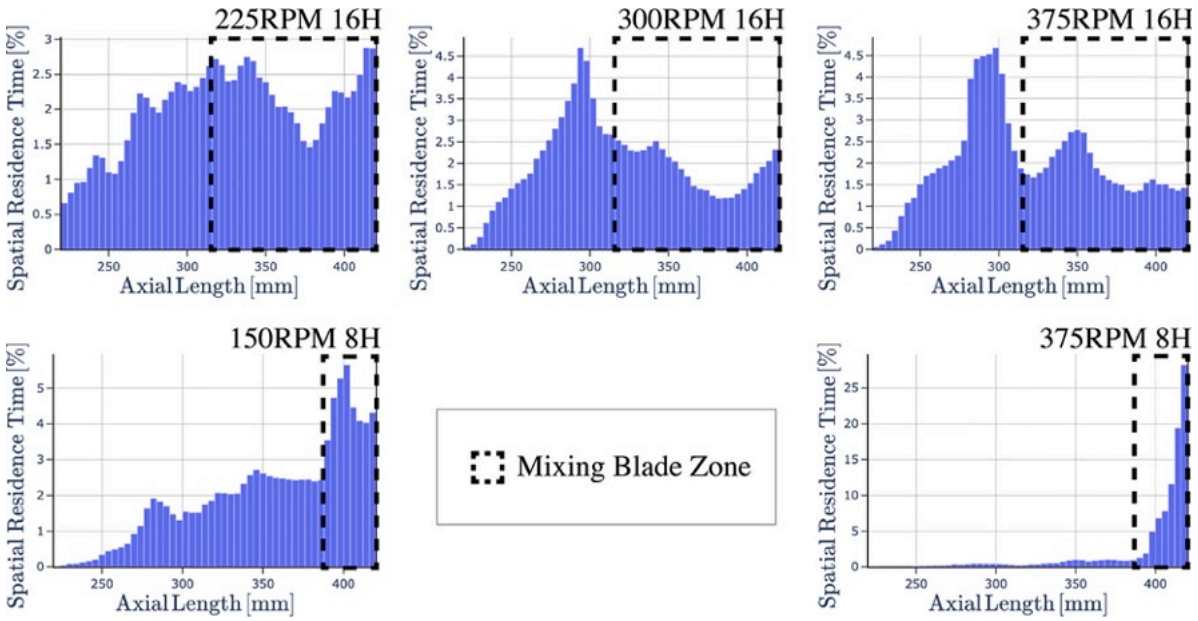


Fig. 10. Spatial Residence Time plots, normalised by the area under the graph, for the various speeds and their given blade configuration. The region of interest for the calculation spans between 220 mm to 420 mm. A black dashed line denotes the Mixing Blade Zone and corresponds to where the mixing zone starts along the axial length (mm), the zones start at 310 mm and 390 mm for the 16H and 8H respectively. To remove any erroneous tracers, a filter was applied to the calculation excluding points which had; traces shorter than 200 mm, min velocity of 0.01 m/s, max velocity of 3 m/s, and points with relative error >95th percentile.

valuable to industrial users of continuous blenders, who will naturally want to avoid the process conditions which give rise to them.

Our results show that the '8H' systems – those possessing a lower number of mixing blades – exhibited a larger number of less-desirable transit modes than the '16H' systems, with a shift from axial to centrifuging motion as the blade rotation rate is increased. For the 16 mixing blade case, we observed a similar increase in the percentage of centrifugal trajectories, though this apparent shift is less statistically significant.

Secondly, we have introduced a 'Lagrangian Micromixing' metric, similar in interpretation to the more conventional 'dispersion' metric used in prior PEPT studies (Martin et al., 2007; Windows-Yule et al., 2020) but capable of handling sparse, discontinuous data in rotating reference frames. The data obtained using this metric suggest that the 16 mixing blade system at the highest test blade rotation rate exhibited the strongest (micro)mixing conditions, with the 8H case at the lowest RPM producing the weakest (micro)mixing conditions.

Finally, we have developed a generalisable PEPT auto-correlation function suitable for continuous systems. As the autocorrelation function employed can be meaningfully interpreted as a measure of order and thus, by definition, an indicator of the presence of chaos, it provides another valuable predictor of mixing. This parameter once again indicates that improved mixing conditions may be achieved with more mixing blades and at a higher RPM. These data, combined with additional data in the form of spatial residence time distributions, show the existence of a high-hold-up 'folding region' at the interface of the push-blade and mixing blade regions, creating in essence an extended mixing zone. This folding region is observed only for the 16-blade configuration at relatively high ($\gtrsim$300 RPM) blade rotation rates.

Overall, our results suggest that – for the range of parameters tested – improved mixing conditions may be achieved for the combination of more mixing blades and higher RPM. The positive influence of high blade rotation rate in particular is a potentially pleasing finding for the field, as it reduces the need for a compromise between mixing quality and throughput. Nonetheless, these data were acquired only using a comparatively simple, non-cohesive powder, and a relatively low feed rate and (thus) fill fraction. Further work should be performed using additional materials and feed rates in order to assess the generality of our results.

It is important to keep in mind that more mixing or improved mixing conditions may not always have a positive effect. In the case of powder lubrication with, for example, magnesium stearate, overzealous mixing may lead to over-lubricated tablets; which then result in reduced tablet tensile strength (Mosig and Kleinebudde, 2015) and slower disintegration/dissolution rates (Nickerson et al., 2018). Therefore, processing parameters like the 8H (at high speed) may be better suited for a given formulation and specific use case.

In addition to the information gained directly from our results, the detailed, three-dimensional data obtained provide a valuable calibration/validation data set for future DEM models of continuous blender systems (Windows-Yule and Neveu, 2022).

CRediT authorship contribution statement

O. Jones-Salkey: Conceptualization, Data curation, Formal analysis, Investigation, Methodology, Visualization, Writing – original draft, Writing – review & editing. **A.L. Nicusan:** Data curation, Formal analysis, Investigation, Software, Validation,Visualization, Writing – original draft, Writing – review & editing. **C.R.K. Windows-Yule:** Conceptualization, Funding acquisition, Methodology, Project administration, Resources, Supervision, Writing – review & editing. **A. Ingram:** Conceptualization, Funding acquisition, Project administration, Resources, Supervision, Writing – review & editing. **D. Werner:** Data curation, Investigation, Methodology, Software, Validation. **S. Clifford:** Conceptualization, Funding acquisition, Project administration, Resources, Supervision, Writing – review & editing. **G.K. Reynolds:** Conceptualization, Funding acquisition, Project administration, Resources,Supervision, Writing – review & editing.

Declaration of competing interest

The authors declare the following financial interests/personal relationships which may be considered as potential competing interests: Owen Jones-Salkey reports financial support was provided by Engineering and Physical Sciences Research Council.

Data availability

Data will be made available on request.

Acknowledgements

We would like to acknowledge Dr. James Holman (GEA) for generously allowing us to purchase the GEA CDB-1 Linear Blender Prototype.

Experimental work on PEPT was carried out as part of an Engineering Doctorate programme funded by EPSRC, United Kingdom through the Centre for Doctoral Training in Formulation Engineering (grant no. EP/L015153/1), and from AstraZeneca plc, United Kingdom. The computations described in this paper were performed using the University of Birmingham's BEAR Cloud service, which provides flexible resource for intensive computational work to the University's research community. See http://www.birmingham.ac.uk/bear for more details.

References

Baxter, G., Olafsen, J., 2007. Experimental evidence for molecular chaos in granular gases. Phys. Rev. Lett. 99 (2), 028001.

Bekaert, B., Van Snick, B., Pandelaere, K., Dhondt, J., Di Pretoro, G., De Beer, T., Vervaet, C., Vanhoorne, V., 2022. In-depth analysis of the long-term processability of materials during continuous feeding. Int. J. Pharm. 614 (December 2021), 121454. http://dx.doi.org/10.1016/j.ijpharm.2022.121454.

Bhalode, P., Ierapetritou, M., 2020. A review of existing mixing indices in solid-based continuous blending operations. Powder Technol. 373, 195–209. http://dx.doi.org/10.1016/j.powtec.2020.06.043.

Boonkanokwong, V., Remy, B., Khinast, J.G., Glasser, B.J., 2016. The effect of the number of impeller blades on granular flow in a bladed mixer. Powder Technol. 302, 333–349. http://dx.doi.org/10.1016/j.powtec.2016.08.064, URL https://www.sciencedirect.com/science/article/pii/S0032591016305575?casa_token=ST4jsTngb-oAAAAA:aV8PqFfZ-1c3C-t5xLT_8xVrnBiy426HlqqXTNlNh01PmIT4IzHMjjt2Uy1YEeseQA271nptRjs#f0105.

Burcham, C.L., Florence, A.J., Johnson, M.D., 2018. Continuous manufacturing in pharmaceutical process development and manufacturing. Annu. Rev. Chem. Biomol. Eng. 9 (1), 253–281. http://dx.doi.org/10.1146/annurev-chembioeng-060817-084355.

Campbell, C.S., 1997. Self-diffusion in granular shear flows. J. Fluid Mech. 348, 85–101.

Che, H., Al-Shemmeri, M., Fryer, P.J., Lopez-Quiroga, E., Wheldon, T.K., Windows-Yule, K., 2023. PEPT validated CFD-DEM model of aspherical particle motion in a spouted bed. Chem. Eng. J. 453, 139689.

Ebrahimi, M., Yaraghi, A., Ein-Mozaffari, F., Lohi, A., 2018. The effect of impeller configurations on particle mixing in an agitated paddle mixer. Powder Technol. 332, 158–170. http://dx.doi.org/10.1016/j.powtec.2018.03.061, URL https://www.sciencedirect.com/science/article/pii/S0032591018302547?casa_token=Ilnk67Yn6nMAAAAA:ELDsV2aW51OEAxX3hzyUQoWl_Q2S7sg9OAHJ0CKLQ-Btl_Jsw9LBhtj0Ofe0sxNkBwdop3_Pc48#f0025.

Gao, Y., Ierapetritou, M., Muzzio, F., 2011a. Investigation on the effect of blade patterns on continuous solid mixing performance. Canadian J. Chem. Eng. 89 (5), 969–984. http://dx.doi.org/10.1002/cjce.20530, URL https://onlinelibrary.wiley.com/doi/10.1002/cjce.20530.

Gao, Y., Muzzio, F.J., Ierapetritou, M.G., 2012. Optimizing continuous powder mixing processes using periodic section modeling. Chem. Eng. Sci. 80, 70–80. http://dx.doi.org/10.1016/j.ces.2012.05.037, URL https://www.sciencedirect.com/science/article/pii/S0009250912003181?casa_token=ekRMR8ElnJ4AAAAA:8ju5z1WMyR3MIO9ry04pJwNXZfq3L-kUGr-Fa7ns3R-YNT9dWj6RiZYo6YCaRAoIIssTEKIr_PM.

Gao, Y., Vanarase, A., Muzzio, F., Ierapetritou, M., 2011b. Characterizing continuous powder mixing using residence time distribution. Chem. Eng. Sci. 66 (3), 417–425. http://dx.doi.org/10.1016/j.ces.2010.10.045.

Herald, M., Wheldon, T., Windows-Yule, C., 2021. Monte Carlo model validation of a detector system used for positron emission particle tracking. Nucl. Instrum. Methods Phys. Res. A 993, 165073.

International Council for Harmonisation of Technical Requirements for Pharmaceuticals for Human Use (ICH), 2012. Committee for Human Medicinal Products (CHMP) ICH Quality IWG Points to consider for ICH Q8/Q9/Q10 guidelines. Eur. Med. Agency 44 (February), URL www.ema.europa.eu.

International Council for Harmonisation of Technical Requirements for Pharmaceuticals for Human Use (ICH), 2023. ICH guideline Q13 on continuous manufacturing of drug substances and drug products. Eur. Med. Agency 31 (March), URL https://www.ema.europa.eu/en/ich-guideline-q13-continuous-manufacturing-drug-substances-drug-products-scientific-guideline.

Jones-salkey, O., Chu, Z., Ingram, A., Windows-yule, C.R.K., 2023. Reviewing the impact of powder cohesion on Continuous Direct Compression (CDC) Performance, cdc. pp. 1–48.

Lee, S.L., O'Connor, T.F., Yang, X., Cruz, C.N., Chatterjee, S., Madurawe, R.D., Moore, C.M., Yu, L.X., Woodcock, J., 2015. Modernizing pharmaceutical manufacturing: from batch to continuous production. J. Pharmaceutical Innov. 10 (3), 191–199. http://dx.doi.org/10.1007/s12247-015-9215-8.

Leimkuhler, B., Matthews, C., 2015. Molecular dynamics. Interdiscip. Appl. Math. 39, 443.

Martin, T., Seville, J., Parker, D., 2007. A general method for quantifying dispersion in multiscale systems using trajectory analysis. Chem. Eng. Sci. 62 (13), 3419–3428.

Megarry, A.J., Swainson, S.M., Roberts, R.J., Reynolds, G.K., 2019. A big data approach to pharmaceutical flow properties. Int. J. Pharm. 555 (October 2018), 337–345. http://dx.doi.org/10.1016/j.ijpharm.2018.11.059.

Morrison, A.J., Govender, I., Mainza, A.N., Parker, D.J., 2016. The shape and behaviour of a granular bed in a rotating drum using Eulerian flow fields obtained from PEPT. Chem. Eng. Sci. 152, 186–198. http://dx.doi.org/10.1016/j.ces.2016.06.022.

Mosig, J., Kleinebudde, P., 2015. Critical evaluation of root causes of the reduced compactability after roll compaction/dry granulation. J. Pharm. Sci. 104 (3), 1108–1118.

Nickerson, B., Kong, A., Gerst, P., Kao, S., 2018. Correlation of dissolution and disintegration results for an immediate-release tablet. J. Pharm. Biomed. Anal. 150, 333–340.

Nicuşan, A.L., Windows-Yule, C.R., 2020. Positron emission particle tracking using machine learning. Rev. Sci. Instrum. 91 (1), 13329. http://dx.doi.org/10.1063/1.5129251.

Palmer, J., Reynolds, G.K., Tahir, F., Yadav, I.K., Meehan, E., Holman, J., Bajwa, G., 2020. Mapping key process parameters to the performance of a continuous dry powder blender in a continuous direct compression system. Powder Technol. 362, 659–670. http://dx.doi.org/10.1016/j.powtec.2019.12.028.

Parker, D., Forster, R., Fowles, P., Takhar, P., 2002. Positron emission particle tracking using the new Birmingham positron camera. Nucl. Instrum. Methods Phys. Res. A 477 (1–3), 540–545.

Pernenkil, L., Cooney, C.L., 2006. A review on the continuous blending of powders. Chem. Eng. Sci. 61 (2), 720–742. http://dx.doi.org/10.1016/j.ces.2005.06.016.

Portillo, P.M., Vanarase, A.U., Ingram, A., Seville, J.K., Ierapetritou, M.G., Muzzio, F.J., 2010. Investigation of the effect of impeller rotation rate, powder flow rate, and cohesion on powder flow behavior in a continuous blender using PEPT. Chem. Eng. Sci. 65 (21), 5658–5668. http://dx.doi.org/10.1016/j.ces.2010.06.036.

Roth, W.J., Almaya, A., Kramer, T.T., Hofer, J.D., 2017. A demonstration of mixing robustness in a direct compression continuous manufacturing process. J. Pharm. Sci. 106 (5), 1339–1346. http://dx.doi.org/10.1016/j.xphs.2017.01.021.

Sarkar, A., Wassgren, C.R., 2009. Simulation of a continuous granular mixer: Effect of operating conditions on flow and mixing. Chem. Eng. Sci. 64 (11), 2672–2682. http://dx.doi.org/10.1016/j.ces.2009.02.011, URL https://www.sciencedirect.com/science/article/pii/S0009250909001080.

Siraj, M.S., 2014. Single-blade convective powder mixing: The effect of the blade shape and angle. Powder Technol. 267, 289–301. http://dx.doi.org/10.1016/j.powtec.2014.07.024, URL https://www.sciencedirect.com/science/article/pii/S0032591014006561#f0015.

Težyk, M., Milanowski, B., Ernst, A., Lulek, J., 2015. Recent progress in continuous and semi-continuous processing of solid oral dosage forms: A review. Drug Dev. Ind. Pharmacy 42 (8), 1195–1214. http://dx.doi.org/10.3109/03639045.2015.1122607.

Tomita, Y., Nagato, T., Takeuchi, Y., Takeuchi, H., 2020. Control of residence time of pharmaceutical powder in a continuous mixer with impeller and scraper. Int. J. Pharm. 586, 119520. http://dx.doi.org/10.1016/j.ijpharm.2020.119520.

Van Snick, B., Holman, J., Vanhoorne, V., Kumar, A., De Beer, T., Remon, J.P., Vervaet, C., 2017. Development of a continuous direct compression platform for low-dose drug products. Int. J. Pharm. 529 (1–2), 329–346. http://dx.doi.org/10.1016/j.ijpharm.2017.07.003, http://www.sciencedirect.com/science/article/pii/S0378517317306026, https://linkinghub.elsevier.com/retrieve/pii/S0378517317306026.

Vanarase, A.U., Osorio, J.G., Muzzio, F.J., 2013. Effects of powder flow properties and shear environment on the performance of continuous mixing of pharmaceutical powders. Powder Technol. 246, 63–72. http://dx.doi.org/10.1016/j.powtec.2013.05.002.

Vanhoorne, V., Vervaet, C., 2020. Recent progress in continuous manufacturing of oral solid dosage forms. Int. J. Pharm. 579, http://dx.doi.org/10.1016/j.ijpharm.2020.119194.

Wahlich, J., 2021. Review: Continuous manufacturing of small molecule solid oral dosage forms. Pharmaceutics 13 (8), http://dx.doi.org/10.3390/pharmaceutics13081311.

Werner, D., Davison, H., Robinson, E., Sykes, J., Seville, J., Wellings, A., Bhattacharya, S., Monsalve, D.S., Wheldon, T.K., Windows-Yule, C., 2023. Effect of system composition on mixing in binary fluidised beds. Chem. Eng. Sci. 118562.

Wildman, R., Hansen, J.-P., Parker, D., 2002. Velocity auto-correlation functions in three-dimensional vibro-fluidized granular beds. Phys. Fluids 14 (1), 232–239.

Wildman, R., Huntley, J., Hansen, J.-P., Parker, D., Allen, D., 2000. Single-particle motion in three-dimensional vibrofluidized granular beds. Phys. Rev. E 62 (3), 3826.

Windows-Yule, C., Herald, M., Nicuşan, A., Wiggins, C., Pratx, G., Manger, S., Odo, A., Leadbeater, T., Pellico, J., de Rosales, R.T., et al., 2022a. Recent advances in positron emission particle tracking: A comparative review. Rep. Progr. Phys. 85 (1), 016101.

Windows-Yule, C., Neveu, A., 2022. Calibration of DEM simulations for dynamic particulate systems. Pap. Phys. 14, 140010.

Windows-Yule, K., Nicuşan, L., Herald, M.T., Manger, S., Parker, D., 2022b. Positron Emission Particle Tracking. IOP Publishing.
Windows-Yule, C., Rosato, A., Rivas, N., Parker, D., 2014. Influence of initial conditions on granular dynamics near the jamming transition. New J. Phys. 16 (6), 063016.
Windows-Yule, C., Seville, J., Ingram, A., Parker, D., 2020. Positron emission particle tracking of granular flows. Annu. Rev. Chem. Biomol. Eng. 11, 367–396.
Windows-Yule, C., Tunuguntla, D.R., Parker, D., 2016. Numerical modelling of granular flows: A reality check. Comput Part. Mech. 3, 311–332.
Yang, Z., Fryer, P., Bakalis, S., Fan, X., Parker, D., Seville, J., 2007. An improved algorithm for tracking multiple, freely moving particles in a positron emission particle tracking system. Nucl. Instrum. Methods Phys. Res. A 577 (3), 585–594.
Zheng, C., Li, L., Nitert, B.J., Govender, N., Chamberlain, T., Zhang, L., Wu, C.Y., 2022. Investigation of granular dynamics in a continuous blender using the GPU-enhanced discrete element method. Powder Technol. 412 (July), 117968. http://dx.doi.org/10.1016/j.powtec.2022.117968.

Appendix Three

Attached Publication for Chapter 5

Publication Jones-Salkey et al. 2024 [61] has been included below:

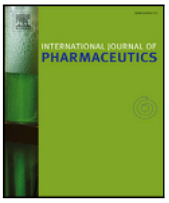
International Journal of Pharmaceutics 651 (2024) 123796



Contents lists available at ScienceDirect

International Journal of Pharmaceutics

journal homepage: www.elsevier.com/locate/ijpharm





Using AI/ML to predict blending performance and process sensitivity for Continuous Direct Compression (CDC)

O. Jones-Salkey [a,b,*], C.R.K. Windows-Yule [a], A. Ingram [a], L. Stahler [b], A.L. Nicusan [a], S. Clifford [b], L. Martin de Juan [c], G.K. Reynolds [b]

[a] School of Chemical Engineering, University of Birmingham, Edgbaston, Birmingham, UK
[b] Oral Product Development, Pharmaceutical Technology & Development, Operations, AstraZeneca, Macclesfield, UK
[c] Oral Product Development, Pharmaceutical Technology & Development, Operations, AstraZeneca, Gothenburg, SWE

ARTICLE INFO

Keywords:
Machine learning
Artificial intelligence
Mixing
Blending
Continuous Direct Compression
Prediction
Formulation

ABSTRACT

Utilising three artificial intelligence (AI)/machine learning (ML) tools, this study explores the prediction of fill level in inclined linear blenders at steady state by mapping a wide range of bulk powder characteristics to processing parameters. Predicting fill levels enables the calculation of blade passes (strain), known from existing literature to enhance content uniformity. We present and train three AI/ML models, each demonstrating unique predictive capabilities for fill level. These models collectively identify the following rank order of feature importance: RPM, Mixing Blade Region (MB) size, Wall Friction Angle (WFA), and Feed Rate (FR). Random Forest Regression, a machine learning algorithm that constructs a multitude of decision trees at training time and outputs the mode of the classes (classification) or mean prediction (regression) of the individual trees, develops a series of individually useful decision trees. but also allows the extraction of logic and breakpoints within the data. A novel tool which utilises smart optimisation and symbolic regression to model complex systems into simple, closed-form equations, is used to build an accurate reduced-order model. Finally, an Artificial Neural Network (ANN), though less interrogable emerges as the most accurate fill level predictor, with an r^2 value of 0.97. Following training on single-component mixtures, the models are tested with a four-component powdered paracetamol formulation, mimicking an existing commercial drug product. The ANN predicts the fill level of this formulation at three RPMs (250, 350 and 450) with a mean absolute error of 1.4%. Ultimately, the modelling tools showcase a framework to better understand the interaction between process and formulation. The result of this allows for a first-time-right approach for formulation development whilst gaining process understanding from fewer experiments. Resulting in the ability to approach risk during product development whilst gaining a greater holistic understanding of the processing environment of the desired formulation.

1. Introduction

A significant volume of research on continuous powder blending has focused on understanding how processing parameters affect performance using metrics such as residence time distributions and dispersion. Vanarase and Muzzio (2011), Vanarase et al. (2013), Holman et al. (2021), Van Snick et al. (2017), Hurley et al. (2022), while other – typically simulation-based – studied have demonstrated the differences that particle properties have on processing efficacy (Gao et al., 2011, 2012b,a; Sarkar and Wassgren, 2009, 2010; Toson et al., 2018). However, there is little work mapping physical experimental bulk powder characteristics to processing conditions in the blender. The only research done to the researchers' knowledge lay with that of Bekaert et al. (2022a,b), who investigated blend properties in a horizontal blender and the development of an empirical predictive model in an incline blender.

With the advent of readily-available, open-source Artificial Intelligence and Machine Learning tools, this study looks to leverage these methodologies to propose a novel framework to approach new pharmaceutical development projects. These methods allow the de-convolution of material properties and processing parameters by mapping processing outcomes to powder characteristics and processing parameters. This, in turn, allows for the prediction of key process outputs, such as the fill level within the blender and (thus) the strain experienced by the formulation, which has been shown to be a good predictor for blending performance (Vanarase and Muzzio, 2011; Jones-salkey et al., 2023a; Bekaert et al., 2022a).

* Corresponding author.
E-mail addresses: o.jones-salkey@hotmail.com, OXJ807@student.bham.ac.uk (O. Jones-Salkey).

https://doi.org/10.1016/j.ijpharm.2024.123796
Received 27 November 2023; Received in revised form 3 January 2024; Accepted 5 January 2024
Available online 6 January 2024
0378-5173/© 2024 The Authors. Published by Elsevier B.V. This is an open access article under the CC BY license (http://creativecommons.org/licenses/by/4.0/).

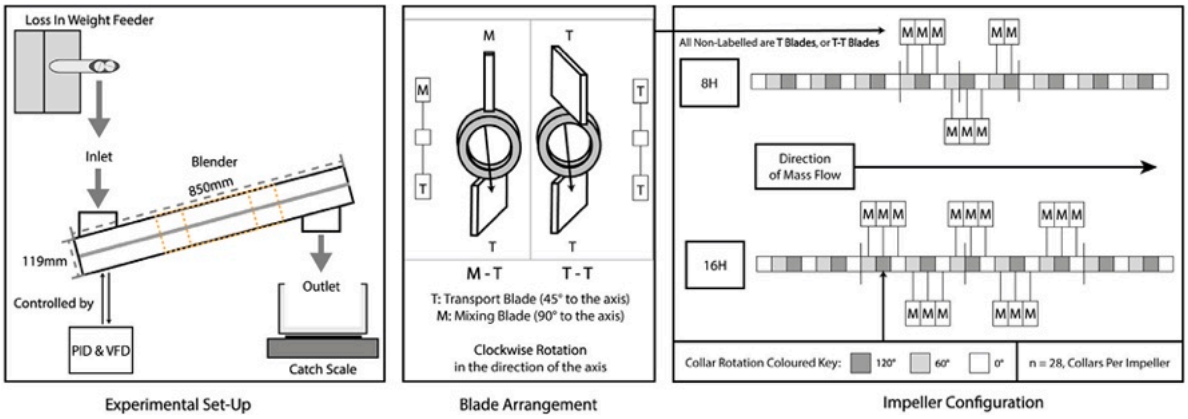


Fig. 1. The above figure graphically describes the Experimental Set-Up, Blade Arrangement, and Impeller configuration used for the experiments.

The utilisation of the three different models in the study ideally highlights the individual strengths of using each of the specific modelling methods. Random Forest Regression (RFR) can 'pull the logic' from the data by providing insights into feature importance and parameter relationships. Individual 'trees' extracted from the model may also provide useful guidance to system operators. PyTorch's Artificial Neural Networks (ANN), on the other hand, fit highly complex non-linear functions to the data to enable accurate and reliable predictions of the data surface, though are somewhat more of a 'black box', offering only limited physical insight regarding the outputs they produce. Finally, we use M^2E^3D, a tool that utilises evolutionary AI and symbolic regression to transform complex systems into simple equations (Nicusan and Windows-Yule, 2022a,b); the methodology of the tool is discussed further in Section 4.5 and accessible on GitHub: https://github.com/uob-positron-imaging-centre/MED.

Ultimately, by using these tools, this study unveils a correlation between fill level and optimum strain, which holds true for varied processing and material properties. The discussion focuses on how this relation develops by relating it to current literature and exploring space–time optimisation and optimum Peclet Numbers in specific regime-like behaviour. The study then discusses the use of such tools in an industrial setting by touching on how best to use this mapping ability to inform decisions to mitigate risk whilst navigating the complexities of drug project development.

2. Equipment

2.1. Prototype GEA, CDB-1, Linear Blender

A prototype of the commercially available GEA CDB-1 Linear Blender (GEA, Dusseldorf, Germany) was used for these experiments. The blender, made of stainless steel (316L), has an internal radius of 59 mm and a volume of 8.2L at a 15° incline to the horizontal. The equipment is driven by a motor paired with a proximity sensor (to measure the rotation of the impeller's shaft) and feed-back controlled variable frequency drive — allowing RPM to be set and maintained.

The shaft of the mixer has 28 removable collars each with two paddle blades the orientations of which can be adjusted from 0° (parallel to shaft axis) to 90° (orthogonal to shaft). Resulting in the ability, with the adjustable paddle blades, to simply change the angle and position of the collars to create a blade configuration. In this study, the 'number of mixing blades' refers to the helical organisation of 90° (to the axis) radial mixing blades from the centre of the mixer out towards the ends of the blender. In effect, the mixing blades are aligned in a helix along the shaft with 60° rotation between adjacent collars; thus increasing the number of mixing blades increases the size of the mixing zone. Ultimately, allowing the categorical variable (of a set configuration) to be considered continuous (as the number of blades varies the size of the mixing zone). The remaining blades in the configuration are aligned in transport orientation, at 45° to the axis. Fig. 1 displays these orientations and their positions in the configurations investigated; 8 mixing blades (8H) and 16 mixing blades (16H). These configurations are the same as the two configurations used in the PEPT study reported by Jones-salkey et al. (2023b).

Each blade configuration is examined across five blender speeds: 150 rpm, 225 rpm, 300 rpm, 375 rpm and 450 rpm. This choice allows the investigation across the full range of relevant blending speeds, exhibited by the CDB-1. Palmer et al. (2020) investigated in increments of 150 rpm, demonstrating a significant difference in mixing performance. In this work, we have reduced the increments to 75 rpm to provide better resolution and more reliable model fitting. Each configuration runs every material at 10 kg/h and 20 kg/h feed rate. Additionally, 3 materials (which are very commonly used filler excipients) run at 26.25 kg/h and 50 kg/h.

2.2. GEA, Compact Powder Feeder

The powder is fed to the blender using a Loss-In-Weight (LIW) GEA Compact Feeder (GEA, Dusseldorf, Germany). The LIW feeder holds roughly 2L of material and can operate in gravimetric (constant mass/time) and volumetric (constant screw speed, effectively constant volume/time) modes. Furthermore, the feeder is accompanied by a combination of a top-up ball valve, with varying volume inserts, and a 10L chute facilitating automatic system refills.

Gravimetric feeding operates by controlling screw speed to maintain a constant mass/time. Thus, a target feed rate can be maintained in the presence of powder flow disturbances, which may occur due to transient disturbances within the hopper or during powder transfer into the conveying screw volume. Therefore, gravimetric operation should be prioritised and the system's mechanical components should be configured to comfortably achieve the desired mass/time setpoint.

The calibration for the feeder is discussed in the following method Section 4.1. The calibration allows for each experiment to have the highest gravimetric feeding up-time, meaning the feeding of each powder is as accurate and reliable as possible.

2.3. Mettler Toledo, Catch Scale

The XS64000LX Mettler Toledo Balance (Mettler Toledo, Greifensee, Switzerland) was used to monitor the mass flow rate at the blender's outlet, recording mass (g) over time (s). Real-time response from the catch scale is used to monitor the mass flow rate from the outlet to ensure the system is operating at steady-state and to determine the residence mass at the end of the run. The scale is linked to Mettler Toledo's LabX software which records the mass at a frequency of 2 Hz, saving it to an output file. The position of the balance, relative to the

Table 1
Characterisation results for the ten materials and the surrogate formulation.

#) Material	Grade	Abbreviation	Basic Flowability Energy (BFE) [mJ]	Bulk Density [kg/L]	WFA @ 2 kPa, 0.4Ra	1/FFC @ 2 kPa	d10 [μm]	d50 [μm]	d90 [μm]
(1) MCC	Avicel PH-101	PH101	202	0.35	13.4	0.26	26.3	69.4	142
(2) MCC	Avicel PH-102	PH102	191	0.35	15.2	0.15	33.1	113	240
(3) MCC	Avicel PH-105	PH105	81.9	0.37	49.4	0.47	7	21	49
(4) MCC	Vivapur 350	VP350	124	0.86	3.87	0.01	377	432	509
(5) Lactose	Pharmatose 110M	P110M	119	0.73	10.2	0.14	78.9	153	219
(6) Lactose	Pharmatose 200M	P200M	128	0.60	44.5	0.31	21.8	57.8	122
(7) Lactose	Pharmatose 450M	P450M	100	0.47	11.4	0.63	3	21	56
(8) Lactose	Lactose FF316	316FF	274	0.61	36.5	0.08	39.8	92.9	173
(9) Mannitol	Pearlitol 200SD	PT200SD	297	0.54	14.5	0.03	40.3	143	238
(10) DCPA	DCPA A-Tab	ATAB	253	0.74	16.3	0.02	48.2	168	305
(F) Formulation	Surrogate	–	242	0.58	11.6	0.12	23	123	257

system, can be seen in Fig. 1. The fill level is then calculated from the residence mass and the bulk density of that powder, the calculation is discussed in the following Section 4.3.1.

3. Materials & characterisation

3.1. Material list

Nine commonly used commercial excipients were used in this study, comprising: Avicel PH-101, Microcrystalline Cellulose, abbreviated to 'PH-101' (DuPont, Cork, Ireland), Avicel PH-102, Microcrystalline Cellulose, abbreviated to 'PH-102' (DuPont, Cork, Ireland), Avicel PH-105, Microcrystalline Cellulose, abbreviated to 'PH-105' (DuPont, Cork, Ireland), Vivapur 350, Microcrystalline Cellulose, abbreviated to 'VP350' (JRS Pharma, Rosenberg, Germany), Fast Flo 316, Lactose Monohydrate, abbreviated to 'FF316' (Kerry, Tralee, Ireland), Pharmatose 110M, Lactose Monohydrate, abbreviated to 'PH110M' (DFE Pharma, Veghel, Holland), Pharmatose 200M, Lactose Monohydrate, abbreviated to 'PH200M' (DFE Pharma, Veghel, Holland), Pharmatose 450M, Lactose Monohydrate, abbreviated to 'PH450M' (DFE Pharma, Veghel, Holland), A-Tab, Dicalcium Phosphate Anhydrous, abbreviated to 'A-Tab' (Innophos, New Jersey, USA), and Pearlitol 200SD, Mannitol, abbreviated to 'PT200SD' (Roquette, Lestrem, France). In addition, the formulation utilises two additional materials: Powdered Paracetamol, abbreviated to 'pAPAP' (Mallinckrodt, USA) and Gycolys, Sodium starch glycolate (SSG), abbreviated to 'Gycolys' (Roquette, Lestrem, France). Furthermore, the drug surrogate formulation (F) in Table 1, is made up of 4 materials at the following weight percentages: Powdered Paracetamol (27% *w/w*), Avicel PH-102 (41% *w/w*), DCPA A-TAB (27% *w/w*), and Glycolys (5% *w/w*).

The materials list was selected according to use in commercial formulations and their relation to one another, with the intention of filling the characterisation space occupied by typical formulations. The first step was to select the more common formulation materials (i.e. PH102, 316FF and P200M), which had innately different material properties. Secondly, alternative grades of the same material were selected to evaluate the differences between the grades, allowing us to evaluate the effect of particle size distribution on both bulk characteristics and ultimate process outcomes. Lastly, after evaluating the characterisation space, additional materials were selected that either filled the characterisation spaces (e.g. PT200SD), provided an extreme value (e.g. VP350), or would be considered a good filler excipient for CDC formulations (e.g. ATAB), resulting in the final material list for the experiments.

3.2. Material characterisation & methods

The powders in Section 3.1 were subjected to a series of powder characterisation tests to determine intrinsic properties and flow behaviour. These are described below and the results are given in Table 1. All characterisation measurements were repeated in triplicate, from which the mean value is used.

Basic Flowability Energy (BFE) was measured using the Freeman FT4 Powder Rheometer (FT4, Freeman Technology, Tewkesbury, UK). BFE is, effectively, a measure describing the energy required for a stainless steel blade to initiate and sustain the bulk flow of a powder. Powders in the FT4 rheometer are exposed to a comparatively similar form of excitation to those in the CDB-1, suggesting that this measurement method may provide useful predictors of the powders' behaviours in the blender. For more information on the measurement technique see Freeman (2007) and for evaluation of the dynamics within the environment see Hare et al. (2015). In the present work, each powder went under four conditioning cycles and four test cycles.

Bulk density was measured using a 50 ml glass measuring cylinder and scale, where the powder was loosely deposited into the cylinder amounting to the maximum (50 ml) line. The powder mass is recorded and the bulk density is calculated (weight/volume). The samples were prepped by shaking the 250 ml holding vessel, ensuring the powder was not consolidated prior to pouring the powder into the measuring cylinder. Pouring the powder from the holding vessel, the cylinder is then filled to the measuring cylinder's 50 ml volume mark, the mass is recorded and used to calculate the bulk density. After each measurement, the powder was returned to the holding vessel before shaking the powder and taking another measurement. Furthermore, there was no manual intervention, agitation or extraction of powder while filling the cylinder — if the volume was not correctly poured the first time, the measurement was removed and repeated. Lastly, the bulk densities were all measured at the same time, negating the influence of humidity when comparing the results to one another.

Flow Function Coefficient (FFC, (using a consolidation pressure of 2 kPa) and Wall Friction Angle (WFA (0.4 Ra @ 2 kPa)) are two measurements describing powder cohesion and powder adhesion, respectively, characterised using the Schulze Ring Shear Tester (Dr. Dietmar Schulze, Wittenburg, Germany). For additional information on FFC and WFA see both Schwedes and Schulze (1990) and Schulze and Schulze (2021). Additionally, the FFC values were transformed into their reciprocal to linearise the measurement sensitivity. This is because it is difficult to discern differences between high values of FFC compared to low values of FFC.

Particle Size Distribution (PSD) was obtained from dynamic image analysis using the QICPIC Rodos (Sympatec GmbH, Clausthal-Zellerfeld, Germany), resulting in d10, d50 and d90 measurements. The Rodos powder disperser was set to 0.6 bar pressure and the M5 lens was used for all measurements.

It shows that the materials demonstrate a wide range of material properties (seen in Table 1), spanning those that would be appropriate for a typical pharmaceutical formulation (Megarry et al., 2019), offering a variation of suitably significant magnitude to successfully monitor their impact. The BFE can be varied from 81.9 to 297.2 mJ; Bulk Density from 0.346 to 0.86 kg/L; WFA from 3.87 to 49.4°; 1/FFC from 0.01 to 0.47; d10 from 3 to 367 μm; d50 from 21 to 432 μm; d90 from 49 to 509 μm.

VP350 has the highest bulk density, FFC and particle size distribution, and lowest WFA, whereas, Avicel PH-105 has the lowest BFE, lowest bulk density, and smallest particle size distribution, with the highest WFA. This is a rather striking result since both of these materials are different grades of the same material (MCC).

The characterisation techniques used in this study were selected based on their fulfilment of one or more of the following criteria:

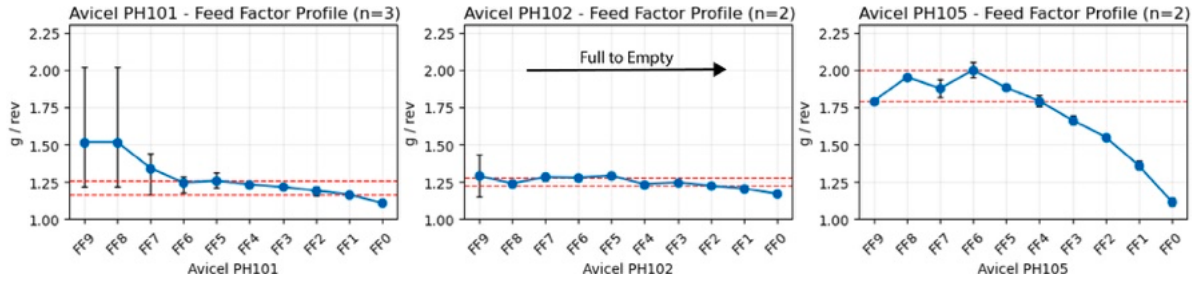


Fig. 2. Three example feed factor profiles, showcasing the profiles for the three different grades of the same material, Avicel (MCC). Error bars indicate the range of values from the duplicate/triplicate calibration runs (indicated by n = in the graph's title). The red dashed lines indicate the feed factor at which the top-up occurred. The following windows were used for the three powders: FF1 to FF4 (0.8L top-up) for Avicel 101, FF2 to FF6 (0.8L top-up) for Avicel 102, and FF4 to FF6 (0.4L top-up) for Avicel 105.

First, they closely resemble the processing environment — for example, the basic flowability energy, BFE, which directly involves the motion of a rotating impeller through a non-compacted particulate medium. Second, they are extensively used in literature to describe a particular behaviour — for example the FFC, which is widely considered to be an accurate measurement technique for quantifying powder cohesion. Third, they are simple and/or widely accessible measurements that succinctly detail bulk powder behaviour, such as bulk density. Furthermore, the fewer measurement techniques used for an accurate prediction, the lower the number of material characterisation experiments required to make a prediction; as such, we have deliberately chosen parameters which encode a considerable amount of information about the system into a single parameter. The result is a set of measurements which can be performed with relative speed and ease, and require minimal use of proprietary equipment.

It is finally worth briefly noting that while for the comparatively free-flowing powders and formulations explored here, a simple poured bulk density measurement is found to be sufficient when exploring more cohesive powders, it may be wise to instead use the FT4's conditioned bulk density measurement, so as to ensure a more reproducible and representative measurement. For our materials, the two were found to be equivalent for all materials tested.

4. Methods

4.1. Feeder calibration

Before the feeder is used to take a measurement, it must be calibrated to ensure the system configuration can accurately dose the desired gravimetric (mass/time) feed rate. Therefore, duplicate/triplicate calibration runs are used to determine the feed factor profile and the hopper top-up strategy.

Feed factor is defined as the mass delivered (from the feeder spout) per screw revolution (g/rev). Due to the differences in the physical properties of the materials used, the loading of the conveying screw and behaviour within the hopper will vary with each material, so each one must be calibrated prior to each investigation.

The feed factor profile is gained through GEA's calibration method, which effectively measures the feed factors whilst emptying the hopper from full with volumetric feeding. The hopper is separated into 10% fill level intervals (F_n), the mass fill of the hopper is then divided into 10 slices in the vertical direction, and the average feed factor within each of those intervals is stored against that hopper fill level. The resultant profile (see Fig. 2) provides insight into the stability of powder dosing, at constant screw speed, with the expectation that free-flowing powders will have minimal change in feed factor across the full range of fill levels. Had a material being discharged suffered from disturbances to feeding, changes to either the gear ratio or screw type/pitch would have been tested to ensure a more consistent feed. Fortunately, the calibration was assessed for all materials and found that the same gearbox ratio of 63:1 and a pair of conveying screws with a concave pitch of 10 mm width were appropriate for all tests.

Lastly, the feed factors are also used to define the stable operating region for the hopper fill level for triggering a hopper top-up event. This was done by plotting mean feed factors from F_9 (full hopper) to F_0 (empty hopper) (100% into 10% intervals, respectively) and identifying the most stable region during discharge. From this, the time and volume of the top-up event were defined, for each material; this event was to be initiated during the stable period of the volumetric emptying and the volume of top-up was selected to be the total volume dispensed over the identified stable region. This was then validated and optimised to ensure the automatic refills occurred with the largest proportion of gravimetric feeding to volumetric feeding. For three different grades of the same powder, the refill window is indicated by red dashed lines in Fig. 2.

This methodology ensures that the system operates with the utmost accuracy and reliability. The stable operating region, describes the operating window that is most resistant to feeding variance under volumetric operation, signifying that the feeding is the least sensitive to the fill level within the hopper. This is because the powder above compresses the powder below, as explained in Engisch and Muzzio (2015). This means that during a top-up event, when the feeder switches from gravimetric to volumetric, the feeder will show a consistent and accurate feed in grams per revolution, which is indicated by the aforementioned feed factor profile.

4.2. Residence mass (RM) measurements

Residence mass (RM) is defined as the mass of powder within the blender's mixing volume during steady-state operation. Several studies discuss the importance of residence mass for improving the macro mixing potential of pharmaceutical blenders (Portillo et al., 2007, 2010; Van Snick et al., 2017). Notably, it is a measurement that can be directly, and physically gathered, without the use of sensors, detectors, or imaging devices. Furthermore, RM's utility is really described by its sensitivity to other processing parameters and material properties. For instance, increasing RPM decreases the RM (discussed in Section 5.1) and allows for the calculation of Mean Residence Time (using Eq. (1)). The result is a great variable for evaluating mixing due to the coupled attachment of material, RPM and MRT — two of the three variables are required to evaluate strain discussed in Section 4.3.2, using Eq. (3).

$$\text{Mean Residence Time (s)} = \frac{\text{Residence Mass (g)}}{\text{Feed Rate (g/s)}} \quad (1)$$

The experiment begins with setting the blender to the desired RPM for the experiment. Once the blender is at speed, the LabX software for the catch scale is then set to record the mass (over time) from the outlet of the blender. Simultaneously, the GEA Compact Feeder communicates with TwinCAT 2 software (Beckhoff, Henley-on-Thames, United Kingdom) through tags appropriate for operation e.g. weight in the hopper, gravimetric mode, and screw speed. After initiating the recording of data, for both dispensing and receiving through the catch scale, the feeder is then set to dispense gravimetrically at the desired setpoint for the experiment.

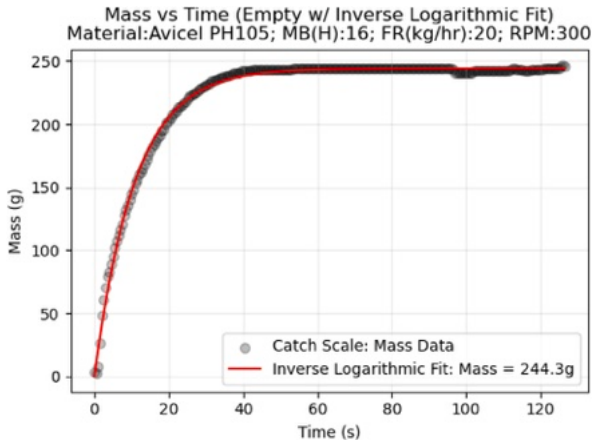


Fig. 3. Example of a '450 RPM Empty', where the offset (remaining mass in the blender) would then be added to the asymptote collected from the curve fitting to gain the final residence mass at steady state.

The powder is dispensed into the blender via the feeder. Steady state is then monitored and confirmed when the dispensing mass flow rate matches the mass flow rate received on the catch scale. While building mass to steady state, RPM is maintained by the feedback loop from the proximity sensor and variable frequency drive. Once steady state has been achieved all processing equipment is stopped simultaneously- and the residence mass within the blender is measured.

To measure the mass, in the most time-effective manner, the system is powered up to the fastest speed (450 RPM) with no powder flow into the system, and the resident mass is captured in the catch scale — demonstrated using Fig. 3. The result is mass removal which is a function of the RPM used.

It is known that 450 rpm, with no feeding, would not fully empty the blender so it was necessary to determine the residual mass. So it was assumed, and then checked, that this residual mass was independent of the speed history. Thus the residual mass was collected at the end of a run of five graduated rpm speeds (150 to 450 RPM) and treated as an 'offset', where it was manually added to the '450 RPM empty' residence masses. This was done for each of the feed rates and the blade configurations, despite the minimal difference being seen between changes in feed rate.

After a "450 RPM Empty" was done, the next RPM, with the same blade configuration and feed rate could then be done. Given the mass amounts are time-dependent, in particular the 450 RPM Empty, the removal of mass over time to the catch scale was recorded and the run stopped when the mass amount remained stable — see Fig. 3. To ensure each of these emptying processes was consistent an inverse log curve was fitted to the '450 RPM empty' residence masses, ensuring we could gather the mass at $t = \infty$. Ultimately, this meant that the residence mass values saw minor changes (in the order of a few grams), but the application of the same 'time-independent' methodology meant that the masses collected were consistently gathered.

The response, RM, serves as the backbone of this experiment, however, the response is best described as fill level (%), which can calculated from RM using Eq. (2).

Using fill level, instead of residence mass, results in simpler contextualisation when evaluating the powder relative to the blender's total volume. Providing a better sense of clarity when comparing different powders against one another, or considering powder behaviour in different blender systems/geometries.

In the discussion (Section 6.2) fill level is used, in place of RM, when evaluating the optimum process parameters to find the ideal regime behaviour across different materials.

4.3. Calculations

4.3.1. Fill level

Fill level [%], is defined as the percentage volume the powder occupies within the mixing volume.

$$\text{Fill Level (\%)} = \frac{(\text{Residence Mass}/\text{Bulk Density})}{\text{Mixer Volume}} \tag{2}$$

4.3.2. Strain

Strain (ω) can be considered as a measure of 'work done' to the powder. In the case of a continuous blender, it can be defined as the mean number of blade passes the powder flux would experience (Vanarase and Muzzio, 2011).

$$\text{Strain } (\omega) = \frac{FL \times \rho \times v_{blender}}{\dot{m}} \times \text{RPM} \tag{3}$$

The influence of the mixing blades is implicitly expressed in this equation due to how the mixing blades alter the fill volume and thus the mean residence time of the powder at a steady state. where RPM is the rotation rate of the agitator in rotations per minute; $\dot{m}$ is the feed rate in kg/h; FL is the fill level (as a fraction) of the powder at steady state; $v_{blender}$ is the volume of the blender in m^3; and ρ is the bulk density of the powder in kg/m^3.

4.4. Predictive modelling

4.4.1. Random forest regression

Despite the numerous insightful findings drawn from various studies using methods such as Partial Least Squares (PLS), Bekaert et al. (2022c), Dhondt et al. (2022), Vanarase et al. (2013), Bekaert et al. (2022a) the method presents a few key constraints. For instance, PLS is inherently linear and tends to obscure the intricate interplay of variables behind its principal components. In contrast, Random Forest Regression (RFR) offers the ability to capture non-linear relationships, providing a descriptive, 'logic-like' portrayal of the variables' interaction. When the primary focus is comprehending the system from both a material and processing perspective, it is crucial to understand these interactions and their resulting sensitivities.

RFR is a machine learning algorithm which combines the predictions of multiple decision trees to produce a more accurate and robust model. In this context, x represents an individual input data point (or a set of feature values) for which we want to predict an output, while y is the actual output or response value corresponding to that input. Hence, for each instance of x, we are trying to predict its corresponding y value. This can simply be depicted as multiple trees each making a prediction for a single x, and then aggregating those predictions to get $\hat{y}(x)$.

In this formulation, $\hat{y}(x)$ denotes the predicted value for the dependent variable based on the input x, aggregating the insights from all n decision trees. Mathematically, given n decision trees, the prediction of RFR for an instance x is given by:

$$\hat{y}(x) = \frac{1}{n}\sum_{i=1}^{n} T_i(x) \tag{4}$$

In the context of the equation, $T_i(x)$ represents the prediction of the ith tree. Each tree is sculpted using bootstrapped data subsets, a technique where random samples are drawn with replacements from the original dataset, allowing some observations to be repeated in each sample. At every decision point, whether it is a split or a branching, a random selection of features (variables) is integrated to ensure that the trees are decor related and there is reduced inter-tree correlation. This inherent randomness can be observed in both the data samples and feature subsets. These techniques enhance the model's generalisation potential, making it more robust and accurate.

To train the model, the entire dataset was randomly split into a train:test split of 80:20 (203:51, datapoints respectively) and training

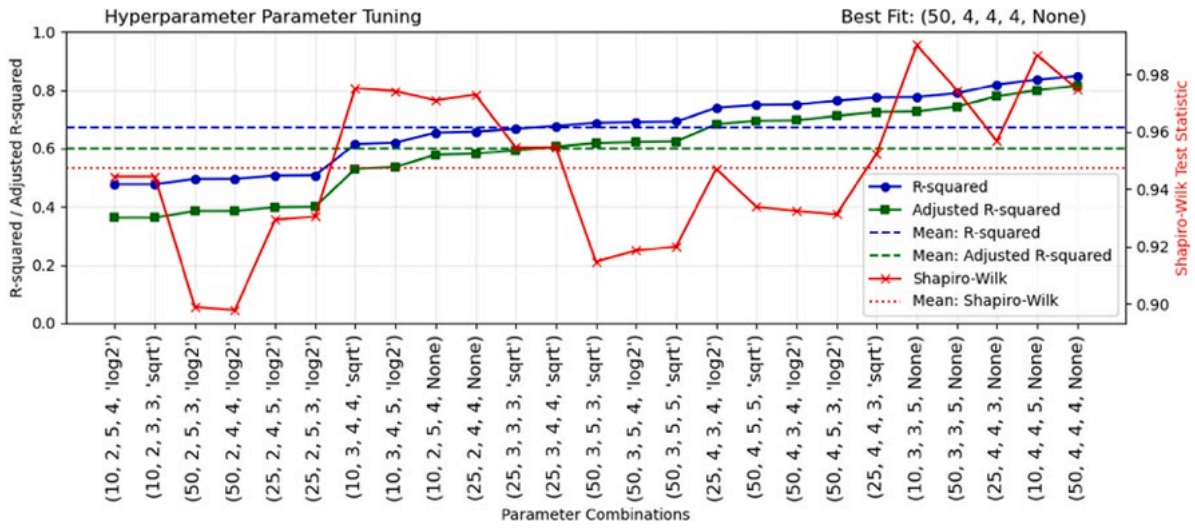


Fig. 4. Random Forest Regression (RFR) model parameter tuning. Results were ordered from worst (left) to best (right) r^2 value, with the secondary axis plotting the assessment of the residual's normal distribution using the Shapiro–Wilk Test (SWT)– higher SWT scores indicate a normal distribution. The *x*-axis shows the combination of the following 5 hyperparameters (in respective order): number of estimators, maximum depth, minimum number of samples to split, minimum number of samples for a leaf and maximum features.

data passed into the tuning stage of modelling. The RFR model was tuned by training approximately 240 models with different combinations of 'sensible' hyperparameter values: the number of estimators, max depth range, minimum samples to split, minimum samples for leaf, and maximum features range (for additional information on RFR see Sci-Kit's documentation: https://scikit-learn.org/stable/modules/generated/sklearn.ensemble.RandomForestRegressor.html).

To clarify the function of the aforementioned (RFR) hyperparameters, the following explanation(s) is provided:

- **Number of Estimators**: Specifies the total number of decision trees within the forest. Increasing the number of trees can improve the model's performance, but there is a threshold beyond which accuracy gains are marginal, trading-off for an increased computational cost.
- **Max Depth Range**: Designates the maximum depth or levels each tree can achieve. Deeper trees can discern more intricate data relationships but risk overfitting. An optimal depth strikes a balance between bias and variance.
- **Minimum Samples to Split**: Specifies the minimum number of samples required for a decision tree split. Increasing this value can prevent the model from incorporating small patterns that may be noise, which serves as a regularisation technique.
- **Minimum Samples for Leaf**: Specifies the minimum number of samples required to be at a leaf node (end of tree branch). Increasing this value, like the prior hyperparameter, can prevent overfitting and enhance generalisation across training examples.
- **Maximum Features Range**: During optimal split determination, the number of features to consider is specified. Random feature selection for each split promotes tree decorrelation and model generalisation.

Sensibility – which is applicable to the rest of the study – is defined as the thought experiments that align the complexity of the model to the size and complexity of the dataset one is looking to model. This means that if one has a large and complex dataset, one could approach it with a complex multi-layered model, with values that will de-convolute the complexity found within the data. Alternatively, with a simpler dataset, utilising the same modelling framework or hyperparameters, one would be at risk of overfitting the data — rendering the model impractical. Therefore, thought is put into the hyperparameter selection to ensure the risk of overfitting is minimal, with the tuning operating at a 'sensible' range. The results from the initial 'sensible' hyperparameters provide feedback to this initial tuning phase and through iteration, the model can be refined to generate a suitable and robust model.

The resultant fitted models were then rank-ordered for r^2 (and adjusted) and plotted alongside the residual's frequency distribution, which is then quantified by the Shapiro–Wilk test (SWT); The Shapiro–Wilk test (SWT) is a statistical analytical test which checks whether a sample comes from a normally distributed population. The null hypothesis (1) assumes that the data is normally distributed, while the alternative hypothesis (0) assumes otherwise. A normal distribution would indicate a lesser propensity for the model to under- or over-predict values, while a narrow distribution indicates lesser error between the measured and predicted values; both a normal and narrow distribution are thus desirable.

The final selected model (Fig. 5), which held the following hyperparameter values: number of estimators (50), max depth range (4), minimum samples to split (4), minimum samples for leaf (4), and maximum features range (None), possessed a high r-squared value of 0.85 (showing a good fit) whilst demonstrating a good normal distribution of the residuals (quantified by the SWT, which was 0.97) — see Fig. 4. Any additional hyperparameters were held at SciKit Learn's default values.

The RFR model's performance is shown in Fig. 5, by the Parity Plot and Feature Importance graph. The Parity plot is the use of the model to predict the 'test' data, which is not used to train the model and shows a good r^2 fit of 0.848. However, there is considerable spread in places, leading to higher RMSE values — namely the cluster of points that are over-predicting at 10% fill. Furthermore, there is greater variability at the higher fill levels but this is potentially due to increased sparsity of data points at higher percentages. This sparsity at these higher fills, is a feature of the experiment, due to RPM highly dominating the system, irrespective of material or alternative process parameters (discussed in Section 5.1); the result is a higher number of points around lower fill levels due to increased RPMs.

The generated data from the full experimental dataset indicates that most operations should be at or below the 35% fill mark. However, further experimentation within these higher fill levels, through both material and process changes (e.g. higher feed rates), would provide the model with greater reasoning, and therefore, the improved capability to predict these fills.

The model was intentionally limited, in terms of accurate predictive capacity, to be able to derive the 'logic' from the system. In this simplified model, only the most important features will be shown, with the most contrasting changes between turning at each feature. This is

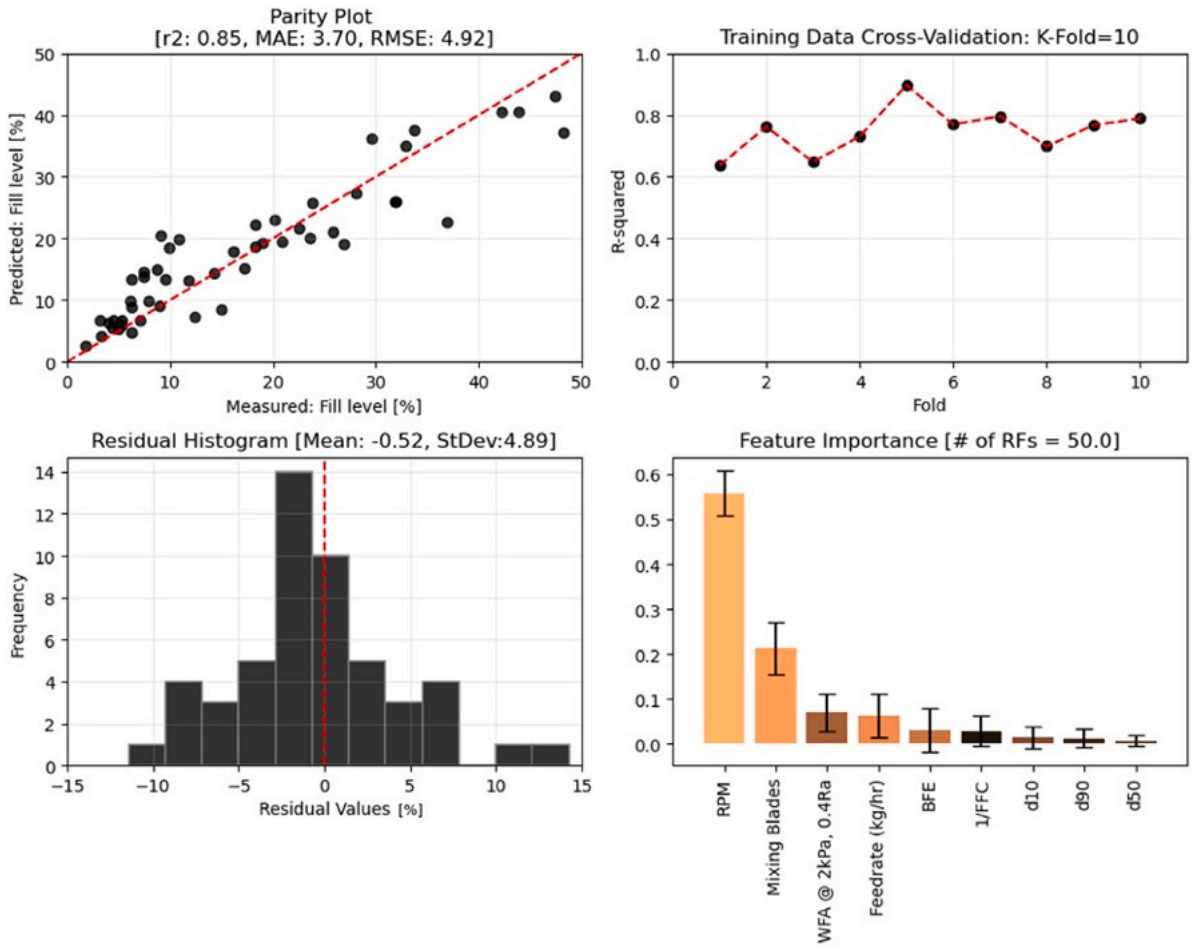


Fig. 5. Random Forest Regression (RFR) model performance. The top left graph shows a parity plot of the measured vs predicted fill level. Top right, training data (only) k-fold cross-validation. Bottom left, RFR's residual histogram. Finally, the bottom right shows the Feature Importance (FI) of each of the parameters on the RFR's predictive capability, higher indicates more importance. The error bars show the standard deviation of the FI across the $n = 20$ generated estimators.

done in contrast to having fewer samples to split and minimum samples for leaf – which would result in more and longer branches to reach the answer – giving rise to less granular predictions. Accordingly, these trees with higher complexity result in a cumbersome tree with many turns, inevitably resulting in the loss of 'what factors *really* matter'.

4.4.2. Artificial Neural Network (PyTorch)

Artificial Neural Networks (ANN or NN) have demonstrated a great ability to make predictions from data on a wide range of applications. The following ANN model was developed from the guidance provided by Goodfellow et al. (2016) comprehensive book on machine learning (ML); the book covers foundational elements of ML in detail, with Chapters 5 and 7 playing a pivotal role in this model's creation.

ANNs function by propagating input data through layers of artificial neurons. These neurons apply a linear transformation followed by a non-linear activation function. Mathematically, each layer's output, h, is computed as:

$$h = \sigma(W x + b) \tag{5}$$

In Eq. (5), σ represents the activation function empowering the model to capture intricate relationships between inputs and outputs. The term W stands for the weights, which dictate the significance of each input. The bias b adjusts the neuron's output, while x is the input to the neuron. As data is fed into the network, it undergoes transformations by each layer. The process, known as forward propagation, continues until the final layer produces the network's output or prediction. The connections between neurons, characterised by the weights and biases, determine the strength and nature of the relationships the network captures. However, after a single forward propagation, the network's predictions may not be accurate. This is where *backpropagation* comes into play. Backpropagation is an optimisation algorithm used for minimising the error in the predictions. It works by computing the gradient of the loss function with respect to each weight by the chain rule and iteratively adjusting the weights and biases in the direction that reduces the error. An *epoch* refers to one complete forward and backward pass of all the training examples. By running multiple epochs, the network continues to refine its weights and biases, aiming to enhance its prediction accuracy over time.

ANNs are complex systems that require iteration to configure and fine-tune model performance. The following hyperparameters (used for the model) are detailed and described below:

- **Architecture**:
  This study employs PyTorch to construct an Artificial Neural Network. Given the dataset's size, this architecture was chosen to be relatively simple to prevent overfitting, which occurs when the model becomes too closely tailored to the training data and performs poorly on unseen data.
  - **Input Layer**: Comprises 9 nodes, corresponding to the number of features in the dataset.
  - **Hidden Layers**: Two layers with 41 and 14 nodes respectively. These layers process and transform the input data.
  - **Output Layer**: A single-node layer, providing the final prediction.

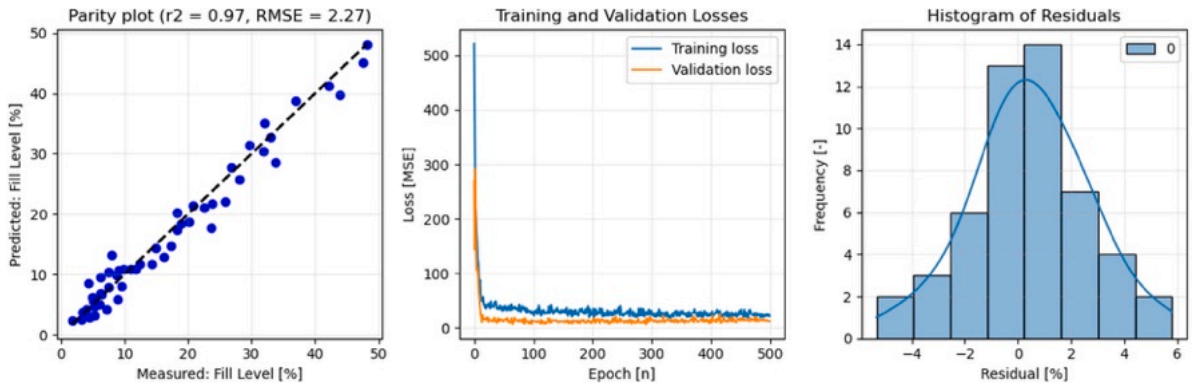


Fig. 6. ANN training and performance: Left, parity plot of the measured vs. predicted fill level percentage. Centre, training and validation losses (in MSE (Mean Squared Error)) of the model vs. the number of epochs. Right, histogram of the residuals (measured-predicted). The relative root mean squared error was 12%.

- **Hidden Layer Nodes (Linear)**: Each node applies a linear transformation to the data, based on the weights and biases. Using the following equation: $h = \sigma(Wx + b)$. These nodes within the network form the basis of the prediction.
- **Activation Function (ReLU)**: Defined as $\sigma(z) = \max(0, z)$. It introduces non-linearity into the network, allowing the model to understand and represent complex relationships in the data.
- **Dropout Rate (0.0155)**: A regularisation method where a fraction of neurons are randomly deactivated during each training iteration. This helps in preventing the model from over-relying on specific neurons and mitigates overfitting.
- **Learning Rate (0.0185)**: Determines the magnitude of adjustments made to the network's weights during training. A smaller learning rate means slower convergence but possibly more precise outcomes, while a larger rate could speed up the training but risk overshooting the optimal solution.
- **Epochs (500)**: Refers to the number of times the entire dataset is presented to the network during training. More epochs can allow for better learning, up to a point, after which overfitting might occur.
- **Batch Size (32)**: The number of data samples processed before the model's internal parameters are updated. Using batches is more memory-efficient than using the entire dataset.
- **Optimiser (ADAM)**: An optimisation algorithm that adjusts the weights of the network. ADAM is known for its adaptive properties, where individual learning rates are computed for each parameter.
- **Loss Criterion (Mean Squared Error (MSE))**: Measures the squared differences between the predicted and actual values. The goal during training is to minimise this value.
- **Data Normalisation (MinMaxScaler)**: Transforms features to lie in a range between 0 and 1. This ensures that no particular feature dominates the learning process due to its scale, leading to more balanced and efficient training.
- **Other Hyperparameters**: Any parameters not explicitly mentioned were kept at PyTorch's default settings to maintain stability and general best practices in training.

The Python package OpTuna was utilised to methodically search for the best combination of two vital parameters: learning rate and dropout rate. The learning rate determines how quickly the model updates its weights in response to the calculated error, while the dropout rate is a technique where certain neurons are randomly "dropped" or deactivated during training to enhance model robustness. OpTuna's search spanned across 100 combinations, bounded within $1e^{-5}$ to $1e^{-1}$ for the learning rate and 0.0 to 0.5 for the dropout rate. The performance of the model was gauged through a combination of metrics, visualised in Fig. 6.

First, a key indicator of a good model includes a steady decrease in the training and validation loss (centre), indicating that the model is learning, and a close match between these two loss curves, suggesting minimal overfitting. The training loss provides a measure of the model's error on the data it is actively learning from, effectively the loss seen at its current epoch. The validation loss measures the error on a separate subset of data not used during training (unseen data at the current epoch), offering insights into the model's ability to generalise to new, unseen data.

Second, once the model has been trained on the 'training data' (80% of the dataset) the model is asked to predict the remaining 'test' (20%) data, the result is the parity plot (left) — which further validates/indicates the model's ability to predict unseen data. The fit of the model can be quantified by an RMSE of 2.27 and a high r^2, which in this case is exceptional with 0.97.

Third, a residual histogram plots the distribution of the actual data minus the predicted data. A narrow and normal distribution here would conclude that the model has minimal bias under or over-predicting across the range of predicted test values. In addition, the frequency distribution of the residuals is greatly improved compared to the RFR's.

Lastly, the developed ANN was investigated using SHAP (SHapley Additive exPlanations) analysis, a method rooted in game theory (Lundberg and Lee, 2017); further details and documentation can be found at https://github.com/slundberg/shap. Effectively SHAP treats each discrete data point as a player and allows the 'game' to unfold to determine which features are the most 'useful' for predicting the response variable. The resultant is a graph (Fig. 7) similar to that found in the RFR's Feature Importance (Fig. 5).

The top-performing features match in the same rank order for both models; highlighting the reliability of these factors in the prediction of fill level. The remaining features differ in rank order suggesting the models utilise the remainder of the variables differently. Alternatively, it suggests that the variables (and/or the differences between them) are statistically insignificant compared to the important ones.

4.5. Symbolic regression — M^2E^3D

Multiphase Materials Exploration via Evolutionary Equation Discovery — or M^2E^3D, further abbreviated simply to MED, is a data-driven tool for discovering analytical equations modelling the underpinning physics or correlations of industrial systems that are too complex to be modelled from first principles (Nicusan and Windows-Yule, 2022a,b). The core algorithm of M^2E^3D is its symbolic regression engine, the *SymbolicRegression.jl* library written in the Julia programming language (Cranmer et al., 2020; Bezanson et al., 2017), which discovers analytical expressions f mapping given input values X to a measured output $y = f(X)$; the general algorithmic steps are:

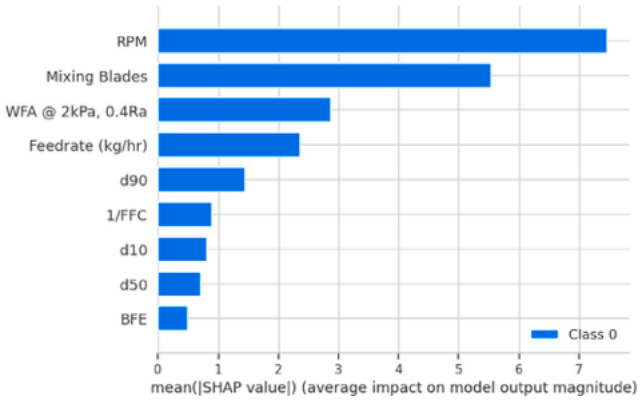


Fig. 7. ANN SHAP analysis, showing the mean of the modulus SHAP Values. Effectively, the average impact of each of the variables on the output magnitude. This is then ranked-ordered from the most influential feature to the least. The scale quantifies the relative importance of the variables.

1. The user selects the operators available to the symbolic regression engine, including common binary operators (addition, multiplication, etc.) and unary operators (log, sin, etc.) or custom functions — allowing users to incorporate some domain knowledge into the equation search, e.g. if the process outputs are modelled against system geometry, trigonometric functions might be included.
2. The operators, along with inputs and fitting coefficients are combined in a tree to form equations (see Fig. 8).
3. The free coefficients are fitted against the measured data y and the residuals are computed $f(X) - y$.
4. An evolutionary algorithm is used to minimise both residuals **and equation complexity** (the latter measured simply as the number of branches in the equation tree) - this multi-objective optimisation problem is necessary to discover sensible, physical, interpretable equations rather than overfitted chains of functions.
5. The process of equation generation - fitting - evaluating - evolving is continued until the best-performing equations at each level of complexity are found to stabilise (i.e. not change between generations) - and hence a Pareto front of equation complexity-accuracy is found.

The main advantages of the technique include:

- **Interpretability**: the equations found give insight into the underlying physics governing the system, while coefficients bear physical units which, again, allow physical interpretation of the correlations found.
- **Robustness against noise**: as equation complexity is also minimised, the most persistent underlying physical terms are identified, naturally removing measurement noise.
- **Requiring few measurements**: if the system is governed by underlying physical laws whose inputs are included in the training data, identifying them requires $O(10)$ data points, which is orders of magnitude lower than what surrogate models and neural networks typically require.
- **Ability to solve the inverse problem**: oftentimes it is not just a predictive model that is desired, but the ability to dynamically change a process input to achieve a fixed output (e.g. fill level); this is possible by rearranging the equations found and can be integrated in continuous on-line process control schemes.
- **Allowing some degree of extrapolation**: unlike virtually all surrogate modelling approaches, if an underlying physical law is identified (e.g. Stokes' law in fluid flow), it can be extrapolated beyond the input training data range to a point (e.g. in the previous example, until turbulence becomes significant).

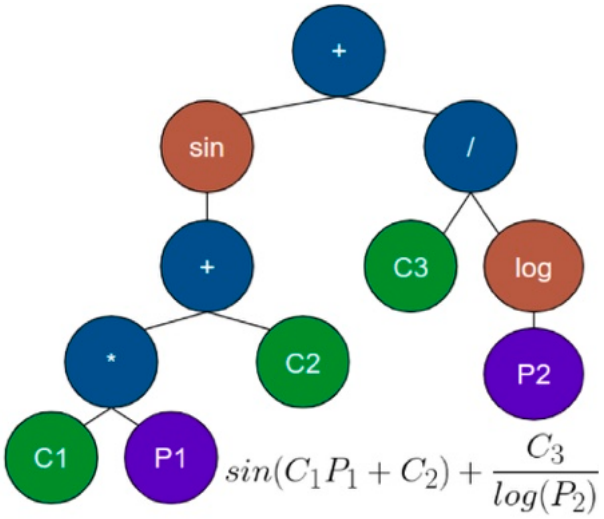


Fig. 8. M^2E^3D representation of an example analytical model (bottom right), built as a tree with its nodes (circles) representing input parameters (purple), constants which need fitting (green), binary operators (blue) and unary operators (orange).

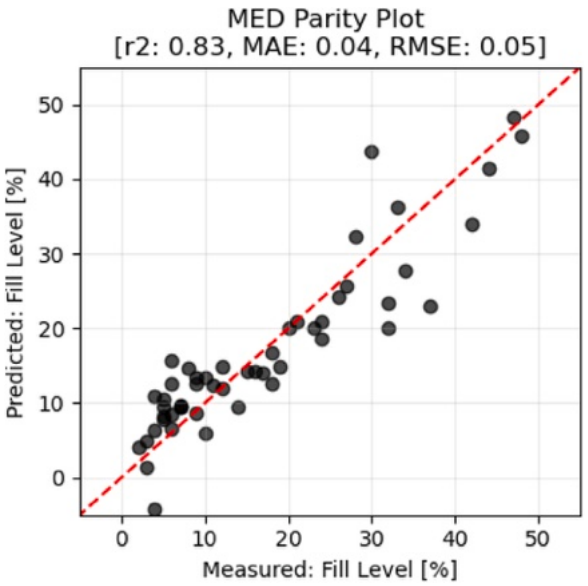


Fig. 9. M^2E^3D Parity Plot, measured vs predicted.

Both the algorithm and the codebase for M^2E^3D can be found on GitHub: https://github.com/uob-positron-imaging-centre/MED)

M^2E^3D has been trained on the same 80:20 train-test split data as the other AI/ML methods and produced an equation (Eq. (6)) whose specific form and interpretation are discussed below. The equation was then used to predict the test data and produced the parity plot shown in Fig. 9. It is recognised that there is a single prediction with a negative fill level, this would be considered erroneous and scrapped (since a negative fill level is impossible), but displays the potential limitation of selecting an equation which is not complex enough. M^2E^3D could also be told to use different or more complex operators and re-trained, this may improve the tool's ability to generate more suitable equations — for the training of this model, it was limited to binary operators.

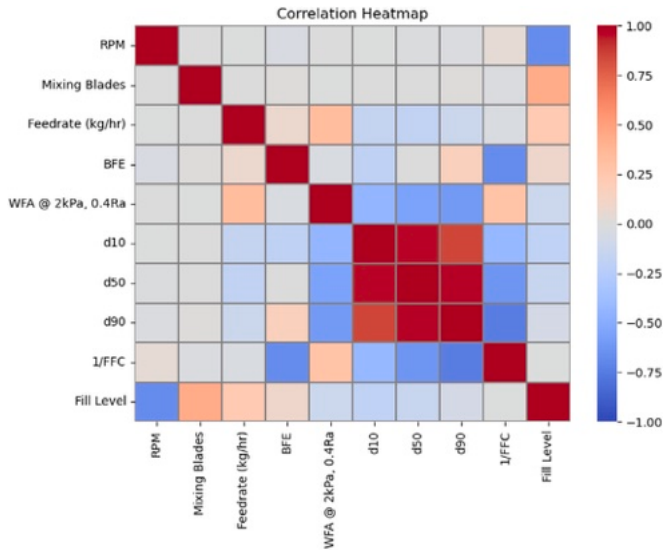


Fig. 10. Correlation Heatmap (−1 to +1) between process parameters, material properties and response variable (fill level). The colour bar indicates the positive correlation (+1, Red) and negative correlation (−1, Blue).

5. Results

5.1. General data trends

The correlation between the response and variables (normalised between +1 and −1) was calculated and plotted as a heat map 10. The correlations between the response variable, Fill Level, and the other variables highlight the effect that variables have on the response. For instance, it shows that RPM is highly negatively correlated with Fill Level, whereas Mixing Blades are moderately positively correlated with Fill Level. It is of particular interest how the material properties are related to the Fill Level — but there are no correlations of a moderate magnitude that point to a specific characteristic being a significant influence.

Plotting the fill level against RPM (shown in Fig. 11) produces a clear, negative linear trend, and in some cases resembles a reverse Sigmoidal curve. Fig. 11, shows the fill level response against the three processing parameters: RPM, Mixing Blades, and Feed Rate. As mentioned, RPM dominates the system, reducing the fill level, irrespective of both material properties and mixing blade configuration. A higher feed rate sees a translation upwards, effectively increasing the fill level – but not necessarily changing the shape of the curve – this is seen to have an increased effect for a higher mixing blade configuration (16H). Perhaps this is due to a decrease in axial transport in the centre of the mixing volume, and so there is less direct transport of the powder from the inlet to the outlet. Moreover, increasing the higher mixing blade configuration, resulted in higher fill levels across the rpm range but had a lesser effect at higher RPMs — again suggesting RPM is the most influential parameter on fill level. These observations agree well with prior experimental and numerical studies (Portillo et al., 2008, 2010; Vanarase and Muzzio, 2011; Van Snick et al., 2017; Palmer et al., 2020; Zheng et al., 2022).

5.2. Model: Random forest regression

Evaluating the general data trends with a single material property provides no significant distinction or correlation. This may be due to the difficulty of discerning a true pattern with a single bulk characteristic — as it would be considered too granular. Therefore, we can better understand their behaviour by modelling how these bulk characteristics interact with other material characteristics or process parameters.

The decision tree (35 of 50), seen in Fig. 12, showcases an example of the logic output. The tree can be interpreted by moving down the tree from the initial top node. Each node then passes another if statement, questioning *if* the assessed sample possesses values greater or less than what the node is asking, which will decide the following node. The final box (called a *'leaf'*) contains the predicted (value) Fill Level %, for the specific path of logic gates used to reach the leaf.

The results align with Section 5.1, insofar as saying that both RPM and Mixing Blades show great significance on the final fill level as these parameters dictate the breadth of the fill levels, sitting at Tier 1 and 2 of the tree. Interestingly, BFE, WFA, d10 and RPM show on the 3rd tier but these are shown to be dependent on the fill level at this point. Furthermore, this is reflected in the initial correlation plot (Fig. 10), meaning that at higher fill levels BFE and WFA are shown to be factors to make a further distinction on the fill level.

Furthermore, when evaluating the positional importance of a node it is also important to consider the colour of the node — which highlights the mean fill level of all samples at the current node. It is shown at higher fill levels (where motion is likely more frictionally dominated), particle physical properties influence the prediction, demonstrated by the position and colour association of BFE, WFA and FFC. Whereas at lower fill levels (where motion is more likely collisionally dominated) the rotation rate seems to dominate; intuitively described by the increased influence of processing parameters due to the reduction of powder volume and the resultant increase in both the frequency and intensity of particle–wall collision and reduction of particle–particle contacts.

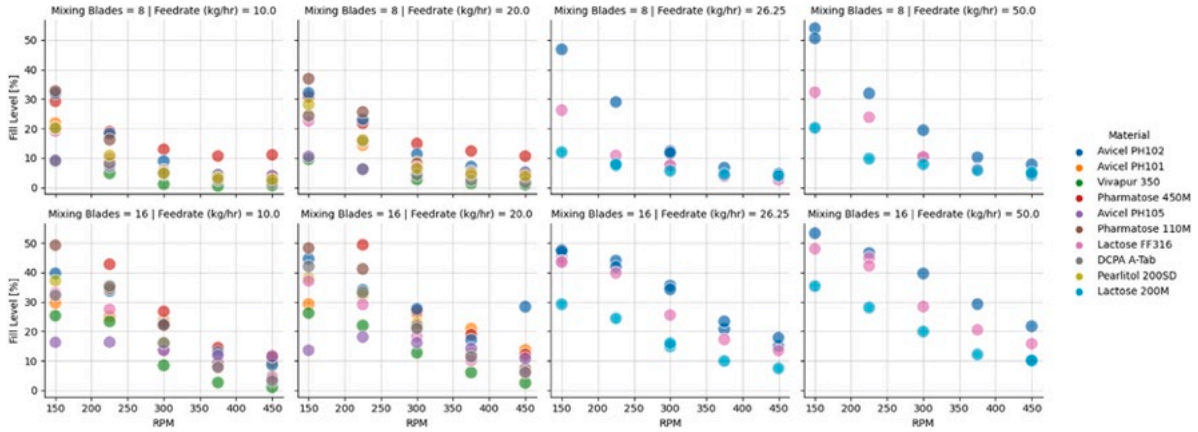


Fig. 11. Scatter graphs showing the fill level response of the materials used for the experiment with respect to the three processing parameters: RPM, Mixing Blades, and Feedrate (kg/h).

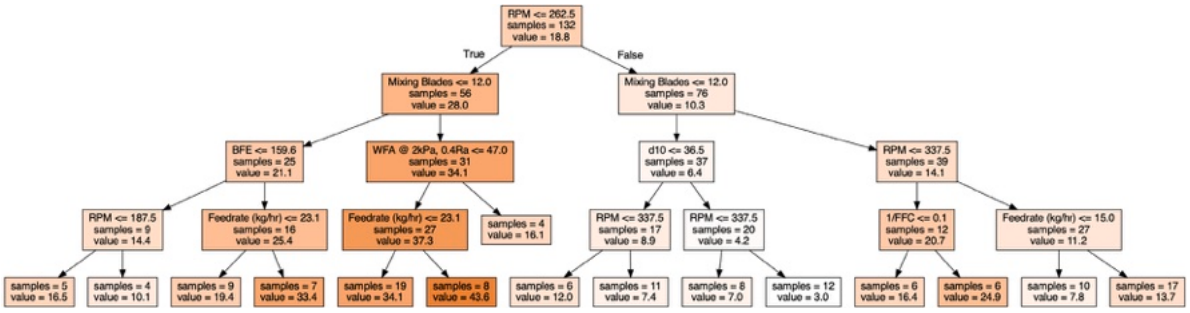


Fig. 12. Decision Tree (35 of 50) from the Random Forest Regression Model, with darker colours indicating high Fill Level. Samples refer to the number of data points, and value is the mean Fill Level for those samples – in percentage (%) – for that node.

5.3. Model: PyTorch ANN feature analysis & contour mapping

The wall friction angle (WFA @ 2 kPa, 0.4 Ra) is shown to be the material characteristic with the greatest feature importance in the model, which holds true for both ANN and RFR models. The practical application of understanding this is formulation adjustment. Different excipients can be paired with the existing blend or powder, in order to modify the final powder characteristic. The result of this allows a quality-by-design approach, as the prediction allows for the understanding of how sensitive a particular property is to processing parameters. This is especially important when building in robustness and early mitigation of risks associated with potential batch-to-batch variation. This operational sensitivity is best shown in Fig. 13, where the two highest-ranking operational parameters have been plotted against the range of WFA values used to train the model. Thus, the sensitivity of the material property can be effectively gauged.

The model shows that the effect of WFA on fill level is, generally, lower at rpms greater than 300 — agreeing with the RFR decision tree (Fig. 12). At these RPMs, the fill level is lower, typically ranging from 6%–20%, which complements the previous discussion point (from the previous section) on collision-based bulk motion/mixing. The mixing blade configuration comes into play by holding up more mass, promoting a higher fill level. This interaction, which promotes more 'frictional' mixing, results in a more complex interaction between the WFA and the discussed process parameters. This is best demonstrated by the change of shape and colour across the three contour plots.

The application of this knowledge in a practical setting suggests that: if there were (for example) a perturbation from the feeder and thus a slight transient change in the formulation's WFA (due to compositional change), this combination of parameters would provide greater confidence that the fill level (and thus the desired process outcome) will be preserved. This methodology and philosophy build in key quality by design aspects to harmonise formulation development and operational robustness.

5.4. Model: M^2E^3D's symbolic regression

While ANNs and random forest regressors can be interrogated to some extent – as has been demonstrated in the preceding sections – they remain, to some extent 'black boxes'. M^2E^3D's methodology (discussed in Section 4.5), meanwhile, produces complete, closed-form equations to describe the behaviours of the systems to which it is applied. For the present data set, the M^2E^3D equation which provided the highest 'score' was the following:

$$\text{Fill Level} = 100 \times \left(0.0032 \times \text{Feed Rate} - 0.003 \times \text{WFA} - 0.0004 \times \text{d10} + \frac{4.284 \times \text{Mixing Blades}}{\text{RPM}} \right) \quad (6)$$

The linear equation can also be viewed as separate terms (seen in (8)), where the following terms can be used as descriptors for their relation to the fill level. Furthermore, these equation terms can be evaluated using an ANOVA. To do this, the M^2E^3D Equation's terms were gathered and fit into an OLS (ordinary least squares) model before assessing the statistical significance of each of the terms.

Table 2
ANOVA Table for the generated M^2E^3D equation (see Eq. (6)) based on the split terms (See Eq. (7) and Eq. (8)), showing the sum squared variance (sum_sq), degrees of freedom (df), F-Statistic (F) and P-Statistic (PR(>F)).

	sum_sq	df	F	PR(>F)
Term1	0.38	1	7.1e+15	0.00e+00
Term2	0.35	1	6.8e+15	0.00e+00
Term3	0.29	1	6.2e+15	0.00e+00
Term4	2.96	1	2.0e+16	0.00e+00
Residual	0.00	249	nan	nan

The ANOVA results can be found in Table 2. Each term was found to have significance in predicting fill level, which was expected as M^2E^3D ensured that every term was significant. However, by assessing the sum squared variance of the prediction based on each term's sensitivity – quantified as the change in the predicted fill level in response to a standardised perturbation, such as a 1% or 10% increase from the mean value of each term – we can determine their relative importance in predicting fill level. The rank order is as follows: $t4 \gg t1 > t2 > t3$. This indicates that the fourth term is responsible for the largest range of variability in the prediction. These findings align with the other modelling (in Sections 5.2 and 5.3) methods as they show RPM and Mixing Blades to be the most important features for predicting.

$$\text{'}Predicted = 100 \times (t1 + t2 + t3 + t4)\text{'} \quad (7)$$

$$\begin{aligned} &W here: \\ &[Predicted] \rightarrow \text{Fill Level} \\ &[t1] \rightarrow (0.0032 \times \text{Feed Rate}) \\ &[t2] \rightarrow (-0.003 \times \text{WFA}) \\ &[t3] \rightarrow (-0.0004 \times \text{d10}) \\ &[t4] \rightarrow \left(\frac{4.284 \times \text{Mixing Blades}}{\text{RPM}} \right) \end{aligned} \quad (8)$$

6. Discussion

6.1. Blind formulation validation and model comparison

The described models (Sections 5.2–5.4) have been developed with the same single excipient data. In this section, we test whether – despite this considerable limitation in their training data – they can accurately predict the behaviours of a full pharmaceutical blend. The same experiments were run using a 4-component blend which served as a surrogate for a real drug formulation — the active compound of the campaigned drug is replaced with powdered paracetamol, ensuring the

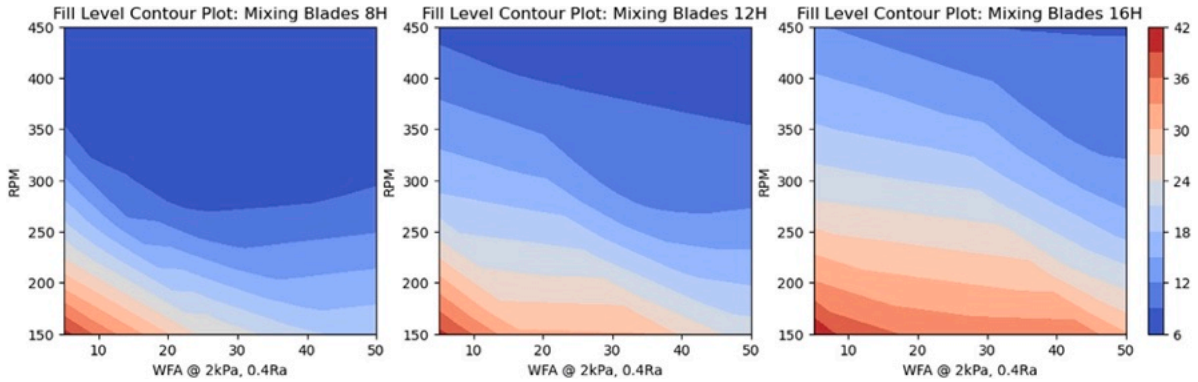


Fig. 13. Fill Level Contour Plot Prediction using the ANN as a function of RPM and WFA. The (shared) colour bar indicates the fill level in percentage for the 3 plots. The held values for the contour plot are as follows: RPM (150–450), MB (8, 12, 16), Feed Rate (22 kg/h), BFE (188 mJ), WFA (5–50), d10 (61 μm), d50 (122 μm), d90 (206 μm), 1/FFC (0.189).

final characteristics of the surrogate blend remain representative of the campaign. The surrogate was validated by ensuring the bulk properties of the surrogate formulation and the true formulation still possessed similar bulk physical characteristics (notably the bulk density and FFC), after the proprietary API was switched out. The bulk characteristic behaviours of this blend were gathered using the same methodology described in Section 3.1, and included in the final row of Table 1.

The experiments measured the fill level of the surrogate formulation at 3 speeds (250, 350, 450 rpm) at 15 kg/h feed rate and 16 mixing blades. The blend's material characteristics were then measured and used to predict the fill level. The results can be seen in Fig. 14. The models were all, to varying degrees of precision, able to predict the fill level of the blend and the variation thereof with RPM. This means that, despite the complexity of a multi-component formulation, there is a correlation between the formulation's characteristics and the resultant fill level. This is an important and potentially exciting finding, as it suggests that the models developed may be used to predict the behaviours of new formulations with no additional training.

The prediction accuracy ranked the model's Mean Absolute Error (MAE) in the following order ANN (1.4), M^2E^3D (3.7), and then RFR (4.6). The contour plots between the ANN and M^2E^3D are similar, displaying similar fills in the same areas. ANN and M^2E^3D differ in terms of linearity, M^2E^3D generally presents a very linear progression of contours — with tighter packing (of boundaries) in the lower corner and wider packing at the maximum. ANN showcases complex shapes and curvature, which has been shown to be advantageous for prediction. RFR, on the other hand, shows almost categorical boundaries. highlighting that despite the granularity of the model, there are some key features which allow for reliable fill level prediction. Ultimately, the following can be said: using each of the predictive methods provides a trade-off between accuracy and conceptual understanding. By using all three tools, however, one can achieve both highly accurate prediction, as well as strong mechanistic insight.

It is finally important to note that data-driven models have the highest predictive accuracy within the bounds of their training data — that is to say, while our models show impressive predictive capabilities within the parameter ranges upon which they were trained, this same level of accuracy cannot be assured outside this parameter space. Nonetheless, as we conduct more experiments, the model can be retrained, and the predictive confidence boundary correspondingly expanded. Furthermore, if the blender used were not fixed in inclination, it could be another processing variable for the training data. Thus making it possible to evaluate the mixing conditions across a wide set of inclinations, improving applicability for other commercial blenders.

6.2. Predicting mixing performance

Strain, determined as the number of blade passes through a given powder (calculated using Eq. (3)) has been demonstrated to be a strong predictor of good mixing in several prior publications (Vanarase and Muzzio, 2011; Portillo et al., 2008; Palmer et al., 2020; Vanarase et al., 2013; Zheng et al., 2022).

Using the validated ANN, we can input a given blend's material properties to calculate the strain from the predicted fill level. The resultant strain values across the range of processing parameters can then be plotted as a set of surface plots in Fig. 15. The detailed landscape describes the interaction between the formulation's properties and the range of processing parameters in the context of mixing performance. The surface plots seen in Fig. 15 are generated for the surrogate formulation (detailed in Table 1). The surface plots are then coloured by the ANN's prediction of the fill level at those same conditions. The fact that the model is able to predict the surrogate accurately (demonstrated in Section 6.1) provides confidence in the surface's shape and position of the colours.

It is immediately interesting to note that, irrespective of processing conditions, the optimum strain seems to consistently be found at or near a fill level of 1/3. The correlation suggests that the material in the blender has reached an idealised balance between the RPM and Mean Residence Time. To speculate on exactly why this occurs; it seems to suggest that the powder is, at this fill level, exhibiting regime-like behaviour which promotes ideal mixing conditions.

To better describe the hypothesis of optimum strain occurring around 1/3 fill level, it is useful to consider similar surrogate systems which show regime-like behaviour. There are two situations that can be conceptually related: rotating drums and fluidised beds.

- **Rotating Drums** utilise a single continuous motion within a batch vessel to mix the granular media within. Thus, when different processing conditions are used, the granular media (e.g. powder) within the drum demonstrate different bulk motion behaviours, which are described as regimes. Increasing the rotating speed of the drum, results in a progressive pulling of the granular media up the side of the drum in the direction of motion, resulting in regimes labelled as (from low to high RPM) rocking, rolling, cascading, cataracting, and centrifuging (to name a few) (Morrison et al., 2016). The transitions between these regimes are known to be affected not only by drum RPM, but also fill level — as is the mixing achieved thereby Arntz et al. (2008). If mixing is intended for the media, motions which cause high levels of granular dispersion (cascading/cataracting) result in improved mixing. In the context of the incline linear blender, the described 1/3 fill level suggests that this fill may be the balance for adequate powder volume for the powder to mix into (increasing MRT, and therefore macro mixing), whilst providing a sufficient mixing rate (RPM).

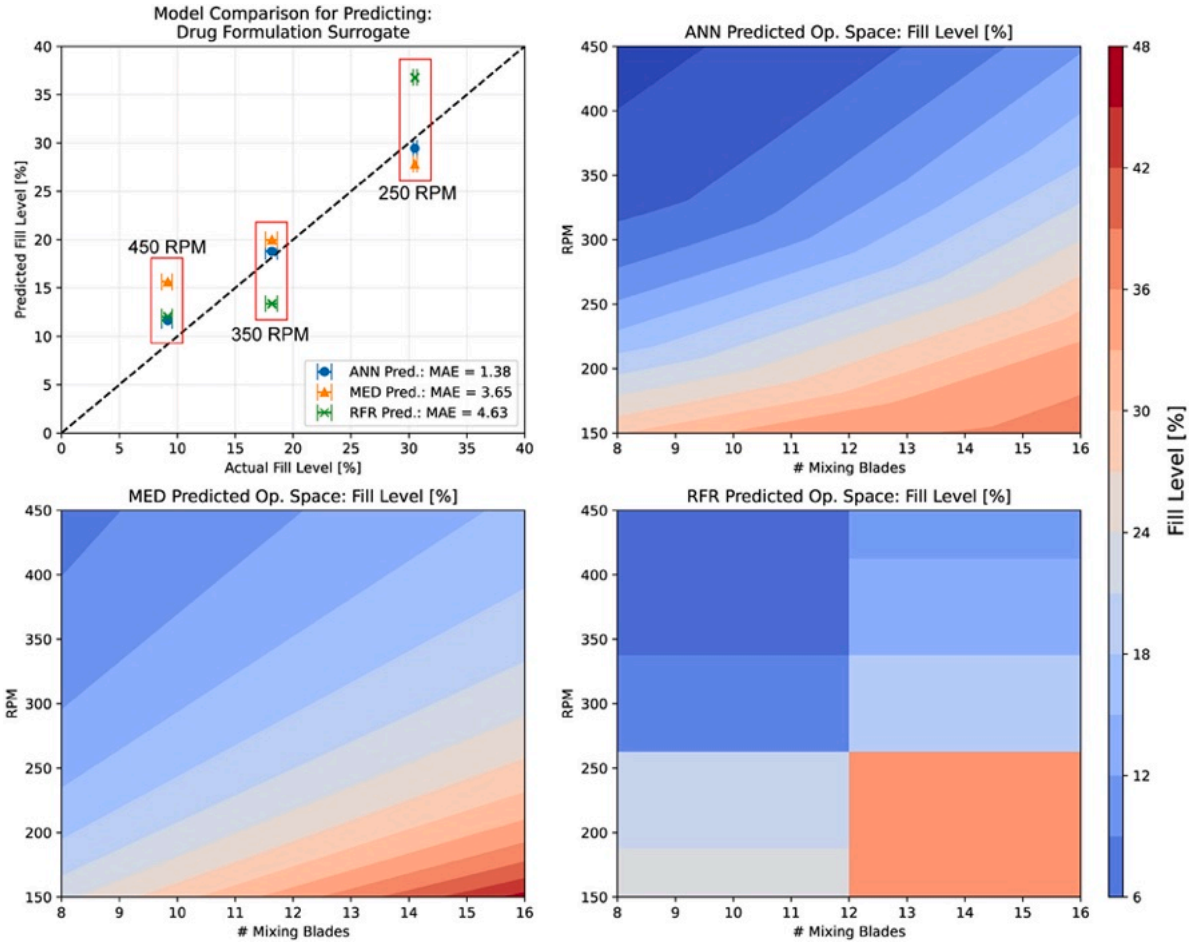


Fig. 14. Parity Plot between the experimental and predicted fill levels. The parity plot shows the three different models predicting the fill level. Each experiment was repeated 3 times, the mean is shown and the bars indicate the range of values (on the *x*-axis). Each model demonstrates the operating space between the RPM and mixing blades. The three models are ranked by the MAE (Mean Absolute Error) prediction of the experiment. Subsequently, an example of the design space showing the two most important processing parameters is plotted for each of the models. The model's contour plots are indicated by the graph's title. Furthermore, all contour graphs share the same colour bar and number of gradient steps (12) between the min and max.

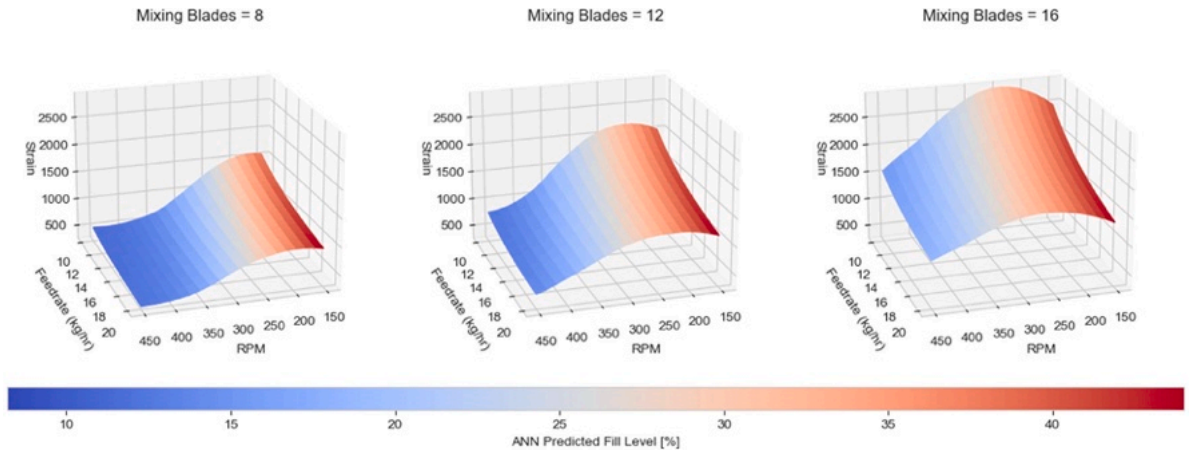


Fig. 15. Surface plots showing the strain by the three processing parameters for the drug surrogate formulation. The continuous parameters (those that can change during operation) share the same plot as the strain. The colour bar indicates the ANN predicted fill level, the three graphs share the same colour scale — allowing comparison.

- **Vibrofluidised Beds** utilise mechanical agitation in the form of vibration to cause an effective reduction in gravity, invoking fluid-like or even gaseous motion of dicrete solid particles (Rosato and Windows-Yule, 2020). To achieve this, a certain amount of agitation (i.e. a suitably high vibration strength) is necessary for the powder bed to reach fluidisation. Similarly, in the context of the inclined linear blender, the rpm agitator also has a mechanical agitation influence. The suggestion for the incline linear blender is that at a suitably high rpm (Froude Number), the motion of the impeller causes the powder to reach this fluidised state, in

which the effects of both gravity and inter-particular cohesion are sufficiently overcome to markedly reduce the resistance to inter-particular mixing.

Thus the hypothesis describes the resulting regimen as a combination of the two situations but in the context of continuous powder blending, where the powder flux receives enough work through agitation, leading to semi-fluidised behaviour. This overcomes the effects of gravity and inter-particulate cohesion of the powder, therefore promoting the local displacement and replacement of powder leading to improved micromixing. When paired with higher 'H' mixing blade configurations (otherwise described as larger mixing zones) there is an increase in axial slippage, which promotes the similarly described re-constitutive behaviour as the cascading regime seen with rotating drums. This, in turn, explains that for a given powder (or formulation), feed rate and blade configuration there is an optimum rpm, at which the powder reaches this regime; which coincides with the blender being 1/3 full. Either side of this apparent optimal fill level leads into contact-dominated mixing (for higher rpms) or friction-dominated mixing (lower rpms) — similar to that outlined by Zheng et al. (2022).

However, to attain this regime at a higher strain value- and therefore improved mixing, blade configuration is key, as it will manage the bulk mass — due to its role of promoting both axial and radial transport. In the context of this study, that would be the 16H configuration (when compared to 8H and 12H), which should, by these standards, supply adequate transport at the base (inlet), improved 'slippage' and radial dispersion in the mixing region, and lastly enough transport at the latter part of the barrel to remove sufficiently blended powder. This is supported further by the 'folding region' seen in the Positron Emission Particle Tracking (PEPT) study of Jones-salkey et al. (2023b) which describes localised spatial residence time retention of powder in the former part of the barrel, just prior to the mixing zone.

While it is possible that this is a specific feature of the helical mixing blade configuration (H) arrangement, the findings implicitly suggest that alternative blade configurations can form different regime-like behaviour. Nevertheless, in this instance, it would be sensible to offer the use of the H-configuration in order to exploit the described feature. It would be interesting to evaluate alternative configurations, like those discussed in Van Snick et al. (2017), to see if they present varied regime-like behaviour; and if not, would the configurations they describe present different processing sensitivities to those regimes?

To expand upon the insights from Fig. 15, let us examine how the proposed theory compares with the broader literature on this subject.

Building on the work of Kushner and Schlack (2014), who explored the scaling of blending powdered lubricant in both bin and tubular batch blenders, they highlighted a parameter K that could scale blending across vessel sizes spanning five orders of magnitude, given a constant Froude number of 0.4. Here, K denotes the 'amount of mixing', which is the product of the 'number of rotations (r)', the 'batch blender's characteristic length scale (L)', and the 'fraction of headspace ($F_{\text{headspace}}$)'.

K can be broken down into two components: 'mixing intensity' ($L \times F_{\text{headspace}}$) and 'mixing duration' (r). Specifically, the characteristic length roughly indicates the mixing region and the headspace gives the powder room to move, facilitating mixing. These combine to show the dispersive potential of each rotation. Meanwhile, the number of rotations conveys the number of times the powder undergoes dispersive rotations. Fortunately, for batch systems, these two components are decoupled, meaning 'mixing intensity' can be compensated by increasing 'mixing duration', and vice versa.

Transitioning this concept from batch to continuous processes leads to the formulation of the strain equation (strain = rpm × mean residence time), where rpm and mean residence time encapsulate the mixing intensity and duration, respectively. In continuous systems, however, since the MRT is a function of RPM (assuming a constant feed rate), one cannot independently adjust intensity and duration, emphasising that a balance is required.

Critical to these discussions is the underlying principle that regardless of scaling in batch or varied continuous setups primarily depends on fostering particle–particle interactions — the real catalyst for mixing. This becomes evident in bulk powder flow regimes, especially visible in granular mixing within rotating drums.

Relevant studies by Van Snick et al. (2017), Palmer et al. (2020), Bekaert et al. (2022a), and Zheng et al. (2022) offer deeper insights. The first three emphasise that maximising strain results in better content uniformity in both horizontal and inclined (15°) linear powder blenders. The latter provides context on regimes.

Interestingly, Bekaert et al. (2022a), using a horizontal mixer, found no interaction between the number of blade passes and blend properties, which contrasts the findings of this study. The interpretation is that the inclination of the blender seems to play a pivotal role in powder transport, which is best illustrated by materials showing different fill levels at the same rpm- see Fig. 11. This highlights the importance of understanding how the material properties interact with the geometrical differences.

Van Snick et al. (2017) indicated that in the same blender used in this study (15° linear blender), accurate and consistent content uniformity was achieved at intermediate residence mass and an intermediate rpm. This finding was reinforced when comparing two different blade configurations under identical conditions.

Moreover, Palmer et al. (2020) demonstrated that after achieving a certain strain, there is only a minimal further increase in blend uniformity, effectively stating that there is an effective 'ideal strain' for a formulation which achieves optimal mixing for a minimal time- and energy-expenditure. Thus, by utilising this tool we can predict the maxima and work back towards this 'effective' strain. Such insights enable researchers to pinpoint the optimal strain for increased processing efficiency whilst ensuring consistent content uniformity. Furthermore, an additional graph shows a V-shaped dip in the Peclet Number (Pe) plotted against fill level, with the lowest point (of this V-shaped dip) at around 1/3 fill level. Pe number is a ratio which indicates a balance between advective and diffusive transport rates; which could be effectively described as a balance of micro-to-macro mixing. A Pe of one, seems to occur at the fill level that provides the highest strain (demonstrated in Fig. 15).

Lastly, Zheng et al. (2022) utilised calibrated DEM simulations to identify two distinct regimes, which transition at an intermediate RPM of 250. This aligns with the first logic gate in the RFR decision tree shown in Fig. 12; whilst it is important to note, the model has similarly outlined this RPM across the ten different excipients and remains comparable to the simulation.

In conclusion, the body of literature, when analysed in tandem with the findings from Fig. 15, and the related discussions provide a comprehensive rationale of the behaviour being exhibited under these conditions. The significance of this should provide both researchers and industry professionals with an initial look into continuous blending regimens.

6.3. Application: Identifying the strain window

One potential practical application of these tools could be to adjust the process to compensate for a large disturbance. For example, APC could be used to reduce the RPM, and therefore increase the MRT, in response to a large disturbance. Following the disturbance, the RPM can be returned back to the steady-state set-point.

Referring to Palmer et al. (2020), the lowest rpm on the APC should match the most suitable point on the exponential decay curve, which could be effectively termed 'Strain Point (ω_P)'. This represents the minimum blade passes needed for desired content uniformity. Given that cohesive species are given an effective shear rate (tip-speed) to sufficiently break particle agglomerates/aggregates. This leads to questions for future research: *"what is the minimum tip speed required for effective blending of cohesive powders"* and *"are two **equal** strain values*

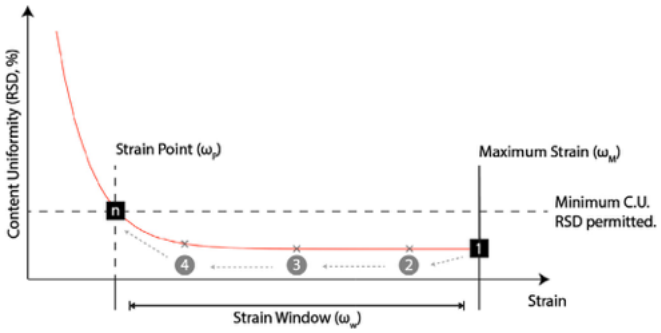


Fig. 16. Graphical Representation of the Strain Window (ω_W). Points 2, 3, and 4, indicate guided experiments to find the Strain Point (ω_P) — or the expansion of the current Strain Window (ω_W).

with different RPMs similar for mixing?" especially concerning values above or below the specific shear requirement for a formulation.

The predictive toolkit highlighted in Figs. 13, 14, and 15 enables the identification of 'Maximum Strain' (ω_M) for specific processing parameters, verifiable through subsequent experimentation. Upon confirming the attainment of minimum shear, our focus shifts to optimising the 'Strain Window' (ω_W), which is the difference between ω_M and ω_P, as depicted in Fig. 16. We can direct our experiments to maintain content uniformity around the ideal RPM, as illustrated by points 2 and 3 in the figure. These experimental points establish a strain window from the lowest acceptable strain value to ω_M. Further exploration, as seen at point 4, could widen this window. For a comprehensive understanding of the process limits, additional guided experimentation, towards point n (ω_P), may be performed to identify the threshold of failure.

It is noteworthy that theoretically, the toolkit could streamline experimentation to just three pivotal points. This top-down approach defines a steady-state set-point and establishes bounds for upper and lower RPM ranges. Similarly, it can assess the impact of other variables like feed rate changes on blend properties.

The deployment of these modelling tools is instrumental in developing robust control strategies, offering a nuanced understanding of the process and its operational parameters up to the point of failure. This outlines a safer operating domain, ensuring the product meets critical quality attributes. The use of these tools allows this understanding to be achieved with reduced experimentation, which is particularly important as extensive large-scale experimentation can slow development as well as impact on cost and sustainability. Furthermore, they can verify the consistency of processes or formulations, valuable for modifications like reformulation or changes to processing set-points. This process similarity can be corroborated through a series of validation trials, affirming the model's accurate prediction of the operational landscape.

7. Conclusion

In this paper, we have developed several machine learning/artificial intelligence models for predicting the performance of a continuous pharmaceutical blender, whilst also facilitating new insight into the fundamental behaviours thereof.

The methods used include RandomForestRegression (RFR), which extracts logic from the data; a novel symbolic regression and evolutionary AI tool (M^2E^3D), which produces complete, closed-form equations, effectively creating a reduced order model of the data; and Artificial Neural Networks (ANN), which provide more accurate predictions at the expense of a less-interpretable model. All three models independently identified the agitator speed (RPM), the number of mixing blades, the wall friction angle (WFA, 2 kPa with 0.4 Ra coupon) and the feed rate (kg/h) as the most important features for the prediction of fill level, and thus the strain experienced by the powder — an important predictor for mixing. By interrogating the models further, we were also able to gain valuable insight into the dynamics and mechanics of the blender explored, through prediction of the operating space.

In terms of pure predictive capability, the ANN demonstrated the greatest strength, both for the single components on which it was trained, as well as in further blind validation, predicting the behaviour of a 4-component formulation to a high degree of accuracy. Its ability to accurately predict the fill level of a previously unseen formulation, containing an API not included in its training data set, shows considerable promise for such an approach, in the future, to be used as a means of reducing the time and cost currently associated with bringing new drugs to market.

It is worth noting that we have discovered an interesting correlation between the maximum strain and 1/3 fill level (during steady state) in the prediction of the operating space. This correlation applies regardless of formulation or variable processing parameters, and it represents a crucial set point for blending processes that use a 15-degree incline blender. By achieving this, 1/3 fill level, set point during operation, a balance between advective and diffusive mixing can be attained. It is of further interest if other fill-level, and thus space–time, optimisations exist for other blending platforms and inclinations.

The magnitude of strain can be increased if the process is intensified — in effect simultaneously increasing both RPM and MRT. Yet, since RPM and MRT are coupled, increasing RPM will decrease MRT. Therefore, it is important to consider both the feed rate and the blade configuration. Decreasing the feed rate will increase MRT while decreasing the number of radial mixing blades will decrease MRT.

Given that maximising throughput is often desired, the blade configuration should be adjusted to include more radial mixing blades to retain higher fill levels (at the same RPM) and the RPM should be increased — thus intensifying the process. Similarly, this resolves the issue for highly agglomerated species, where using a higher RPM provides a higher tip speed, which then acts to break the highly agglomerated species. There may be slight differences between the clinical commercial equipment and the prototype (used in this study), however, the fundamental understanding remains the same. To validate this observation, we performed additional runs using various blade configurations, feed rates, and surrogate formulations (as detailed in Section 2.1). These runs were not included in the model training. However, they have shown that the maximum strain is also consistently observed at a fill level of 1/3. In addition, these findings were checked against a backlog of development runs for other formulations using the GMP-compliant CDC-50 from GEA and saw the same relationship of around a 1/3 fill level delivering the highest strain values.

Ultimately, the predictive tools described in this publication can find this optimum range of processing parameters for a newly characterised formulation and then evaluate both the operational and formulation stability of that formulation within the blender. Said tools thus stand to both mitigate risk and reduce wastage of time, energy and materials during product development through prediction of the variability at these early phases, meaning a directed first-time-right approach to experimentation, validation and process establishment, carrying benefits both economic and environmental.

CRediT authorship contribution statement

O. Jones-Salkey: Writing – review & editing, Writing – original draft, Visualization, Validation, Software, Project administration, Methodology, Investigation, Formal analysis, Data curation, Conceptualization. **C.R.K. Windows-Yule:** Writing – review & editing, Writing – original draft, Supervision, Project administration, Conceptualization. **A. Ingram:** Writing – review & editing, Writing – original draft, Supervision, Resources, Project administration, Conceptualization. **L. Stahler:** Writing – original draft, Methodology, Investigation, Data curation. **A.L. Nicusan:** Writing – review & editing, Writing – original draft, Visualization, Software, Methodology, Formal analysis. **S.**

Clifford: Validation, Supervision, Resources, Project administration, Methodology, Investigation, Conceptualization. **L. Martin de Juan:** Supervision, Project administration, Investigation, Conceptualization. **G.K. Reynolds:** Writing – review & editing, Supervision, Resources, Project administration, Investigation, Funding acquisition.

Declaration of competing interest

The authors declare the following financial interests/personal relationships which may be considered as potential competing interests: Andrew Ingram reports financial support, administrative support, equipment, drugs, or supplies, and writing assistance were provided by AstraZeneca. If there are other authors, they declare that they have no known competing financial interests or personal relationships that could have appeared to influence the work reported in this paper.

Data availability

The authors do not have permission to share data.

Acknowledgements

Experimental work was carried out as part of an Engineering Doctorate programme funded by EPSRC, United Kingdom through the Centre for Doctoral Training in Formulation Engineering (grant no. EP/L015153/1), and from AstraZeneca plc, United Kingdom. The computations described in this paper were performed using the University of Birmingham's BEAR Cloud service, which provides flexible resource for intensive computational work to the University's research community. See http://www.birmingham.ac.uk/bear for more details.

References

Arntz, M., den Otter, W.K., Briels, W.J., Bussmann, P., Beeftink, H., Boom, R., 2008. Granular mixing and segregation in a horizontal rotating drum: a simulation study on the impact of rotational speed and fill level. AIChE J. 54 (12), 3133–3146.

Bekaert, B., Grymonpré, W., Novikova, A., Vervaet, C., Vanhoorne, V., 2022a. Impact of blend properties and process variables on the blending performance. Int. J. Pharm. 613 (September 2021), http://dx.doi.org/10.1016/j.ijpharm.2021.121421.

Bekaert, B., Van Snick, B., Pandelaere, K., Dhondt, J., Di Pretoro, G., De Beer, T., Vervaet, C., Vanhoorne, V., 2022b. Continuous direct compression: Development of an empirical predictive model and challenges regarding PAT implementation. Int. J. Pharm. X 4 (December 2021), 100110. http://dx.doi.org/10.1016/j.ijpx.2021.100110.

Bekaert, B., Van Snick, B., Pandelaere, K., Dhondt, J., Di Pretoro, G., De Beer, T., Vervaet, C., Vanhoorne, V., 2022c. In-depth analysis of the long-term processability of materials during continuous feeding. Int. J. Pharm. 614 (December 2021), 121454. http://dx.doi.org/10.1016/j.ijpharm.2022.121454.

Bezanson, J., Edelman, A., Karpinski, S., Shah, V.B., 2017. Julia: A fresh approach to numerical computing. SIAM Rev. 59 (1), 65–98.

Cranmer, M., Sanchez-Gonzalez, A., Battaglia, P., Xu, R., Cranmer, K., Spergel, D., Ho, S., 2020. Discovering symbolic models from deep learning with inductive biases. In: NeurIPS 2020. arXiv:2006.11287.

Dhondt, J., Bertels, J., Kumar, A., Van Hauwermeiren, D., Ryckaert, A., Van Snick, B., Klingeleers, D., Vervaet, C., De Beer, T., 2022. A multivariate formulation and process development platform for direct compression. Int. J. Pharm. 623 (June), 121962. http://dx.doi.org/10.1016/j.ijpharm.2022.121962.

Engisch, W.E., Muzzio, F.J., 2015. Feedrate deviations caused by hopper refill of loss-in-weight feeders. Powder Technol. 283, 389–400. http://dx.doi.org/10.1016/j.powtec.2015.06.001.

Freeman, R., 2007. Measuring the flow properties of consolidated, conditioned and aerated powders—a comparative study using a powder rheometer and a rotational shear cell. Powder Technol. 174 (1–2), 25–33.

Gao, Y., Ierapetritou, M., Muzzio, F., 2012a. Periodic section modeling of convective continuous powder mixing processes. AIChE J. 58 (1), 69–78. http://dx.doi.org/10.1002/aic.12563, arXiv:0201037v1, http://doi.wiley.com/10.1002/aic.12563, https://onlinelibrary.wiley.com/doi/10.1002/aic.12563.

Gao, Y., Muzzio, F.J., Ierapetritou, M.G., 2012b. Optimizing continuous powder mixing processes using periodic section modeling. Chem. Eng. Sci. 80, 70–80. http://dx.doi.org/10.1016/j.ces.2012.05.037, URL https://www.sciencedirect.com/science/article/pii/S0009250912003181?casa_token=ekRMR8ElnJ4AAAAA:8ju5z1WMyR3MIO9ry04pJwNXZfq3L-kUGr-Fa7ns3R-YNT9dWj6RiZYo6YCaRAoIIssTEKIr_PM.

Gao, Y., Vanarase, A., Muzzio, F., Ierapetritou, M., 2011. Characterizing continuous powder mixing using residence time distribution. Chem. Eng. Sci. 66 (3), 417–425. http://dx.doi.org/10.1016/j.ces.2010.10.045.

Goodfellow, I., Bengio, Y., Courville, A., 2016. Deep Learning. MIT Press, http://www.deeplearningbook.org.

Hare, C., Zafar, U., Ghadiri, M., Freeman, T., Clayton, J., Murtagh, M., 2015. Analysis of the dynamics of the FT4 powder rheometer. Powder Technol. 285, 123–127.

Holman, J., Tantuccio, A., Palmer, J., van Doninck, T., Meyer, R., 2021. A very boring 120 h: 15 million tablets under a continuous state of control. Powder Technol. 382, 208–231. http://dx.doi.org/10.1016/j.powtec.2020.12.073, URL https://linkinghub.elsevier.com/retrieve/pii/S003259102031250X.

Hurley, S., Tantuccio, A., Escotet-espinoza, M.S., Flamm, M., Metzger, M., 2022. Development and use of a residence time distribution (RTD) model control strategy for a continuous manufacturing drug product pharmaceutical process. Pharmaceutics 14 (2), http://dx.doi.org/10.3390/pharmaceutics14020355.

Jones-salkey, O., Chu, Z., Ingram, A., Windows-yule, C.R.K., 2023a. Reviewing the Impact of Powder Cohesion on Continuous Direct Compression (CDC) Performance, No. Cdc. pp. 1–48.

Jones-salkey, O., Nicusan, A.L., Windows-yule, C.R.K., Ingram, A., Werner, D., 2023b. Application of Positron Emission Particle Tracking (PEPT) for the evaluation of powder behaviour in an incline linear blender for Continuous Direct Compression (CDC). Int. J. Pharm. 645 (May), 123361. http://dx.doi.org/10.1016/j.ijpharm.2023.123361.

Kushner, J., Schlack, H., 2014. Commercial scale validation of a process scale-up model for lubricant blending of pharmaceutical powders. Int. J. Pharm. 475 (1–2), 147–155. http://dx.doi.org/10.1016/j.ijpharm.2014.08.036.

Lundberg, S.M., Lee, S.-I., 2017. A unified approach to interpreting model predictions. In: Advances in Neural Information Processing Systems. pp. 4765–4774.

Megarry, A.J., Swainson, S.M., Roberts, R.J., Reynolds, G.K., 2019. A big data approach to pharmaceutical flow properties. Int. J. Pharm. 555 (October 2018), 337–345. http://dx.doi.org/10.1016/j.ijpharm.2018.11.059.

Morrison, A.J., Govender, I., Mainza, A.N., Parker, D.J., 2016. The shape and behaviour of a granular bed in a rotating drum using Eulerian flow fields obtained from PEPT. Chem. Eng. Sci. 152, 186–198. http://dx.doi.org/10.1016/j.ces.2016.06.022.

Nicusan, A.-L., Windows-Yule, K., 2022a. PyMED: Multiphase Materials Exploration via Evolutionary Equation Discovery. Zenodo, http://dx.doi.org/10.5281/zenodo.7215239.

Nicusan, A.-L., Windows-Yule, K., 2022b. M2E3D: Multiphase Materials Exploration via Evolutionary Equation Discovery.

Palmer, J., Reynolds, G.K., Tahir, F., Yadav, I.K., Meehan, E., Holman, J., Bajwa, G., 2020. Mapping key process parameters to the performance of a continuous dry powder blender in a continuous direct compression system. Powder Technol. 362, 659–670. http://dx.doi.org/10.1016/j.powtec.2019.12.028.

Portillo, P.M., Ierapetritou, M.G., Muzzio, F.J., 2008. Characterization of continuous convective powder mixing processes. Powder Technol. 182 (3), 368–378. http://dx.doi.org/10.1016/j.powtec.2007.06.024, URL https://www.sciencedirect.com/science/article/pii/S0032591007003142?pes=vor&entityID=https%3A%2F%2Fidp.bham.ac.uk%2Fshibboleth#fig1.

Portillo, P.M., Muzzio, F.J., Ierapetritou, M.G., 2007. Hybrid DEM-compartment modeling approach for granular mixing. AIChE J. 53 (1), 119–128. http://dx.doi.org/10.1002/aic.11054, arXiv:0201037v1, URL http://doi.wiley.com/10.1002/aic.11054.

Portillo, P.M., Vanarase, A.U., Ingram, A., Seville, J.K., Ierapetritou, M.G., Muzzio, F.J., 2010. Investigation of the effect of impeller rotation rate, powder flow rate, and cohesion on powder flow behavior in a continuous blender using PEPT. Chem. Eng. Sci. 65 (21), 5658–5668. http://dx.doi.org/10.1016/j.ces.2010.06.036.

Rosato, A., Windows-Yule, K., 2020. Influence of key parameters. Segregation in Vibrated Granular Systems. Academic Press, pp. 197–218. http://dx.doi.org/10.1016/b978-0-12-814199-1.00018-4, URL https://www.sciencedirect.com/book/9780128141991/segregation-in-vibrated-granular-systems#book-description.

Sarkar, A., Wassgren, C.R., 2009. Simulation of a continuous granular mixer: Effect of operating conditions on flow and mixing. Chem. Eng. Sci. 64 (11), 2672–2682. http://dx.doi.org/10.1016/j.ces.2009.02.011, URL https://www.sciencedirect.com/science/article/pii/S0009250909001080.

Sarkar, A., Wassgren, C., 2010. Continuous blending of cohesive granular material. Chem. Eng. Sci. 65 (21), 5687–5698. http://dx.doi.org/10.1016/j.ces.2010.04.011.

Schulze, D., Schulze, D., 2021. Flow properties of bulk solids. In: Powders and Bulk Solids: Behavior, Characterization, Storage and Flow. Springer, pp. 57–100.

Schwedes, J., Schulze, D., 1990. Measurement of flow properties of bulk solids. Powder Technol. 61 (1), 59–68.

Toson, P., Siegmann, E., Trogrlic, M., Kureck, H., Khinast, J., Jajcevic, D., Doshi, P., Blackwood, D., Bonnassieux, A., Daugherity, P.D., am Ende, M.T., 2018. Detailed modeling and process design of an advanced continuous powder mixer. Int. J. Pharm. 552 (1–2), 288–300. http://dx.doi.org/10.1016/j.ijpharm.2018.09.032, URL https://www.sciencedirect.com/science/article/pii/S0378517318306835?via%3Dihub.

Van Snick, B., Holman, J., Vanhoorne, V., Kumar, A., De Beer, T., Remon, J.P., Vervaet, C., 2017. Development of a continuous direct compression platform for low-dose drug products. Int. J. Pharm. 529 (1–2), 329–346. http://dx.doi.org/10.1016/j.ijpharm.2017.07.003, URL http://www.sciencedirect.com/science/article/pii/S0378517317306026, https://linkinghub.elsevier.com/retrieve/pii/S0378517317306026.

Vanarase, A.U., Muzzio, F.J., 2011. Effect of operating conditions and design parameters in a continuous powder mixer. Powder Technol. 208 (1), 26–36. http://dx.doi.org/10.1016/j.powtec.2010.11.038.

Vanarase, A.U., Osorio, J.G., Muzzio, F.J., 2013. Effects of powder flow properties and shear environment on the performance of continuous mixing of pharmaceutical powders. Powder Technol. 246, 63–72. http://dx.doi.org/10.1016/j.powtec.2013.05.002.

Zheng, C., Li, L., Nitert, B.J., Govender, N., Chamberlain, T., Zhang, L., Wu, C.Y., 2022. Investigation of granular dynamics in a continuous blender using the GPU-enhanced discrete element method. Powder Technol. 412 (July), 117968. http://dx.doi.org/10.1016/j.powtec.2022.117968.

References

1. Ghosh TK and Roy J. Tablet and Capsule Machine Instrumentation. CRC Press, 2012
2. Lieberman HA, Lachman L, and Schwartz JB. Pharmaceutical Dosage Forms - Tablets. 1989; 1
3. Banker GS and Rhodes CT. Modern Pharmaceutics. Marcel Dekker Inc., 2002
4. Allen Jr. LV and Ansel HC. Ansel's Pharmaceutical Dosage Forms and Drug Delivery Systems. 10th. Lippincott Williams & Wilkins, 2014
5. Shargel L and Yu AB. Applied Biopharmaceutics & Pharmacokinetics. 7th. McGraw-Hill Education, 2015
6. Voigt R. Pharmaceutical Technology: Tabletting Technology. Thieme, 2012
7. Sharma D et al. Orally Disintegrating Tablets: Formulation, Preparation Techniques, and Evaluation. Journal of Applied Pharmaceutical Science 2013
8. Khan D, Kirby D, Bryson S, Shah M, and Rahman Mohammed A. Paediatric specific dosage forms: Patient and formulation considerations. International Journal of Pharmaceutics 2022; 616:121501. DOI: 10.1016/j.ijpharm.2022.121501. Available from: https://doi.org/10.1016/j.ijpharm.2022.121501
9. Norman J et al. Emerging Trends in Oral Drug Delivery: A Review. International Journal of Pharmaceutical Sciences and Research 2017

10. Gibson SC. Pharmaceutical Manufacturing Handbook: Production and Processes. John Wiley & Sons, 2009

11. Nasr MM. Quality by design: A new framework for the development and manufacturing of medicines. Pharmaceutical Engineering 2011; 31:42–50

12. Plumb K. Continuous processing in the pharmaceutical industry: changing the mind set. Chemical Engineering Research and Design 2005; 83:730–8

13. Juran J. M. Juran on quality by design: the new steps for planning quality into goods and services. Simon and Schuster, 1992

14. Sangshetti JN, Deshpande M, Zaheer Z, Shinde DB, and Arote R. Quality by design approach: Regulatory need. Arabian Journal of Chemistry 2017; 10:S3412–S3425. DOI: 10.1016/j.arabjc.2014.01.025. Available from: http://dx.doi.org/10.1016/j.arabjc.2014.01.025

15. Yu LX, Amidon G, Khan MA, Hoag SW, Polli J, Raju GK, and Woodcock J. Understanding pharmaceutical quality by design. eng. AAPS Journal 2014 Jul; 16:771–83. DOI: 10.1208/s12248-014-9598-3. Available from: https://pubmed.ncbi.nlm.nih.gov/24854893%20https://www.ncbi.nlm.nih.gov/pmc/articles/PMC4070262/

16. Vogt FG and Kord AS. Development of quality-by-design analytical methods. Journal of pharmaceutical sciences 2011; 100:797–812

17. Zhang L and Mao S. Application of quality by design in the current drug development. Asian journal of pharmaceutical sciences 2017; 12:1–8

18. Lee SL et al. Modernizing Pharmaceutical Manufacturing: from Batch to Continuous Production. Journal of Pharmaceutical Innovation 2015

19. Wahlich J. Review: Continuous manufacturing of small molecule solid oral dosage forms. Pharmaceutics 2021; 13. DOI: 10.3390/pharmaceutics13081311

20. Plumb K. Continuous Processing in Pharmaceutical Manufacturing. Wiley, 2015

21. Desai PM, Vaerenbergh GV, Holman J, Liew CV, and Heng PWS. Continuous manufacturing: the future in pharmaceutical solid dosage form manufacturing. Pharmaceutical Bioprocessing 2015 Sep; 3:357–60. DOI: 10.4155/pbp.15.19

22. Ierapetritou M, Muzzio F, and Reklaitis G. Perspectives on the continuous manufacturing of powder-based pharmaceutical processes. 2016

23. Huang Z, Scicolone JV, Gurumuthy L, and Davé RN. Flow and bulk density enhancements of pharmaceutical powders using a conical screen mill: A continuous dry coating device. Chemical Engineering Science 2015; 125:209–24. DOI: 10.1016/j.ces.2014.05.038. Available from: http://dx.doi.org/10.1016/j.ces.2014.05.038

24. Vanarase AU, Osorio JG, and Muzzio FJ. Effects of powder flow properties and shear environment on the performance of continuous mixing of pharmaceutical powders. Powder Technology 2013 Sep; 246:63–72. DOI: 10.1016/j.powtec.2013.05.002

25. Jones-salkey O, Chu Z, Ingram A, and Windows-yule CRK. Reviewing the Impact of Powder Cohesion on Continuous Direct Compression (CDC) Performance. 2023 :1–48

26. Kehlenbeck V and Sommer K. Possibilities to improve the short-term dosing constancy of volumetric feeders. Powder Technology 2003; 138:51–6. DOI: 10.1016/j.powtec.2003.08.040

27. Escotet-Espinoza MS. Phenomenological and residence time distribution models for unit operations in a continuous pharmaceutical manufacturing process. 2018 :312

28. Engisch WE and Muzzio FJ. Method for characterization of loss-in-weight feeder equipment. Powder Technology 2012; 228:395–403. DOI: 10.1016/j.powtec.2012.05.058. Available from: http://dx.doi.org/10.1016/j.powtec.2012.05.058

29. Engisch WE and Muzzio FJ. Loss-in-Weight Feeding Trials Case Study: Pharmaceutical Formulation. Journal of Pharmaceutical Innovation 2015; 10:56–75. DOI: 10.1007/s12247-014-9206-1

30. Engisch WE and Muzzio FJ. Feedrate deviations caused by hopper refill of loss-in-weight feeders. Powder Technology 2015; 283:389–400. DOI: 10.1016/j.powtec.2015.06.001. Available from: http://dx.doi.org/10.1016/j.powtec.2015.06.001

31. Bekaert B, Van Snick B, Pandelaere K, Dhondt J, Di Pretoro G, De Beer T, Vervaet C, and Vanhoorne V. In-depth analysis of the long-term processability of materials during continuous feeding. International Journal of Pharmaceutics 2022; 614:121454. DOI: 10.1016/j.ijpharm.2022.121454. Available from: https://doi.org/10.1016/j.ijpharm.2022.121454

32. Van Snick B, Holman J, Vanhoorne V, Kumar A, De Beer T, Remon JP, and Vervaet C. Development of a continuous direct compression platform for low-dose drug products. International Journal of Pharmaceutics 2017 Aug; 529:329–46. DOI: 10.1016/j.ijpharm.2017.07.003. Available from: http://www.sciencedirect.com/science/article/pii/S0378517317306026%20https://linkinghub.elsevier.com/retrieve/pii/S0378517317306026

33. Simonaho SP, Ketolainen J, Ervasti T, Toiviainen M, and Korhonen O. Continuous manufacturing of tablets with PROMIS-line - Introduction and case studies from continuous feeding, blending and tableting. European Journal of Pharmaceutical Sciences 2016; 90:38–46. DOI: 10.1016/j.ejps.2016.02.006. Available from: http://dx.doi.org/10.1016/j.ejps.2016.02.006

34. García-Muñoz S, Butterbaugh A, Leavesley I, Manley LF, Slade D, and Bermingham S. A flowsheet model for the development of a continuous process for pharmaceutical tablets: An industrial perspective. AIChE Journal 2018 Feb; 64:511–25. DOI: 10.1002/aic.15967. Available from: https://onlinelibrary.wiley.com/doi/10.1002/aic.15967

35. Gyürkés M, Madarász L, Köte Á, Domokos A, Mészáros D, Beke K, Nagy B, Marosi G, Pataki H, Nagy ZK, et al. Process design of continuous powder blending using residence time distribution and feeding models. Pharmaceutics 2020; 12:1119. DOI: 10.3390/pharmaceutics12111119. Available from: https://doi.org/10.3390/pharmaceutics12111119

36. Beretta M, Hörmann TR, Hainz P, Hsiao WK, and Paudel A. Investigation into powder tribo-charging of pharmaceuticals. Part I: Process-induced charge via twin-screw feeding. International Journal of Pharmaceutics 2020; 591. DOI: 10.1016/j.ijpharm.2020.120014

37. Beretta M, Hörmann TR, Hainz P, Hsiao WK, and Paudel A. Investigation into powder tribo–charging of pharmaceuticals. Part II: Sensitivity to relative humidity. International Journal of Pharmaceutics 2020; 591. DOI: 10.1016/j.ijpharm.2020.120015

38. Prescott JK and Barnum RA. On powder flowability. Pharmaceutical technology 2000; 24:60–0

39. Rhodes MJ. Introduction to particle technology. John Wiley & Sons, 2008

40. Windows-Yule K, Nicuşan L, Herald MT, Manger S, and Parker D. Comparison with other techniques. *Positron Emission Particle Tracking: A comprehensive guide*. IOP Publishing, 2022

41. Windows-Yule CR and Neveu A. Calibration of DEM simulations for dynamic particulate systems. Papers in Physics 2022; 14:1–13. DOI: 10.4279/pip.140010

42. Leung LY, Mao C, Srivastava I, Du P, and Yang CY. Flow Function of Pharmaceutical Powders Is Predominantly Governed by Cohesion, Not by Friction Coefficients. Journal of Pharmaceutical Sciences 2017; 106:1865–73. DOI: 10.1016/j.xphs.2017.04.012. Available from: http://dx.doi.org/10.1016/j.xphs.2017.04.012

43. Thornton C. Granular Dynamics, Contact Mechanics and Particle System Simulations: A DEM study. Vol. 24. 2015 :1–195. DOI: 10.1007/978-3-319-18711-2

44. Kojima T and Elliott JA. Effect of silica nanoparticles on the bulk flow properties of fine cohesive powders. Chemical Engineering Science 2013; 101:315–28. DOI: 10.1016/j.ces.2013.06.056. Available from: http://dx.doi.org/10.1016/j.ces.2013.06.056

45. Meyer K and Zimmermann I. Effect of glidants in binary powder mixtures. Powder Technology 2004; 139:40–54. DOI: 10.1016/j.powtec.2003.09.007

46. Escotet-Espinoza MS, Scicolone JV, Moghtadernejad S, Sanchez E, Cappuyns P, Van Assche I, Di Pretoro G, Ierapetritou M, and Muzzio FJ. Improving Feedability of Highly Adhesive Active Pharmaceutical Ingredients by Silication. Journal of Pharmaceutical Innovation 2021; 16:279–92. DOI: 10.1007/s12247-020-09448-y

47. Tran DT, Majerová D, Veselý M, Kulaviak L, Ruzicka MC, and Zámostný P. On the mechanism of colloidal silica action to improve flow properties of pharmaceutical excipients. International Journal of Pharmaceutics 2019; 556:383–94. DOI: 10.1016/j.ijpharm.2018.11.066. Available from: https://doi.org/10.1016/j.ijpharm.2018.11.066

48. López A, Vivacqua V, Hammond R, and Ghadiri M. Analysis of screw feeding of faceted particles by discrete element method. Powder Technology 2020; 367:474–86. DOI: 10.1016/j.powtec.2020.03.064. Available from: https://doi.org/10.1016/j.powtec.2020.03.064

49. Krantz M, Zhang H, and Zhu J. Characterization of powder flow: Static and dynamic testing. Powder Technology 2009; 194:239–45. DOI: 10.1016/j.powtec.2009.05.001. Available from: http://dx.doi.org/10.1016/j.powtec.2009.05.001

50. Lumay G, Pillitteri S, Marck M, Monsuur F, Pauly T, Ribeyre Q, Francqui F, and Vandewalle N. Influence of mesoporous silica on powder flow and electrostatic proper-

ties on short and long term. Journal of Drug Delivery Science and Technology 2019; 53:1–7. DOI: 10.1016/j.jddst.2019.101192

51. Neveu A, Francqui F, and Lumay G. Measuring powder flow properties in a rotating drum. Measurement 2022; 200:111548

52. Patel D, Francqui F, Defrêne RJL, and Neveu A. Influence of additives on the electrostatic charge build-up of excipients. Powder Technology 2003; 132:192–8. DOI: 10.1016/S0032-5910(03)00077-1

53. Ramirez-Dorronsoro JC, Jacko RB, and Kildsig DO. Chargeability measurements of selected pharmaceutical dry powders to assess their electrostatic charge control capabilities. AAPS PharmSciTech 2006; 7:1–8. DOI: 10.1208/pt0704103

54. Escotet-Espinoza MS, Moghtadernejad S, Oka S, Wang Z, Wang Y, Roman-Ospino A, Schäfer E, Cappuyns P, Van Assche I, Futran M, Muzzio F, and Ierapetritou M. Effect of material properties on the residence time distribution (RTD) characterization of powder blending unit operations. Part II of II: Application of models. Powder Technology 2019; 344:525–44. DOI: 10.1016/j.powtec.2018.12.051. Available from: https://doi.org/10.1016/j.powtec.2018.12.051

55. Escotet-Espinoza MS, Moghtadernejad S, Scicolone J, Wang Y, Pereira G, Schäfer E, Vigh T, Klingeleers D, Ierapetritou M, and Muzzio FJ. Using a material property library to find surrogate materials for pharmaceutical process development. Powder Technology 2018; 339:659–76. DOI: 10.1016/j.powtec.2018.08.042. Available from: https://doi.org/10.1016/j.powtec.2018.08.042

56. Shier AP, Kumar A, Mercer A, Majeed N, Doshi P, Blackwood DO, and Verrier HM. Development of a predictive model for gravimetric powder feeding from an API-rich materials properties library. International Journal of Pharmaceutics 2022; 625:122071. DOI: 10.1016/j.ijpharm.2022.122071. Available from: https://doi.org/10.1016/j.ijpharm.2022.122071

57. Yadav IK, Holman J, Meehan E, Tahir F, Khoo J, Taylor J, Benedetti A, Aderinto O, and Bajwa G. Influence of material properties and equipment configuration on loss-in- weight feeder performance for drug product continuous manufacture. Powder Technology 2019; 348:126–37. DOI: 10.1016/j.powtec.2019.01.071. Available from: https://doi.org/10.1016/j.powtec.2019.01.071

58. Gamble JF, Akseli I, Ferreira AP, Leane M, Thomas S, Tobyn M, and Wadams RC. Morphological distribution mapping: Utilisation of modelling to integrate particle size and shape distributions. International Journal of Pharmaceutics 2023; 635:122743. DOI: 10.1016/j.ijpharm.2023.122743

59. Pereira Diaz L, Brown CJ, Ojo E, Mustoe C, and Florence AJ. Machine learning approaches to the prediction of powder flow behaviour of pharmaceutical materials from physical properties. Digital Discovery 2023; 2:692–701. DOI: 10.1039/D2DD00106C

60. Owasit A, Tripathi S, Davé R, and Young J. Predicting Powder Blend Flowability from Individual Constituent Properties Using Machine Learning. Pharmaceutical Research 2025; 42:665–83. DOI: 10.1007/s11095-025-03855-x

61. Jones-Salkey O, Windows-Yule C, Ingram A, Stahler L, Nicusan A, Clifford S, Juan LM de, and Reynolds G. Using AI/ML to predict blending performance and process sensitivity for Continuous Direct Compression (CDC). International Journal of Pharmaceutics 2024; 651:123796

62. Shi G, Lin L, Liu Y, Chen G, Luo Y, Wu Y, and Li H. Pharmaceutical Application of Multivariate Modelling Techniques: A Review on the Manufacturing of Tablets. RSC Advances 2021; 11:8323–45. DOI: 10.1039/d0ra08030f. Available from: https://pubs.rsc.org/en/content/articlelanding/2021/ra/d0ra08030f

63. Breiman L. Random forests. Machine learning 2001; 45:5–32

64. Goodfellow I, Bengio Y, and Courville A. Deep Learning. http://www.deeplearningbook.org. MIT Press, 2016

65. Schmidt M and Lipson H. Distilling Free-Form Natural Laws from Experimental Data. Science 2009; 324:81–5. DOI: 10.1126/science.1165893

66. Angelis D, Sofos F, and Karakasidis TE. Artificial intelligence in physical sciences: Symbolic regression trends and perspectives. Archives of Computational Methods in Engineering 2023 :1

67. De Souter L, Waeytens R, Van Hauwermeiren D, Grymonpré W, Bekaert B, Nopens I, and De Beer T. Elucidation of the powder flow pattern in a twin-screw LIW-feeder for various refill regimes. International Journal of Pharmaceutics 2023; 631. DOI: 10.1016/j.ijpharm.2022.122534

68. Muzikova J, Louzenska M, and Pekarek T. A STUDY OF COMPRESSION PROCESS AND PROPERTIES OF TABLETS WITH MICROCRYSTALLINE CELLULOSE AND COLLOIDAL SILICON DIOXIDE. Acta Poloniae Pharmaceutica 2016; 73:1259–65

69. Apeji YE and Olowosulu AK. Quantifying the effect of glidant on the compaction and tableting properties of paracetamol granules. J Res Pharm 2020; 24:1–12

70. Uzunović A and Vranić E. Effect of magnesium stearate concentration on dissolution properties of ranitidine hydrochloride coated tablets. Bosnian journal of basic medical sciences / Udruženje basičnih mediciniskih znanosti = Association of Basic Medical Sciences 2007; 7:279–83. DOI: 10.17305/bjbms.2007.3060

71. Bolhuis GK and Armstrong NA. Excipients for direct compaction - An update. Pharmaceutical Development and Technology 2006 Jan; 11:111–24. DOI: 10.1080/10837450500464255. Available from: http://www.tandfonline.com/doi/full/10.1080/10837450500464255

72. Bridgwater J. Fundamental powder mixing mechanisms. Powder Technology 1976; 15:215–36. DOI: 10.1016/0032-5910(76)80051-4

73. Cooke MH, Stephens DJ, and Bridgwater J. Powder mixing - a literature survey. Powder Technology 1976; 15:1–20. DOI: 10.1016/0032-5910(76)80025-3

74. Laurent BF and Bridgwater J. Influence of agitator design on powder flow. Chemical Engineering Science 2002 Sep; 57:3781–93. DOI: 10.1016/S0009-2509(02)00317-2. Available from: https://www.sciencedirect.com/science/article/pii/S0009250902003172

75. Van Snick B, Grymonpré W, Dhondt J, Pandelaere K, Di Pretoro G, Remon JP, De Beer T, Vervaet C, and Vanhoorne V. Impact of blend properties on die filling during tableting. International Journal of Pharmaceutics 2018; 549:476–88. DOI: 10.1016/j.ijpharm.2018.08.015. Available from: https://doi.org/10.1016/j.ijpharm.2018.08.015

76. Palmer J, Reynolds GK, Tahir F, Yadav IK, Meehan E, Holman J, and Bajwa G. Mapping key process parameters to the performance of a continuous dry powder blender in a continuous direct compression system. Powder Technology 2020 Feb; 362:659–70. DOI: 10.1016/j.powtec.2019.12.028

77. Venables HJ and Wells JI. Powder mixing. Drug Development and Industrial Pharmacy 2001; 27:599–612. DOI: 10.1081/DDC-100107316

78. Asachi M, Nourafkan E, and Hassanpour A. A review of current techniques for the evaluation of powder mixing. Advanced Powder Technology 2018; 29:1525–49. DOI: 10.1016/j.apt.2018.03.031. Available from: https://doi.org/10.1016/j.apt.2018.03.031

79. Portillo PM, Vanarase AU, Ingram A, Seville JK, Ierapetritou MG, and Muzzio FJ. Investigation of the effect of impeller rotation rate, powder flow rate, and cohesion on powder flow behavior in a continuous blender using PEPT. Chemical Engineering Science 2010; 65:5658–68. DOI: 10.1016/j.ces.2010.06.036

80. Poux M, Fayolle P, Bertrand J, Bridoux D, and Bousquet J. Powder mixing: Some practical rules applied to agitated systems. Powder Technology 1991; 68:213–34. DOI: 10.1016/0032-5910(91)80047-M

81. Sebastian Escotet-Espinoza M, Moghtadernejad S, Oka S, Wang Y, Roman-Ospino A, Schäfer E, Cappuyns P, Van Assche I, Futran M, Ierapetritou M, and Muzzio F. Effect of tracer material properties on the residence time distribution (RTD) of continuous powder blending operations. Part I of II: Experimental evaluation. Powder Technology 2019 Jan; 342:744–63. DOI: 10.1016/j.powtec.2018.10.040

82. Gao Y, Vanarase A, Muzzio F, and Ierapetritou M. Characterizing continuous powder mixing using residence time distribution. Chemical Engineering Science 2011 Feb; 66:417–25. DOI: 10.1016/j.ces.2010.10.045

83. Vanarase AU and Muzzio FJ. Effect of operating conditions and design parameters in a continuous powder mixer. Powder Technology 2011; 208:26–36. DOI: 10.1016/j.powtec.2010.11.038. Available from: http://dx.doi.org/10.1016/j.powtec.2010.11.038

84. Fan LT, Chen Ym, and Lai FS. Recent developments in solids mixing. Powder Technology 1990 Jun; 61:255–87. DOI: 10.1016/0032-5910(90)80092-D. Available from: https://www.sciencedirect.com/science/article/pii/003259109080092D

85. Rosato AD and Windows-Yule C. Segregation in vibrated granular systems. Academic Press, 2020 :197–218

86. Rennie PR, Chen XD, Hargreaves C, and MacKereth AR. Study of the cohesion of dairy powders. Journal of Food Engineering 1999; 39:277–84. DOI: 10.1016/S0260-8774(98)00158-7

87. De Villiers MM. Description of the kinetics of the deagglomeration of drug particle agglomerates during powder mixing. International Journal of Pharmaceutics 1997; 151:1–6. DOI: 10.1016/S0378-5173(97)04893-X

88. Mehrotra A, Muzzio FJ, and Shinbrot T. Spontaneous separation of charged grains. Physical Review Letters 2007; 99:1–4. DOI: 10.1103/PhysRevLett.99.058001

89. Mazumder MK, Sims RA, Biris AS, Srirama PK, Saini D, Yurteri CU, Trigwell S, De S, and Sharma R. Twenty-first century research needs in electrostatic processes applied to industry and medicine. Chemical Engineering Science 2006 Apr; 61:2192–211. DOI: 10.1016/j.ces.2005.05.002. Available from: https://linkinghub.elsevier.com/retrieve/pii/S0009250905003878

90. Bekaert B, Grymonpré W, Novikova A, Vervaet C, and Vanhoorne V. Impact of blend properties and process variables on the blending performance. International Journal of Pharmaceutics 2022; 613. DOI: 10.1016/j.ijpharm.2021.121421

91. Gao Y, Ierapetritou M, and Muzzio F. Periodic section modeling of convective continuous powder mixing processes. AIChE Journal 2012 Jan; 58:69–78. DOI: 10.1002/aic.12563. arXiv: 0201037v1 [physics]. Available from: http://doi.wiley.com/10.1002/aic.12563%20https://onlinelibrary.wiley.com/doi/10.1002/aic.12563

92. Pingali K, Mendez R, Lewis D, Michniak-Kohn B, Cuitino A, and Muzzio F. Mixing order of glidant and lubricant - Influence on powder and tablet properties. International Journal of Pharmaceutics 2011; 409:269–77. DOI: 10.1016/j.ijpharm.2011.02.032. Available from: http://dx.doi.org/10.1016/j.ijpharm.2011.02.032

93. Portillo PM, Ierapetritou MG, and Muzzio FJ. Characterization of continuous convective powder mixing processes. Powder Technology 2008 Mar; 182:368–78. DOI: 10.1016/j.powtec.2007.06.024. Available from: https://www.sciencedirect.com/science/article/pii/S0032591007003142?pes=vor&entityID=https%3A%2F%2Fidp.bham.ac.uk%2Fshibboleth#fig1

94. Werner D, Davison H, Robinson E, Sykes JA, Seville JPK, Wellings A, Bhattacharya S, Monsalve DAS, Wheldon TK, and Windows-Yule CRK. Effect of system composition on mixing in binary fluidised beds. Chemical Engineering Science 2023 :118562

95. Goldhirsch I. Introduction to granular temperature. Powder Technology 2008; 182:130–6. DOI: 10.1016/j.powtec.2007.12.002

96. Ogawa S. Multitemperature theory of granular materials. *Proc. of the US-Japan Seminar on Continuum Mechanical and Statistical Approaches in the Mechanics of Granular Materials, 1978*. Gakajutsu Bunken Fukyu-Kai. 1978 :208–17

97. Gao Y, Muzzio FJ, and Ierapetritou MG. Optimizing continuous powder mixing processes using periodic section modeling. Chemical Engineering Science 2012 Oct; 80:70–80. DOI: 10.1016/j.ces.2012.05.037. Available from: https://www.sciencedirect.com/science/article/pii/S0009250912003181?casa_token=ekRMR8ElnJ4AAAAA:8ju5z1WMyR3MIO9ry04pJwNXZfq3L-kUGr-Fa7ns3R-YNT9dWj6RiZYo6YCaRAoIIssTEKIr_PM

98. Sarkar A and Wassgren CR. Simulation of a continuous granular mixer: Effect of operating conditions on flow and mixing. Chemical Engineering Science 2009 Jun; 64:2672–82. DOI: 10.1016/j.ces.2009.02.011. Available from: https://www.sciencedirect.com/science/article/pii/S0009250909001080

99. Tomita Y, Nagato T, Takeuchi Y, and Takeuchi H. Control of residence time of pharmaceutical powder in a continuous mixer with impeller and scraper. International Journal of Pharmaceutics 2020 Aug; 586:119520. DOI: 10.1016/j.ijpharm.2020.119520

100. Karner S and Urbanetz NA. Arising of electrostatic charge in the mixing process and its influencing factors. Powder Technology 2012; 226:261–8. DOI: 10.1016/j.powtec.2012.04.062. Available from: http://dx.doi.org/10.1016/j.powtec.2012.04.062

101. Haycocks N, Goldschmidt NA, and Thomsen U. Temperature & humidity requirements in pharmaceutical facilities. https://ispe.org/pharmaceutical-engineering/september-october-2021/temperature-humidity-requirements-pharmaceutical. (accessed Mar 31, 2023). 2023 Mar

102. Tran D, Komı=́nová P, Kulaviak L, and Zámostnỳ P. Evaluation of multifunctional magnesium aluminosilicate materials as novel family of glidants in solid dosage products. International Journal of Pharmaceutics 2021; 592:120054

103. Toson P, Siegmann E, Trogrlic M, Kureck H, Khinast J, Jajcevic D, Doshi P, Blackwood D, Bonnassieux A, Daugherity PD, and Ende MT am. Detailed modeling and process design of an advanced continuous powder mixer. International Journal of Pharmaceutics 2018 Dec; 552:288–300. DOI: 10.1016/j.ijpharm.2018.09.032. Available from: https://www.sciencedirect.com/science/article/pii/S0378517318306835?via%3Dihub

104. Kale DP, Zode SS, and Bansal AK. Challenges in translational development of pharmaceutical cocrystals. Journal of Pharmaceutical Sciences 2017; 106:457–70

105. Health and Executive S. ATEX and Explosive Atmospheres. https://www.hse.gov.uk/fireandexplosion/atex.htm. Accessed: 2023-01-10. 2016

106. Health and Executive S. Dangerous Substances and Explosive Atmospheres Regulations (DSEAR). https://www.hse.gov.uk/fireandexplosion/dsear.htm. Accessed: 2023-01-10. 2016

107. Alam MA, Liu YA, Dolph S, Pawliczek M, Peeters E, and Palm A. Benchtop NIR method development for continuous manufacturing scale to enable efficient PAT application for solid oral dosage form. International Journal of Pharmaceutics 2021; 601:120581. DOI: 10.1016/j.ijpharm.2021.120581. Available from: https://doi.org/10.1016/j.ijpharm.2021.120581

108. Montgomery DC. Design and Analysis of Experiments. John Wiley & Sons, 2017

109. Hill AM, Barber MJ, and Gotham D. Estimated costs of production and potential prices for the WHO Essential Medicines List. BMJ global health 2018; 3:e000571

110. Hill A, Gotham D, Fortunak J, Meldrum J, Erbacher I, Martin M, Shoman H, Levi J, Powderly WG, and Bower M. Target prices for mass production of tyrosine kinase inhibitors for global cancer treatment. BMJ open 2016; 6:e009586

111. Witte C, Pérez L, Fernandez M, and Weskamp T. Decarbonizing API manufacturing: Unpacking the cost and regulatory requirements. McKinsey & Company 2024. Accessed: 2024-12-30. Available from: https://www.mckinsey.com/industries/life-sciences/our-insights/decarbonizing-api-manufacturing-unpacking-the-cost-and-regulatory-requirements

112. Iansiti M and Nadella S. Democratizing Transformation. Harvard Business Review 2022 May; 100. Accessed: 2024-12-30:36–45. Available from: https://hbr.org/2022/05/democratizing-transformation

113. Burcham CL, Florence AJ, and Johnson MD. Continuous manufacturing in pharmaceutical process development and manufacturing. Annual Review of Chemical and Biomolecular Engineering 2018 Jun; 9:253–81. DOI: 10.1146/annurev-chembioeng-060817-084355. Available from: https://doi.org/10.1146/annurev-chembioeng-060817-084355

114. Vanhoorne V and Vervaet C. Recent progress in continuous manufacturing of oral solid dosage forms. International Journal of Pharmaceutics 2020; 579. DOI: 10.1016/j.ijpharm.2020.119194

115. Lee SL, O'Connor TF, Yang X, Cruz CN, Chatterjee S, Madurawe RD, Moore CM, Yu LX, and Woodcock J. Modernizing Pharmaceutical Manufacturing: from Batch to Continuous Production. Journal of Pharmaceutical Innovation 2015; 10:191–9. DOI: 10.1007/s12247-015-9215-8. Available from: https://doi.org/10.1007/s12247-015-9215-8

116. Roth WJ, Almaya A, Kramer TT, and Hofer JD. A Demonstration of Mixing Robustness in a Direct Compression Continuous Manufacturing Process. Journal of Pharma-

ceutical Sciences 2017; 106:1339–46. DOI: 10.1016/j.xphs.2017.01.021. Available from: http://dx.doi.org/10.1016/j.xphs.2017.01.021

117. International Council for Harmonisation of Technical Requirements for Pharmaceuticals for Human Use (ICH). ICH guideline Q13 on continuous manufacturing of drug substances and drug products. European Medicines Agency 2023; 31. Available from: https://www.ema.europa.eu/en/ich-guideline-q13-continuous-manufacturing-drug-substances-drug-products-scientific-guideline

118. International Council for Harmonisation of Technical Requirements for Pharmaceuticals for Human Use (ICH). Committee for Human Medicinal Products (CHMP) ICH Quality IWG Points to consider for ICH Q8/Q9/Q10 guidelines. European Medicines Agency 2012; 44. Available from: www.ema.europa.eu

119. Pernenkil L and Cooney CL. A review on the continuous blending of powders. Chemical Engineering Science 2006; 61:720–42. DOI: 10.1016/j.ces.2005.06.016

120. Tężyk M, Milanowski B, Ernst A, and Lulek J. Recent progress in continuous and semi-continuous processing of solid oral dosage forms: A review. Drug Development and Industrial Pharmacy 2015; 42:1195–214. DOI: 10.3109/03639045.2015.1122607

121. Windows-Yule CRK, Seville JPK, Ingram A, and Parker DJ. Positron emission particle tracking of granular flows. Annual review of chemical and biomolecular engineering 2020; 11:367–96

122. Windows-Yule K, Nicu\csan L, Herald MT, Manger S, and Parker D. Positron Emission Particle Tracking. IOP Publishing, 2022

123. Boonkanokwong V, Remy B, Khinast JG, and Glasser BJ. The effect of the number of impeller blades on granular flow in a bladed mixer. Powder Technology 2016 Nov; 302:333–49. DOI: 10.1016/j.powtec.2016.08.064. Available from: https://www.sciencedirect.com/science/article/pii/S0032591016305575?casa_token=ST4jsTngb-

oAAAAA:aV8PqFfZ-1c3C-t5xLT_8xVrnBiy426HlqqXTNlNh01PmIT4IzHMjjt2Uy1YEeseQA27f0105

124. Siraj MS. Single-blade convective powder mixing: The effect of the blade shape and angle. Powder Technology 2014 Nov; 267:289–301. DOI: 10.1016/j.powtec.2014.07.024. Available from: https://www.sciencedirect.com/science/article/pii/S0032591014006561#f0015

125. Gao Y, Ierapetritou M, and Muzzio F. Investigation on the effect of blade patterns on continuous solid mixing performance. Canadian Journal of Chemical Engineering 2011 Oct; 89:969–84. DOI: 10.1002/cjce.20530. Available from: https://onlinelibrary.wiley.com/doi/10.1002/cjce.20530

126. Ebrahimi M, Yaraghi A, Ein-Mozaffari F, and Lohi A. The effect of impeller configurations on particle mixing in an agitated paddle mixer. Powder Technology 2018 Jun; 332:158–70. DOI: 10.1016/j.powtec.2018.03.061. Available from: https://www.sciencedirect.com/science/article/pii/S0032591018302547?casa_token=Ilnk67Yn6nMAAAAA:ELDsV2aW51OEAxX3hzyUQoWl_Q2S7sg9OAHJ0CKLQ-Btl_Jsw9LBhtj0Ofe0sxNkBwdop3_Pc48#f0025

127. Windows-Yule C, Tunuguntla DR, and Parker D. Numerical modelling of granular flows: a reality check. Computational particle mechanics 2016; 3:311–32

128. Windows-Yule C and Neveu A. Calibration of DEM simulations for dynamic particulate systems. Papers in Physics 2022; 14:140010

129. Che H, Al-Shemmeri M, Fryer PJ, Lopez-Quiroga E, Wheldon TK, and Windows-Yule K. PEPT validated CFD-DEM model of aspherical particle motion in a spouted bed. Chemical Engineering Journal 2023; 453:139689

130. Parker DJ, Forster RN, Fowles P, and Takhar PS. Positron emission particle tracking using the new Birmingham positron camera. Nuclear Instruments and Methods in

Physics Research Section A: Accelerators, Spectrometers, Detectors and Associated Equipment 2002; 477:540–5

131. Windows-Yule CRK, Herald MT, Nicu\csan AL, Wiggins CS, Pratx G, Manger S, Odo AE, Leadbeater T, Pellico J, Rosales RTM de, et al. Recent advances in positron emission particle tracking: a comparative review. Reports on Progress in Physics 2022; 85:16101

132. Herald M, Wheldon T, and Windows-Yule C. Monte Carlo model validation of a detector system used for positron emission particle tracking. Nuclear Instruments and Methods in Physics Research Section A: Accelerators, Spectrometers, Detectors and Associated Equipment 2021; 993:165073

133. Zheng C, Li L, Nitert BJ, Govender N, Chamberlain T, Zhang L, and Wu CY. Investigation of granular dynamics in a continuous blender using the GPU-enhanced discrete element method. Powder Technology 2022; 412:117968. DOI: 10.1016/j.powtec.2022.117968. Available from: https://doi.org/10.1016/j.powtec.2022.117968

134. Megarry AJ, Swainson SM, Roberts RJ, and Reynolds GK. A big data approach to pharmaceutical flow properties. International Journal of Pharmaceutics 2019; 555:337–45. DOI: 10.1016/j.ijpharm.2018.11.059

135. Yang Z, Fryer PJ, Bakalis S, Fan X, Parker DJ, and Seville JPK. An improved algorithm for tracking multiple, freely moving particles in a positron emission particle tracking system. Nuclear Instruments and Methods in Physics Research Section A: Accelerators, Spectrometers, Detectors and Associated Equipment 2007; 577:585–94

136. Nicuşan AL and Windows-Yule CR. Positron emission particle tracking using machine learning. Review of Scientific Instruments 2020 Jan; 91:13329. DOI: 10.1063/1.5129251. Available from: https://doi.org/10.1063/1.5129251

137. Wildman RD, Huntley JM, Hansen JP, Parker DJ, and Allen DA. Single-particle motion in three-dimensional vibrofluidized granular beds. Physical Review E 2000; 62:3826

138. Morrison AJ, Govender I, Mainza AN, and Parker DJ. The shape and behaviour of a granular bed in a rotating drum using Eulerian flow fields obtained from PEPT. Chemical Engineering Science 2016; 152:186–98. DOI: 10.1016/j.ces.2016.06.022. Available from: http://dx.doi.org/10.1016/j.ces.2016.06.022

139. Leimkuhler B and Matthews C. Molecular dynamics. Interdisciplinary applied mathematics 2015; 39:443

140. Wildman RD, Hansen JP, and Parker DJ. Velocity auto-correlation functions in three-dimensional vibro-fluidized granular beds. Physics of Fluids 2002; 14:232–9

141. Windows-Yule CRK, Rosato AD, Rivas N, and Parker DJ. Influence of initial conditions on granular dynamics near the jamming transition. New journal of physics 2014; 16:63016

142. Bhalode P and Ierapetritou M. A review of existing mixing indices in solid-based continuous blending operations. Powder Technology 2020; 373:195–209. DOI: 10.1016/j.powtec.2020.06.043. Available from: https://doi.org/10.1016/j.powtec.2020.06.043

143. Baxter GW and Olafsen JS. Experimental evidence for molecular chaos in granular gases. Physical review letters 2007; 99:28001

144. Campbell CS. Self-diffusion in granular shear flows. Journal of Fluid Mechanics 1997; 348:85–101

145. Martin TW, Seville JPK, and Parker DJ. A general method for quantifying dispersion in multiscale systems using trajectory analysis. Chemical engineering science 2007; 62:3419–28

146. Mosig J and Kleinebudde P. Critical evaluation of root causes of the reduced compactability after roll compaction/dry granulation. Journal of Pharmaceutical Sciences 2015; 104:1108–18

147. Nickerson B, Kong A, Gerst P, and Kao S. Correlation of dissolution and disintegration results for an immediate-release tablet. Journal of Pharmaceutical and Biomedical Analysis 2018; 150:333–40

148. Holman J, Tantuccio A, Palmer J, Doninck T van, and Meyer R. A very boring 120 h: 15 million tablets under a continuous state of control. Powder Technology 2021 Apr; 382:208–31. DOI: 10.1016/j.powtec.2020.12.073. Available from: https://doi.org/10.1016/j.powtec.2020.12.073%20https://linkinghub.elsevier.com/retrieve/pii/S003259102031250X

149. Hurley S, Tantuccio A, Escotet-espinoza MS, Flamm M, and Metzger M. Development and Use of a Residence Time Distribution (RTD) Model Control Strategy for a Continuous Manufacturing Drug Product Pharmaceutical Process. Pharmaceutics 2022; 14. DOI: 10.3390/pharmaceutics14020355

150. Sarkar A and Wassgren C. Continuous blending of cohesive granular material. Chemical Engineering Science 2010; 65:5687–98. DOI: 10.1016/j.ces.2010.04.011. Available from: http://dx.doi.org/10.1016/j.ces.2010.04.011

151. Bekaert B, Van Snick B, Pandelaere K, Dhondt J, Di Pretoro G, De Beer T, Vervaet C, and Vanhoorne V. Continuous direct compression: Development of an empirical predictive model and challenges regarding PAT implementation. International Journal of Pharmaceutics: X 2022; 4:100110. DOI: 10.1016/j.ijpx.2021.100110. Available from: https://doi.org/10.1016/j.ijpx.2021.100110

152. Nicusan AL and Windows-Yule K. PyMED: Multiphase Materials Exploration via Evolutionary Equation Discovery. Version 0.1.0. 2022 Oct. DOI: 10.5281/zenodo.7215239. Available from: https://doi.org/10.5281/zenodo.7215239

153. Nicusan AL and Windows-Yule K. M2E3D: Multiphase Materials Exploration via Evolutionary Equation Discovery. Version 0.1.0. 2022 Apr

154. Jones-salkey O, Nicusan AL, Windows-yule CRK, Ingram A, and Werner D. Application of Positron Emission Particle Tracking (PEPT) for the evaluation of powder behaviour in an incline linear blender for Continuous Direct Compression (CDC). International Journal of Pharmaceutics 2023; 645:123361. DOI: 10.1016/j.ijpharm.2023.123361. Available from: https://doi.org/10.1016/j.ijpharm.2023.123361

155. Freeman R. Measuring the flow properties of consolidated, conditioned and aerated powders—a comparative study using a powder rheometer and a rotational shear cell. Powder Technology 2007; 174:25–33

156. Hare C, Zafar U, Ghadiri M, Freeman T, Clayton J, and Murtagh M. Analysis of the dynamics of the FT4 powder rheometer. Powder Technology 2015; 285:123–7

157. Schwedes J and Schulze D. Measurement of flow properties of bulk solids. Powder technology 1990; 61:59–68

158. Schulze D and Schulze D. Flow properties of bulk solids. Powders and Bulk solids: Behavior, characterization, storage and flow 2021 :57–100

159. Portillo PM, Muzzio FJ, and Ierapetritou MG. Hybrid DEM-compartment modeling approach for granular mixing. AIChE Journal 2007 Jan; 53:119–28. DOI: 10.1002/aic.11054. arXiv: 0201037v1 [physics]. Available from: http://doi.wiley.com/10.1002/aic.11054

160. Cavinato M, Artoni R, Bresciani M, Canu P, and Santomaso AC. Scale-up effects on flow patterns in the high shear mixing of cohesive powders. Chemical Engineering Science 2013; 102:1–9. DOI: 10.1016/j.ces.2013.07.037

161. Dhondt J, Bertels J, Kumar A, Van Hauwermeiren D, Ryckaert A, Van Snick B, Klingeleers D, Vervaet C, and De Beer T. A multivariate formulation and process

development platform for direct compression. International Journal of Pharmaceutics 2022; 623:121962. DOI: 10.1016/j.ijpharm.2022.121962. Available from: https://doi.org/10.1016/j.ijpharm.2022.121962

162. Lundberg SM and Lee SI. A unified approach to interpreting model predictions. *Advances in Neural Information Processing Systems*. 2017 :4765–74

163. Cranmer M, Sanchez-Gonzalez A, Battaglia P, Xu R, Cranmer K, Spergel D, and Ho S. Discovering Symbolic Models from Deep Learning with Inductive Biases. NeurIPS 2020 2020. arXiv: 2006.11287 [cs.LG]

164. Bezanson J, Edelman A, Karpinski S, and Shah VB. Julia: A fresh approach to numerical computing. SIAM review 2017; 59:65–98

165. Arntz M, Otter WK den, Briels WJ, Bussmann P, Beeftink H, and Boom R. Granular mixing and segregation in a horizontal rotating drum: a simulation study on the impact of rotational speed and fill level. AIChE journal 2008; 54:3133–46

166. Rosato A and Windows-Yule K. Influence of key parameters. Academic Press, 2020 :197–218. DOI: 10.1016/b978-0-12-814199-1.00018-4. Available from: https://www.sciencedirect.com/book/9780128141991/segregation-in-vibrated-granular-systems#book-description

167. Kushner J and Schlack H. Commercial scale validation of a process scale-up model for lubricant blending of pharmaceutical powders. International Journal of Pharmaceutics 2014; 475:147–55. DOI: 10.1016/j.ijpharm.2014.08.036. Available from: http://dx.doi.org/10.1016/j.ijpharm.2014.08.036

168. Lekhal A, Girard K, Brown M, Kiang S, Khinast J, and Glasser B. The effect of agitated drying on the morphology of l-threonine (needle-like) crystals. International Journal of Pharmaceutics 2004; 270:263–77

169. Parikh DM. Handbook of pharmaceutical granulation technology. Drugs and the pharmaceutical sciences 2005; 81

170. Hare C and Ghadiri M. Attrition of paracetamol and aspirin under bulk shear deformation. Chemical Engineering Science 2015; 125:13–9

171. Goh WP, Sinha K, Nere NK, Ho R, Bordawekar S, Sheikh A, and Ghadiri M. Breakage assessment of lath-like crystals in a novel laboratory-scale agitated filter bed dryer. Pharmaceutical Research 2022; 39:3209–21